Towards 'Smarter' Systems: Key Cyber-Physical Performance-Cost Tradeoffs in Smart Electric Vehicle Charging with Distributed Generation

HERON, JOHN,WILFRED

Towards 'Smarter' Systems

Key Cyber-Physical Performance-Cost Tradeoffs in Smart Electric Vehicle Charging with Distributed Generation

John Wilfred Heron

A Thesis presented for the degree of
Doctor of Philosophy

Department of Engineering
Durham University
United Kingdom

November 2020

Towards 'Smarter' Systems

Key Cyber-Physical Performance-Cost Tradeoffs in Smart Electric Vehicle Charging with Distributed Generation

John Wilfred Heron

Submitted for the degree of Doctor of Philosophy

November 2020

Abstract: The growing penetration of electric vehicles (EV) into the market is driving sharper spikes in consumer power demand. Meanwhile, growing renewable distributed generation (DG) is driving sharper spikes in localised power supply. This leads to growing temporally unsynchronised spikes in generation and consumption, which manifest as localised over- or undervoltage and disrupt grid service quality. Smart Grid solutions can respond to voltage conditions by curtailing charging EVs or available DG through a network of cyber-enabled sensors and actuators. How to optimise efficiency, ensure stable operation, deliver required performance outputs and minimally overhaul existing hardware remains an open research topic.

This thesis models key performance-cost tradeoffs relating to Smart EV Charging with DG, including architectural design challenges in the underpinning Information and Communications Technology (ICT). Crucial deployment optimisation balancing various Key Performance Indicators (KPI) is achieved. The contributions are as follows:

- Two Smart EV Charging schemes are designed for secondary voltage control in the distribution network. One is optimised for the network operator, the

other for consumers/generators. This is used to evaluate resulting performance implications via targeted case study.

- To support these schemes, a multi-tier hierarchical distributed ICT architecture is designed that alleviates computation and traffic load from the central controller and achieves user fairness in the network. In this way it is scalable and adaptable to a wide range of network sizes.

- Both schemes are modelled under practical latency constraints to derive interlocking effects on various KPIs. Multiple latency-mitigation strategies are designed in each case.

- KPIs, including voltage control, peak shaving, user inconvenience, renewable energy input, CO_2 emissions and EV & DG capacity are evaluated statistically under 172 days of power readings. This is used to establish key performance-cost tradeoffs relevant to multiple invested bodies in the power grid.

- Finally, the ICT architecture is modelled for growing network sizes. Quality-of-Service (QoS) provision is studied for various multi-tier hierarchical topologies under increasing number of end devices to gauge performance-cost tradeoffs related to demand-response latency and network deployment.

Declaration

The work in this thesis is based on research carried out in the Department of Engineering at Durham University. No part of this thesis has been submitted elsewhere for any degree or qualification.

Acknowledgements

I have not undertaken this odyssey of work alone. Here, I recognise the invaluable assistance provided to me by others as I set about this journey.

First, for providing guidance, support and always being on my side from start to finish, I would like to thank my supervisor Prof. Hongjian Sun. I express my deepest gratitude for all of the discussions, feedback, enthusiasm and advice that was available at short notice for the duration of my PhD study, and encouragement during the most troublesome moments.

Second, I would like to accredit the invaluable assistance of Prof. Peter Matthews for finding me a database of accurate 1s windspeed data that was intrinsic to the contributions of this research. Similarly, I would like to thank the OREC group for providing this data and Dr. Donatella Zapallá for her encouragement when debugging its post-processing. Also thanks to Prof. Phil Blythe and Dr. Graeme Hill at Newcastle University for providing electric vehicle charging data and Dr. Andrew Crossland for providing carbon emissions data from MyGridGB. Without this input, key conclusions reached in this thesis would not have been possible.

Third, I must thank the research teams who hosted me on my industrial secondments. Special mention to Dr. Velissarios Gezerlis and Dr. Tilemachos Doukoglou at OTE Labs in Athens, Dr. Jan Schuurmans at DotX Control Solutions in Amsterdam and Dr. Omid Alizadeh-Mousavi at DEPsys in Lausanne. In each of these locations I was provided with warm hospitality, keen input, discerning insight and inspiration for my ongoing projects.

Finally, I am indebted to the close friends and family whose support and encouragement made even the most trying moments of this PhD tolerable. I want to thank Alra for her love and patience through the ups and downs of the last three years. I want to thank my family members for their Herculean proof-reading efforts at the eleventh hour. And Henrik, Wesley and Jeanne, whose friendship provided welcome respite from the everyday pressures of academia, and with whom I have shared many fond memories over the years.

With great [charging] *power comes great responsibility.*

— Spiderman

Dedicated to

Captain Fluffers

for doing what he does best

Contents

List of Figures

List of Tables

Nomenclature

AC	Alternating Current
BER	Bit Error Rate
CCU	Central Control Unit
CD	Continuous Deviations
CMR	Continuous Margin Reduction
COR	Smart Correction
CO_2	Carbon Dioxide
CP	Control Pilot pin, IEC 61851
CPO	Charge Point Operator
CUR	Smart Curtailment
CS	Charging Station
CSMS	Charging Station Management System
DC	Direct Current
DG	Distributed Generation
DGC	Distributed Generation Controller
DSO	Distribution System Operator
EMS	Energy Management System
EV	Electric Vehicle
EVSE	Electric Vehicle Supply Equipment
GUI	Graphic User Interface
HC	Hosting Capacity
HTTP	Hypertext Transfer Protocol

ICT	Information and Communications Technology
ICU	Intermediary Control Unit
IEC	International Electrotechnical Commission
IEEE	Institute for Electrical and Electronics Engineers
IP	Internet Protocol
IR	Interval Reduction
ISO	International Organisation for Standardisation
JSON	JavaScript Object Notation
KPI	Key Performance Indicator
LC	Local Controller
LV	Low Voltage (240V)
MV	Medium Voltage (12.66kV)
MW	MegaWatt
OCPP	Open Charge Point Protocol
OSCP	Open Smart Charging Protocol
OpenADR	Open Automated Demand Response
PAPR	Peak-to-Average Power Ratio
PE	Protective Earth pin, IEC 61851
PP	Proximity Pilot pin, IEC 61851
PV	Photovoltaic
p.u.	per unit
QoS	Quality of Service
SCADA	Supervisory Control and Data Acquisition
SD	Smart Device
TCP	Transmission Control Protocol
TD	Trigger Deviations
TMR	Trigger Margin Reduction
TSO	Transmission System Operator
TWh	TeraWatt-hour

UK	United Kingdom
USA	United States of America
VDSL	Very High Speed Digital Subscriber Line
VEN	Virtual End Node
VTN	Virtual Top Node
XMPP	eXtensible Messaging and Presence Protocol
XML	eXtensible Markup Language

Chapter 1

Introduction

In 2019, useful energy consumed from the United Kingdom's (UK) National Grid summed to roughly 346 TWh. Meanwhile, 26 TWh of technical losses were incurred, roughly 8% of useful output [1]. Technical losses are from energy dissipated in the conducting lines and equipment, and magnetic losses in transformers. These are normally considered inherent to the power network, and a loss in income for the energy provider. Assuming perfect power factor correction on the load side, technical losses result simply from having to transport power over large geographical distances. Thus it is inherently desirable to reduce distance between generator and consumer.

Recently, renewable generation has seen growing emphasis as an effective means against global climate change. In 2019, the share of renewable generation in overall electric power output reached a record high of 37% in the UK [1]. Further, a 6% surge in distributed generation (DG) was observed - this is fed directly into the distribution network alongside consumers (e.g. residential small-scale wind and solar power), rather than first being fed into long-distance transmission lines. Continuing this trend, the National Grid expects by 2030, 50% of all generation will be connected at the distribution level [2], [3].

However, grid hardware was designed for traditional unidirectional transfer only, and under specific power constraints. DG can lead to localised power congestion

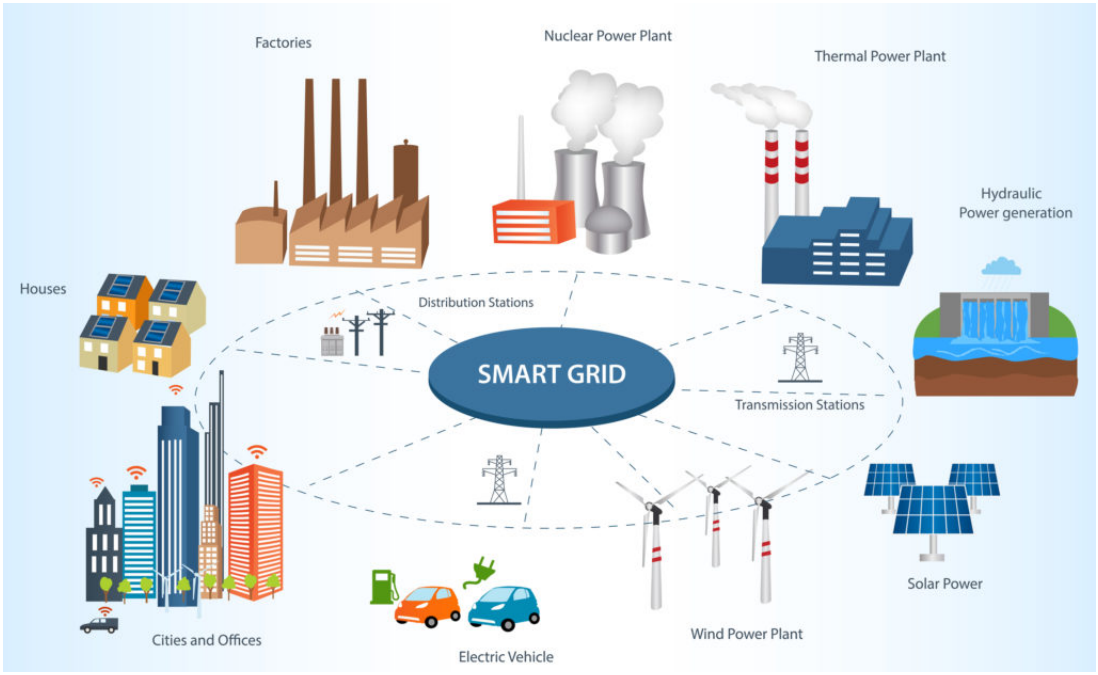

Figure 1.1: Smart Grids are the key to supporting all-electric vehicles in the power network [10]

and reverse power flow, for which the network was not necessarily designed. Further, renewable generation is highly dependent on weather conditions, meaning its availability is non-correlated with consumer demand. Changes in weather can lead to sudden spikes or troughs in localised power conditions leading to disruptions in power quality. For this reason, limits are placed on DG, typically 15-20% of peak load [4].

Further, the increasing number of electricity-consuming devices is leading to sharper spikes in consumer demand. The National Grid expects by 2040 all cars sold will be purely electric [3]. Typical UK daily household energy consumption ranges from 5-20kWh per day [5], while electric vehicle (EV) battery capacity ranges 20-100kWh [6]–[9]. Ownership of a fully EV will represent huge increase in household energy demand.

Predictions of rising temporally unsynchronised spikes in generation and consumption has led to growing concern whether the traditional power grid can continue to be operated within stable limits. The solution lies in coordination of numerous cyber-enabled sensors and actuators permeated throughout the grid - the Smart

Grid - shown Fig. 1.1. This development mirrors the increasing deployment of cyber devices globally, e.g. Internet-of-Things (IoT). How to intelligently control generators, loads and storage devices in the power network to optimise efficiency and ensure stable operation is an ongoing driver of Smart Grid research.

Smart Charging solutions aim to mitigate spikes in supply and demand by exploiting the 'discretionary' power requirement of EVs - it does not matter exactly when EV charging takes place, so long as it is charged when the consumer requires. Thus it is possible, within certain timing constraints, to adjust net demand according to available supply in a way that meets various Key Performance Indicators (KPIs). In this way, Smart Charging stands to deliver precise and colocated actuation at fine granularity in the distribution network, and can synergise with renewable supply such that the capacity of both EVs and DG can be improved.

1.1 Thesis Objectives

This thesis targets four critical research areas in Smart Charging development. A literature review elaborating on, and exposing, these three open topics is provided in Chap. 2. The topics are as follows:

1.1.1 Divergent Optimisation Standpoints

First, Smart Charging can be approached from two optimisation objectives:

(A) For peak shaving in the network, i.e. to flatten peak load. This means power equipment, which is sized according to peak load, can be minimally replaced to accommodate rising demand. Equipment can be operated closer to its limits and power efficiency more effectively optimised, reducing technical losses and operating costs.

(B) To maximise power transfer when it is cheap, i.e. during non-peak times or when renewable generation is strong. This reduces consumer energy prices and can better buffer high DG penetrations.

These two objectives (A) and (B) can be misaligned. Strong renewable generation can lead to cheap electricity during peak loading hours. In this case, the operator desires peak shaving, while consumers/generators desire peak charging. This dichotomy is largely unanswered in Smart Charging research. This thesis explicitly models the performance implications of both optimisation standpoints via targeted case studies.

1.1.2 Practical Latency Constraints

Smart Grid solutions require a pervasive ICT infrastructure to connect numerous sensors and actuators. Fine-granularity control also requires optimisation over increasingly numerous links and buses. For this reason, cost of data collection as well as computation complexity in the optimisation algorithm are significant investment concerns relating to operational latency.

Further, operating bodies in the power network are not traditionally accustomed to latency-critical applications and this is reflected in deployed hardware (e.g. SCADA data from wind turbines is collected at 10 minute intervals). Latency reduction beyond a certain minimum may require extensive reconfiguring and replacement of existing infrastructure and is hence a significant cost concern.

Practical latency constraints are routinely overlooked in Smart Charging research. Perfect knowledge of grid status, energy prices, driving patterns and loading is generally assumed everywhere in the network, and that the 'sense-compute-actuate' response cycle can occur with zero latency. This thesis explicitly models KPIs under various practical latency constraints, and designs an underpinning ICT architecture such that traffic burden, centralised computation and hardware investment are all jointly minimised.

1.1.3 Balancing KPIs over multiple concerned parties

Finally, successful Smart Charging requires willing participation and coordination from various concerned participants in the power network. How to guarantee satisfaction for each participant remains unclear.

Successful Smart Charging requires numerous participating EVs. However, delayed EV charging is an inconvenience to EV owners. Economically, this can be realised via user subscription, where EV owners are compensated for potential charging delay with cheaper energy prices. KPIs such as Voltage Control and Peak Shaving, which are of strong concern for the network operator, must be correctly balanced against User Inconvenience such that compensation can be quantified and sufficiently high subscription numbers can be maintained.

Further, Smart Charging can significantly reduce overall carbon emissions by delaying EV charging from peak hours in the early evening to overnight when released CO_2/kWh is lowest. By buffering for instability introduced from renewable generation, it can also improve DG capacity in the network. DG Energy Input and daily CO_2 Emissions incentivise investment in renewable systems, and are therefore KPIs for renewable expansion. However, due to statistical variation in both supply and demand, DG may require curtailment. The statistical interaction between Smart Charging, DG penetration and CO_2 emissions highly relevant to encouraging investment in DG.

Finally, Sec. 1.1.2 described how infrastructure investment relating to practical latency constraints is a key driver for deployment budget. All KPIs are balanced against practical latency constraints as a running theme throughout this thesis.

Smart Grid services stand to uproot the conventional economic structure of power distribution. This thesis explicitly models key performance-cost tradeoffs relating to six KPIs: Voltage Control, Peak Shaving, User Inconvenience, DG Input, CO_2 Emissions and Deployment Cost.

1.1.4 Steps towards Decentralisation

There is a notable progression of 'decentralisation' evident in the literature on Smart Grid control. However, existing installations adopt a centralised communications paradigm only. Moreover, decentralisation is a formidable step, involving at the very least significant installation and reprogramming of new and existing infrastructure. This thesis proposes a distributed communications architecture to support both Smart Charging schemes that serves to decentralise computation and traffic load in the network without radical infrastructural overhaul.

1.2 Thesis Contributions

The contributions of this thesis are as follows:

- Two Smart Charging schemes are designed relevant to diverging optimisation objectives of operator and consumer/generator:

  1. ***Smart Curtailment (CUR):*** achieves peak shaving, allowing minimal additions to power infrastructure and lower costs for the network operator.
  2. ***Smart Correction (COR):*** optimally adapts charging load to available renewable generation, maximising cost-efficiency for consumers/generators.

  These can simultaneously achieve voltage control in the distribution network and dramatic rise in EV and DG capacity.

- A multi-tier hierarchical distributed ICT architecture and protocol is designed to alleviate computation and traffic load without extensive infrastructural overhaul. Further, this is compatible with Smart Charging and Demand-Response communications standards. Thus the system is scalable and adaptable to a variety of network sizes and asset arrangements, and is readily applicable in the industrial environment.

- KPIs for Voltage Control, Peak Shaving, User Inconvenience, DG Energy Input, CO_2 Emissions and Deployment Cost for both schemes are evaluated statistically under 172 days of input power profiles, and key performance-cost tradeoffs are identified.

- These tradeoffs are modelled subject to practical operational latency constraints, and multiple latency-mitigation strategies are evaluated.

- Finally, key performance-cost tradeoffs relating to traffic load and deployment cost are analysed for the proposed ICT architecture. Demand-response latency is analysed for various network topologies as the number of client users increases. The conclusions in this case are also general to numerous Smart Grid and IoT configurations.

1.3 Thesis Outline

This thesis is organised into five chapters. Chapter 2 conducts a background and literature review of the topic, and the research contributions are spread over chapters 3-5. These summarise and expand upon two publications (**I**, **II** in Sec. 1.4), which are attached in the appendices, and one manuscript (**III**) that is pending peer review at the time of writing.

Chapter 2 outlines key background material and surveys recent literature on Smart Grid research topics relating to this thesis. Two mathematical models for analysing power flow in the transmission and distribution network are defined, and key shortcomings of traditional grid control mechanisms for emerging power requirements are identified. Smart Grid ICT architectures and various Smart Charging solutions are reviewed, along with recent open Smart Charging communications standards. Finally, the scope of research and contributions of this thesis are elaborated.

Chapter 3 begins by defining the system model general to both Smart Charging schemes, describing the underpinning ICT architecture and the test platform on

which they are statistically assessed. It then completes in depth analysis of the first scheme, Smart Curtailment (CUR), under ideal and practical latency constraints. KPIs are evaluated statistically and key cost-performance tradeoffs are identified. This chapter expands upon the published work in **(I)** listed below.

Chapter 4 analyses the second scheme, Smart Correction (COR). This is mathematically formulated for its crucial algorithmic differences with CUR. Operation of the two schemes is compared under ideal and then practical latency constraints. Finally, KPIs are statistically evaluated and key performance-cost tradeoffs for the two schemes are compared in detail. This chapter expands upon the work in **(III)** that has been submitted for publishing pending review.

Chapter 5 designs a testbed simulation to evaluate latency reduction in the ICT architecture for growing numbers of client devices. Protocols, module structure and graphic user interface is described, before round-trip latency is analysed specific to traffic accumulation at the mid-tier aggregator. Statistical results are then presented and key performance-cost tradeoffs are identified linking to demand-response latency with ICT deployment cost. This chapter expands upon the published work in **(II)** listed below.

Finally, Chapter 6 concludes the thesis, summarising key research contributions and outlining future work.

1.4 Publications

The relevant publications included in this thesis are as follows

(I) J. W. Heron and H. Sun, "Smart Electric Vehicle Charging with Ideal and Practical Communications in Smart Grids," in *Proc. 2019 IEEE Global Communications Conference (GLOBECOM)*, Waikoloa, HI, USA, 2019, pp. 1-6.

(II) J. W. Heron, J. Jiang, H. Sun, V. Gezerlis and T. Doukoglou, "Demand-Response Round-Trip Latency of IoT Smart Grid Network Topologies," in

IEEE Access, vol. 6, pp. 22930-22937, 2018.

(III) J. W. Heron, H. Sun, O. Alizadeh-Mousavi and A. Crossland "Key Performance-Cost Tradeoffs in Smart Electric Vehicle Charging with Distributed Generation," submitted to *IET Smart Grid*, August 2020 (pending review)

In addition to the publications above, the author is primary contributor to further publications that are not related to the main thesis objective:

(IV) J. W. Heron and H. Sun, "Dynamic Time and Power Allocation for Opportunistic Energy Efficient Cooperative Relay," in *Proc. 2017 IEEE 86th Vehicular Technology Conference (VTC-Fall)*, Toronto, ON, 2017, pp. 1-5.

(V) J. W. Heron, H. Sun and H. Haas, "LiFi for the Vehicular Environment: A Survey," Submitted to *IEEE Transactions on Intelligent Transport Systems*, July 2020 (pending review)

Chapter 2

Background and Literature Survey

This chapter outlines key background material and surveys recent literature relating to the contributions of this thesis. This chapter is in two sections.

In Section 2.1, background material is reviewed. Two concise mathematical models are derived to describe prevalent power flow issues in the transmission and distribution network. These models are used to identify key shortcomings of traditional grid control methods and the need for Smart Grid implementation in future energy services.

In Section 2.2, literature is surveyed on key research topics. First, ICT constraints relevant to data exchange between sensors and actuators are introduced, and networked control paradigms in Smart Grid communications architectures are reviewed. Smart Charging is then presented, along with relevant extension to Vehicle-to-Grid (V2G) configurations, as a means to deliver various KPIs in the power network. Finally, recent open Smart Charging and Demand-Response communications standards are then summarised. Finally, Section 2.3 concludes the topic.

2.1 Background

This section builds a model for power transfer in the transmission and distribution network, defining an optimisation problem for physical design targets. Traditional

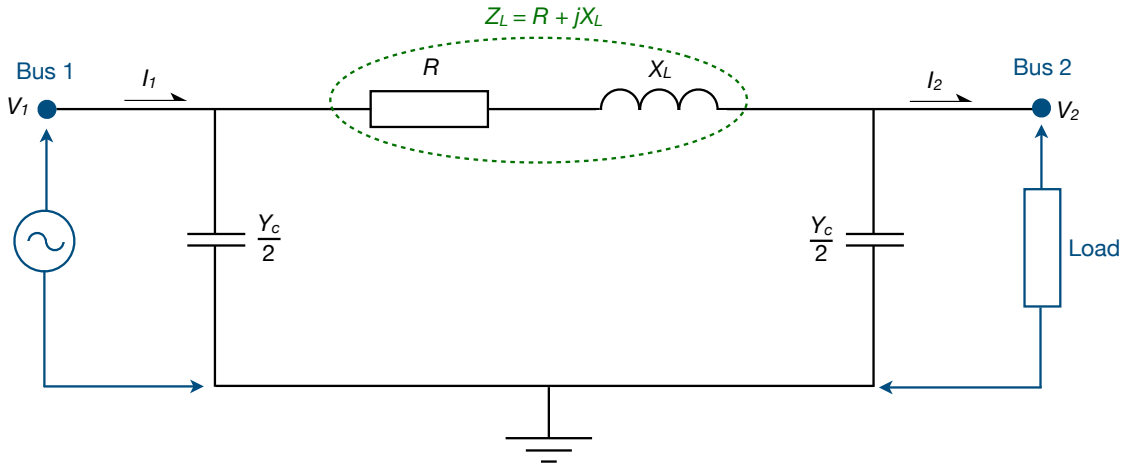

Figure 2.1: Π-equivalent model of a medium length (80-240km) transmission line between two buses (per transmission phase)

network control is then described, along with its shortcomings with respect to future energy services. With this basis, 'Smart' systems are introduced in Sec. 2.2.1.

2.1.1 Modelling the Power Network

The power network transports three-phase alternating current (AC) electricity between nodes or 'buses', connected via transmission and distribution lines. For any bus b in the network, the voltage phasor V_b may be represented by

$$V_b = |V_b|e^{j\theta_b} \tag{2.1.1}$$

Where $|V_b|$ denotes the root-mean-square voltage, θ_b denotes phase angle with respect to the node's current phasor I_b, and $j = \sqrt{-1}$.

A transmission line connecting two buses 1 & 2 may be modelled by its Π-equivalent circuit shown in Fig. 2.1. Here, V_1, I_1 and V_2, I_2 represent voltage and current phasors at the output of a net power injection from a source/generator, and net power ejection to the load, respectively. If a balanced load exists on all three transmission phases, only a single phase need be analysed. R is the AC conductive resistance of the line. X_L is the inductive reactance due to the formation of a magnetic field around a current-carrying conductor. Y_C is the capacitive admittance that develops due to voltage difference between phase conductors and between a

phase conductor and the ground.

Fig. 2.1 is an approximation applicable to medium length transmission lines in the range 80-240km. In short transmission lines (less than 80km), the capacitive admittance is often negligible. This is commonly assumed in distribution networks, since the distances are short and the voltage is comparatively low. In this case, the line can be modelled simply by its series impedance $Z_L = R + jX_L$. In longer transmission lines (more than 240km), the shunt capacitance can no longer be approximated to two equal parts at the sending and receiving end, and the model must consider parameters uniformly distributed along the line. The contributions of this thesis relate to the distribution network, so analysis is limited to short-range lines, and medium-range for comparison.

With Kirchoff's Laws the circuit in Fig. 2.1 can be described

$$\begin{bmatrix} I_1 \\ \\ I_2 \end{bmatrix} = \begin{bmatrix} \frac{Y_C}{2} + \frac{1}{Z_L} & -\frac{1}{Z_L} \\ \\ \frac{1}{Z_L} & -\left(\frac{Y_C}{2} + \frac{1}{Z_L}\right) \end{bmatrix} \begin{bmatrix} V_1 \\ \\ V_2 \end{bmatrix} \tag{2.1.2}$$

However, a generalised method is required to model a complex interaction of multiple nodes and lines. To do this, Fig. 2.1 can be redescribed by the equivalent Bus Injection Model in Fig. 2.2. Here, current direction is generalised, since any node could have net injection or ejection of power. Current is positive going into a bus, and negative going out. All nodes can then be described by

$$\overrightarrow{I} = \begin{bmatrix} I_1 \\ I_2 \end{bmatrix} = \begin{bmatrix} y_{11} + y_{12} & -y_{12} \\ -y_{12} & y_{22} + y_{12} \end{bmatrix} \begin{bmatrix} V_1 \\ V_2 \end{bmatrix} = \boldsymbol{Y}\overrightarrow{V} \tag{2.1.3}$$

Note that eq. (2.1.3) corresponds exactly with eq. (2.1.2), since the current direction I_2 has been redefined.

Using this notation, steady-state power flow in any network size can be modelled. For example, the four node system in Fig. 2.3. Each bus is connected to all other buses by a transmission line, and each bus may serve as a net injection or net ejection of power. Each current injection must be equal to the sum of currents flowing out

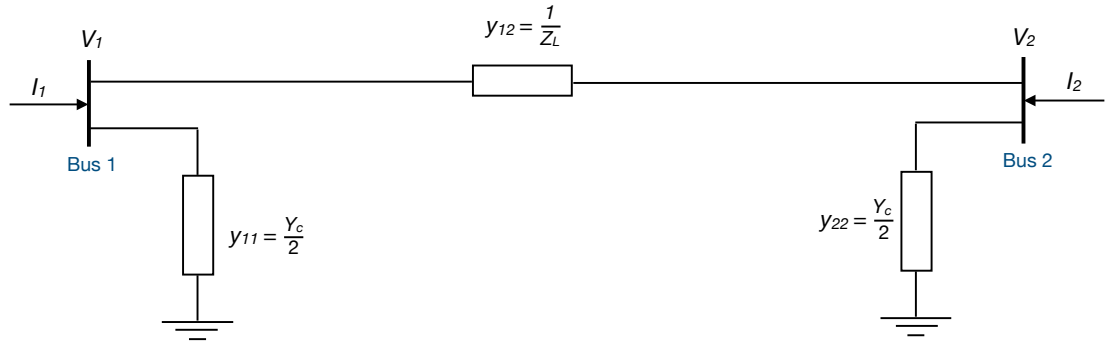

Figure 2.2: Equivalent Bus Injection Model of a transmission line between two buses

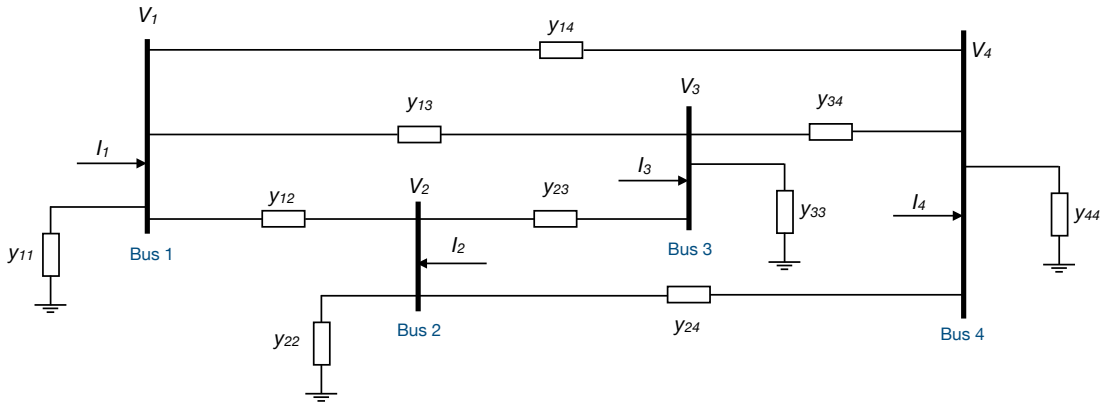

Figure 2.3: Four bus power network

of the bus. Hence, for buses $b = 1, ..., B$ we may generalise

$$I_b = V_b y_{bb} + \sum_{x=1}^{B} (V_b - V_x) y_{bx} \tag{2.1.4}$$

giving the Generalised Bus Injection Model [11], which fully defines voltage and current phasors for any network of B buses connected in topology defined by the $B \times B$ admittance matrix $\boldsymbol{Y}$:

$$\overrightarrow{I} = \begin{bmatrix} I_1 \\ I_2 \\ \vdots \\ I_B \end{bmatrix} = \begin{bmatrix} \sum_{b=1}^{B} y_{1b} & -y_{12} & \cdots & -y_{1B} \\ -y_{12} & \sum_{b=1}^{B} y_{2b} & \cdots & -y_{2B} \\ \vdots & \vdots & & \vdots \\ -y_{1B} & -y_{2B} & \cdots & \sum_{b=1}^{B} y_{Bb} \end{bmatrix} \begin{bmatrix} V_1 \\ V_2 \\ \vdots \\ V_B \end{bmatrix} = \boldsymbol{Y}\overrightarrow{V} \tag{2.1.5}$$

$\boldsymbol{Y}$ is symmetric since $y_{bx} = y_{xb}$. Line admittance $y_{bx} = \gamma_{bx} + j\beta_{bx}$, where γ_{bx} and β_{bx} are line conductance and susceptance. If there is no connection between two buses,

$y_{bx} = 0$. We can then define net apparent power injection into bus b

$$S_b = V_b I_b^* = P_b + jQ_b \tag{2.1.6}$$

Where * denotes the complex conjugate, and P_b, Q_b are the real and reactive power injection, respectively. Using the notation $Y_{bx} = \Gamma_{bx} + j\mathrm{B}_{bx}$ to be the element in row b and column x of $\boldsymbol{Y}$, from (2.1.5) the current and power injection at any bus b may be expressed

$$I_b = \sum_{x=1}^{B} V_x Y_{bx} \tag{2.1.7}$$

$$S_b = V_b \sum_{x=1}^{B} V_x^* Y_{bx}^* \tag{2.1.8}$$

Separating real and imaginary terms, (2.1.8) gives real and reactive power injections

$$P_b = \sum_{x=1}^{B} |V_b||V_x| \Big(\Gamma_{bx} \cos(\theta_b - \theta_x) + \mathrm{B}_{bx} \sin(\theta_b - \theta_x) \Big) \tag{2.1.9}$$

$$Q_b = \sum_{x=1}^{B} |V_b||V_x| \Big(\Gamma_{bx} \sin(\theta_b - \theta_x) + \mathrm{B}_{bx} \cos(\theta_b - \theta_x) \Big) \tag{2.1.10}$$

These are the standard power flow equations, which can be used to fully define power flow in a network using two complex variables $\{S_b, V_b\}$ or four real variables $\{P_b, Q_b, |V_b|, \theta_b\}$ at each bus. This is critical in maintaining suitable network operation. Voltage $|V_b|$ must be kept within statutory limits for correct operation of connected devices and machines. Power factor $\cos\theta_b$ at each node must be kept close to 1 to minimise reactive power flow. The maximum real and reactive power transferred over any one link is constrained by the current carrying capacity of the connecting cable. Thus an optimisation problem may be formulated to determine the optimum balance of generation and consumption within a network of buses for a given performance indicator, e.g. such that the cost of generation and line loss is minimised, while each bus in the network is kept within its predefined constraints. This commonly takes the form

$$\min_{\substack{P_b,Q_b,|V_b|,\theta_b \\ \forall\ b=[1,B]}} \quad f\Big(P_b, Q_b, |V_b|, \theta_b\Big) \tag{2.1.11a}$$

$$\text{s. t.} \quad P_b^{\min} \leq P_b \leq P_b^{\max}, \tag{2.1.11b}$$

$$Q_b^{\min} \leq Q_b \leq Q_b^{\max}, \tag{2.1.11c}$$

$$|V_b|^{\min} < |V_b| < |V_b|^{\max}, \tag{2.1.11d}$$

$$|S_{bx}| \leq |S_{bx}|^{\max} \quad \forall\ x = 1, ..., B \tag{2.1.11e}$$

Where $f\Big(\overrightarrow{\mathrm{x}}\Big)$ is some cost function of the variable set $\overrightarrow{\mathrm{x}} = [P_b, Q_b, |V_b|, \theta_b]^{\mathrm{T}}$, and S_{bx} is the sending end apparent power transfer along the line between b and x. The solution to this problem allows for optimal balance of demand and supply.

However, in practice, several problems arise. The expected difficulty in solving an optimisation problem such as (2.1.11) depends on the underlying characteristics of the objective function $f(\overrightarrow{\mathrm{x}})$ and the feasible set (2.1.11b)-(2.1.11e). Specifically, both the objective function and feasible set must be convex, else solving the problem is NP-hard [12], [13]. Nonlinear equality constraints such as (2.1.11b) and (2.1.11c) (incl. (2.1.9) and (2.1.10)) do not meet the definition of convexity [14]. Therefore, the solution involves significant computational intensity that rapidly become intractable for networks with a large number of buses. How best to apply assumptions, simplifications and relaxations to this non-convex feasible set, while still maintaining acceptable optimality, forms an ongoing point of research, extensively covered in [15]. Standard relaxations differ for the transmission and distribution environment, and will be briefly summarised in turn.

Transmission Network

Transmission Networks are characterised by high voltages and long thick cables, normally forming a mesh-type network topology as in Fig. 2.4. This leads to three traditional approximations:

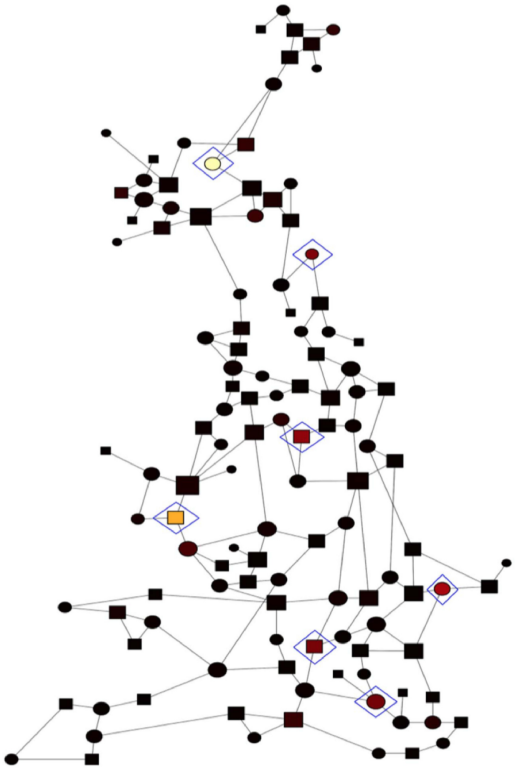

Figure 2.4: The UK transmission network [16]. Circular nodes denote net generators, square nodes denote net consumers.

1. The resistance of transmission cables is significantly less than the reactance, and therefore negligible

$$\Gamma_{bx} \approx 0 \quad \forall\, b, x \tag{2.1.12}$$

2. The difference in phase angle between two connected buses is small

$$\sin(\theta_b - \theta_x) \approx \theta_b - \theta_x, \quad \cos(\theta_b - \theta_x) \approx 1 \qquad \forall\, b, x \tag{2.1.13}$$

3. The difference in voltage magnitudes between connected buses is small

$$|V_b| \approx 1\text{p.u.} \quad \forall\, b \tag{2.1.14}$$

This leads to the standard direct current (DC) power flow equations

$$P_b = \sum_{x=1}^{B} \mathrm{B}_{bx}(\theta_b - \theta_x) \tag{2.1.15}$$

$$Q_b = \sum_{x=1}^{B} \mathrm{B}_{bx}(|V_b| - |V_x|) \approx 0 \tag{2.1.16}$$

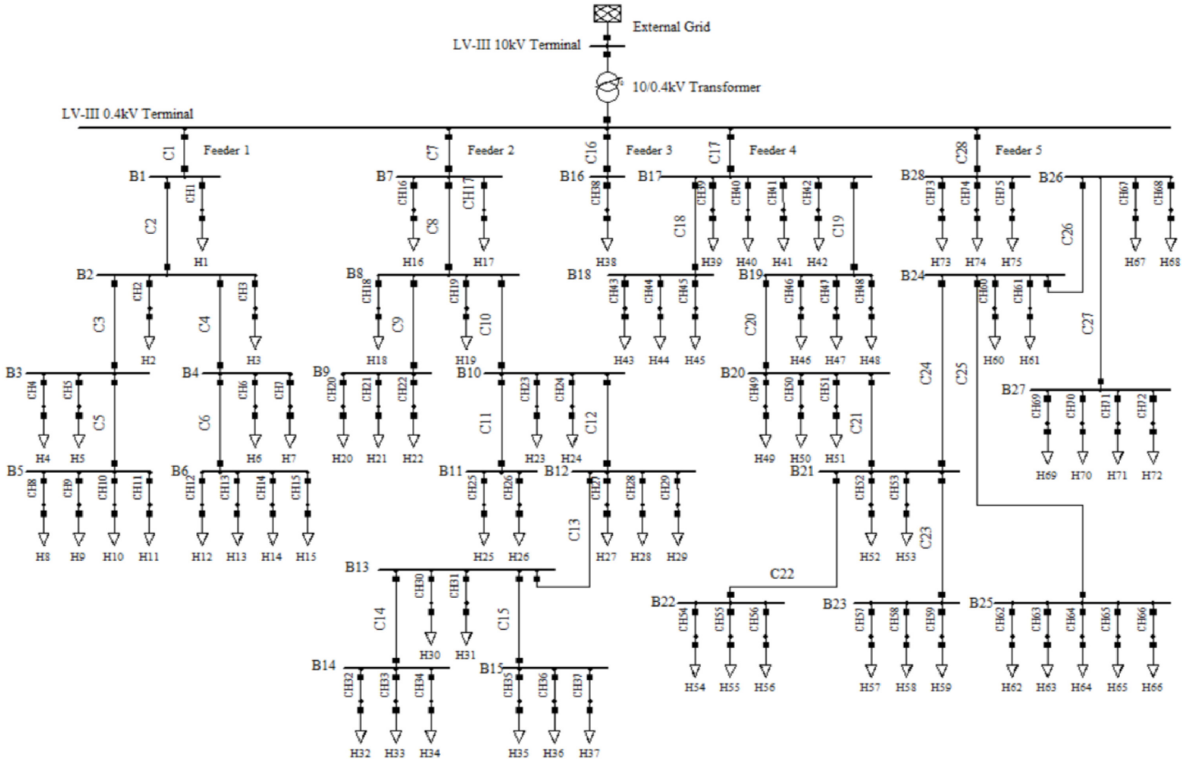

Figure 2.5: A danish residential distribution network, from [18].

Where bus voltage difference and reactive power flow between nodes are ignored. Note that B_{bx} refers to the susceptance between buses b and x, and B refers to number of buses. More accurate relations that do not ignore voltage and reactive power are achieved in [17] using approximations with first order Taylor series and linear planes to approximate quadratic and trigonometric terms, respectively, in (2.1.9) and (2.1.10).

Distribution Network

The traditional approximations made for Transmission networks do not apply at the Distribution level. Distribution networks have characteristically lower voltages, thus resistance and voltage drops between buses are non-negligible. They also typically have radial/hierarchical topology, as in Fig. 2.5, so these voltage effects, as well as phase angle differences, may be compounded over the length of the feeder. This means the assumptions typically made to simplify power flow in the transmission network cannot be made for distribution.

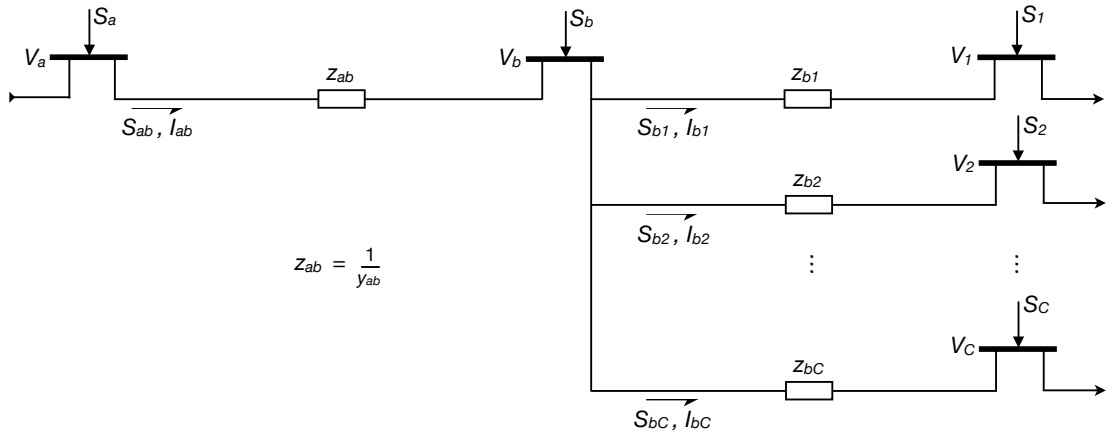

Figure 2.6: Equivalent Branch Flow Model

To better accommodate this radial topology, the Bus Injection Model from (2.1.5)-(2.1.8) may be reformulated as the equivalent Branch Flow Model, shown Fig. 2.6. This takes a recursive structure for each node along a chain of buses extending from the feeder input. Along this chain, denoting any bus a that is parent of bus b, which in turn has child nodes $c = 1, ..., C$, power flow may be defined

$$\sum_{c=1}^{C} S_{bc} = S_{ab} - z_{ab}|I_{ab}|^2 + S_b \tag{2.1.17}$$

$$I_{bc} = y_{bc}(V_b - V_c) \tag{2.1.18}$$

$$S_{bc} = V_b I_{bc}^* \tag{2.1.19}$$

These are commonly re-expressed by Baran & Wu's DistFlow equations [19], [20]

$$\sum_{c=1}^{C} S_{bc} = S_{ab} - z_{ab}|I_{ab}|^2 + S_b \tag{2.1.20}$$

$$|V_b|^2 - |V_c|^2 = 2\mathrm{Re}\left(z_{bc}^* S_{bc}\right) - |z_{bc}|^2 |I_{bc}|^2 \tag{2.1.21}$$

$$|V_b|^2 |I_{bc}|^2 = |S_{bc}|^2 \tag{2.1.22}$$

Performing this calculation first recursively along a branch and then consecutively along parallel branches permits full definition for complex variables $\{S_b, V_b\}$, in the same manner as the Bus Injection Model in (2.1.5)-(2.1.8). Since the two models are equivalent, the optimisation problem in (2.1.11) is unchanged and the feasible set remains non-convex. A way to simplify this problem is to neglect nonlinear power losses $z_{ab}|I_{ab}|^2$. This results in linear optimisation constraints, allowing for a

conservative estimation of voltage drop. More accurate (and more computationally intensive) estimations can be achieved using second-order cone relaxations to convert the power balance equations into convex quadratic inequalities, and semi-definite relaxations for matrix inequality constraints [15].

2.1.2 Traditional Control in the Power Network

The traditional power network is designed to transfer unidirectional output from municipal bulk synchronous generators to residential and industrial consumers. The aggregated power demand is generally predictable, and satisfactory balance is maintained from suitable contingency arrangement, dispatch forecasting and primary, secondary and tertiary control mechanisms.

National power networks are commonly designed with '$N-1$ contingency'. This means that grid operators ensure the network can continue to operate successfully if any one of the bulk generators in the grid fail. This involves maintaining suitable spinning reserve at power stations and careful forethought in the transmission network mesh topology so that lines are not overloaded.

Meanwhile, day-to-day balance is maintained by economic dispatch. Many economic models exist, but generally suppliers and distributors conduct transactions based on day-ahead price forecasting. Distribution networks are governed by a Distribution System Operator (DSO), who predicts tomorrow's net demand profile and bids for the required power to the Transmission System Operator (TSO). This operator compiles all the bids according to a certain cost minimisation function and dispatches tomorrow's generation profile to individual power stations.

Most load forecasting models can predict daily load profile within an accuracy of 95% [22]. The remaining 5% is corrected via frequency control mechanisms. An imbalance of load and generation will alter the AC frequency of transmitted electricity. Power stations are fitted with automatic turbine governors which will increase/decrease power output in order to restore balance in the system in a process

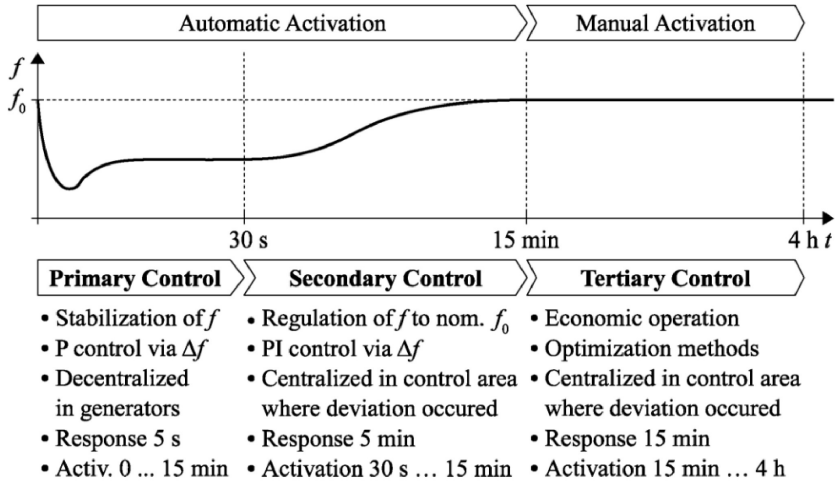

Figure 2.7: Frequency trace following a sudden increase in power demand [21]

called primary frequency control. The system operator then instructs power stations to further increase/decrease generation in order to restore the nominal grid frequency (50Hz in the UK). This is known as secondary frequency control, and may be conducted manually or automatically via an algorithm. Critically, transmission lines must not be loaded beyond their capacity limits. Tertiary control is then implemented for restoring economic operation. This is illustrated in Fig. 2.7 [21]. The statutory limit of mains frequency deviation in the UK is ±0.5Hz, and voltage deviation 0.96-1.1p.u (in Europe 0.9-1.1p.u.). In the event that these limits are exceeded, e.g. following a large unplanned disturbance, measures such as mandatory load shedding are implemented to ensure the generators are not loaded beyond their spinning reserve and continue to operate within their limits.

The significant practical differences between the transmission and distribution network in operating voltage, network topology and managing entity mean there is a natural separation between the two systems. The TSO maintains acceptable conditions in the transmission network (e.g. using the Bus Injection Model (2.1.7)-(2.1.8)), while the DSO maintains the distribution network (e.g. with Branch Flow (2.1.17)-(2.1.19)). The TSO sees only bulk changes in aggregated power demand taken from the step-down transformer at input to each distribution feeder, and the DSO sees only bulk changes in transmission frequency and supply voltage. Thus the

intricacies of one operator are normally invisible to the other.

This traditional form of power control is entirely satisfactory for the purpose for which it was designed - unidirectional power transfer with only small deviations from forecasted demand. Stability over the adjustment period of seconds to minutes is generally not problematic due to large spinning inertia maintained in the power plants themselves, as well as induction motor demand spread throughout the network particularly in industrial consumers. This spinning inertia determines the initial slope of frequency deviation following a disturbance, and is deliberately kept substantial so as to permit adequate response time. However, the next section will show how emerging power applications (such as DG and EV charging) lead to question this traditional control paradigm.

2.1.3 Limitations of Traditional Power Control

In the transmission network, rise in renewable generation can lead to instability. Renewable generation fluctuates rapidly with weather conditions, leading to sudden changes in net demand profile that cannot be precisely forecasted. This leads to more significant frequency and voltage deviations following a distrubance. Further, renewable power plants generally have small or no spinning inertia. The increasing share of renewable generation in network-wide power production means the potency of maintained spinning inertia is effectively reduced, shortening the critical response time for outage to be prevented.

In the distribution network, problems associated with excessive renewable generation have been documented in numerous studies [4], [23]–[27]. Significantly, they include rapid voltage fluctuations, overvoltage, reverse power flow, localised power congestions and increased line losses. These are compounded by rising numbers of EVs, which bring large increase in peak loading patterns.

Rapid Voltage Fluctuations

Voltage control in the distribution network is traditionally achieved using on-line tap changers and reactive power compensation. Under high DG penetrations, the effectiveness of this regulation is reduced, as rapid fluctuations in availability can lead to sudden surges in real and reactive power flow. For example, under partial cloud cover PV generators have been reported to drop from 100% to 30% in 5-10 seconds [25], [28]. Tap changers, voltage regulators and voltage controlled capacitor banks all have typical delays of 30-90 seconds [29], therefore voltage spikes and slumps of a minute or longer may occur before a control can be effectively applied.

This problem is compounded by high penetrations of EVs. An EV can consume more kWh in a single charge than the average household in one day. Synchronised charging patterns, e.g. when numerous owners return home from work, mean charging load varies significantly with time of day and is non-correlated with renewable supply. The combined stochastic mismatch between spikes and slumps in supply and demand mean the system must contend with increasingly volatile inputs. Over- or undervoltage conditions outside acceptable limits disrupt power quality for the end user, and at extremes may trigger passive protection elements that lead to shedding and outage which may take hours to reconnect.

Overvoltage

Overvoltage is particularly significant when large DG is located at the end of long and lightly loaded feeders. When generation at a bus is greater than the load, the surplus power is injected back into the network. When this occurs at the end of a long feeder, the impedance of the line can be remarkably high, leading to sharp voltage rise [4]. A case study of this phenomenon is provided in [30]. Commonly, this necessitates control action such as curtailment at the power source, which can incur significant economic cost [26].

Reverse Power Flow

Under high DG penetrations, if generation exceeds total network load, power flow direction is reversed and the feeder starts exporting power to neighbouring feeders or to the transmission system. Distribution infrastructure is traditionally designed for unidirectional power flow and no DG. Reverse power flow is not traditionally accounted for in overcurrent and voltage regulation equipment, and may trigger passive protection devices, interrupt grid service quality, and/or overload transformers and equipment [27].

Localised Power Congestion

The distribution network's radial topology means that localised power congestions can appear in individual branches. The location of DG must therefore be tightly controlled to verify that the feeder sections between DG plants and substation have enough capacity to distribute the power under peak conditions.

This issue is also compounded by high penetrations of EVs. The mobile nature of EVs means that spikes in consumption may vary geographically as well as temporally following day-to-day mass migrations, e.g. arrival at a football match or into/out of city centres. This means that load can suddenly spike in a specific chain of the distribution feeder. Surges in real and reactive power flow occur in a more stochastic and volatile manner, complicating stable operation.

Increases Line Losses

For low to moderate DG penetrations, line losses tend to decrease to a minimum as power is transported across shorter distances. However, for high penetrations, losses tend to increase. First, localised power congestions can lead to greater loading conditions than anticipated for normal operation, leading to greater losses in the connected equipment. Second, losses are incurred by fluctuations in reactive power flow, resulting from frequent on-off switching of voltage-controlled capacitor banks as well as frequent operation of tap changers and line voltage regulators. This can also

lead to greater reactive power supplied from the transmission system, which incurs significant additional losses [23]. Finally, overall bus voltage increase as a result of DG increases no-load losses of distribution transformers [29]. All these factors have important economic impacts that offset expected gains from DG.

2.1.4 Towards 'Smarter' Systems

Future energy requirements point towards a more volatile power profile that is less geographically correlated throughout the network. Power requirements are increasing due to rise in and concentration of human population. Further, the diversity of generator and consumer types is rising as a result of various social, environmental and economic pressures. Traditional assumptions for grid control are no longer viable, and power disruptions can no longer be compensated by shortsighted traditional techniques.

Smart Grid solutions aim to harness the communication layer that is increasingly implemented at all levels in the power network. By appropriate deployment of sensors, actuators and underpinning ICT, control units can gain advantage over traditional grid control paradigms by operating in a coordinated and decentralised manner. How best to design coordination algorithms in this way forms the unifying objective of Smart Grid research.

2.2 Literature Survey

Sec. 2.1 described physical and practical operation of the traditional power system along with its shortcomings with respect to emerging power requirements. This section surveys selected Smart Grid solutions relevant to contributions of this thesis.

2.2.1 Communications for a Smarter Grid

Traditional control of power flow operates on a short-sighted, reactionary basis, where deviations from forecasted demand are first detected and then corrected normally within a matter of minutes. Emerging power requirements begin to question this response time. Advantage can be gained from using permeated sensors to trigger coordinated control actions with wider reach and finer granularity in the nearby infrastructure. With more numerous and pervasive sensors and actuators, more targeted and precise power flow decisions can be achieved to enhance relevant KPIs.

Sensors and actuators must be connected in a bidirectional ICT network. Given the ubiquitous nature of the grid and the demand for numerous and pervasive sensors and actuators, architectural design of this ICT network is of key significance. Architectures can generally be characterised into four types based on their underlying topology: Centralised, Distributed, Decentralised and Independent.

Centralised Control

The simplest and most common solution involves a central control unit connected to all sensors and actuators in the system. This maintains complete control over all actuating entities, ensures full visibility since all sensor readings are gathered to the same centre, and allows all actuating devices to have simple act-on-command interfaces, which reduces overall complexity and cost. However, this comes at the cost of optimisation complexity, traffic load on the ICT network, and system vulnerability [14].

Under centralised architecture, finer control granularity means the central unit must monitor increasingly comprehensive intricacies of all buses in the network as well as their interconnections. A fast response to disturbance requires that these intricacies be monitored frequently, so that the operator is aware of every change in the network. As the number of connected devices grows, the complexity of optimisation increases and greater computation resources are required to manage

it. Computing hardware is significant to system cost. As granularity of control increases, e.g. to many thousands of nodes at each distribution bus, there is concern that the power network is too vast and complex to be optimally micromanaged from a single controlling entity under practical deployment budgets [14].

Further, as the number of connected devices grows, so does traffic load on the underpinning ICT system. Under a purely centralised network, N_S sensors and N_A actuators require $N_S + N_A$ dedicated links with the central controller every coordination interval. For thousands of nodes or more, the overhead required can add significant traffic requirements. The power network does not traditionally rely on latency-critical data systems, so the necessary addition of ICT hardware is a significant cost constraint.

A centralised architecture also means there is only one point of failure in the system. If the central controller cannot operate successfully, the whole system is undermined. If communication links between controller and actuators are disrupted or intercepted, this may significantly affect localised stability. The additional encryption layers necessary to guard against cyber-attack increase both communication and processing overheads, further adding to system cost.

As the number of end devices grows in the system, these concerns are driving architectural developments that alleviate burden on the central controller. Key considerations include how to design signals that laconically express essential information about local/general operating conditions, how to structure the communications topology so these signals are efficiently exchanged, and how to process these signals to make tangible real-time actuations.

Distributed Control

In Distributed architectures, decisions are made locally at actuating devices, however, these decisions depend on external signals broadcast periodically from a central controller. The broadcasted signals capture global system trends based on aggregated

sensor data. Centralised computation load is alleviated since actuators compute signals independently, and the ICT system is simplified since outward communication is broadcast common to all nodes in the network. Two approaches are possible, based on Dual Decomposition [31] and Population Game Theory [14], [32], [33].

In Dual Decomposition, every actuating node b has its own cost function $f_b\left(\overrightarrow{x_b}\right)$ and its own constraints, particularly regarding net power injection S_b. The optimisation problem in (2.1.11) can then be redefined at each individual node

$$\min_{\overrightarrow{x}_b} \quad \sum_{b=1}^{B} f_b\left(\overrightarrow{x_b}\right) \tag{2.2.1a}$$

$$\text{s. t.} \quad \sum_{b=1}^{B} S_b = 0, \tag{2.2.1b}$$

$$S_{b\min} \leq S_b \leq S_{b\max} \tag{2.2.1c}$$

where $\overrightarrow{x_b}$ is the vector set of optimisation variables relevant to bus b. The only global constraint is the network-wide balance in supply and demand. A signal summarising this balance is broadcast to all nodes every time period. Based on this signal, each node solves its local optimisation problem via convex optimisation techniques and iteratively compensates for global mismatch via e.g. the water-filling method. Before the next iterative actuation is implemented, each node first evaluates whether it will violate local capacity limits. This method is shown to converge mathematically to global optimum at a rate proportional to the number of nodes [31].

Dual Decomposition assumes optimisation over a continuous domain, whereas flexible loads tend to operate at discrete power levels. Introducing nonlinear constraints to represent these discrete power levels renders this problem non-convex and computationally impractical. A solution is to apply population game theory by transforming the problem into a game consisting of thousands of players each with a discrete strategy set [32], [33]. The aim of each node in its strategy decision is to reduce the global system cost function ($f\left(\overrightarrow{\mathrm{x}}\right)$ in (2.1.11)), thus each strategy revision should incrementally reduce overall system cost, where the Nash equilibrium corresponds to the global optimum. The central controller senses the current

strategy distribution, and broadcasts the gradient of the optimisation cost function with respect to each strategy. This is then used by the actuating nodes to decide on strategy revision for the next iteration. This method has shown fast convergence in simulation compared to dual decomposition, however requires a more complex communication framework.

Distributed architectures are a promising solution to the problems of centralised control for large network sizes. However, they solve only half of ICT issue, since N_S dedicated links are still required between sensors and central controller. The requirement of reliable communication from the central controller also adds vulnerability to cyber attack. Decentralised control offers solution to these issues.

Decentralised Control

Decentralised architecture involves no central controller. Instead, nodes iteratively exchange signals with their neighbouring nodes in order to make local decisions. Like distributed algorithms, the problem of concentrated computation is resolved, and traffic load in the ICT network is reduced since control messages are distributed throughout the network instead of concentrating to a single central point. Further, anomalies of any malfunctioning device can be inferred in neighbouring nodes via signal exchanges, where actuation can be modified to isolate these nodes and maintain normal operation - i.e. this framework is resistant to malfunction and attack.

Consensus methods [34] can be used to coordinate decentralised devices for grid monitoring, power balance and preventative actuation. Here, actuation devices repeatedly exchange information with one another to gain an agreement on the global state of the network, e.g. “total demand is equal to total supply”. Based on its local sensor information and incoming messages from neighbouring nodes, each node will have an opinion about the operating state of the network (e.g. congested, stressed, healthy, etc.). This opinion is exchanged repeatedly among immediate neighbours, and an equilibrium is eventually reached. The consensus can then be used similarly

to a broadcasted signal in distributed methods. With appropriate configuration, treatment of a strong anomalous opinion base among colocated nodes can be used to detect localised congestions e.g. within a radial branch of the distribution network, allowing local actuators to respond to local disturbances. A survey of use of complex network theory to model emerging smart grid control applications in more elaborate grid topologies is provided in [35].

Independent Control

In an independent architecture, control decisions are made fully independently. There is no information exchange between actuating nodes, and only locally available information is used (e.g. bus voltage, frequency, power flow between adjacent nodes, etc.). This is already implemented for primary frequency control in traditional power systems, so is not without precedent.

Primal-dual dynamics [36] and machine learning [37], [38] have been used to incorporate additional variables to this control paradigm. With no dependence on an ICT system, independent control requires minimal processing time and investment, and makes cyber-attacks impossible. However, there is no guarantee of convergence to optimality without information on the global system state. Uncoordinated deployment of control processes without regard for optimality can lead to unexpected harmonics in the system. For example, if all flexible loads are programmed to trigger upon detection of a localised overvoltage, the connection of all loads simultaneously may overcompensate the system, leading to oscillations which are hard to predict. Thus, independent control is apt for processes where response time is critical, however will not guarantee cost-efficient steady-state operations. To incorporate convergence to an optimum steady-state solution, communication between nodes is required.

Transition Towards Decentralisation

There is a natural progression of 'decentralisation' evident in the literature on Smart Grid control. However, distributed and decentralised architectures currently only exist in theory and simulation. Moreover, decentralisation is a formidable step, involving at the very least significant installation and reprogramming of new and existing smart devices. This implies significant capital investment. Further, grid services cannot be interrupted during transition, and once implemented the system cannot be easily overhauled. This impediment has limited decentralised implementations so far.

As a result, alterations that serve to 'decentralise' computation and traffic load in a centralised architecture without radical infrastructural overhaul are highly valuable. An example is use of a hierarchical ICT topology, as proposed in the authors previous work in [39]. This makes use of an aggregator in a three-tier framework to alleviate traffic burden in a centralised network of smart devices, and studies design tradeoffs between latency and investment in mid-layer hardware. A natural progression is to offload key decision-making processes to the mid-tier aggregators, thus alleviate centralised computation load. These two steps form key contributions of this thesis.

2.2.2 Smart Loading for the Smarter Grid

How best to match supply with demand forms the fundamental question of Smart Grid control. This problem can be approached from different sides - supply or demand. In traditional 'supply-side' management, power system operators seek to predict required demand profile and then match it with corresponding generation. However, emerging power applications make this approach harder to render. Sophisticated machine learning methods for demand forecasting have been studied, surveyed in [40]. Similarly, a survey on uncertainty quantification in economic dispatch for renewable energy sources is provided in [41].

The traditional 'supply-side' approach will not be made obsolete. However, this

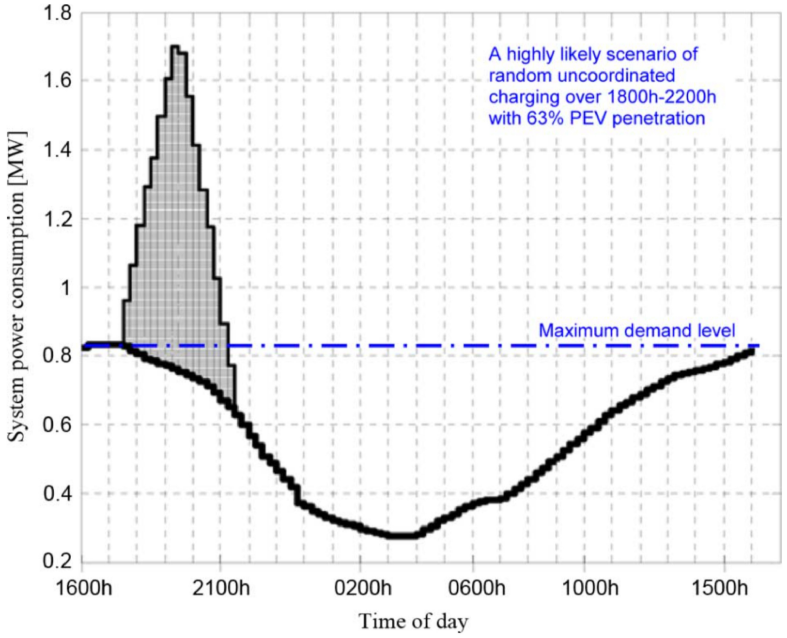

Figure 2.8: A prediction for random uncoordinated EV charging from [44]

problem may also be approached from 'load-side'. Consumer power demand may be categorised as Fixed or Flexible. Fixed loads (e.g. lights, television, kettle) have a specific power requirement that must be provided exactly and on-demand. Flexible loads (e.g. EVs) have a discretionary power requirement, i.e. it does not matter exactly when vehicle charging takes place so long as the battery is charged when the consumer requires it. Thus it is possible, within certain timing constraints, to compensate for spikes in supply and demand by adjusting flexible loads. This process known is as Smart Loading. An overview of novel and traditional Smart Loading strategies is provided in [42]. Meanwhile [43] reviews potential synergies between EV charging and DG.

Smart Electric Vehicle (EV) Charging

Smart loading solutions follow concerns on the effects of high EV penetration on daily household demand profile. Typical daily household energy consumption in the UK ranges from 5-20 kWh [5], while typical EV battery capacity ranges from 20-100 kWh [6]–[9]. Owning an EV will represent huge increase in household energy consumption. Further, a plausible scenario is that numerous EV owners will return

home from work in the early evening, during a time of already peak demand, and immediately plug in their vehicles. Predictions of the effects random uncoordinated charging may have on the power network range from significant to disastrous, as shown in Fig. 2.8 from [44].

Optimal Smart Charging can be sought from two objectives - from the perspective of the consumer/generator, or from that of the network operator.

Consumers and DG Investors: For users and producers of grid power, the objective is to maximise power transfer when it is cheap - cheap to use, or cheap to produce. This occurs, for example, during non-peak times or when renewable generation is strong. How to cost-efficiently coordinate such a system forms a large part of Smart Charging studies. A control strategy using dynamic pricing in the distribution network is presented in [45] which achieves symbiotic interaction between EVs and distributed generation. An EV charging scheme using online maximum sensitivities selection combined with distributed wind power and real-time pricing is provided in [46].

Network Operator: For the network provider, Smart Charging can be used to flatten peak loads. For example, instead of charging EVs in the early when most people return home from work, charge them overnight when consumer demand is low. A flatter power profile allows for smaller and more predictable disturbances to the system, and key outputs can be more effectively controlled. Power equipment, which is sized according to peak load, need not be supplemented to accommodate a large rise in peak demand. Equipment can be operated closer to its limits and power transfer efficiency more effectively optimised. All this can significantly reduce operating costs, which can eventually translate to cheaper energy prices for consumers. How to coordinate this forms a second large part of research. A short-term load-forecasting algorithm based on artificial neural networks and statistical load curves is presented in [47], where photovoltaic input and battery energy storage is shown to achieve

significant peak shaving. A fuzzy logic based strategy for a residential distribution system is demonstrated in [22] to ensure bus voltage magnitude is kept within allowable operating limits. This achieves satisfactory daily voltage profile without need for detailed system modelling or optimisation. A fast-converging scheme is presented in [48] incorporating intrinsic randomness of arrival time, departure time and charging time to minimise peak demand in the system. A coordination algorithm based on three designated charging time zone priorities is simulated for varying EV penetration in a residential distribution network in [44] to improve voltage profile. It was shown that with correct management of charge allocation, over 63% penetration of EVs could be tolerated in a distribution network with no increase in peak load, and no alterations in existing hardware.

This dichotomy of design objectives between user and operator is often ignored in Smart Charging research. An assessment of these diverging objectives is provided in [49] for increasing penetrations of distributed wind generation. It is shown that these two Smart Charging objectives do not necessarily coincide, and indeed may compete. For example, if renewable generation leads to the cheapest electricity at a time coinciding with peak demand, the triggering of price-driven flexible loads combined with the already existing peak in fixed loading may lead to unexpected surges. The consumer benefits from cheap electricity in this scheme, however the operator must implement significant additional capacity in power equipment, thus incurring losses. Any Smart Charging solution must consider these potentially competing economic objectives, and this is explicitly modelled in this thesis.

Vehicle-to-Grid

Smart Charging can be extended with the realisation that an EV battery need not only be load while connected for charging. Provided a minimum charging requirement is met, it represents significant energy storage that can give power to the grid as well as draw from it. Thus an EV becomes a ‘prosumer’ - either producer or consumer of power as required. A bidirectional charger can allow the EV to inject real or reactive

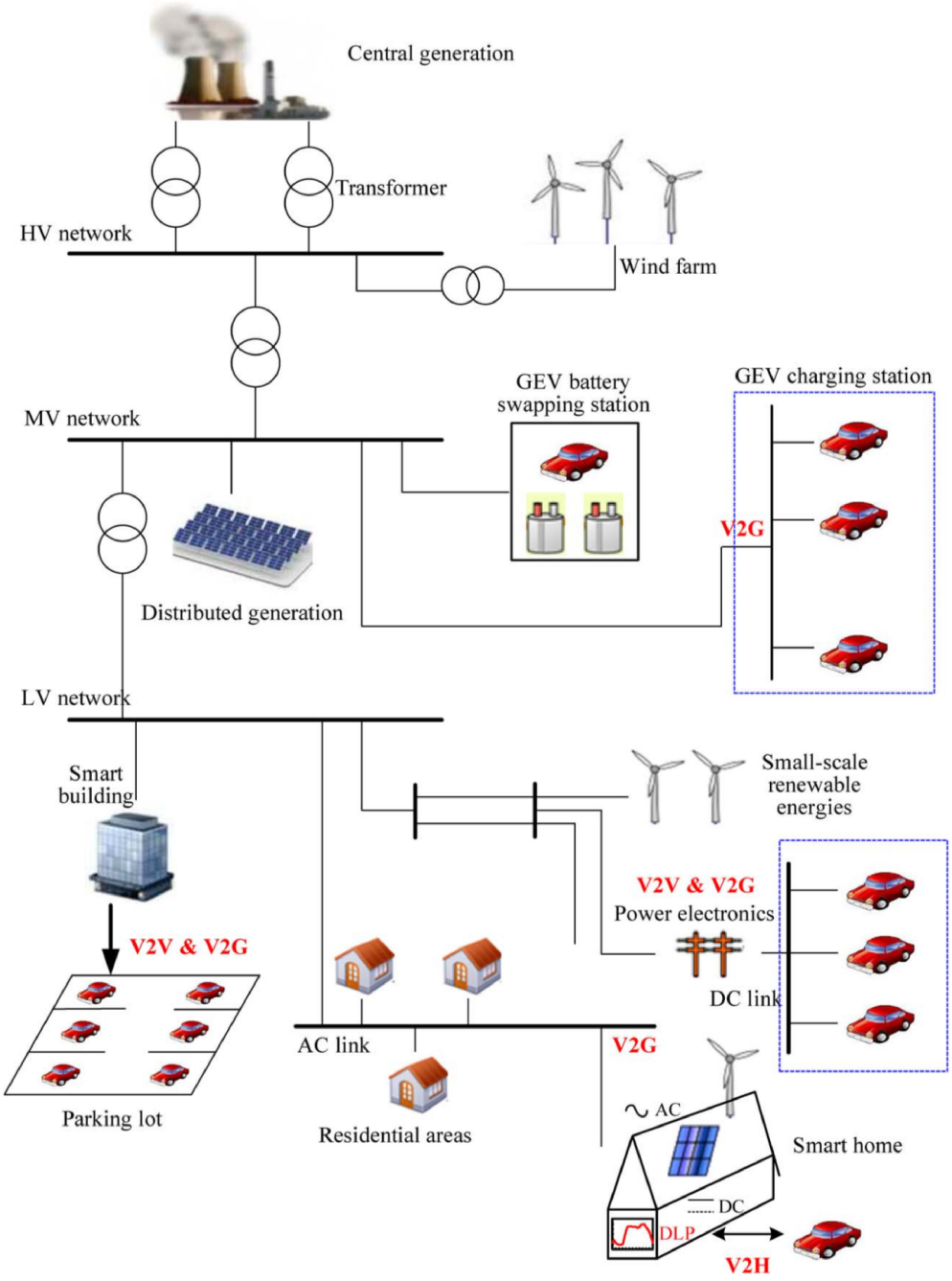

Figure 2.9: Vehicle-to-Grid (V2G) from [50]

power to achieve voltage regulation at a localised ultra-fine granularity. Groups of aggregated EVs could achieve this on a community-wide scale. Connected groups of EVs distributed throughout the network could even contribute to the overall grid. Thus, Smart Charging can be used for trough filling as well as peak shaving, further improving network-wide power profile. Further, the primary transport objective of EVs means that their availability is concentrated in comparable density to that of

the human population. This concept, known as Vehicle-to-Grid (V2G) illustrated Fig. 2.9, has compelling potential to achieve precise, colocated and decentralised actuation at fine granularity, with minor additions to existing infrastructure. It paints a pretty picture.

The feasibility of V2G is based on the assumption of large-scale EV penetration, which is only achievable on a 10-15 year horizon. In nearer terms, more contained applications such as vehicle-to-home (V2H), vehicle-to-building (V2B), or vehicle-to-community (V2C) have been proposed. A survey of V2G methods in escalating size and network-significance is provided in [50].

This is a hot topic in Smart Grid research. Experimental results for a prototype on-board EV battery charger is presented in [51] for several bidirectional operation modes (V2G, V2H and Vehicle-for-Home (V4H)). Outage management for V2B applications is discussed in [52]. A V2G control algorithm for peak shaving/valley filling using target curves is developed in [53], taking into account vehicle requirements, load demands, and significant system constraints. It is shown that V2G can be more economical, more effective and faster when compared to other peak shaving/valley-filling methods. An autonomous V2G control scheme is proposed in [54], providing distributed spinning reserve for unexpected intermittency of renewable energy sources. A droop control based approach is employed based on frequency deviation at the plug-in terminal, and a fast and synchronised response is demonstrated. A comparable design concept is used in [21], where droop control is combined with hierarchical model predictive control at an EV charging aggregator to cope with temporal and spatial EV variability. A home energy management system for a distributed small-scale V2H and V2G operation combined with renewable generation and two-way energy trading is presented in [55]. Electricity bill reduction based on various comparative case studies is demonstrated. Finally, by way of practical accomplishment, the Johan Cruyff Football Arena in Amsterdam recently implemented bidirectional charging stations combined with 148 Nissan Leaf batteries and a 1MW photovoltaic system, allowing fans to contribute to the power

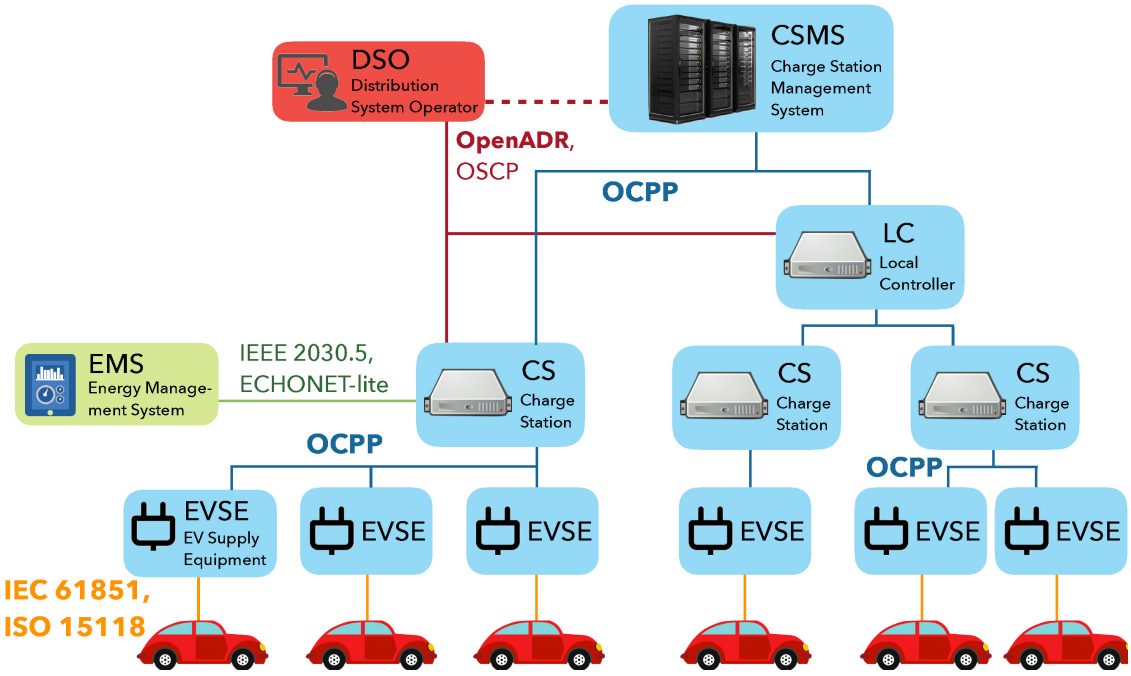

Figure 2.10: OCPP centralised topology, interoperable with a number of other energy management standards

consumption of the stadium while they are watching the game [56].

As with Smart Charging models, V2G systems may be designed with various objectives in mind, e.g. PAPR, loss minimisation, cost/efficiency/emission optimisation, peak shaving, power compensation, etc. The issue of diverging priorities between prosumer and operator is again significant. Practical concerns are also prevalent. Not all EVs support bidirectional charging, and the technology requires widespread availability of V2G-enabled vehicles to be effective. Further, there is concern over the effect of bidirectional charging on battery life and corresponding warranty responsibility. How to economically incentivise V2G participation among users is also unclear, since, without compensation in some way, bidirectional charging is altruistic from a user perspective. This technology is still in its infancy, however presents exciting prospects for next generation power services.

2.2.3 Open Smart Charging Standards

Smart Charging can be practically realised by a number of competing communications standards, however all assume the same hierarchical centralised topology shown

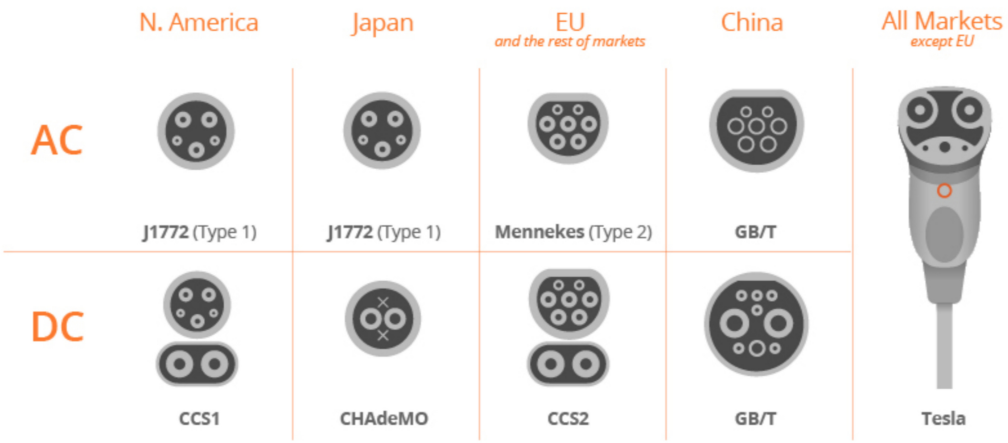

(a) EV Charging Plug Standards [59]

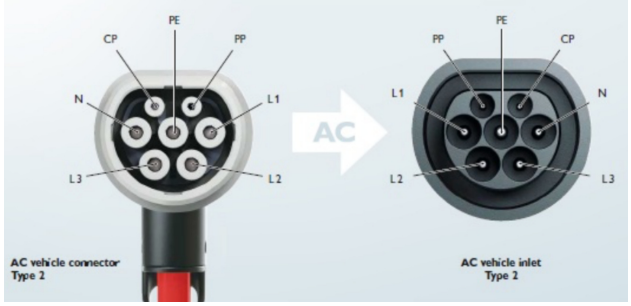

(b) Mennekes Type 2 (Three phase) [60].

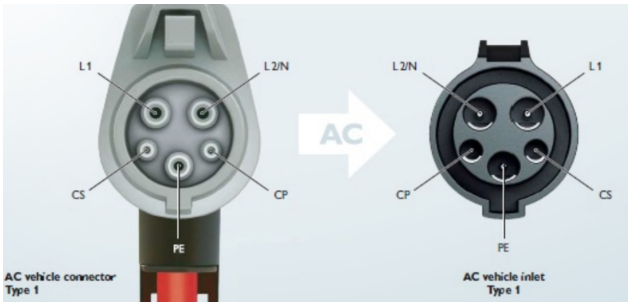

(c) J1772 Type 1 (Single Phase) [60].

Figure 2.11: EV Charging Plug Standard Pin Connections.

Fig. 2.10. The nomenclature is as follows. A central Charging Station Management System (CSMS) connects to all Charging Stations (CS) either directly or via Local Controllers (LC). CSs are responsible for managing a collection of geographically colocated charging points or EV Supply Equipments (EVSE). There can only be one EV charging at an EVSE at any one time. LCs are an optional extra tier, responsible for managing a collection of CSs.

Power transfer between EV and EVSE is covered by IEC 61851 [57] and ISO 15118 [58] standards. However, Smart Charging for grid optimisation requires control of power transfer over a network-wide scale. This is possible by virtue of several bespoke communications standards, the two most prominent of which are Open Charge Point Protocol (OCPPv2.0) and Open Automated Demand Response (OpenADR 2.0b, now IEC 62746-10-1).

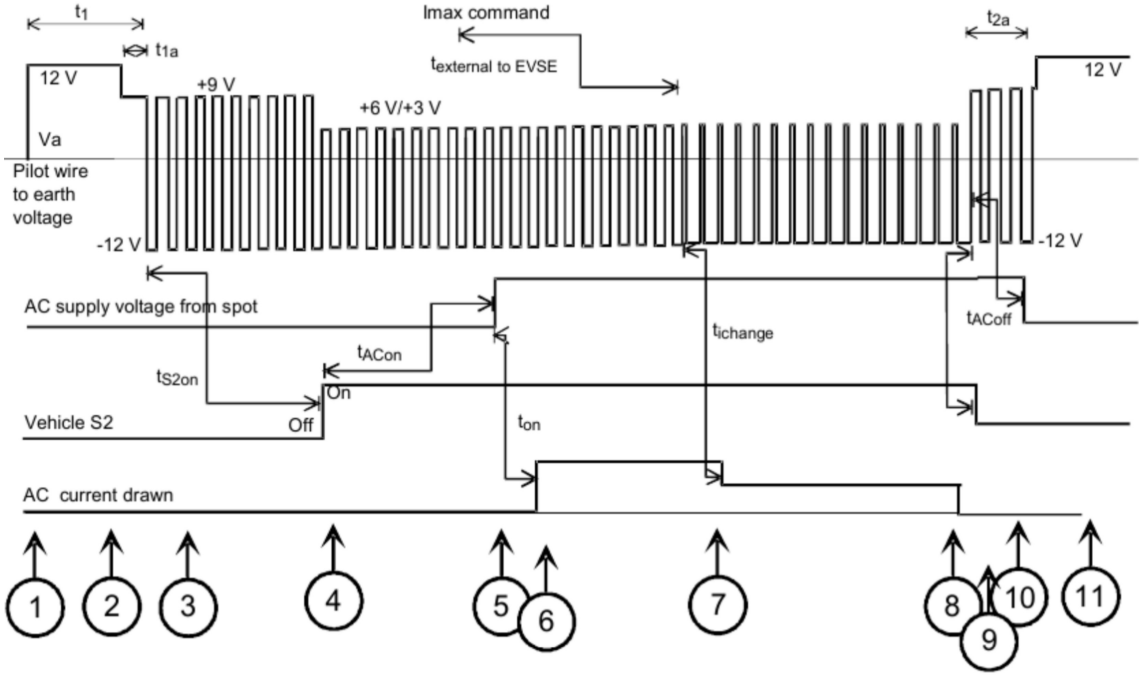

Figure 2.12: Charging Power Negotiation between EVSE and EV on the CP pin in IEC 61851 [57]

IEC 61851

When an EV arrives at a charging point, the EV and EVSE must arrange between them the correct power to charge with. This is achieved with IEC 61851.

There are a variety of EV plug standards dependent on geographical region and manufacturer of EV, however they share typical pin connections as shown Fig. 2.11. L1-3 are the AC power pins, N is neutral, PE is protective earth, PP is proximity pilot to detect when a vehicle is attached, CP is control pilot on which communications take place.

IEC 61851 uses multi-level pulse width modulation (PWM) to indicate the maximum available charging power. Voltage between 3-12V on the common CP pin indicates which stage in the charging process, and the PWM duty cycle indicates the charging power. Charging occurs in 12 steps, as shown Fig. 2.12:

1. EV is not connected and 12V open circuit supply voltage is maintained.

2. EV is connected, causing the voltage to drop to 9V across an internal resistor in the EV charging port.

3. A pilot signal begins from the EVSE, where the duty cycle indicates the maximum charging power available.

4. The EV indicates it is ready to charge by closing a switch across another internal resistor to drop the CP voltage to 6V.

5. EVSE initiates power transfer by making contact to the grid.

6. EV begins charging by making contact across its battery.

7. During charging, power can be adjusted by the EVSE by changing the duty cycle on the CP pin. The EV must respond by adjusting its charging power within 5s, else the connection is broken.

8. EV finishes charging once its desired State of Charge has been achieved.

9. EV is ready to disconnect, opens switch bringing voltage back to 9V.

10. EV disconnects, and voltage is once again 12V.

This simple protocol, available at all AC charging connections, allows either EVSE or EV to reduce the charging power if required and permits Smart Charging at any IP-connected charging point.

The need for more detailed communication between EVSE and EV has led to ISO 15118 being commonly available at charging points. Support for this is indicated by a 5% duty cycle in the IEC 61851 initialisation state. ISO 15118 [58] allows digital messages to be exchanged between EV and EVSE along the CP pin. This enables, for example, authentication, transaction and security information, desired charging profile, EV state of charge, etc. to be exchanged. The standard itself is vast, extending to a complete V2G network stack. However, security concerns and a poor (roughly 60s) update period resulting from an EV-triggered demand-response paradigm means that this standard is generally considered impractical for time-sensitive grid purposes.

L5	Application	JSON (RFC 8259)
		WebSocket (RFC 6455)
L4	Transport	TLS
		TCP (RFC 1006)
L3	Network	IPv4 (RFC 791) / IPv6 (RFC 2460)
L2	Data Link	*Not in specification*
L1	Physical	

Figure 2.13: OCPPv2.0 Protocol Stack

Open Charge Point Protocol (OCPP)

Several standards enable higher layer communication for coordinated Smart Charging between multiple non-colocated EVSEs; however, the two most prominent are Open Charge Point Protocol (OCPP) and Open Automated Demand Response (OpenADR, covered Sec. 2.2.3).

OCPP is the leading standard for EV charging station management, mainly aimed at Charge Point Operators (CPO) for transaction and billing purposes. It has a number of functions including transactions, reservation, authorisation, security, diagnostics, display messages, etc. The latest version of OCPPv2.0 now includes Smart Charging capability, and is highly interoperable with OpenADR and other energy management protocols such as OSCP, IEEE 2030.5, ECHONET-lite, etc. via its External Smart Charging function.

The specification describes message formats in the application layer using Javascript Object Notation (JSON) and WebSocket framework, with remaining layers using standard Transmission Control Protocol / Internet Protocol (TCP/IP) stack, shown Fig 2.13. The use of TCP/IP allows for any IP-connected device to be added to the Smart Charging assets.

OCPP Smart Charging occurs via power limits sent from the central CSMS to individual CSs or LCs. These power limits may be instantaneous, or may also contain a start time and duration. The CS then distributes this overall power demand between all connected vehicles, ensuring that power does not exceed this

fixed limit. Due to the low-latency requirements of authentication, transaction and billing purposes, the standard has scope for multiple prioritised charge profile specifications in seconds.

Several Smart Charging configurations are possible. A CS may be programmed to not exceed a specific power limit during certain times of day according to a certain schedule (General Smart Charging). This schedule may be overridden in real-time via message exchange from CSMS or LC (Central or Local Smart Charging). The schedule may also be overridden by external signals such as from the DSO or a home/building energy management system (External Smart Charging), and is therefore interoperable with other load management standards. In this case, OCPP only requires that the CSMS be updated if any CS is not behaving as expected.

OCPPv2.0 is rapidly becoming the go-to standard for CPOs to remotely manage a network of charging stations, meaning that as more charging points are deployed the capacity for Smart Charging will grow. However, not all CSs are managed by a CPO, and therefore have no need to be OCPPv2.0-enabled. For Smart Charging on these non-OCPP CSs, OpenADR presents a compelling solution.

Open Automated Demand-Response (OpenADR)

OpenADR [61], now standardised as IEC 62746-10-1, is a generalised demand-response message framework for uniform and interoperable signal exchange between utilities, DSOs and energy management and control systems. Unlike OCPP, it is not specific to a network of charging stations and may be extended to include demand-response services to any actuator in the system, such as generator, energy storage, flexible load, sensor aggregator, etc. Further, without the need for complex features such as transaction and billing its structure is highly simplified. This means an OpenADR-enabled Smart Device requires a significantly smaller processor than is required for OCPP.

OpenADR also has specification mainly in the application layer, describing mes-

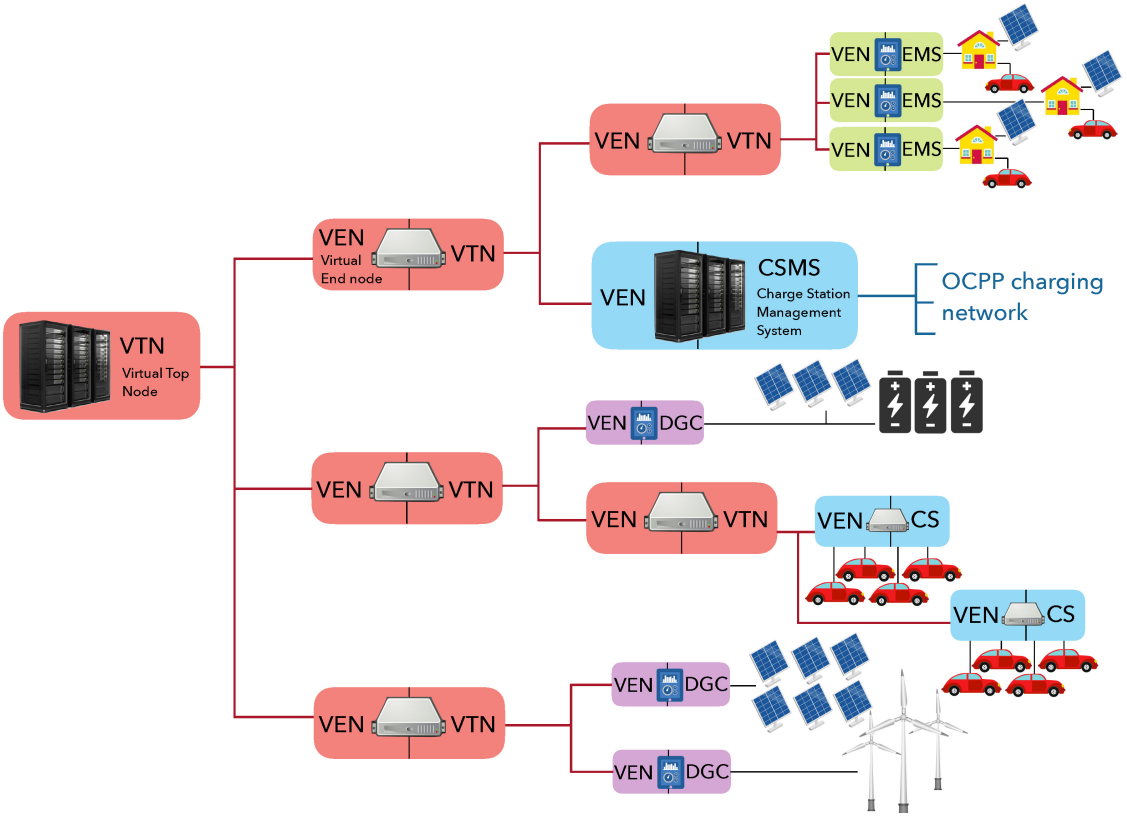

Figure 2.14: Generalised hierarchical topology of OpenADR system. (DGC = Distributed Generation Controller)

sage formats in eXtensible Markup Language (XML), supporting both Hypertext Transport Protocol (HTTP) or eXtensible Messaging and Presence Protocol (XMPP). Other layers use a standard TCP/IP network stack enabling extension to any IP-connected device.

A multi-tiered hierarchical architecture is also assumed, shown Fig. 2.14. Node hierarchy is defined in a two-way link, where a server or Virtual Top Node (VTN) communicates with its clients or Virtual End Nodes (VEN). A VEN may be any a gateway that controls one or more demand-response resources, and may control them using protocols other than OpenADR. A multi-tier hierarchy is enabled since intermediate nodes may act as both VEN and VTN.

Several communication paradigms are possible. In PULL configuration, communication is always instigated by VEN, periodically polling for new messages. In PUSH configuration, both VEN and VTN may initiate messages. Further, several profiles of OpenADR exist. OpenADR 2.0b is relevant to full-featured energy man-

agement solutions [62]. This provides four services, each with a different set of messages:

1. *EiEvent* - This is a curtailment signal sent from VTN to VEN to change power demand/supply of its resource, and contains a start time, duration and information on degree of curtailment or updated energy price. The VEN then responds with either confirmation or rejection of this event.

2. *EiReport* - This is usually sent from VEN to VTN to report energy consumption, status of resources or sensor readings. These may be 'history' reports conveying a series or data points recorded in the past, or real-time reports where an instant reading is sent either periodically or on demand. The VEN must first have all its capabilities (resources, amount of stored data, sampling frequency, etc) registered with the VTN.

3. *EiRegisterParty* - This is used to register a new VEN to a VTN.

4. *EiOpt* - Optional command structure dependent on the nature of the managed asset.

There are two configurations by which OpenADR can be combined with OCPP. First, every OCPP-enabled CS may also be registered as a VEN of the OpenADR VTN. Alternatively, the OCPP central server (CSMS) may be registered as VEN of the OpenADR VTN. On receiving EiEvent requests from the VTN, the CSMS can then aggregate power limits among participating CSs. The VTN must also receive periodic EiReport messages from the CSMS or CSs so that it is aware of the available response assets. In this way, all OCPP-connected CSs can become a demand-response asset of the grid operator in the OpenADR system.

Combined with front end standards IEC 61851 and ISO 15118, OCPP includes practical Smart Charging capability at all OCPP-enabled charging stations. OpenADR extends Smart Charging capability to non-OCPP-enabled charging points as well as combined optimisation with renewable generation controllers and other

demand-response assets. These lay the foundation for practical Smart Charging implementation. However, as described in previous sections, implementation of Smart Charging is impeded by uncertainty over clear optimisation objectives (between operator and consumer/generator), how to economically manage user inconvenience, and how to deliver required service quality under practical communications system constraints. These impediments will construct key contributions of this thesis.

2.3 Summary

The growth of renewable DG combined with the rising penetration of EVs into the automotive market is leading to growing temporally unsynchronised spikes in generation and consumption that disrupt grid service quality. Smart Grid solutions seek to harness a vast network of cyber-enabled sensors and actuators to deliver future energy services. How best to coordinate this populous network of communicating devices, and how best to optimise power delivery given strict performance and budget constraints, are open research topics. This chapter presented background and targeted literature review relevant to the contributions of this thesis.

First, two concise mathematical models were developed to describe power flow in a network of buses. Using these models, key shortcomings in traditional grid control methods were identified, and Smart Grids as an evolving solution were introduced.

Next, Smart Grid ICT architectures are reviewed. Centralised communication is the industry default, permitting full control and visibility of the network and reducing complexity of peripheral devices. However, as the number of Smart Devices grows, problems arise relating to computation load, data traffic burden and security concerns. Alternative Distributed, Decentralised and Independent control architectures to reduce or remove dependence on a central controller are discussed. As the size and granularity of Smart Grid control solutions grow, steps towards a ‘decentralised’ communications paradigm will progress.

Traditional power network control concerns how best to match generation with consumption. Under increasing renewable generation, which cannot be increased or decreased on demand like a municipal power plant, future energy services seek to match demand with supply by adjusting flexible loads. With high battery capacity and discretionary power requirement, EVs are prime candidate. Smart Charging can be optimised from the standpoint of operator or consumer/generator. For the network operator, peak shaving reduces the need to replace power hardware and improves transfer efficiency, thereby reducing operating costs. This can compete with optimal conditions for consumer/generator where cost-efficiency is maximised by using power when it is cheap, i.e. non-peak hours or when renewable generation is strong. This dichotomy of objectives is often ignored in the literature when analysing Smart Charging schemes.

By adding bidirectional charging functionality to a Smart Charging system, vehicle-to-grid (V2G) services are enabled. EVs can thereby present a distributed mobile energy storage solution delivering precise actuation that is approximately concentrated with the density of human population. This has drawn significant research attention, and stands as an exciting logical extension of Smart Charging.

While academia races ahead with V2G and decentralised control paradigms, industrial standards remain grounded. Recent open Smart Charging standards that lay the groundwork for implementation in an industrial context are summarised. Smart Charging is realisable at front-end with IEC 61851, and on a network-wide scale via OCPP and OpenADR. Both network protocols make use of a standard TCP/IP network stack enabling extension to any IP-connected device, and assume multi-tier hierarchical centralised communications architecture.

Despite the bespoke Smart Charging capability in these standards, no widespread practical implementation has been delivered to date due to certain critical research challenges, that were identified in Sec. 1.1 and 1.2. These contributions are delivered succinctly over the coming three chapters.

Chapter 3

Smart Curtailment (CUR)

The UK National Grid estimates that by 2040 all cars sold will be purely electric [3]. A typical UK household's energy consumption ranges 5-20kWh/day [5], while typical EV battery capacity ranges 20-100kWh [6]–[9]. Ownership of an EV will represent significant increase in household energy consumption. Further, synchronised driving patterns are plausible, for example numerous EV owners arriving home from work between already peak loading hours of 6-10pm and immediately charging their vehicles. All this points to ever sharper spikes in consumer power demand.

Meanwhile, various social, economic and environmental pressures concerning greenhouse gas emissions are driving a surge in renewable DG that is fed directly into the distribution network alongside consumers. In 2019, the share of renewable generation in overall electric power output reached a record high of 37% in the UK [1]. Total distributed generation rose 6%, the majority of which was due to added wind and solar power. Continuing this trend, the National Grid expects by 2030, 50% of all generation will be connected at the distribution level [2], [3].

Locally, spikes in supply and demand manifests as over- or under-voltage conditions that can trigger passive protection elements or lead to mandatory load shedding and blackouts. They can also lead to grid congestion, increased line losses, overloading of transformers, feeders and protection equipment as well as high harmonic distortion, that is invisible to the network operator and for which the network was

not necessarily designed. Growing temporally unsynchronised spikes in generation and consumption lead to question whether the traditional power grid can continue to operate within stable limits. For this reason, DSOs place capacity limits on DG penetration (a.k.a the Hosting Capacity HC), typically 15-20% of peak load [4].

Smart EV charging techniques seek to mitigate the effects of supply-demand imbalance by exploiting the discretionary power requirement of EVs: it does not matter exactly when EV charging takes place, so long as the vehicle is charged when the consumer requires. Thus it is possible, within certain timing constraints, to adjust net demand according to grid stability requirements. This can achieve flatter power profile and more predictable disturbances, meaning power equipment, which is sized according to peak load, need be minimally supplemented to accommodate this rising demand. Equipment can be operated closer to its limits and power efficiency more effectively optimised, reducing technical losses and operating costs. Not only can this translate to reduced consumer energy prices, it can also serve as buffer for potentially unstable DG input, increasing the DG capacity in the network.

In line with the scope of research identified in Sec. 1.1 and 1.2, the contributions of this chapter are as follows:

- A curtailment-based Smart Charging scheme (Smart Curtailment, CUR) is designed secondary voltage control and peak shaving in the distribution network. This can dramatically increase EV charging capacity while also delivering multiple KPIs. Under the same scheme, curtailing DG to avoid over-voltage can similarly increase DG capacity.

- A distributed hierarchical communications architecture is developed to support the Smart Curtailment scheme. This architecture jointly minimises central computation load and ICT traffic burden by offloading coordination of demand-response assets onto regional Intermediary Control Units (ICUs). It is also compatible with recent Smart Charging and Demand-Response open communications standards such as OCPP and OpenADR. In this way the scheme is

scalable and adaptable to a variety of network sizes and asset arrangements.

- Constraints of practical operational latency on KPIs is explicitly modelled and two latency-mitigation strategies are presented to balance necessary performance tradeoffs.

- The Smart Curtailment scheme is evaluated for various KPIs: Voltage Control, Peak Shaving, User Inconvenience, DG Energy Input, CO_2 Emissions and Depoloyment Cost. Key performance-cost tradeoffs are identified.

The rest of this chapter is laid out as follows. Sec. 3.1 describes the system model, defining inputs to the system, the test IEEE bus distribution network, and the underpinning communications architecture. The Smart Curtailment scheme (CUR) under zero latency is then evaluated in Sec. 3.3, and operation is described first for EV charging only, and then for combined EV and DG curtailment. Practical latency constraints are then introduced in Sec. 3.4, and two latency mitigation strategies are defined. Statistical performance of the CUR scheme is then evaluated in Sec. 3.5 for 172 days of wind power inputs and cost-performance tradeoffs for various KPIs are evaluated. Finally, Sec. 3.6 concludes the topic.

3.1 System Model

Load is first categorised as flexible or non-flexible. Non-flexible load is any power demand that cannot be delayed, i.e. must be delivered on demand. Flexible load is that for which a reasonable delay can be tolerated, e.g. EVs. Smart Charging seeks to optimise power transfer by intelligently manipulating the timing of flexible loads.

Economically, Smart Charging is possible if priority is decided by user input. 'High priority' users are treated as non-flexible load, and 'low priority' users compensated for potential charging delay with cheaper energy prices. Conceivably, many users with daytime jobs do not care if their EV is charged early evening or overnight,

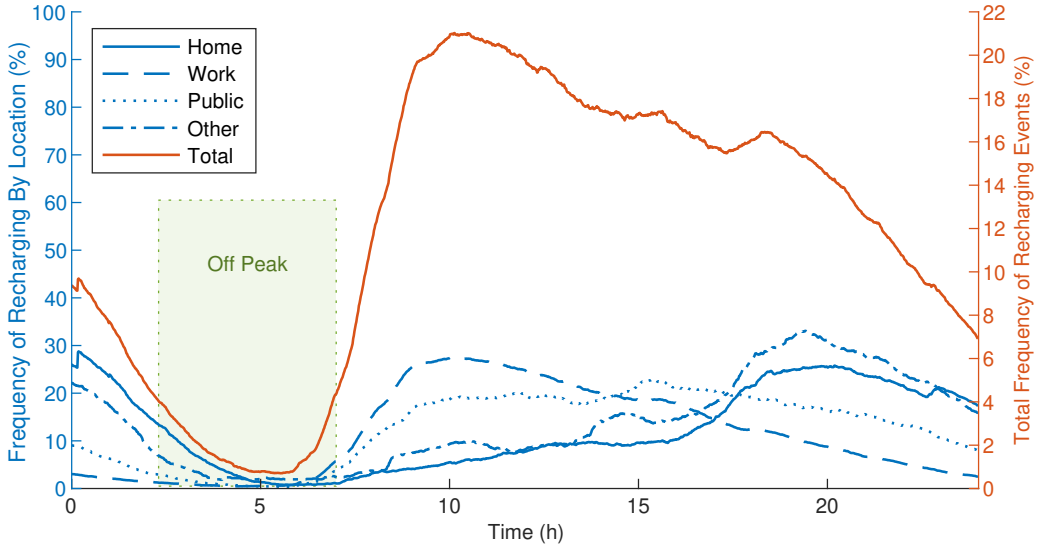

Figure 3.1: Daily variation in active charging events.

and will accept this scheme to save money. In this thesis, non-flexible load refers to traditional household energy demand and flexible load to EVs, although these definitions may be rearranged without loss of generality.

3.1.1 EV Charging Load

Charging behaviour of EVs is statistically quantified in [63], which gathers data from 31,765 EV trips and 16,229 charging events. Charging frequency with time of day is given for 'home', 'work', 'public' and 'other' locations. With this data, a statistical daily variation for expected number of active charging EVs throughout the day is constructed, shown Fig. 3.1. This plots percentage of active charging events by subcategory on the left axis, and percentage of the overall total on the right.

Load curves for 'home' and 'other' charging locations have peak roughly synchronised with household peak loading hours 6-10pm, when many users return home from work. However, many charging events occur at 'work' locations, leading to overall peak around 10am. All locations have roughly synchronised off-peak hours 2.30-7am, during which users are unlikely to be driving and most EV charging is complete. Mean charging power per vehicle was 3.18kW. With this data, average expected load per vehicle $P_{EV}(t)$ is constructed for random uncoordinated charging.

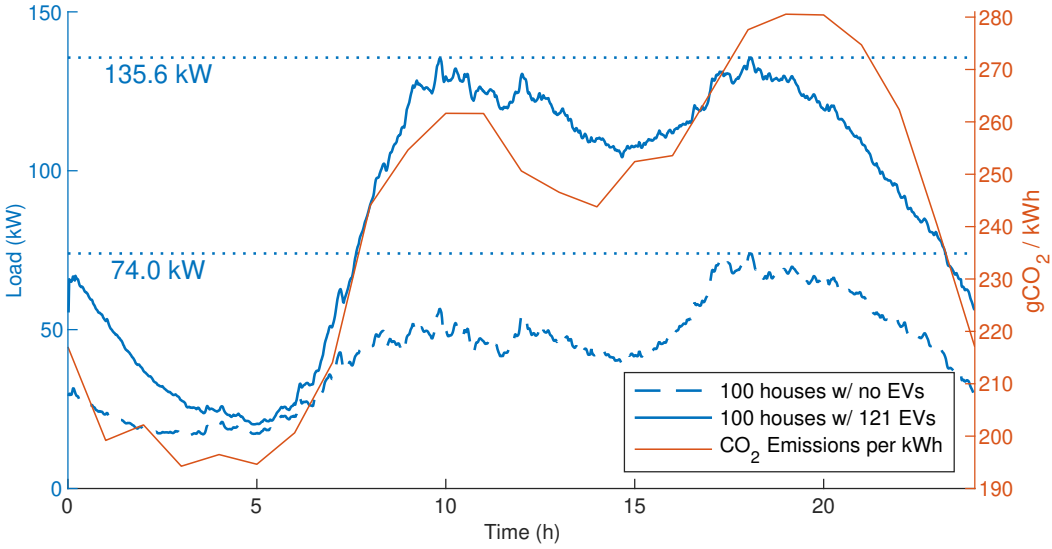

Figure 3.2: The average household in the UK has 1.21 vehicles. This plot shows the increase in expected load profile of 100 households on a cold winter day if all vehicles were electric ($H_b = 100$, $\eta_{EV} = 1.21$). This is overlayed by the carbon emissions per kWh averaged over the month of February 2020. Load and emissions correlate strongly.

3.1.2 Household Load

Electrical power demand of 251 selected households with and without electric heating in the UK is studied in [64]. Approximately 10% of households use electric heating [65]. With this data, expected load curve per household $P_H(t)$ on a cold winter day is also constructed.

The average household in the UK owned 1.21 vehicles in 2017 [66]. When the corresponding EV and household load profiles are combined, shown Fig. 3.2 for 100 households, peak load rises 83%. However, off-peak times are roughly matched 2-6am. This exposes favourable conditions for Smart Charging.

3.1.3 Carbon Emissions

MyGridGB [67] logs and analyses power generation in real-time throughout the UK, where inputs from all forms of power production are used to analyse carbon emissions. Using this data, CO_2 emissions per kWh is gathered at hourly intervals over a period of 30 days. When these 30 days are averaged, a notable pattern emerges that is

highly correlated with loading patterns, shown on the right axis in Fig. 3.2. By charging your EV between the hours of 3-5am instead of 7-8pm you reduce your CO_2 emissions by almost 30%. This suggests that simply by rescheduling EV charging from peak loading hours in the early evening to off-peak hours in the night and early morning, Smart Charging can simultaneously reduce peak load and carbon emissions in the system.

The aggregated CO_2 emissions curve in Fig. 3.2 is used to compute daily CO_2 emissions as a KPI throughout Chap. 3 and 4 assuming all load corresponds to this emissions curve.

3.1.4 Power Network Model

A distribution network of B buses is modelled for household and EV load as follows. Power demand $S_b[n] = P_b[n] + jQ_b[n]$ at each distribution bus $b \in \boldsymbol{B} = \{1, 2, ..., B\}$ at time $t = n\Delta t,\ n \in \mathbb{Z}^+,\ j = \sqrt{-1}$, is defined

$$\left.\begin{aligned} P_b[n] &= H_b\Big(P_H[n] + \eta_{EV} P_{EV}[n]\Big) \\ Q_b[n] &= 0 \end{aligned}\right\} \ \forall\ 0 \leq n < \tfrac{24}{\Delta t} \tag{3.1.1}$$

H_b is the number of houses supplied at each bus b, η_{EV} is network-wide EV penetration, P_H and P_{EV} are average expected household and EV charging load profiles, respectively, per household and per EV. Time interval $\Delta t = \frac{1}{60}$ (1 minute). Power flow between sequential nodes $a, b, c \subset \boldsymbol{B}$, $a \neq b \neq c$ in the network is then defined by the Branch Flow Model [15]

$$\sum_{c=1}^{C} S_{b,c}[n] = S_{a,b}[n] - Z_{a,b}|I_{a,b}[n]|^2 - S_b[n] \tag{3.1.2}$$

$$V_b[n] - V_c[n] = Z_{b,c} I_{b,c}[n] \tag{3.1.3}$$

$$S_{b,c}[n] = V_b[n] I^*_{b,c}[n] \tag{3.1.4}$$

where $c \in [1, 2, ...C]$ are all child nodes of node b, which is in turn child of a. Along the branch $b \to c$: $S_{b,c} = P_{b,c} + jQ_{b,c}$ is sending end complex power transfer, $I_{b,c}$ is

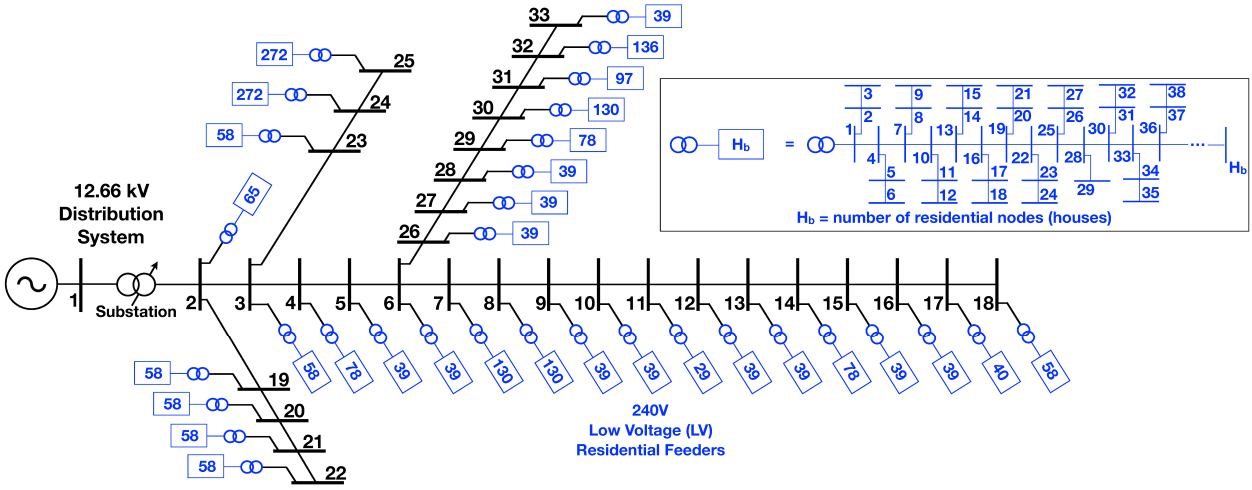

Figure 3.3: IEEE 33 bus 12.66kV distribution network.

current phasor and $Z_{b,c} = R_{b,c} + jX_{b,c}$ is line impedance. S_b is net power drawn from bus b and V_b is voltage phasor. This model allows complex power flow and voltage deviation at each link and bus to be calculated iteratively for each time step n.

This was simulated for the IEEE 33-bus 12.66kV distribution network shown Fig. 3.3, adapted from [68]. Each bus b connects to a low voltage (LV) 240V residential feeder with a varying number of households H_b. Real power demand at each LV node follows the expected average load curve for households P_H and EVs P_{EV}. Power factor correction is perfectly implemented at each bus, and line impedance in the LV feeders is negligible (i.e. the only reactive load is from capacitive and inductive effects of the 12.66kV lines). Bus 1 is slack, with constant voltage $V_1 = 1$ per unit (p.u.), zero net power demand and phase angle.

Matpower [69] is a package of open source Matlab-language M-files for solving steady-state power system simulations. This software is used to compute all network power flow characteristics in Chap. 3 and 4.

Using Matpower, expected load under 0% and 40% EVs is applied with inputs defined in Sec. 3.1.1-3.1.2, and voltage deviation at each bus is derived. Voltage V_b^{low} is shown in Fig. 3.4, which is defined as the most negative bus voltage deviation in

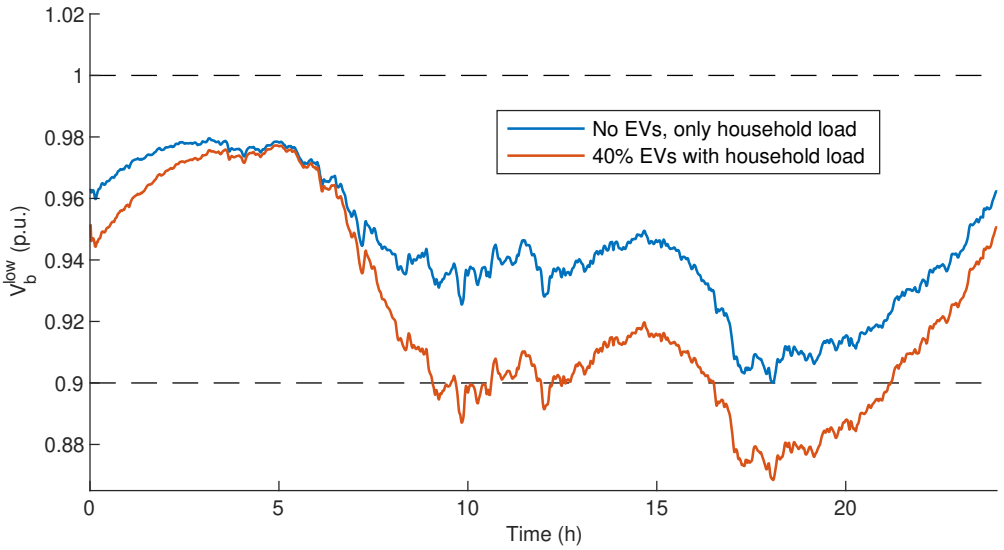

Figure 3.4: V_b^{low} for random uncoordinated charging under 0% and 40% EV penetration. (V_b^{low} is the most negative bus voltage deviation in the network, regardless of which specific bus)

the network, regardless of which specific bus this may be:

$$V_b^{\text{low}}[n] = \min_b \Big(V_1[n], V_2[n], \dots V_B[n] \Big) \tag{3.1.5}$$

I.e. at any particular time, all bus voltages are greater than or equal to V_b^{low}.

In European normal grid operations, voltage deviation at any bus should not exceed the statutory limit of 1 ± 0.1p.u. [14]. The number of houses is chosen in this model such that the lower limit 0.9p.u. is reached under household load only. Thus the network can be considered to have 0% EV Capacity under random uncoordinated charging. EVs bring V_b^{low} well outside of its acceptable range.

3.1.5 Renewable Distributed Generation (DG)

It is desirable to increase the proportion of renewable DG in the power network. However, as outlined in Sec. 2.1.3, excessive DG can lead to problems such as over-voltage, reverse power flow, localised congestions, thermal overloading of equipment and increased line losses. To avoid this, DG must often be curtailed to a maximum value. Renewable generation is effectively free once installed, so to maximise return on investment in renewable systems, DG curtailment must be minimised.

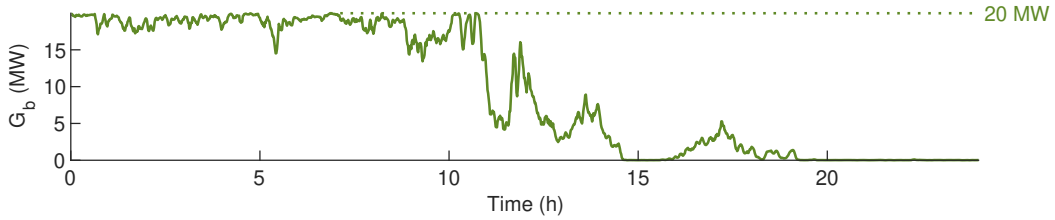

(a) DG wind power input at bus 18.

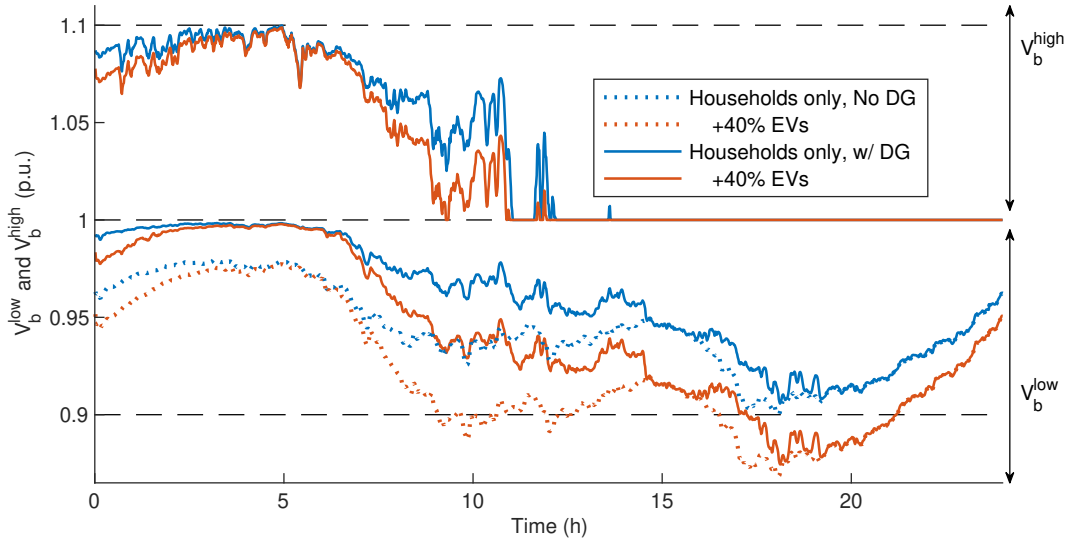

(b) Maximum (V_b^{high}) and minimum (V_b^{low}) worst bus voltages under 20MW DG. All remaining bus voltages fall between the top and bottom curves.

Figure 3.5: Adding DG only increases volatility of voltage deviation.

DG is equivalent in the system to negative load. However, to differentiate from demand, power generation at bus b is denoted G_b. DG Capacity (a.k.a. Hosting Capacity) is defined as the upper limit of DG beyond which overvoltage occurs [4], [70]. In other words, upper worst bus voltage V_b^{high}, which is defined

$$V_b^{\text{high}}[n] = \max_b \Big(V_1[n], V_2[n], \dots V_B[n] \Big) \tag{3.1.6}$$

should not exceed 1.1 p.u.

Wind power generation profile is modelled using windspeed sensor readings gathered at 1s intervals over 172 days from an offshore wind farm in [71]. Power is derived using the Vestas V164-8.0 wind turbine power curve [72], and inertia of the turbine blades accommodated via 5 point rectangular smoothing window.

Problems of excessive DG are most noticeable when concentrated at the end of long and lightly loaded feeders [73]. Fig. 3.5 shows a 20MW wind power input profile

at bus 18, where peak is roughly synchronised with minimum load in the early hours of the morning. Maximum V_b^{high} and minimum V_b^{low} voltage deviations are shown in Fig. 3.5b. Displaying the maximum and minimum voltage deviation (at any bus at any time) in this way means that all other bus voltages fall somewhere between V_b^{high} and V_b^{low}. The dotted lines in Fig. 3.5b are the same as V_b^{low} in Fig. 3.4, shown for comparison. Two points can be observed:

- First, since V_b^{high} now touches the upper limit 1.1 p.u., this may be considered the DG capacity of the unconstrained system. This will be used as benchmark for comparison with the proposed Smart Charging schemes.

- Second, voltage now spans the full range of its acceptable limits and V_b^{low} remains unchanged. This demonstrates how unconstrained DG can lead to increased voltage fluctuations and aggravate volatility, since it is non-synchronised with consumer demand.

This chapter proposes a scheme to synergise EV charging and DG such that capacity of both can be improved simultaneously.

3.2 Communications Architecture

Any Smart Grid scheme requires harnessing the communication capability of numerous cyber-enabled sensors and actuators permeated throughout the grid. This section designs an ICT architecture to underpin the proposed Smart Charging schemes and to explicitly model effects of operational latency on KPIs. First, contributions of this chapter relevant to the proposed ICT architecture are expanded and clarified. Structure, topology and function of the hierarchical tiers are then defined, and operational latency constraints are explained. Contributions continue in Sec. 3.3, where specific interactions of the Smart Curtailment scheme are developed.

3.2.1 Contributions of the ICT Architecture

Practical ICT constraints are inherent in operation of any Smart Grid system. However, these are routinely overlooked in Smart Charging studies, which tend to assume that perfect knowledge of grid status and loading patterns is available everywhere in the network, and that any actuating device can act with zero latency. Where delay is mentioned, e.g. [74], [75], it tends to refer to convergence time and/or control action period of the optimisation scheme, not the mandatory operational latency required from transporting information and response time of actuating devices.

The proposed ICT architecture uses the three-tier hierarchical topology inspired from the author's previous work in [39] (see Chap. 5). This is also compatible with recent open Smart Charging and Demand-Response communications standards such as OpenADR [61] and OCPP [76]. The work in [39] demonstrates that offloading IoT / Smart Grid asset coordination onto regional hubs in a hierarchical topology can effectively alleviate traffic burden in the network. This chapter develops this ICT strategy into a practically applicable demand-response algorithm for Smart Charging that also alleviates computation load at the central controller. The contributions this are as follows:

- A practical arrangement of Smart Devices is proposed in a Distributed control paradigm such that key decision-making processes are offloaded to mid-tier aggregators, serving to alleviate computation load at the central controller. Alleviation of computation and traffic load in this way makes the system scalable and adaptable to a variety of network sizes and asset arrangements.
- A demand-response algorithm for network control at each hierarchical tier is designed, taking into account practical information constraints that are routinely overlooked in the literature.
- The architecture is compatible with recent Smart Charging and Demand-Response communications standards, therefore is readily applicable to the industrial environment without radical infrastructural overhaul.

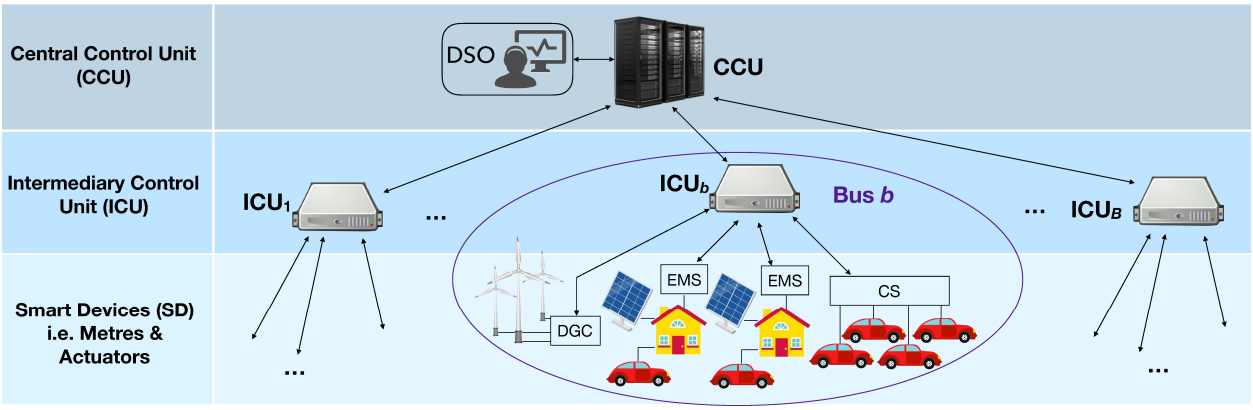

Figure 3.6: Three-tier hierarchical communications topology for the proposed Smart EV Charging scheme.

3.2.2 Hierarchical Topology

A three-tier hierarchical topology is used, shown Fig 3.6. There are three node types: Central Control Unit (CCU), Intermediary Control Units (ICU) and Smart Devices (SD).

- **Central Control Unit (CCU):** This is the main network coordinator, e.g. the DSO, where information from the entire network is gathered. It is connected via data link to various ICUs permeated throughout the network. It receives periodic status beacons from each ICU and based on these beacons, transmits control instructions.

- **Intermediary Control Unit (ICU)** These are mid-tier nodes which co-ordinate regionally colocated demand-response assets via SDs. This alleviates computation load on the CCU as well as traffic load on the ICT system [39]. Every update period, the ICU broadcasts 'Status Request' to its SDs and receives their replies. If a control signal from the CCU is received, actuation instructions are transmitted to relevant SDs. In this system there is one ICU_b for each distribution bus b, but in practice an ICU could exist anywhere numerous demand-response assets must be managed.

- **Smart Devices (SD)** These are bottom-tier nodes that conduct measurements and/or actuations. Practically, they may take the form of home or

building energy management systems (EMS), networked charging stations (CS) and DG controllers (DGC). These will be numerous and pervasive, so operation is kept simple. The SD receives control commands (e.g. curtailment limits) from its ICU, and replies with status messages. Upon receiving a curtailment limit, the SD ensures its overall power does not exceed this limit.

3.2.3 Inter-tier Communication

This architecture is in line with recent open Smart Charging and Demand-Response communications standards OpenADR (now IEC 62746-10-1) [61] and OCPP [76]. A detailed summary of these standards is provided in Sec. 2.2.3.

Upper-tier communication (CCU-ICU) can be achieved with OpenADR, where the CCU is virtual top node (VTN) and ICUs are virtual end nodes (VEN). PUSH protocol is enabled so both may initiate communication. Status beacons are sent via EiReport service, and control commands via EiEvent.

Lower-tier communication (ICU-SD) deploys Smart Charging via OCPP, however is configurable using OpenADR. All SDs are VENs of the ICU VTN. Status requests and/or curtailment limits can be sent from the ICU via EiEvent service, and status information can be reported via EiReport from any sensor or actuator in the LV feeder. The External Smart Charging feature of OCPPv2.0 allows for every OCPP-connected CS to be also managed by the ICU via OpenADR.

3.2.4 Practical Latency Constraints

For effective control, numerous sensor readings and control commands must be transmitted between sensors and actuators permeated in the distribution network over a wide geographical area. These messages must be processed and exchanged over various tiers, and will incur an accumulation of all queueing, processing, transmission and actuation delays. This is illustrated by (ii)-(xi) in Fig. 3.7, which shows the

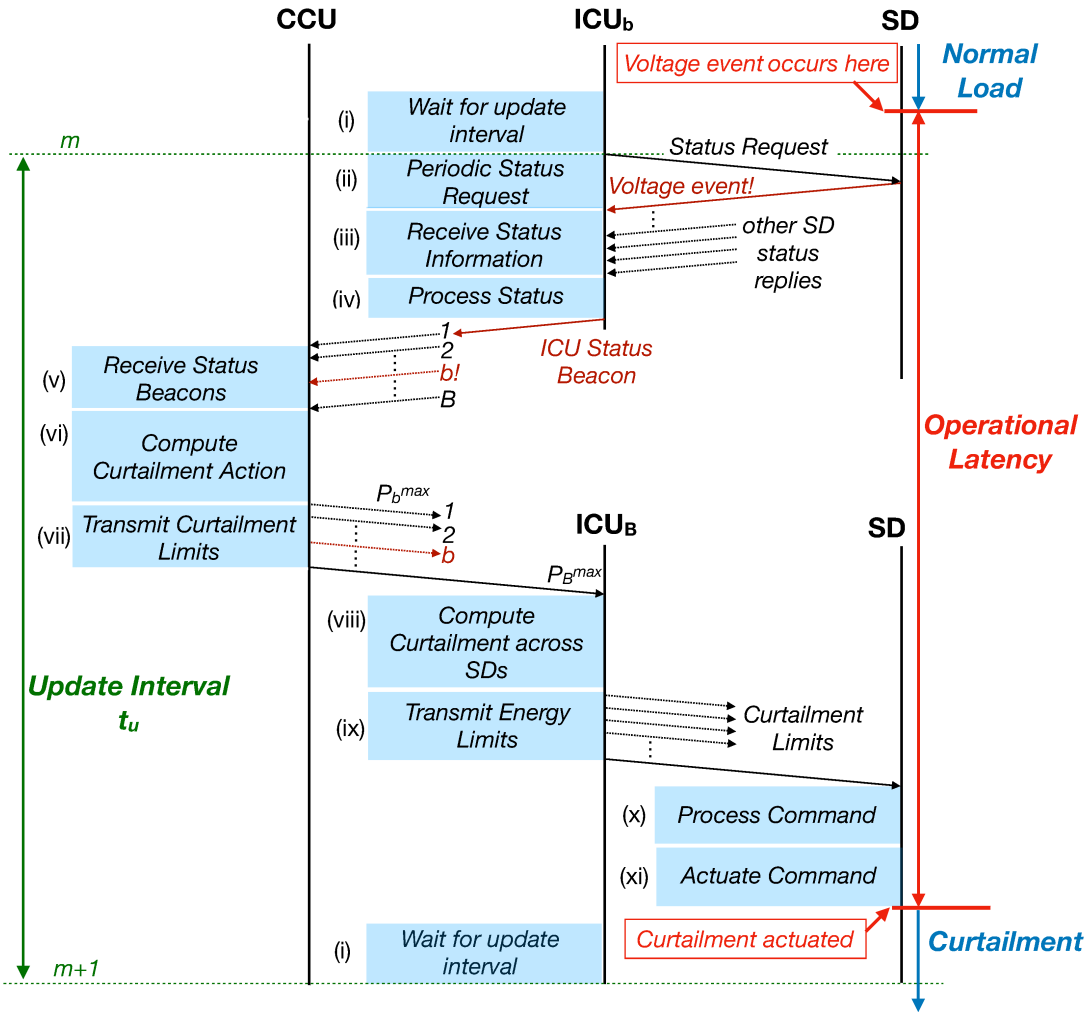

Figure 3.7: Operational Latency accumulation for one curtailment actuation.

latency accumulation as the system responds to a voltage event with curtailment action. This operational latency imposes a minimum update interval t_u within the system, defining granularity of control and the rate at which disturbance events can be detected and compensated. This practical update interval is subject to two systematic constraints:

First, ICT infrastructure represents large investment for a system as ubiquitous as the power network. Using a short update interval with fast sensor readings increases data volume and system traffic, which raises bandwidth requirements and cost of ICT hardware. A tradeoff ensues between granularity of control and cost of data collection.

Second, operating bodies in the power network are traditionally unaccustomed to

latency-critical ICT applications, and update interval is far from homogenised across the industry. OCPP has scope for charging limit duration in seconds, as well as rapid demand-response times due to transaction and billing requirements; however, Supervisory Control and Data Acquisition (SCADA) data is normally collected from wind turbines at 10 minute intervals. Tap changers, voltage regulators and voltage controlled capacitor banks all have typical delays of 30-90 seconds [29]. Any control scheme is subject to the slowest interval available, and this range of update periods and response times mean that significant additional delay may be incurred while waiting for an update command, (i) in Fig. 3.7, or at the actuating SD itself in response to an incoming command (x)-(xi). There will inevitably be a transition period during which slower-than-desired update interval must be tolerated.

Latency can be reduced in the system, but this comes at a cost. Understanding key tradeoffs between practical update period and Smart Charging performance is vital, and forms a key contribution of this thesis.

3.3 Performance under Zero Latency

Curtailment in this scheme can take two forms, depending on the nature of voltage conditions in the network. To prevent undervoltage, EV charging load is curtailed to bring voltage back within bounds (P-curtailment). If there is overvoltage, DG must be curtailed (G-curtailment). Operation of each will be described in turn assuming zero latency in the system.

The role of each ICU_b during P-CUR is summarised in Fig. 3.8. Every update interval $t = mt_u$ where $t_u = k\Delta t,\ k, m \in \mathbb{Z}^+$, each ICU requests status information from its SDs to gather bus voltage $V_b[m]$, active power demand $P_b[m]$ and overall DG input $G_b[m]$, and forwards this to the CCU. It also gathers total EV charging power $P_b^{\text{flex}}[m]$ and stores this locally. Thus the CCU receives three complete status vectors every update interval:

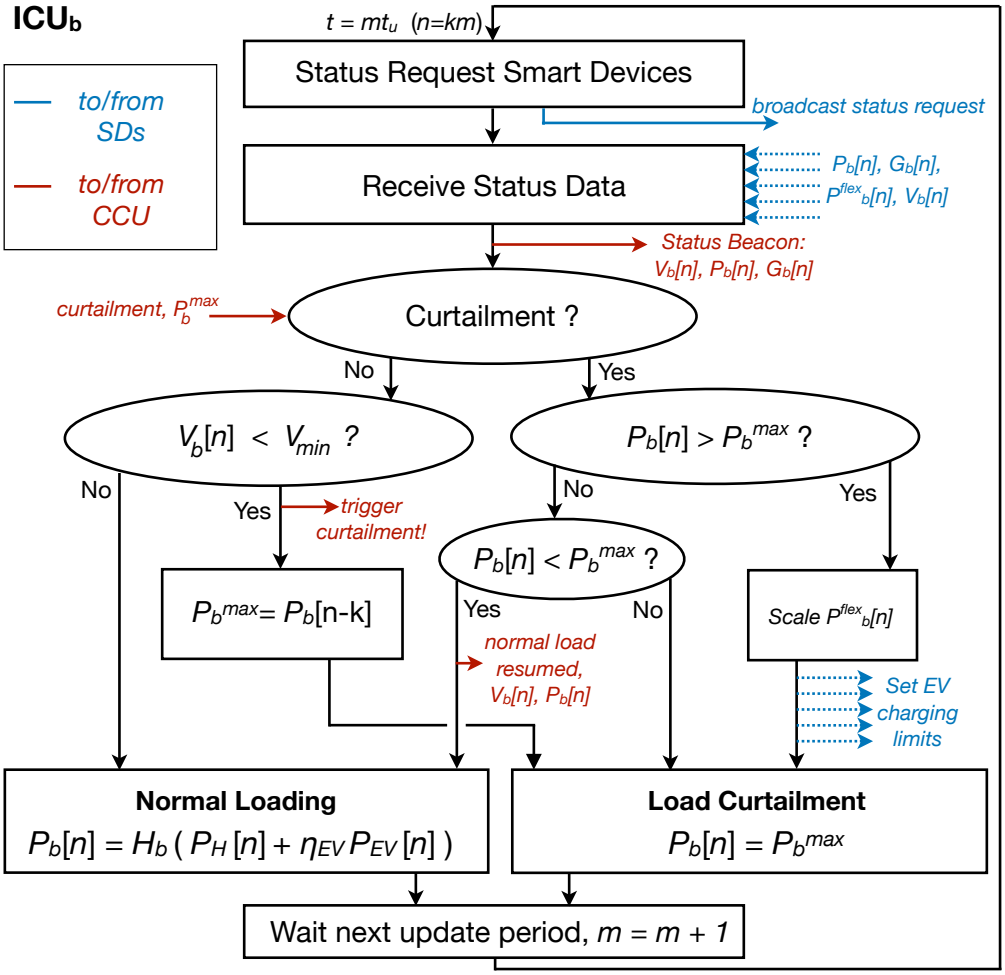

Figure 3.8: Smart EV Charging algorithm at ICU_b.

$$\overrightarrow{V}[m] = \begin{bmatrix} V_1[m] \\ \vdots \\ V_B[m] \end{bmatrix}, \overrightarrow{P}[m] = \begin{bmatrix} P_1[m] \\ \vdots \\ P_B[m] \end{bmatrix}, \overrightarrow{G}[m] = \begin{bmatrix} G_1[m] \\ \vdots \\ G_B[m] \end{bmatrix} \tag{3.3.1}$$

3.3.1 P-Curtailment (P-CUR)

P-curtailment is triggered at interval $m = m_P$ by any bus voltage below the limit $V_{\min}$. If $V_b[m] < V_{\min}$ is detected, ICU_b begins curtailment at bus b and notifies the CCU, which then identifies b as the worst bus w. Due to the radial topology of the distribution network, V_b^{low} will be affected by load changes in any other bus. Therefore, the maximum power vector is chosen by the CCU as the last received

power from each bus before the curtailment trigger

$$\overrightarrow{P}^{\max}[m] = \begin{bmatrix} P_1^{\max}[m] \\ \vdots \\ P_B^{\max}[m] \end{bmatrix} = \begin{bmatrix} P_1[m_P - 1] \\ \vdots \\ P_B[m_P - 1] \end{bmatrix} = \overrightarrow{P}[m_P - 1] \tag{3.3.2}$$

The CCU then notifies each ICU_b of its maximum power $P_b^{\max}$, which launches curtailment at every other bus.

During P-CUR, each ICU_b issues charging limits to all of its connected CSs to ensure $P_b[n]$ does not exceed $P_b^{\max}$. Non-flexible load is met by priority, and the remaining available power is distributed proportionally between all active charging EVs. This limits total network load to

$$P_T[m] = \sum_{b=1}^{B} P_b^{\max}[m] \tag{3.3.3}$$

And ensures V_b^{low} is limited to $V_{\min}$. Assuming the network is designed to meet non-flexible load requirements, it is always possible to reduce flexible load such that V_b^{low} is kept within bounds. The limit $P_b^{\max}$ is maintained at each bus until all delayed charging load is satisfied. At this point, ICU_b resumes normal load and notifies the CCU of its reduced power. This process continues until all EV charging queues at all ICUs are empty, and normal load is resumed.

The CUR scheme requires minimal processing at the CCU since curtailment limits are taken simply as the last received power value from each bus. Further, central processing load is reduced by offloading micromanagement of demand-response assets in a distributed manner to regional ICU controllers.

V_b^{low} and P_T under P-CUR is shown Fig. 3.9. Several KPIs can be derived:

Voltage Control

Under zero DG, P-CUR ensures load is never large enough to bring V_b^{low} below the statutory limit at 0.9pu. Under zero latency, $P_b^{\max}$ can be instantly initiated in response to undervoltage, so perfect voltage control is achieved.

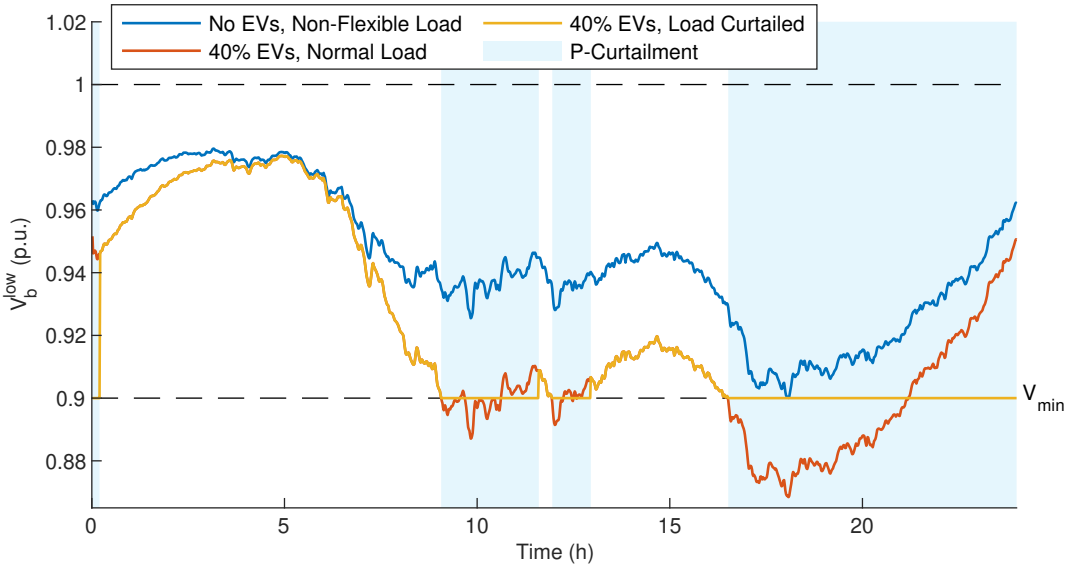

(a) Voltage at worst bus

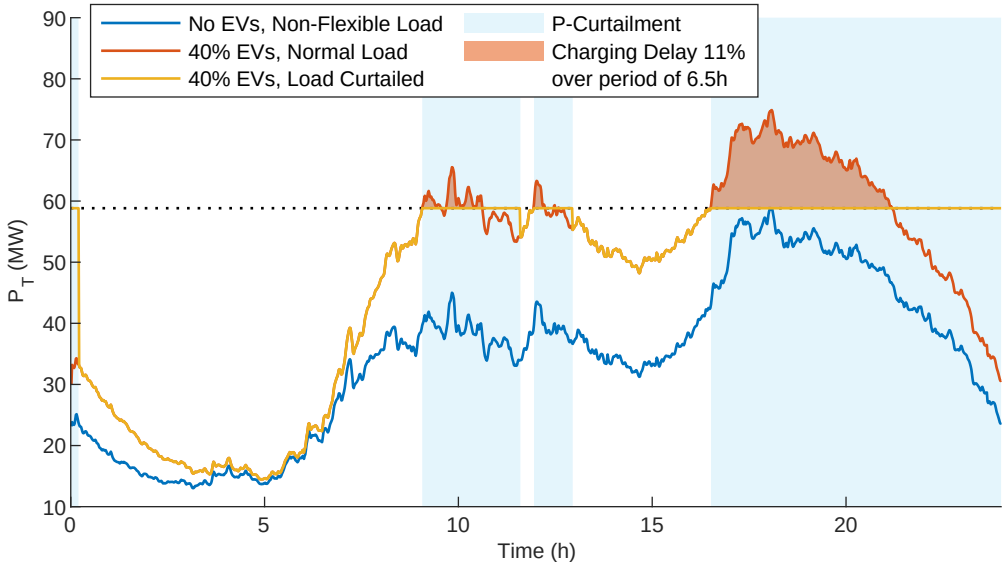

(b) Total real power demand.

Figure 3.9: Power and voltage deviation in *P*-CUR.

Peak Load

Curtailing flexible load subject to voltage conditions inherently reduces peak load in the system.

EV Charging Delay

Curtailing charging load causes delays for subscribing EV owners during peak hours. Delay is incurred only when unconstrained load exceeds curtailed load. This delay period is shown in shaded orange, Fig. 3.9b. Daily charging delay is the ratio of

mean normal to curtailed load during this period, in this case 11% over 6.5h. An EV charging during these peak hours takes on average 11% longer to gain the same amount of charge.

CO_2 Emissions

Daily carbon emissions are calculated by assuming all non-DG power input follows emissions from Fig. 3.2. Since P-CUR reschedules charging load from peak hours to lower emission hours overnight, less CO_2 is emitted overall. This saving grows as η_{EV} increases.

EV Charging Capacity

Undervoltage is avoided, so EV Capacity has increased compared to the unconstrained system (recall from Sec. 3.1.4 that the unconstrained system had 0% EV capacity).

3.3.2 G-Curtailment (G-CUR)

The same process can be used to curtail generation in the network to avoid overvoltage. G-curtailment is triggered at interval $m = m_G$ by any bus voltage above the limit $V_{\max}$. By the same process as P-CUR, any ICU_b that detects an overvoltage may trigger curtailment of DG at all buses according to a maximum generation vector equivalent to the last received generation values at the CCU

$$\overrightarrow{G}^{\max}[m] = \begin{bmatrix} G_1^{\max}[m] \\ \vdots \\ G_B^{\max}[m] \end{bmatrix} = \begin{bmatrix} G_1[m_G - 1] \\ \vdots \\ G_B[m_G - 1] \end{bmatrix} = \overrightarrow{G}[m_G - 1] \tag{3.3.4}$$

Once G-curtailment is triggered, each ICU_b issues generation limits to all subsidiary DGCs to ensure $G_b[n]$ does not exceed $G_b^{\max}$, where generation is split proportionally between all active DG inputs. This limits total DG to

$$G_T[m] = \sum_{b=1}^{B} G_b^{\max}[m] \tag{3.3.5}$$

No DG storage is assumed. Thus, the limit $G_b^{\max}$ is maintained only while generation is available in excess, i.e. $G_b[n]$ may drop below $G_b^{\max}$ at any time.

Sec. 3.1.5 demonstrated that the HC of the network with DG input concentrated at the end of the feeder (bus 18) was roughly 20MW. For comparison, V_b^{low}, V_b^{high}, G_T and P_T under CUR are shown with 62MW wind farm input at bus 18 and 60% EV penetration in Fig. 3.10. Several observations can be made.

Voltage Control

Referring to Fig. 3.10b, CUR effectively contains voltage deviation between statutory limits. However, since there are now two inputs that determine bus voltage, $\overrightarrow{P}$ and $\overrightarrow{G}$, curtailment in either one leads to Continuous Deviations (CD) about $V_{\min}$ or $V_{\max}$. Variation in unconstrained $\overrightarrow{P}$ during G-CUR leads to CD about $V_{\max}$. Unconstrained $\overrightarrow{G}$ during P-CUR leads to CD about $V_{\min}$. During PG-curtailment (i.e. both P- and G-CUR simultaneously), there is no deviation, since both are constant at their curtailed limits.

User Inconvenience

EV charging is spread throughout the network, whereas DG input is concentrated at a single bus. This, combined with the inherent volatility of renewable generation, means CD is much more prominent about $V_{\min}$ (during P-CUR) than about $V_{\max}$.

To cope with CD, Continuous Margin Reduction (CMR) is employed. This is where the margin formed by $V_{\min}$ and $V_{\max}$ is reduced away from statutory limits. However, this also means P_T and G_T must be curtailed at lower thresholds. For EVs, this means longer charging delays for subscribing users. For DG, this means lower average power output, reducing returns on investment in renewable systems. The shorthand G-CMR or P-CMR is used to refer to movement of only $V_{\max}$ or $V_{\min}$, respectively.

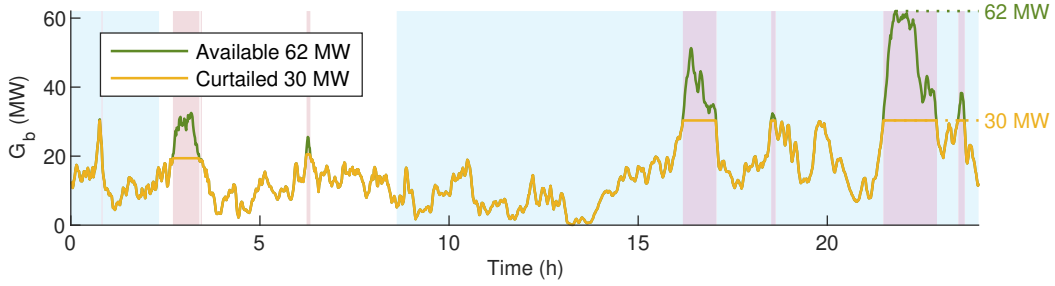

(a) DG Wind Power Input at Bus 18

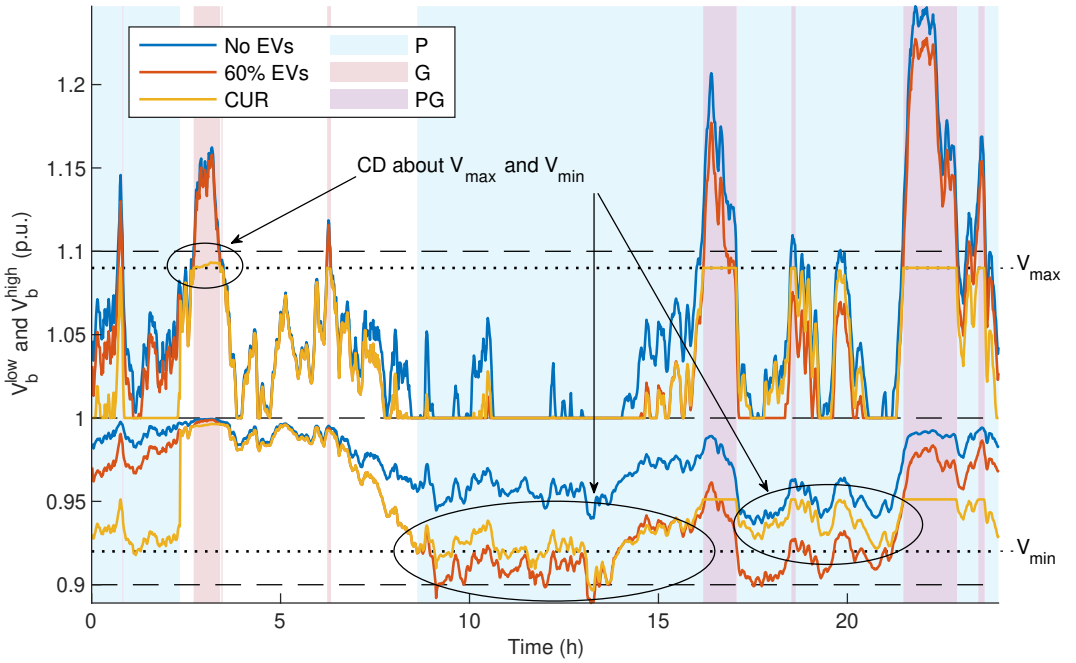

(b) Maximum (top) and Minimum (bottom) Worst Bus Voltages. Continuous Deviations (CD) appear about the limits $V_{\max}$ and $V_{\min}$.

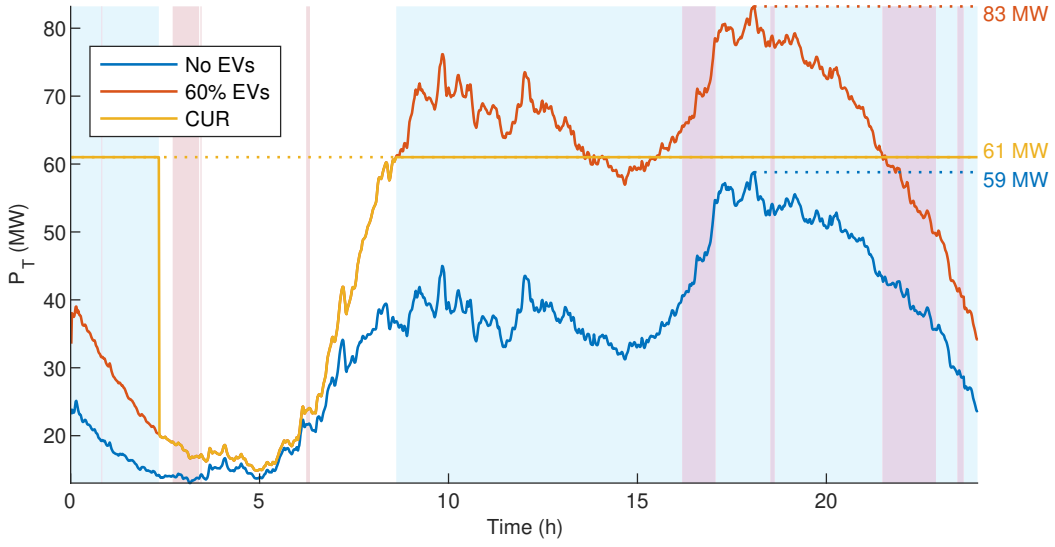

(c) Total Power Demand

Figure 3.10: CUR can effectively improve both EV and DG hosting capacity

CO_2 Emissions

Greater DG penetration brings significantly reduced carbon emissions, since a higher proportion of total power input is renewable.

EV & DG Capacity

Voltage stays within bounds despite rise in EV and DG penetration, reflecting capacity increase of both simultaneously compared to the unconstrained system.

3.4 Practical Latency Constraints

Without the assumption of perfect communication, sensor readings must be gathered at a pre-defined update period incumbent to hardware and bandwidth constraints in the underpinning ICT system. Upon detection of over- or undervoltage, multiple messages must be exchanged in sequence before curtailment is effectively actuated. This latency accumulation imposes an update interval t_u, defining granularity of control in the system.

As discussed in Sec. 3.2, the update interval will be defined largely by two parameters relevant to the system operator. First, demand-response latency in the system is dependent largely on investment in ICT infrastructure, which is designed based on a certain expected data volume. Halving t_u leads to twice the data volume and twice the system traffic, which is significant for a system the size of the power network. Delivering this increased data volume under the same end-to-end latency raises bandwidth requirements and cost of ICT infrastructure. A tradeoff ensues between granularity of control and cost of data collection, and ultimately the update interval may be defined by budget constraints. Understanding the compromises this interval brings is therefore imperative.

Second, power networks are not traditionally accustomed to latency-critical ICT applications, and update interval is far from homogenised across devices. Any control scheme is subject to the slowest update interval available - controlling EV charging at 1s intervals is of limited use if SCADA wind data brings granularity of DG control to 10 minute intervals. There will inevitably be a transition period where the system must cope with slower-than-desired update period before adequate hardware is implemented universally.

Under these practical system latency constraints, certain complications must be dealt with, leading to key performance tradeoffs for the operator.

3.4.1 Latency Effects

Assuming a 10 minute update interval, a delay period of up to 10 minutes may follow an over- or undervoltage event before an appropriate curtailment action is triggered. Voltage deviations during this critical delay period are termed Trigger Deviations (TD). Under CUR, curtailment limits $\overrightarrow{P}^{\max}$ and $\overrightarrow{G}^{\max}$ are static during curtailment, so latency effects on voltage deviation manifest only at the curtailment trigger.

A 10 minute update interval for CUR is modelled in Fig. 3.11, from which several observations can be made.

Trigger Deviations (TD)

TD is visible for both P- and G-curtailment, however there is striking difference in magnitude between the two. For P-curtailment, TD is comparable in size to CD, so is effectively mitigated by CMR. In contrast, TD in G-curtailment vastly outweighs CD. The amount exceeded in both depends on variation in load and DG during this trigger delay, so is stochastic in real time.

TD is also visible in the curtailed DG and load profile in Fig 3.11a and 3.11c. Here, at each curtailment trigger, $\overrightarrow{P}$ and/or $\overrightarrow{G}$ are allowed to deviate freely before curtailment to the last received power value can be effectively actuated, leading to spikes in generation and consumption. In this case, for power consumption the difference is small (peak 76MW curtailed to 72MW), but for DG the difference is significant (peak 44MW curtailed to 29MW). Power equipment is normally sized according to peak power values, so this difference is important from an operator perspective, and it is desirable to limit this spike.

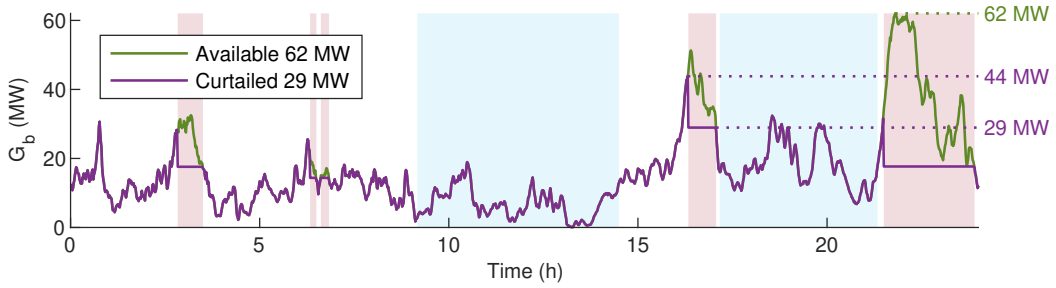

(a) DG Wind Power Input at Bus 18

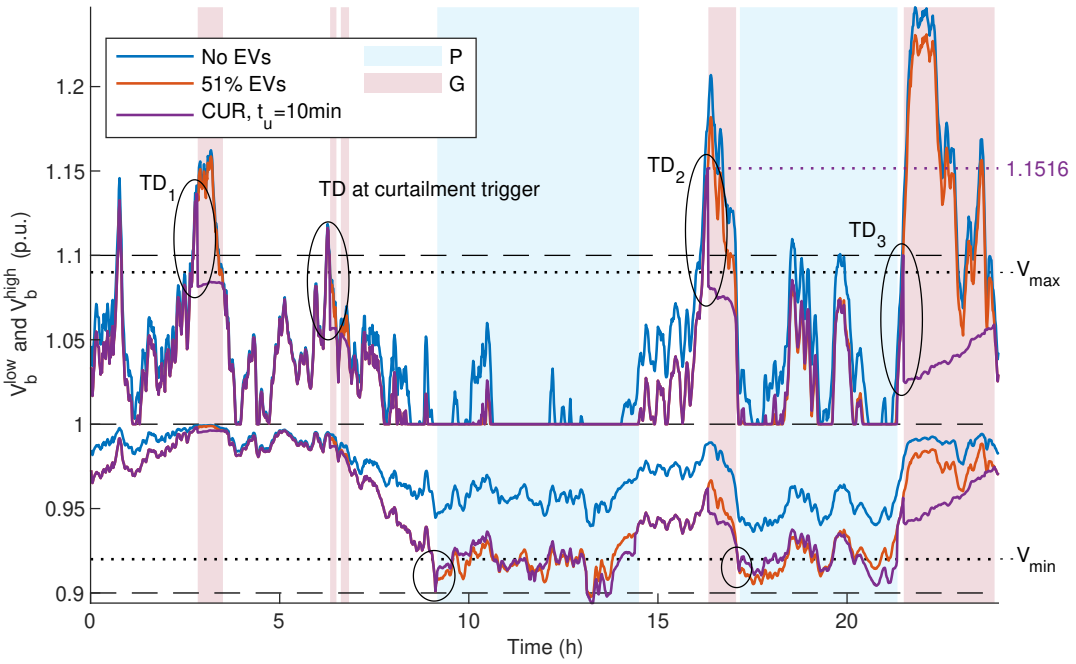

(b) Maximum (top) and Minimum (bottom) worst bus voltages under $t_u = 10$ minutes. The update interval leads to Trigger Deviations (TD) which manifest only at the curtailment trigger.

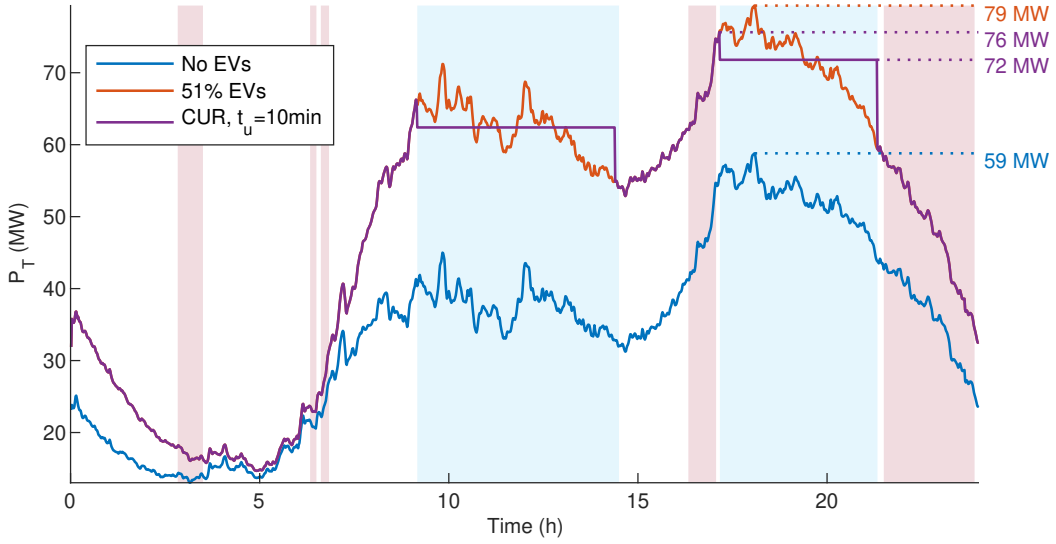

(c) Total Power Demand

Figure 3.11: Practical communications constraints (here $t_u = 10$min.) lead to spikes in generation and consumption. This is most significant for G-curtailment due to volatility of input and concentration at the end of the feeder.

Curtailment Power Limit

The update interval also has effect on the curtailed power. Since $\overrightarrow{P}^{\max}$ and $\overrightarrow{G}^{\max}$ are chosen as the last received values at the CCU before the over- or undervoltage event, the curtailed limit ultimately depends on where the system was 10 minutes prior to the trigger. This leads to a stochastic curtailment value, where G_T may be high (as in TD_1, TD_2 in Fig. 3.11b) or low (TD_3). Since DG is highly volatile, this difference can be significant. In general, the update interval tends towards overcurtailment - i.e. $\overrightarrow{P}^{\max}$ and $\overrightarrow{G}^{\max}$ are lower than for the zero-latency system. Therefore the drawbacks of CMR - delays to EV charging and lower DG output - are made worse.

3.4.2 Latency Mitigation Strategies

A practical update interval leads to two impracticalities in CUR: spikes in generation and consumption that lead to unacceptable voltage deviations, and overcurtailment, which leads to higher charging delays and lower renewable energy output. There are two ways to mitigate these TD effects. One of which is CMR, which has already been seen in the zero latency system. The other, Interval Reduction (IR) involves reducing the update interval t_u. Each will be dealt with in turn.

Continuous Margin Reduction (CMR)

In the same process as was applied under zero latency, reducing the margin $V_{\max}$ can mitigate the sharp TD spike at the G-curtailment trigger, seen Fig. 3.11. This is shown for $V_{\max} = 1.05$pu in Fig. 3.12, where overvoltage is successfully eliminated.

However, this comes at a price. Curtailing DG at $V_{\max}$ =1.05pu leads to a significant increase in severity of G-curtailment. While maximum curtailed generation limit is only reduced from 29MW to 24MW, the system also spends almost 6 hours longer in G-curtailment, meaning that overall delivery of renewable energy is reduced. Just by reducing $V_{\max}$ from 1.09 to 1.05pu, the proportion of daily energy consumption supplied by wind power is reduced from 26% to 22%. This reduction is important

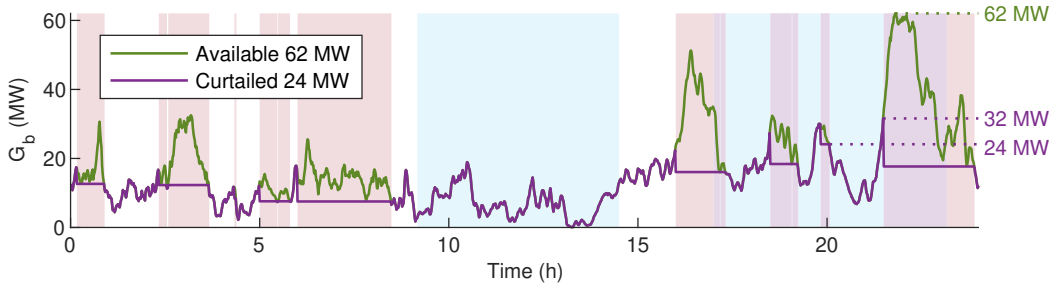

(a) DG wind power input at bus 18.

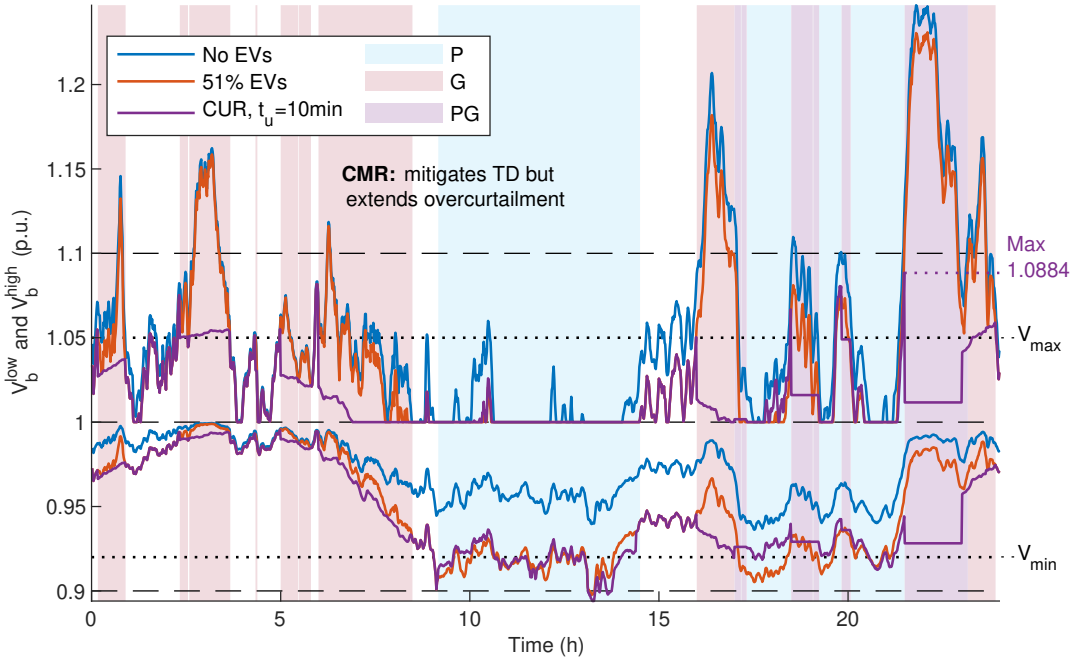

(b) Maximum (top) and Minimum (bottom) worst bus voltages under for $V_{\max} = 1.05$pu.

Figure 3.12: Continuous Margin Reduction (CMR) can mitigate TD in G-CUR, however severity of curtailment is significantly increased.

from a planning perspective since it will strongly limit the return on investment seen from installation of renewable energy systems.

Finally, P- and G-curtailment are linked. Increasing the severity of G-CMR leads to overall lower voltages throughout the network, meaning that P-curtailment is triggered earlier and at lower power. Since charging demand is then satisfied slower, time spent in P-curtailment is increased from 9.4h in Fig. 3.11 to 11.2h in Fig. 3.12. This translates as an increase in average charging delay from 4% to 7% during peak hours.

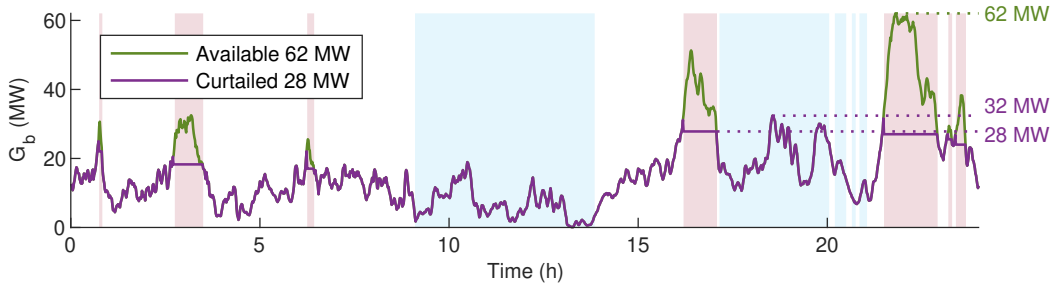

(a) DG Wind Power Input at Bus 18.

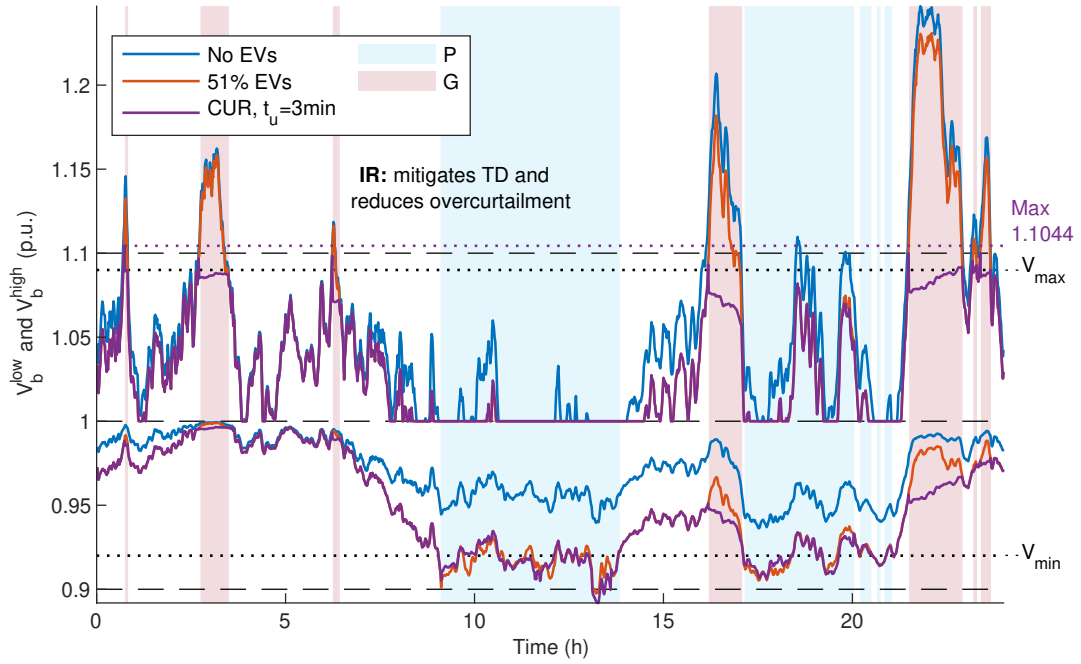

(b) Maximum (top) and Minimum (bottom) Worst Bus Voltages under for $t_u = 3$min.

Figure 3.13: Interval Reduction (IR), i.e. reducing the interval t_u, can strongly mitigate TD in G-CUR without increasing curtailment severity.

Interval Reduction (IR)

Interval reduction, as the name suggests, involves reducing the update interval t_u. In so doing, the time during which load and DG can freely fluctuate during the trigger latency period is reduced, and with it the probability of a strong deviation.

Table 3.1: Comparison of CMR and IR for mitigation of trigger deviations in G-curtailment, CUR

	Fig.	t_u (min.)	$V_{\max}$ (pu)	Voltage Dev.	Charging Delay	Energy from DG
none	3.11	10	1.09	Unacceptable	4.4 %	26.7 %
CMR	3.12	10	1.05	Acceptable	7.4 %	22.7 %
IR	3.13	3	1.09	Acceptable	2.7 %	28.0 %

As shown in Fig. 3.13, reducing the update interval to $t_u = 3\text{min}$ is sufficient to effectively eliminate overvoltage.

Further, since over- and under-voltage are detected and responded to sooner, the TD spike in peak load and DG at the curtailment trigger is decreased. And since $\overrightarrow{P}^{\max}$ and $\overrightarrow{G}^{\max}$ are chosen at more recent values before the over- or undervoltage event, they are chosen at a statistically higher value, meaning that overcurtailment is also reduced. The charging delay is then lower and energy supplied by DG is higher. In this $t_u = 3\text{min}$ system, charging delay drops to 3% and renewable energy supply rises to 28% (from 4% and 27% in the 10min system Fig. 3.11). This is expected since, as t_u is reduced, the system approaches the zero-latency response. For easier comparison, key performance variables for each example under CMR and IR are listed in Tab. 3.1.

3.5 Simulation

To demonstrate key performance-cost tradeoffs and consolidate analysis against a diverse array of inputs, 172 days of windpower profiles, derived from windspeed data in [71], were applied under varying degrees of CMR and IR. The system was tested for each of these 172 days under 80% EV penetration and 40MW wind power input at bus 18. This is twice the DG capacity of the unconstrained system. The following KPIs are evaluated: Voltage Control, Peak Shaving, User Inconvenience, DG Energy Input CO_2 Emissions and Deployment Cost.

3.5.1 Continuous Margin Reduction (CMR)

CMR was tested in two phases. First, P-CMR was tested by incrementing $V_{\min}$ from 0.9 tp 0.96pu. Second, the same was done for G-CMR by with $V_{\max}$ from 1.1 to 1.04pu. During each phase, the other limit was kept constant at 1.1 and 0.9pu,

respectively. Voltage, load and generation profiles were simulated at each bus for each of the 172 days of DG input, and KPIs were evaluated as follows:

Voltage Control

- Voltage area above and below bounds at the maximum and minimum worst buses in the network (units p.u.-hours)
- Peak daily maximum and minimum voltage

Peak Shaving

- Peak load throughout the day

User Inconvenience

- Daily average charging delay during peak hours
- Daily energy supplied by DG

CO_2 Emissions

- Daily CO_2 emissions, based on the average daily carbon emissions curve described in Sec. 3.1.3

This was then repeated for update intervals $t_u = 10$, 5 and 3min. Unconstrained system behaviour was also simulated for each day to serve as control group.

Percentage Overload

Curtailed power demand depends on both the DG input profile and the lower voltage limit $V_{\min}$. Raising $V_{\min}$ leads to P-curtailment being triggered earlier and at lower power. However, if DG is strong near the minimum worst bus voltage, charging load

can be significantly higher before a voltage drop below $V_{\min}$ occurs, meaning that curtailment may not be triggered at all.

System overload occurs on low windpower days where the power limit enforced by $V_{\min}$ is such that curtailed power endures over 24 hours. If the probability of these overloaded days is less than 50%, any forgone EV charging load after these 24 hours will eventually be satisfied in spare capacity on later days, so the system is still within EV charging capacity. If not, however, then the forgone charging load will gradually accumulate, meaning this penetration of EVs cannot be supported long term. For a given EV penetration, percentage overload therefore defines the highest extent of practical P-CMR in the system and the useable range of $V_{\min}$.

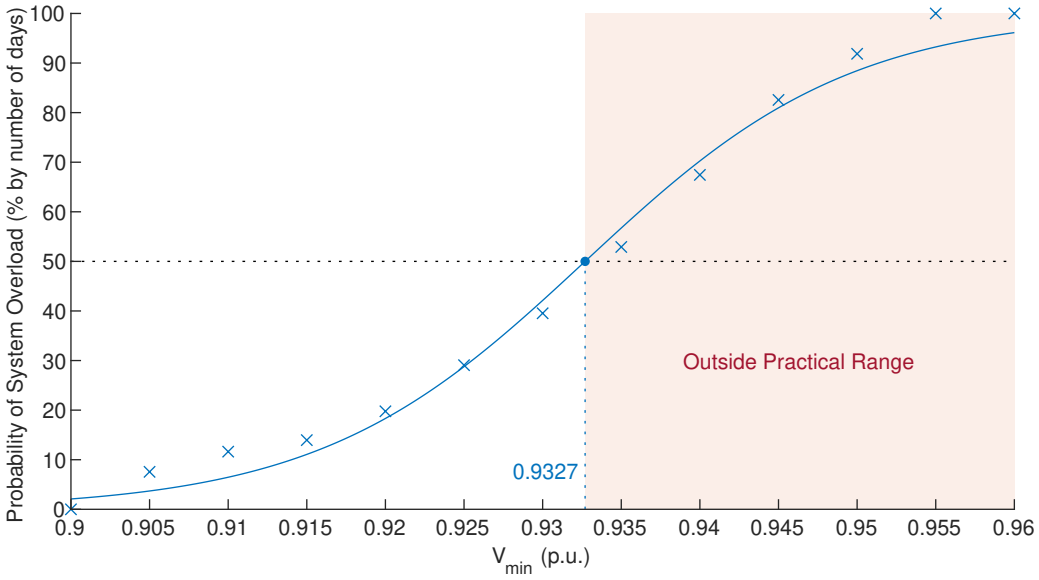

Figure 3.14: CUR - Probability of system overload with increasing $V_{\min}$.

Percentage overload over the 172 days in each $V_{\min}$ category is shown in Fig. 3.14. There is little difference between update intervals here, so only the curve for $t_u = 10$min is shown. Since this percentage cannot be less than 0% and cannot be larger than 100%, the probability is approximated by the logistic curve of the form

$$\boldsymbol{p}(V_{\min}) = \frac{1}{1 + e^{-\alpha(V_{\min} - \beta)}} \tag{3.5.1}$$

where shaping variables α and β are found via generalised least squares regression. This allows the maximum sustainable $V_{\min}$ to be extrapolated, showing that

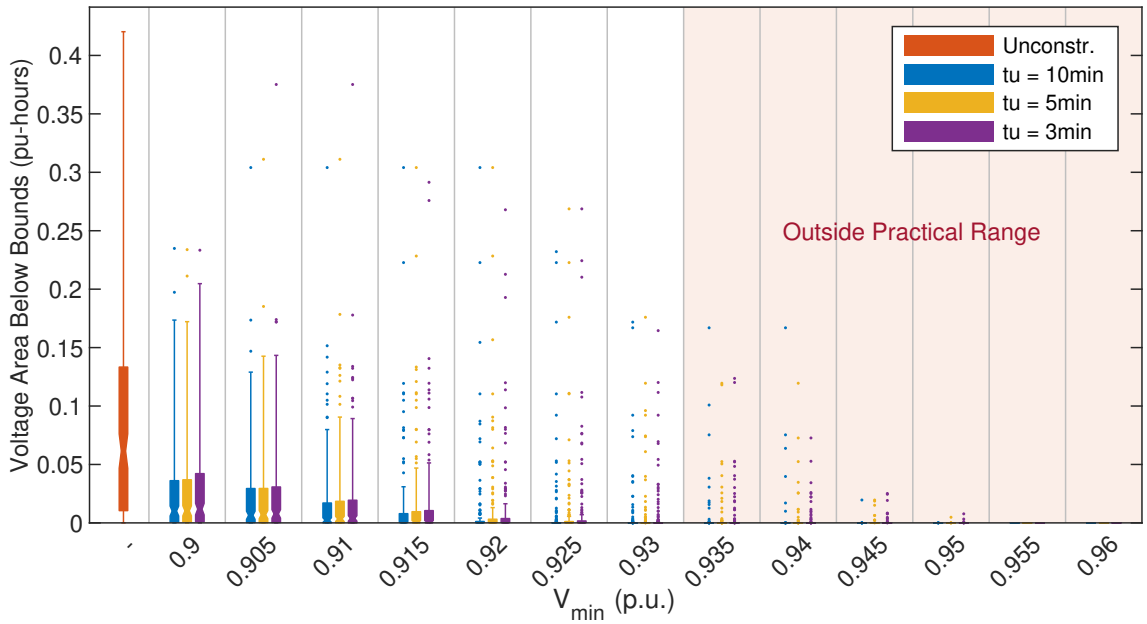

(a) Voltage Area Below Bounds for varying $V_{\min}$ (units pu-hours).

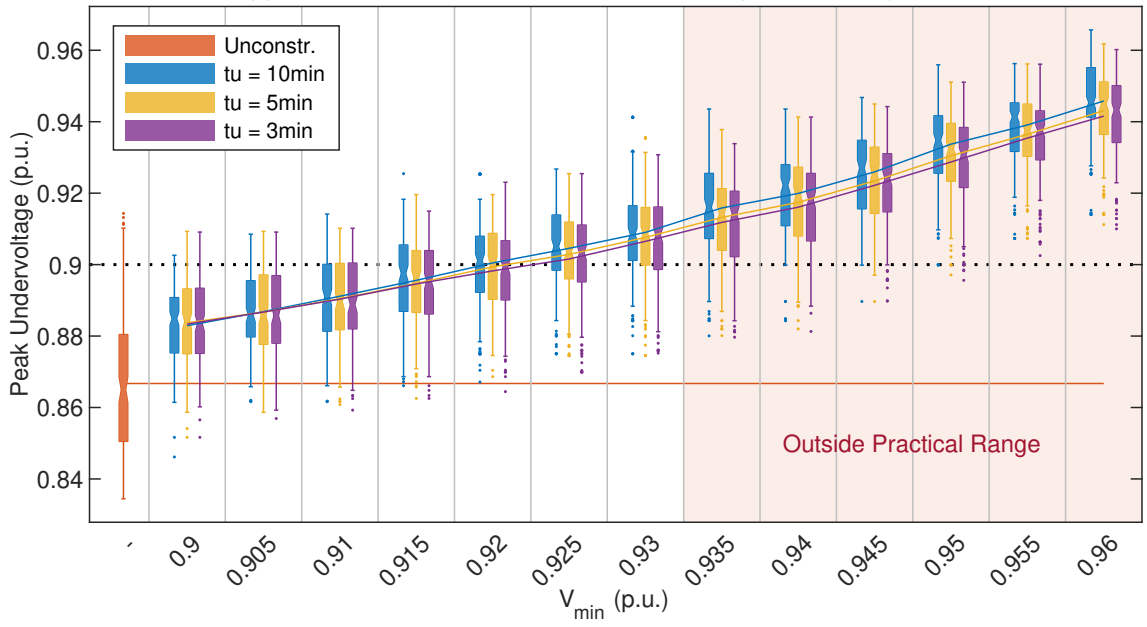

(b) Peak Daily Minimum Voltage for varying $V_{\min}$

Figure 3.15: CUR - Voltage performance of P-CMR.

$V_{\min} > 0.9327$pu cannot practically be sustained in this network arrangement since the 80% EV penetration is then beyond practical charging capacity $\eta_{\text{EV}}^{\max}$. However, data points above this boundary still provide useful for analysing key performance relationships, so are continued below.

Voltage Control

Voltage control is assessed via voltage area above and below bounds, as well as peak upper and lower voltage. These are shown in box and whisker plots for $V_{\min}$ and $V_{\max}$ in Fig. 3.15 and 3.16.

Beginning with $V_{\min}$, in Fig. 3.15, clearly voltage deviations below the statutory limit decrease as $V_{\min}$ increases. Voltage area below bounds, shown Fig. 3.15a, decreases to almost zero for $V_{\min} \geq 0.92$pu. Peak undervoltage, shown Fig. 3.15b, also undergoes a steady upward trend. Voltage deviation under P-curtailment is primarily attributable to CD, which is not affected by system update interval, so there only small visible effect from t_u in both metrics. Since, as described in Sec. 3.4.1, using a smaller update interval reduces overcurtailment in the system, a smaller t_u leads to curtailment marginally closer to the statutory limit, which increases the likelihood of deviation below bounds. For this reason, peak undervoltage is slightly lower, and area below bounds slightly higher, for $t_u = 3$min. Nevertheless, the difference is slight.

The practical range of $V_{\min}$, shown by the region outside the shaded red, indicates it is not possible to entirely remove voltage deviations out of bounds for 80% EV penetration with this scheme configuration alone. Practically, this could be dealt with by a number of additional mitigating processes, one of which is the COR scheme developed in Chap. 4. Alternatively, $V_{\min}$ could be adjusted daily according to expected DG profile.

G-CMR, on the upper voltage bound $V_{\max}$ shown Fig. 3.16, mirrors the effects seen on $V_{\min}$. First, referring to Fig. 3.16a, since the effect of TD is large and CD comparatively small under G-curtailment, the majority of voltage area above bounds occurs during the TD spike. This is overall smaller than the area below bounds, which is principally dependent on CD and deviates over a longer time period. For this reason, voltage area above bounds begins small and falls away sharply.

Peak overvoltage follows a steady downward trend with increasing $V_{\max}$, but is

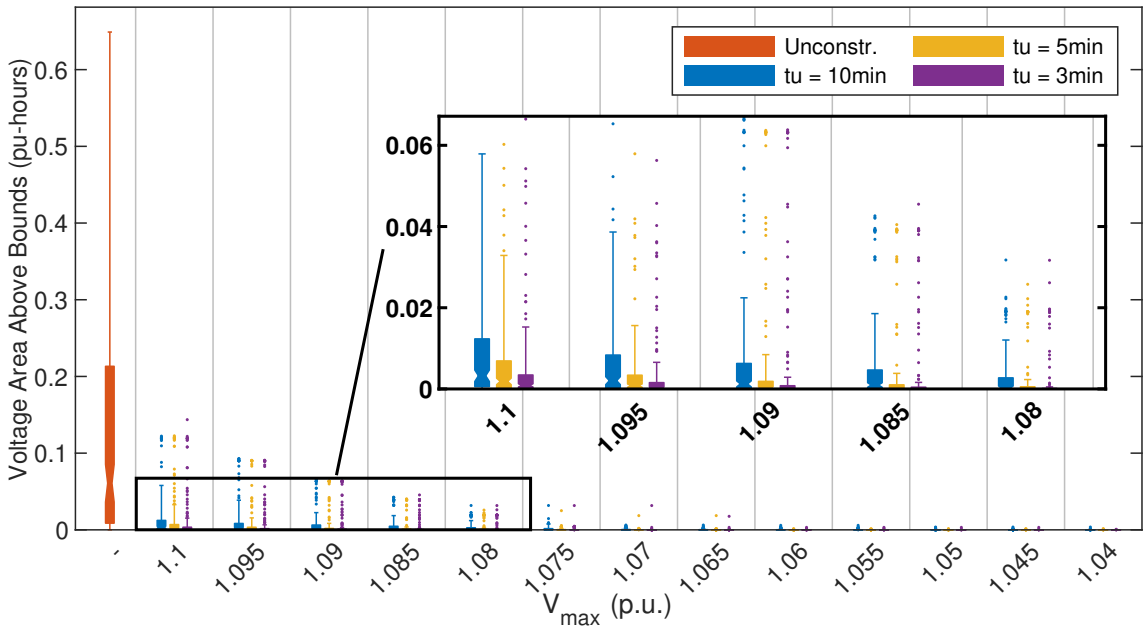

(a) Voltage Area Above Bounds for varying $V_{\max}$ (units pu-hours).

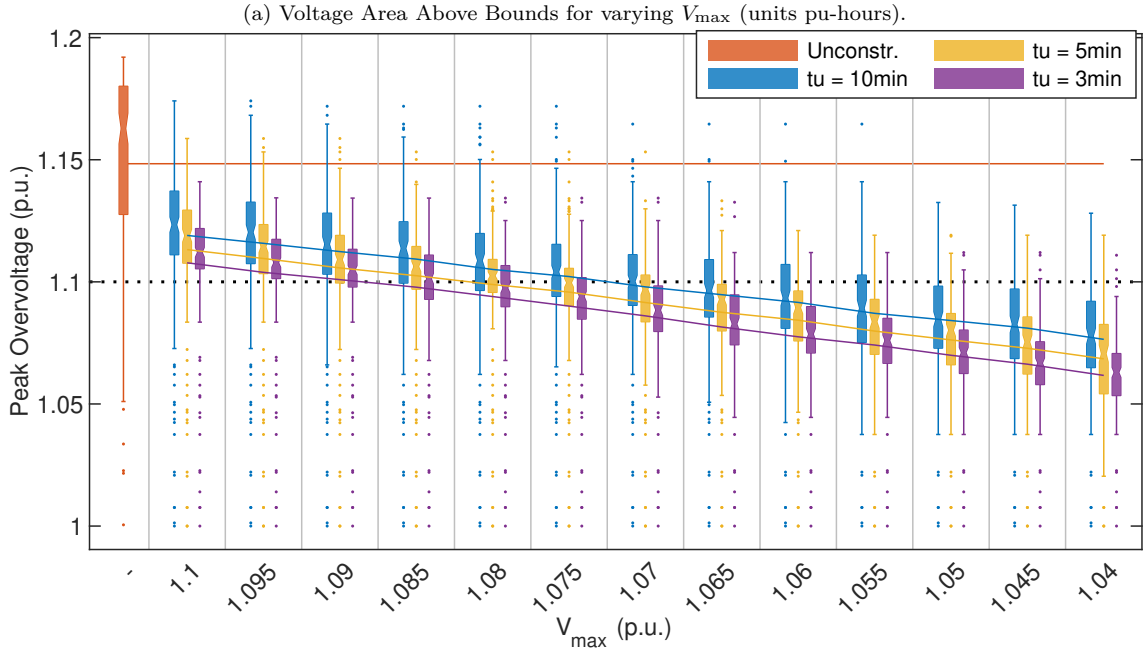

(b) Peak Daily Maximum Voltage for varying $V_{\max}$

Figure 3.16: CUR - Voltage performance of G-CMR.

never fully eliminated. This is due to the volatile nature of the DG input source, and is compounded by its concentration at the end of the feeder. In addition to a steady reduction in peak deviations with $V_{\max}$, there is also high correlation with t_u in every category. This is because TD forms the major source of overvoltage and is mitigated by IR.

These figures show that CUR can decisively improve both voltage control factors over the unconstrained system, demonstrating it is an effective means for voltage

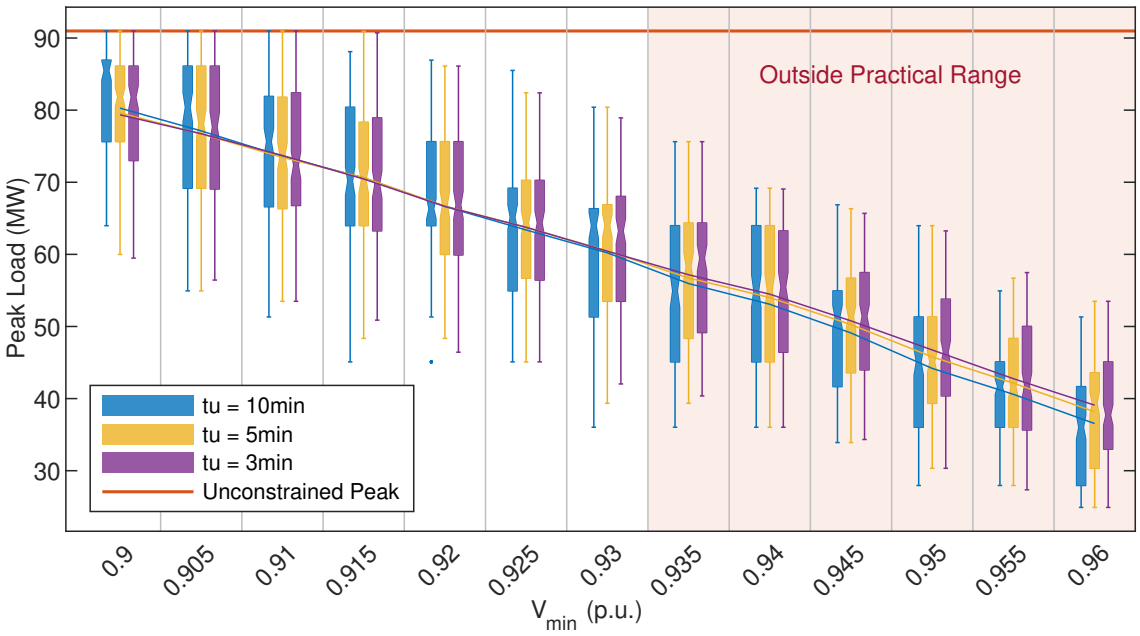

Figure 3.17: Daily Peak Load

control in higher EV and DG penetrated networks.

Peak Shaving

The CUR scheme can significantly improve voltage control; however, key performance tradeoffs are displayed in the power demand profile. Peak load under varying $V_{\min}$ is shown Fig. 3.17. Curtailment in CUR requires that overall power demand is always less than or equal to the unconstrained peak, therefore CUR will by definition effectively serve to reduce expected peak load in the network. Naturally then, increasing $V_{\min}$, i.e. increasing the severity of P-CMR, will reduce peak load. This is important since power hardware is normally sized according to peak load, and reducing this peak may serve to cut implementation and operating costs.

User Inconvenience

Curtailing load and DG comes at cost to user experience.

EV Charging Delay: Since EV users require high power demand to charge their vehicles quickly curtailing load leads to charging delays. The average charging delay per EV user during peak hours is shown in Fig. **??**, which clearly increases

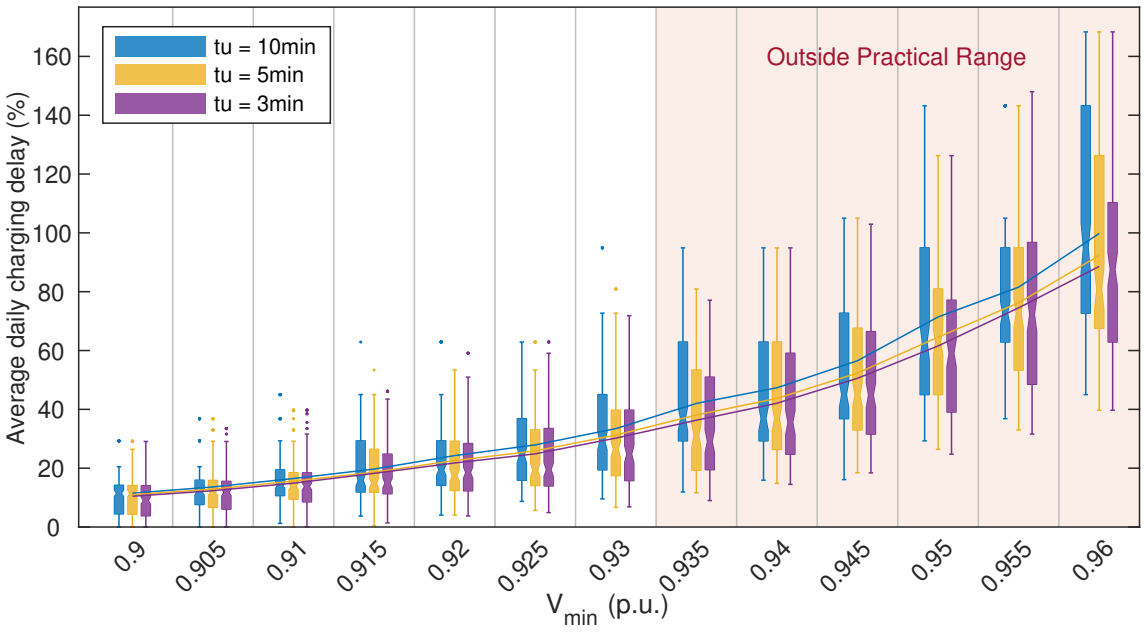

Figure 3.18: Average Charging Delay per EV User

with severity of curtailment. This presents a key tradeoff of the CUR scheme - that a reduction in peak load must be accompanied by an increase in EV charging times. Further, peak load follows a roughly linear downward trend, while charging delay rises exponentially upwards. Increasing $V_{\min}$ from 0.9 to 0.93pu reduces peak load by 25%, and EV charging delay rises from 10% to 30%. Increasing $V_{\min}$ to 0.96pu reduces peak load by the same amount again, but delay then increases to 90% during peak hours. Clearly, this is a key compromise for the system designer.

Here, again, a roughly proportional statistical relationship is displayed between different t_u values, since a higher update interval tends towards overcurtailment. The mean EV charging delay for $t_u = 10$min is consistently higher than that for $t_u = 5$min, which is in turn consistently higher than 3min. A shorter update interval raises the average curtailment power, which leads to marginally lower average charging delay in the system.

DG Energy Input: The overall daily energy supply from DG is shown Fig. 3.19. This is important from the perspective of investment in renewable systems, since energy delivery from renewable sources must be maximised in order to improve return on equipment, instalment and maintenance costs.

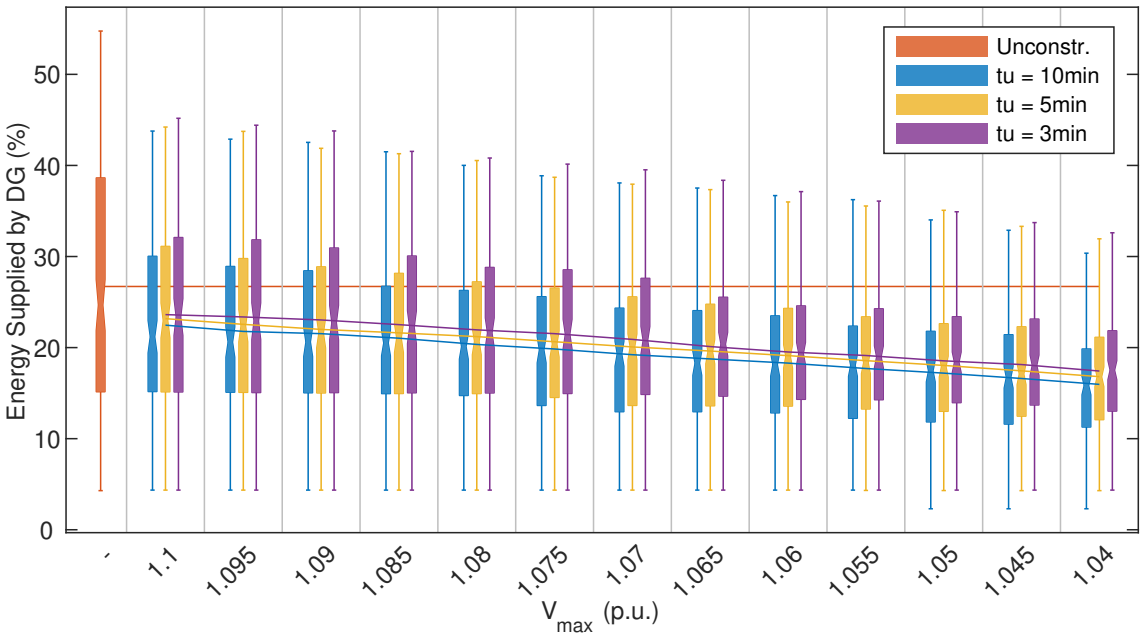

Figure 3.19: CUR - DG input under CMR for varying $V_{\max}$.

Increasing severity of G-CMR is accompanied by a reduction in overall renewable energy supply since DG is curtailed to a lower value; however, the gradient is shallow, dropping from ∼23% at $V_{\max}$ =1.1pu to ∼17% at $V_{\max}$ =1.04pu. Over all categories, DG supply is between 3-10% lower than the unconstrained input.

Peak DG is reduced as t_u decreases since the TD spike is mitigated; however, the value to which it is curtailed is on average higher since DG input is also retracted to a more recent power value. Here, using $t_u = 3$min leads to on average 3% more energy being supplied by renewables than $t_u = 10$min, consistent across all severities of G-CMR.

These figures show that the CUR scheme is inevitably accompanied by a statistical reduction in distributed renewable output. This is a key tradeoff to its voltage control and DG hosting capacity benefits. Since voltage control is improved under the CUR scheme, higher nominal DG capacity can be accommodated meaning that installation of more renewable generation units can be permitted by the DSO. However, since this DG must be routinely curtailed to deliver voltage constraints, the return on investment seen from each additional renewable energy system decreases. This is an important performance metric in cost analysis of energy supply and vital for

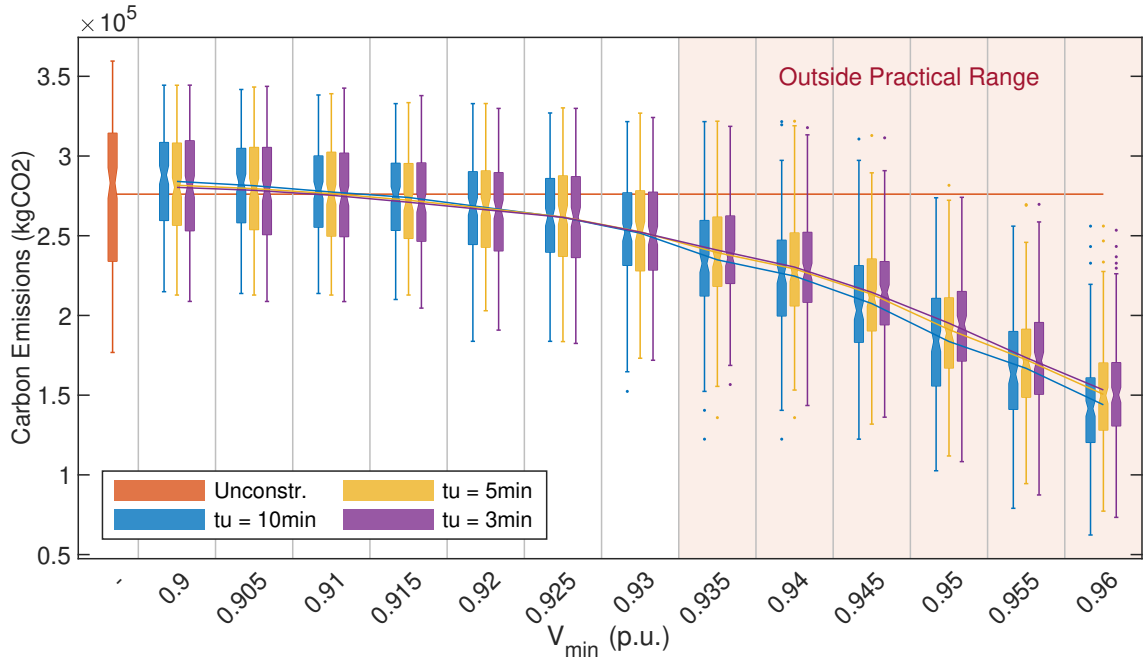

(a) Total Daily CO_2 Emissions for $V_{\min}$.

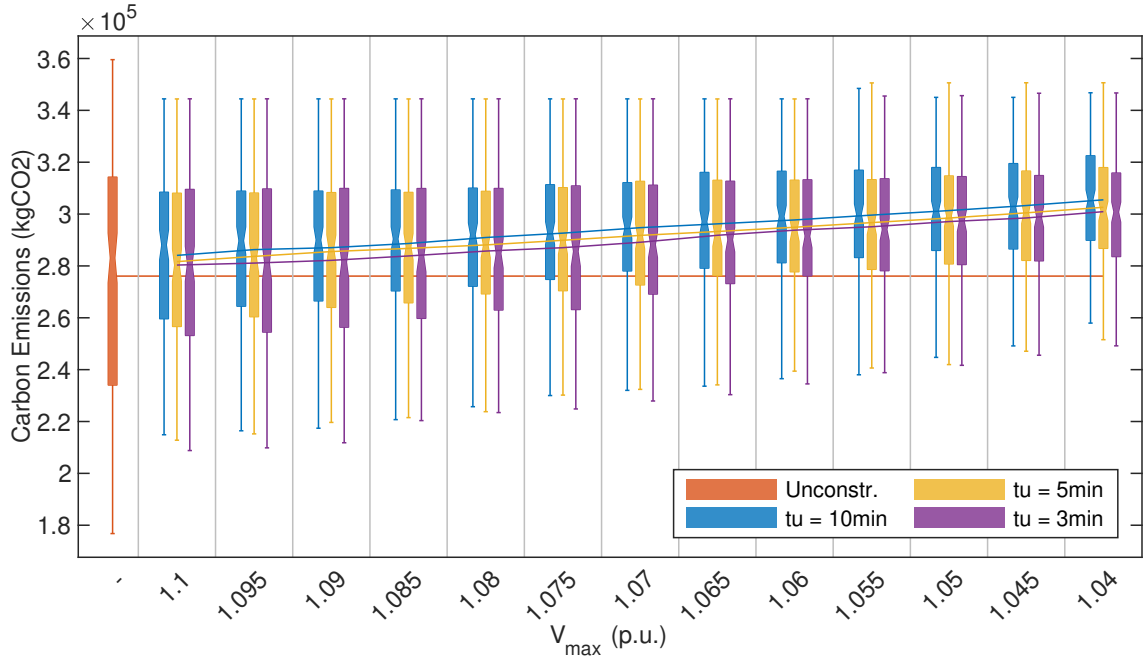

(b) Total Daily CO_2 Emissions for $V_{\max}$.

Figure 3.20: CUR - Carbon Emissions of CMR.

targeted schemes to incentivise household renewable generation.

CO_2 Emissions

Finally, assuming that all non-distributed power supplied to the distribution network (i.e. through the slack bus 1) follows the average daily carbon emissions curve shown

in Fig. 3.2, daily emissions of CO_2 was extracted for each simulation day. This is shown Fig. 3.20.

Unconstrained peak loading hours begin around 9.30am and persists through to roughly 8pm. P-curtailment reduces this peak by delaying excessive power demand into off-peak hours in the night and early morning, which also coincides with times of lowest CO_2 emissions. Increasing the severity of P-curtailment (i.e. increasing $V_{\min}$) pushes more power demand later into these off-peak emission hours and therefore reduces overall CO_2 emissions, as shown Fig. 3.20a.

In contrast, the opposite relationship is seen for G-curtailment. Assuming excessive DG is not stored or otherwise reused, curtailing renewable input will only serve to reduce the daily proportion of energy supplied by renewable sources. This energy is instead supplied from the conventional transmission network, leading to higher CO_2 emissions overall. In turn, these increases are roughly counteracted by the reductions seen from P-curtailment if heavy CMR is employed in both categories.

However, it must be noted that this increase in carbon emissions is in comparison to unconstrained DG input of the same 40MW magnitude, which is accompanied by unacceptable voltage and power instability. Compared to the system in Sec. 3.1.5 which had HC of 20MW only, the carbon emissions are greatly reduced due to overall higher renewable energy input. The CUR scheme achieves both voltage control and decreased carbon emissions due to higher DG penetration. But, excessive G-CMR will reduce these carbon savings.

This establishes another key performance-cost tradeoff. By reducing peak load and correspondingly the need for extensive hardware replacement throughout the distribution network, the CUR scheme presents attractive opportunities to cheaply raise DG penetration to meet carbon emission targets. Required voltage control, EV charging delay and renewable investment will decide the degree of P- and G-CMR in the system, and this must be balanced against associated savings in carbon emissions.

3.5.2 Interval Reduction (IR)

Properly calibrated CMR can effectively stabilise voltage deviations in highly EV and DG penetrated networks. However, G-curtailment is particularly vulnerable to TD spikes due to variability of the renewable input and its concentration at the end of the feeder. As a result, heavy G-CMR is required to effectively limit overvoltage, incurring losses in DG energy input and carbon emissions. IR can limit these TD spikes without heavy G-CMR and therefore gain advantage over the performance-cost tradeoffs identified in Sec. 3.5.1. However, system update interval is a key determinant in Deployment Cost. IR and performance under practical operational latency is used to evaluate this final KPI.

Deployment Cost

To evaluate this, t_u is varied from 10 to 2 minutes with four light G-CMR systems ($V_{\max}$ = 1.1, 1.09, 1.08 and 1.07pu, $V_{\min}$ = 0.9pu) in the same test system described in Sec. 3.5.1. Peak overvoltage, DG Energy input and CO_2 emissions is gathered for each of the 172 days of windpower inputs. These are plotted in Fig. 3.21.

The effect of IR on peak overvoltage is shown in Fig. 3.21a. Looking at the upper whisker in each category, this shows significant peak overvoltage improvement can be achieved. However, the primary advantages of IR are displayed in DG energy supply Fig. 3.21b and carbon emissions Fig. 3.21c. In each of these, a slight upward and downward trend, respectively, is noticeable, which are in the opposite directions to Fig. 3.19 and 3.20b where the slope is significantly steeper. This shows that IR can significantly reduce peak overvoltage without compromising renewable energy supply and carbon emissions which are key tradeoffs of G-CMR.

Since latency-sensitive performance characteristics of CUR are only visible at the curtailment trigger, it can be seen from Fig. 3.15-3.20 that all variables except peak overvoltage are a relatively weak function of t_u. As a result, IR can limit peak overvoltage while avoiding the tradeoffs inherent in CMR. However, IR inherently

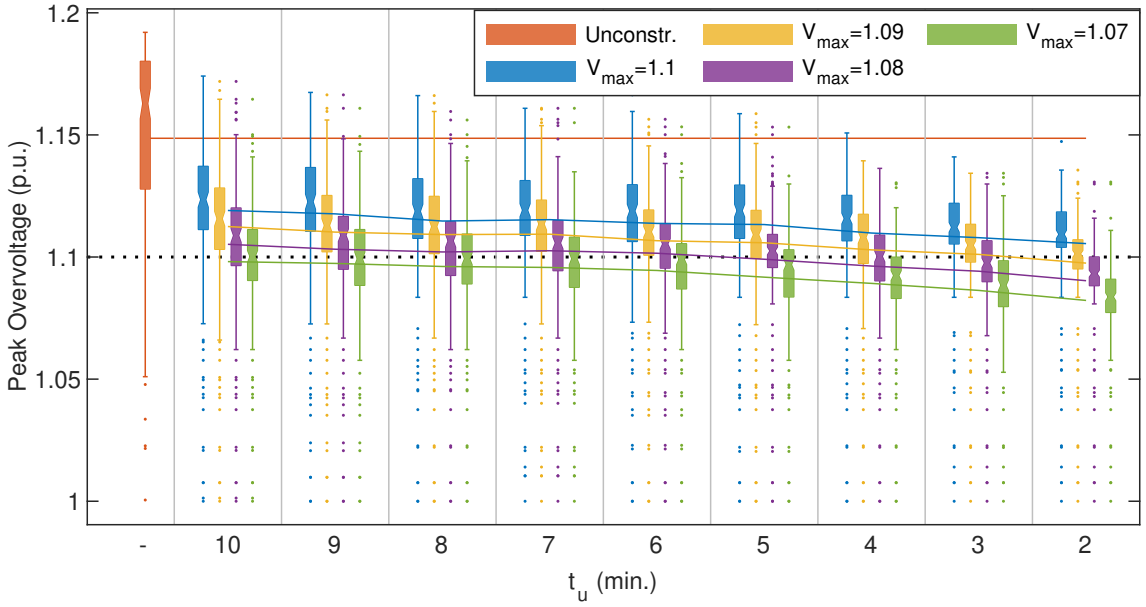

(a) Peak Daily Maximum Voltage.

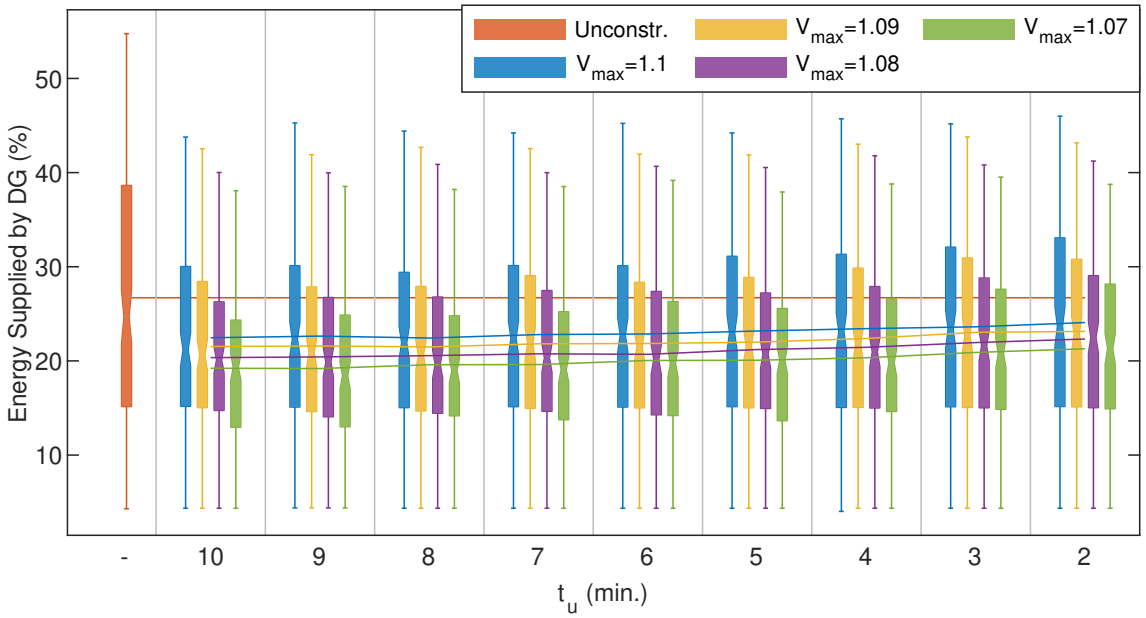

(b) Energy Supplied by DG.

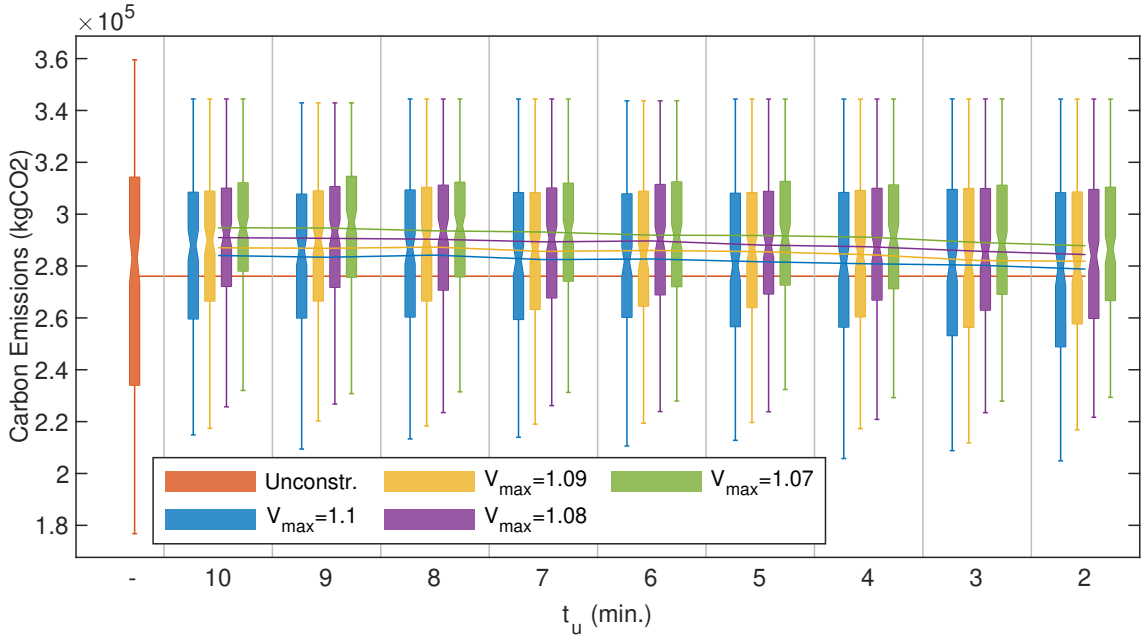

(c) Daily Average CO_2 Emissions.

Figure 3.21: CUR - Key Performance Variables under varying degrees of IR.

leads to increased data traffic in the system and burden on the underpinning ICT hardware that may require extensive replacement/reconfiguration. Reducing t_u from 10 to 2 minutes leads to 5 times the data traffic in the same time interval. Cost of data collection is a key constraint in Smart Grid systems that will grow as the number of served users and Smart Devices increases. Balance between IR and CMR forms the final cost-performance tradeoff.

3.6 Conclusion

The growing penetration of EVs is driving sharper spikes in consumer power demand. Meanwhile, growing renewable DG is driving sharper spikes in localised power supply. This leads to question how to keep the grid running within tolerable limits. Smart Charging schemes provide a way to adjust consumer power demand according to grid requirements. This chapter proposes a curtailment-based Smart Charging scheme using a laconic, scalable and efficient communications architecture that can simultaneously achieve voltage control and peak shaving in the network. This is optimised for the network operator, since peak shaving allows for higher EV penetration to be tolerated with minimal hardware replacement.

The contributions of this chapter are as follows:

- A curtailment-based Smart Charging scheme (Smart Curtailment, CUR) is designed for peak shaving and voltage control in the distribution network. This allows minimal hardware replacement and lower operating costs along with simultaneous increase in EV and DG capacity.
- The scheme uses a distributed hierarchical communications architecture that jointly minimises centralised computation and ICT traffic load by offloading coordination of demand-response assets onto regional Intermediary Control Units (ICUs). It is also compatible with existing open Smart Charging communications standards such as OCPP and OpenADR, and is therefore scalable

and adaptable to a wide range of network sizes and asset arrangements.

- Practical operational latency constraints on KPIs are modelled and two latency-mitigation strategies are identified.

- Key cost-performance tradeoffs are evaluated for the following KPIs: Voltage Control, Peak Shaving, User Inconvenience, DG Energy Input, CO_2 Emissions and Deployment Cost.

CMR was shown to effectively limit voltage deviations about both upper and lower boundaries while simultaneously reducing peak load in the system. This has the advantage of reducing the need for hardware replacement and, correspondingly, implementation and operating costs compared to unconstrained rise in EV and DG penetration. However, this comes at the cost of other KPIs.

P-CMR leads to exponentially increased EV charging delays for users in the system. This is important since user participation is key in any Smart Charging scheme and inconvenience to subscribers is an essential cost constraint. By delaying EV charging load to the night and early morning, *P*-CMR also reduces carbon emissions.

G-CMR reduces daily DG input, effectively limiting the return on investment in renewable generation. This is an inconvenience to users who are expecting a specific payback time on their household renewable system. Further, this reduction in renewable supply also leads to increase in carbon emission.

G-curtailment is highly sensitive to TD spikes due to variation in renewable supply and its concentration at the end of the feeder. Heavy *G*-CMR is required to effectively eliminate overvoltage. Alternatively, IR can reduce peak overvoltage without the negative effects on DG Energy Input and Carbon Emissions. However, this in turn incurs a cost-performance tradeoff by transferring the burden to Deployment Cost.

3.7 Evaluation

The work in this chapter can be aptly compared with several studies in the literature. These can be categorised in to two categories: Smart Charging schemes for Peak Shaving and Smart Charging Control Architecture.

3.7.1 Peak Shaving

In [48], a fast converging distributed demand-response method for Smart Charging is proposed for peak shaving in the distribution network. It incorporates arrival time, departure time and charging time to model EV availability and charging demand in dwillings, then integrating resulting randomness for deterministic demand-response techniques. In this way it investigates effects of charging-discharging rate on peak demand and how this shapes aggregated demand profile. However, for the model to work, users must set a deadline by which a certain amount of energy should be stored in the EV batteries for the next journey, and it assumes the requested charging task is feasible during the EV's connection to the grid. Only peak shaving is considered as a KPI and load profile assumes a constant hourly rate. Further, the system is implemented without DG.

In [44], a real-time Smart Charging algorithm is proposed to coordinate multiple EV charging activities for loss minimisation, voltage control and peak shaving. Users must choose from three designated charging time zone priorities: Red (18.00-20.00), Blue (20.00-01.00) and Green (01.00-08.00). The scheme then performs minimises cost of generation and losses every update period based on real-time energy price information and preferred charging time zones based on priority. The algorithm incorporates optimisation complexity, using Maximum Sensitivities Selection by Jacobian approximation instead of conventional (e.g. genetic algorithm) techiques. Voltage control and peak shaving are considered, and user inconvenience is roughly accounted for via time zone priorites; however, charging delay is not explicitly modelled and it is unclear how to handle users who cannot charge their vehicles

during their preferred time zone due to network constraints. No DG is incorporated and the effect of system update interval on performance is not considered (only $t_u = 5$min is used). Requirement for a "high speed bidirectional communications network" is mentioned, but no ICT architectural solution is proposed.

In [22], a fuzzy logic-based strategy for charging EVs in a residential distribution system is proposed such that system minimum voltage is kept within allowable operating limits. This achieves satisfactory results in terms of daily voltage profile and losses without the need for an optimisation solver; however, optimality is not guaranteed. Only energy price and voltage control are considered and update interval remains constant at $t_u = 15$min. No DG is incorporated and there is no consideration for user fairness in the power allocation algorithm.

All these studies present Smart Charging solutions for a small set of KPIs. None of them consider the comprehensive list of KPIs modelled in this thesis: Voltage Control, Peak Shaving, User Inconvenience, Carbon Emissions and ICT Deployment Cost. Further, all these studies assume perfect knowledge of energy prices, driving patterns and network load is available everywhere in the network instantly and that control actions can be actuated without delay. There is no consideration for how practical operational latency affects each respective KPI, and it remains unclear how sensors and actuators within the schemes should be efficiently implemented via supporting ICT architecture. This chapter delivers on all of these issues.

3.7.2 Communications & Control Architecture

In [75] a distributed Smart Charging power optimisation problem is formulated based on dual decomposition, showing it to rapidly converge from large disturbances to a stable operating point. In the test system, EV capacity was improved from 70 to 700 EVs. Latency resulting from convergence time and control action period is modelled, and delay from communications overhead under fast control timescales is mentioned only. However, practical operational latency resulting from accumulations in the

sense-compute-actuate demand-response cycle are unquantified and its effects on performance are not considered. The study assumes the communication network is "ubiquitous, broadband, reliable and low latency", and that measurement, communications and control nodes can detect bus conditions sufficiently quickly such that all parameters remain within system tolerances. These are key assumptions challenged in this thesis.

Finally, [74] proposes and evaluates a new Smart Charging controller inspired by the slow start mechanism of TCP on the Internet. A comparison scenario follows between solutions based on On Load Tap Changers and Smart Charging voltage control. While this paper mentions sources of delay in response time of a Smart Charging load controller in the introduction, it does not quantify nor analyse effects of this delay on KPIs in the proposed system.

3.8 Summary

First, the system model was described. Household and EV charging power profiles are quantified based on real-world statistical studies. Hourly CO_2 emissions data averaged over the month of February 2020 is shown to strongly correlate with these expected power profiles. Smart Charging presents marked opportunities for peak shaving and carbon emissions reduction since average daily profiles of households, EV charging and CO_2 emissions share roughly similar peak and off-peak timings.

The IEEE 33 bus MV distribution test feeder was then outlined. Each bus in the distribution system supplies a LV residential feeder. The number of houses served by the network is allocated such that non-flexible (household) load brings the minimum worst bus voltage to statutory limits. Thus the test system is unable to tolerate any additional unconstrained EV penetration without voltage deviation below acceptable limits.

DG is then introduced. DG capacity is defined as the upper limit of DG such that maximum bus voltage does not exceed 1.1pu. Wind power generation profiles are

derived from 172 days of 1s windspeed data, with power extracted via wind turbine power curve. This allows a generation profile to be applied to the system based on physical data readings. Noting that problems relating to overvoltage are most noticeable when DG is concentrated at the end of a long feeder, a wind farm input is added at the end of the feeder and unconstrained DG capacity is established.

The communications architecture to support the proposed Smart Charging scheme is then designed. In line with recent Smart Loading communications standards, the scheme uses a distributed three-tier hierarchical topology. The CCU is the central network coordinator, which is connected to an ICU at each distribution bus. ICUs are mid-tier nodes, which coordinate actuators and aggregate sensor readings in their regional area via connection to SDs. Practical latency issues are then discussed. System update interval is identified as a key constraint relating to budget limitations in the underpinning ICT system, and is compounded in the near future by lack of homogeneity across SDs in the industry.

The proposed Smart Curtailment (CUR) scheme is then presented in detail, beginning with operation under zero latency. P-curtailment of EV charging load as a means for voltage control is illustrated, along with effect on peak load and EV charging delay. The P-curtailment scheme is shown to support 81% EV penetration with no rise in peak load from non-flexible loading conditions.

G-curtailment is then shown to significantly improve DG capacity in the system by supporting a 62MW wind farm input at the end of the feeder. Continuous voltage Deviations (CD) are identified due to fluctuations in the unconstrained power variable and CMR is demonstrated as a solution.

Practical latency is then introduced in the CUR scheme by way of a 10 minute update interval. This is shown to produce voltage deviation spikes at the curtailment trigger (Trigger Deviations, TD). In P-curtailment these are comparable in magnitude to CDs, so can be aptly mitigated by CMR. However, TDs in G-curtailment are large in magnitude. Two solutions to cope with this are explored. G-CMR is shown to effectively mitigate TD, however also leads to degraded DG energy input.

Alternatively, Interval Reduction (IR) can effectively mitigate TD without these drawbacks, however incurs additional burden on the ICT system.

Finally, the CUR scheme was tested against 172 days of wind profile input, and key performance-cost tradeoffs were identified. Overload probability was shown to define a practical upper limit on EV charging capacity and a useable range of $V_{\min}$. CMR is shown to effectively limit voltage deviations above and below bounds, and P-CMR achieves significant reduction in both peak load and carbon emissions. However, this comes at the cost of exponentially increasing charging delays for EV users during peak hours. Similarly, G-curtailment reduces daily renewable energy supply, limiting return on investment in renewable systems and increasing overall carbon emissions.

Interval reduction can gain strong advantage over the drawbacks of excessive G-curtailment by reducing peak overvoltage without compromising DG energy input. However, a tradeoff then ensues between Deployment Cost and the remaining KPIs.

The CUR scheme is shown to be an effective solution for voltage control in the distribution network, capable of dramatically increasing both EV and DG capacity while reducing peak load from unconstrained conditions. CMR and IR can be used to tailor the severity of voltage deviations under given targets for user inconvenience, renewable energy input, carbon emissions and deployment cost. These represent key performance-cost tradeoffs for the system operator. Chap. 4 will demonstrate that further advantage over these KPIs can be achieved by adjusting the optimisation objective.

Chapter 4

Smart Correction (COR)

In response to rising penetrations of EVs and DG, Smart Curtailment (CUR) was proposed in Chap. 3 relevant to voltage control and peak shaving in the distribution network. This achieved significant improvement in both the EV and DG capacity while limiting power hardware replacement, thereby reducing costs for the network operator.

However, optimisation objectives for the operator are not always aligned with those for consumers and/or investors in DG systems, who desire to maximise power transfer when it is cheap, e.g. during non-peak times or when renewable generation is strong. This chapter will show that by reformulating optimisation for energy consumers, significant gains in numerous KPIs can be achieved.

This chapter proposes a correction-based Smart Charging scheme (Smart Correction, COR) that can repetitively adjust EV charging load in the distribution network according to available DG. This allows optimum cost-efficiency of EV charging for subscribing users, maximised DG energy input for investors in renewable systems and reduced CO_2 emissions. It also allows for better voltage control, pronounced improvement in EV and DG capacity and enhanced resistance to practical latency effects.

The contributions of this chapter are as follows:

- An adaptive scheme (Smart Correction, COR) is proposed to optimally adapt EV charging load according to available DG input, maximising consumption of renewable energy when it is 'cheap' while maintaining technical voltage limits. This improves performance over various KPIs and achieves strong advantage over the cost-performance tradeoffs identified in Chap. 3.

- The COR scheme uses the same distributed multi-tier hierarchical ICT architecture from Chap. 3 and therefore maintains all of its corresponding advantages - jointly minimised computation and traffic load as well as scalability and adaptability to a wide variety of network sizes and asset arrangements.

- Practical latency constraints of this adaptation are evaluated, and COR is shown to deliver significantly enhanced operational latency mitigation compared to CUR.

- COR is evaluated statistically over 172 wind power profiles, and performance is directly compared with CUR. COR is capable of dramatically improving KPIs: Voltage Control, User Inconvenience, CO_2 emissions and Deployment Cost, as well as deliver higher EV and DG capacity. However, peak shaving is reduced. Key performance-cost tradeoffs in this regard are identified.

The rest of this chapter is laid out as follows. Sec. 4.1 defines the mathematical formulation of the COR scheme. Sec. 4.2 describes operation under zero latency, where key performance characteristics are highlighted and compared with CUR. Sec. 4.3 analyses practical latency constraints in the system and identifies three latency-mitigation solutions relevant to voltage control. Finally, performance of these latency-mitigation strategies is analysed statistically for 172 days of wind power profiles in Sec. 4.4, where performance is compared with CUR and critical cost-performance tradeoffs are discussed. Sec. 4.5 then concludes the topic.

4.1 Mathematical Formulation

COR uses the same ICT framework from Chap. 3, where curtailment is triggered by any bus voltage below $V_{\min}$ or above $V_{\max}$. However, under COR the limits $\overrightarrow{P}^{\max}$ and $\overrightarrow{G}^{\max}$ are repetitively corrected during curtailment to optimise power transfer. The mathematical framework for this is described as follows.

The voltage vector at any time is some function f of the load and DG vectors

$$\overrightarrow{V}[n] = f\Big(\overrightarrow{P}[n], \overrightarrow{G}[n]\Big) \tag{4.1.1}$$

where f will vary between networks with various static characteristics such as number of buses, network topology, line impedances, etc. Assuming small changes in the interval Δt, this can be sequentially approximated via first order Taylor series expansion

$$\overrightarrow{V}[n] = \overrightarrow{V}[n-1] + \boldsymbol{J}_f[n-1]\Big(\Delta\overrightarrow{P}[n] + \Delta\overrightarrow{G}[n]\Big) \tag{4.1.2}$$

$$\Delta\overrightarrow{P}[n] = \overrightarrow{P}[n] - \overrightarrow{P}[n-1] \tag{4.1.3}$$

$$\Delta\overrightarrow{G}[n] = \overrightarrow{G}[n] - \overrightarrow{G}[n-1] \tag{4.1.4}$$

where $\boldsymbol{J}_f[n-1]$ is the Jacobian evaluated at $\overrightarrow{V}[n-1]$, given

$$\boldsymbol{J}_f[n-1] = \begin{bmatrix} \frac{\delta V_1}{\delta P_1} & \frac{\delta V_1}{\delta P_2} & \cdots & \frac{\delta V_1}{\delta P_B} \\ \frac{\delta V_2}{\delta P_1} & \frac{\delta V_2}{\delta P_2} & \cdots & \frac{\delta V_2}{\delta P_B} \\ \vdots & \vdots & & \vdots \\ \frac{\delta V_B}{\delta P_1} & \frac{\delta V_B}{\delta P_2} & \cdots & \frac{\delta V_B}{\delta P_B} \end{bmatrix}\Bigg|_{\overrightarrow{V}[n-1]} \tag{4.1.5}$$

This model includes real power demand only, since statistical or historical data for household, EV and DG reactive power profiles is unavailable to the author at the time of writing.

Every update interval m during curtailment, a change in the limit vector $\Delta\overrightarrow{P}^{\max}[m]$ can be calculated to tailor a specific voltage vector $\overrightarrow{V}'$ in the network. Using (4.1.2),

this can be achieved with

$$\Delta\overrightarrow{P}^{\max}[m] = \boldsymbol{J}_f^{-1}[m]\Big(\overrightarrow{V}' - \overrightarrow{V}[m] - \boldsymbol{J}_f[m]\Delta\overrightarrow{G}[m]\Big) \tag{4.1.6}$$

Where $\overrightarrow{V}[m]$ and $\Delta\overrightarrow{G}[m]$ are gathered by sensor readings. The matrix $\boldsymbol{J}_f[m]$ can be computed in the interval $(m-1) < n < m$ by temporarily changing $P_b^{\max}[n]$ at each bus by a small increment and noting the small change in $\overrightarrow{V}[n]$.

How to optimally allocate $\Delta\overrightarrow{P}^{\max}$ and $\overrightarrow{V}'$ is then flexible to a number of power allocation algorithms mirrored in the literature, e.g. [22], [44], [46], [75], [77]. Computational effort is a strong concern. Eq. (4.1.6) involves complex $B \times B$ matrix operations which may become overly intensive for a large number of buses. Fairness is another. Simply maximising $\sum_{b=1}^{B} P_b^{\max}$ during curtailment may lead to disproportionate power concentration at specific low-sensitivity buses, with large queues occurring elsewhere in the network. The COR scheme considers both of these to achieve simultaneous computational savings and user fairness.

The scheme is formulated in two parts. First, behaviour in undervoltage is defined, where P-correction refers to correction of the curtailed EV charging load during P-curtailment. Next, behaviour in overvoltage (G-correction) and simultaneous over- and under-voltage (PG-correction) is described using the same mathematical framework.

4.1.1 P-Correction (P-COR)

If unconstrained load and DG are such that only undervoltage occurs in the system, only charging load need be curtailed and DG can be left unconstrained. In COR, $\overrightarrow{P}^{\max}$ is adjusted every update interval by a correction vector $\Delta\overrightarrow{P}^{\max}[m]$.

$$\overrightarrow{P}^{\max}[m] = \overrightarrow{P}^{\max}[m-1] + \Delta\overrightarrow{P}^{\max}[m] \tag{4.1.7}$$

Choice of $\Delta\overrightarrow{P}^{\max}$ is key, since it must serve to maximise overall power delivery incumbent to variable DG, while keeping all bus voltages within bounds. It must

also serve to maintain fairness in the network, distributing the available power evenly between buses.

To manage fairness, a curtailment condition is enforced such that the change $\Delta P_T = \sum_{b=1}^{B} \Delta P_b^{\max}$ must be implemented proportionally on each bus, i.e.

$$\Delta \overrightarrow{P}^{\max}[m] = \begin{bmatrix} k_1 \\ \vdots \\ k_B \end{bmatrix} \Delta P_T[m], \quad \sum_{k=1}^{B} k_b = 1 \tag{4.1.8}$$

where k_b are constants taken at the curtailment trigger m_P proportional to power demand at each bus. Load correction every update interval can then be formulated

$$\max \qquad \Delta P_T[m] \tag{4.1.9a}$$

$$\text{s. t.} \qquad \overrightarrow{V}[m] \geq V_{\min} \tag{4.1.9b}$$

This is achieved by reformulating (4.1.1) and (4.1.2)

$$\overrightarrow{V}[n] = f\Big(P_T[n], \overrightarrow{G}[n]\Big) \tag{4.1.10}$$

$$\overrightarrow{V}[n] = \overrightarrow{V}[n-1] + \boldsymbol{J}_{P_T}[n-1]\Delta P_T[n] + \boldsymbol{J}_f[n-1]\Delta\overrightarrow{G}[n] \tag{4.1.11}$$

where $\boldsymbol{J}_{P_T}$ can be calculated from $\boldsymbol{J}_f$ via weighted row addition

$$\boldsymbol{J}_{P_T}[n-1] = \left.\begin{bmatrix} \frac{\delta V_1}{\delta P_T} \\ \vdots \\ \frac{\delta V_B}{\delta P_T} \end{bmatrix}\right|_{\overrightarrow{V}[n-1]} = \left.\begin{bmatrix} \sum_{b=1}^{B} k_b \frac{\delta V_1}{\delta P_b} \\ \vdots \\ \sum_{b=1}^{B} k_b \frac{\delta V_B}{\delta P_b} \end{bmatrix}\right|_{\overrightarrow{V}[n-1]} \tag{4.1.12}$$

The vector $\boldsymbol{J}_{P_T}$ is useful since it eliminates the need to compute a $B \times B$ matrix inverse as in (4.1.6), significantly reducing the computations required.

The maximum in (4.1.9a) occurs when $V_b^{\text{low}}[m] = V_{\min}$, therefore the correction $\Delta\overrightarrow{P}_T[m]$ must be such that it brings the worst bus voltage to technical limits. The question is then which bus to choose as the worst bus, since it is important that the correction $\Delta\overrightarrow{P}_T[m]$ does not bring another bus voltage out of bounds.

By rearranging (4.1.11), a change $\Delta P_{T_b}[m]$ can be defined for each bus that will

bring each $V_b[m]$ to $V_{\min}$

$$\begin{bmatrix} \Delta P_{T_1}[m] \\ \vdots \\ \Delta P_{T_B}[m] \end{bmatrix} = \begin{bmatrix} \frac{V_{\min} - V_1[m] + \sum_{b=1}^{B} \frac{\delta V_1}{\delta P_b}\Big|_{\vec{V}[m]} \Delta G_b[n]}{\frac{\delta V_1}{\delta P_T}\Big|_{\vec{V}[m]}} \\ \vdots \\ \frac{V_{\min} - V_B[m] + \sum_{b=1}^{B} \frac{\delta V_B}{\delta P_b}\Big|_{\vec{V}[m]} \Delta G_b[m]}{\frac{\delta V_B}{\delta P_T}\Big|_{\vec{V}[m]}} \end{bmatrix} \tag{4.1.13}$$

The optimum is then the smallest (most negative) correction.

$$\Delta P_T[m] = \min_b \Big[\Delta P_{T_1}[m], \dots, \Delta P_{T_B}[m]\Big]. \tag{4.1.14}$$

This ensures the new worst bus voltage is always $V_{\min}$.

To summarise, the COR scheme calculates the change in power limit $\Delta P_T[m]$ that will maximise power transfer such that the worst bus voltage V_b^{low} is 'corrected' to the limit $V_{\min}$. This is performed at the CCU every update interval during curtailment based on voltage and DG inputs $\overrightarrow{V}[m], \overrightarrow{G}[m]$ received from the ICUs. Power limits for each bus are then sent out to ICUs individually, who distribute the new available power limit between their associated SDs.

The change $\Delta P_T[m]$ represents the total change in curtailed power limit distributed proportionally on each bus. If any individual ICU_b is unable to meet their power limit $P_b^{\max}[m]$, this will raise V_b^{low} above $V_{\min}$, so the voltage will stay within bounds. The reduced power $P_b[n]$ can then be sent to the CCU on the next control iteration, and k_b updated accordingly such that the power limits at the remaining buses will increase. Therefore the scheme is robust to non-uniform loading patterns within one iteration phase.

4.1.2 G-Correction (G-COR)

Since generation is equivalent to negative load in the system, the same mathematical framework can be applied to correct the limit $\overrightarrow{G}^{\max}$ according to variable load inputs. Certain steps will be skipped in this derivation to avoid excessive repetition.

If unconstrained $\overrightarrow{P}[n]$ and $\overrightarrow{G}[n]$ are such that only the overvoltage limit is breached, only $\overrightarrow{G}[n]$ need be curtailed to prevent overvoltage and $\overrightarrow{P}[n]$ can remain unconstrained. G-COR is triggered at $m = m_G$ following the overvoltage event, where $\overrightarrow{G}^{\max}$ is the vector of upper generation limits for each bus. During G-COR, $\overrightarrow{G}^{\max}$ is corrected every update interval by change $\Delta\overrightarrow{G}^{\max}$

$$\overrightarrow{G}^{\max}[m] = \overrightarrow{G}^{\max}[m-1] + \Delta\overrightarrow{G}^{\max}[m] \tag{4.1.15}$$

To do this, (4.1.1) and (4.1.2) can be reformulated

$$\overrightarrow{V}[n] = f\Big(\overrightarrow{P}[n], G_T[n]\Big) \tag{4.1.16}$$

$$\overrightarrow{V}[n] = \overrightarrow{V}[n-1] + \boldsymbol{J}_f[n-1]\Delta\overrightarrow{P}[n] + \boldsymbol{J}_{G_T}[n-1]\Delta G_T[n] \tag{4.1.17}$$

Where fairness condition is enforced

$$\Delta\overrightarrow{G}^{\max}[m] = \begin{bmatrix} l_1 \\ \vdots \\ l_B \end{bmatrix} \Delta G_T[m], \quad \sum_{l=1}^{B} l_b = 1 \tag{4.1.18}$$

Jacobian $\boldsymbol{J}_{G_T}$ is defined

$$\boldsymbol{J}_{G_T}[n-1] = \left.\begin{bmatrix} \frac{\delta V_1}{\delta G_T} \\ \vdots \\ \frac{\delta V_B}{\delta G_T} \end{bmatrix}\right|_{\overrightarrow{V}[n-1]} = \left.\begin{bmatrix} -\sum_{b=1}^{B} l_b \frac{\delta V_1}{\delta P_b} \\ \vdots \\ -\sum_{b=1}^{B} l_b \frac{\delta V_B}{\delta P_b} \end{bmatrix}\right|_{\overrightarrow{V}[n-1]} \tag{4.1.19}$$

and l_b are constants determined at the G-COR trigger according to available power generation at each bus. It is desirable to maximise renewable generation in the network at any given time, so the correction can be formulated

$$\max \qquad \Delta G_T[m] \tag{4.1.20a}$$

$$\text{s. t.} \qquad \overrightarrow{V}[m] \leq V_{\max} \tag{4.1.20b}$$

I.e. the correction $\Delta G_T[m]$ is chosen every update interval such that it brings $V_b^{\text{high}} = V_{\max}$. To do this, as in (4.1.13), the change $\Delta G_{T_b}[m]$ can be defined for each

bus that will bring each $V_b[m]$ to $V_{\max}$

$$\begin{bmatrix} \Delta G_{T_1}[m] \\ \vdots \\ \Delta G_{T_B}[m] \end{bmatrix} = \begin{bmatrix} \frac{V_{\max} - V_1[m] - \sum_{b=1}^{B} \frac{\delta V_1}{\delta P_b}\Big|_{\vec{V}[m]} \Delta P_b[n]}{\frac{\delta V_1}{\delta G_T}\Big|_{\vec{V}[m]}} \\ \vdots \\ \frac{V_{\max} - V_B[m] - \sum_{b=1}^{B} \frac{\delta V_B}{\delta P_b}\Big|_{\vec{V}[m]} \Delta P_b[m]}{\frac{\delta V_B}{\delta G_T}\Big|_{\vec{V}[m]}} \end{bmatrix} \tag{4.1.21}$$

Where the minimum (most negative) correction ensures the new maximum bus voltage is always $V_{\max}$

$$\Delta G_T[m] = \min_b \Big[\Delta G_{T_1}[m], \dots, \Delta G_{T_B}[m]\Big]. \tag{4.1.22}$$

G-COR and P-COR are similar bar a few minor differences. The change $\Delta G_T[m]$ represents change in overall generation limit distributed proportionally on each bus such that the maximum bus voltage does not exceed $V_{\max}$. This is performed at the CCU every update interval based on received voltage and DG sensor readings from each ICU. However, unlike P-COR, which is maintained until all delayed flexible load is satisfied, G-COR persists at each bus only while DG is available. If G_b falls below $G_b^{\max}[m]$ at any bus, unconstrained DG is resumed at that bus and V_b^{high} drops below $V_{\max}$. The reduced G_b is then reported back to the CCU on the next control iteration and l_b updated such that the generation limits at the remaining buses increase. Therefore the scheme is robust to fluctuations in DG between update periods and can adapt within one iteration period.

4.1.3 PG-Correction (PG-COR)

If both $\overrightarrow{P}[n]$ and $\overrightarrow{G}[n]$ continue to increase, eventually a voltage vector is reached that spans the full breadth of technical limits. I.e. there is simultaneously one bus voltage below $V_{\min}$ and another exceeding $V_{\max}$. In this case, both $\overrightarrow{P}[n]$ and $\overrightarrow{G}[n]$ must be curtailed simultaneously.

PG-COR is formulated by simultaneous correction equations for buses a and b,

where a is corrected to $V_{\max}$ and b is corrected to $V_{\min}$

$$\begin{cases} \overset{a,b}{\Delta G_T}[m] = \dfrac{V_{\max} - V_a[m] - \frac{\delta V_a}{\delta P_T}\overset{a,b}{\Delta P_T}[m]}{\frac{\delta V_a}{\delta G_T}} \\ \overset{a,b}{\Delta P_T}[m] = \dfrac{V_{\min} - V_b[m] - \frac{\delta V_b}{\delta G_T}\overset{a,b}{\Delta G_T}[m]}{\frac{\delta V_b}{\delta P_T}} \end{cases} \tag{4.1.23}$$

These can be solved for any bus combination (a, b) by substitution, since $\boldsymbol{J}_{P_T}$ and $\boldsymbol{J}_{G_T}$ are known at the CCU. Namely,

$$\overset{a,b}{\Delta P_T}[m] = \frac{\frac{\delta V_b}{\delta G_T}\Big(V_{\max} - V_a\Big) - \frac{\delta V_a}{\delta G_T}\Big(V_{\min} - V_b\Big)}{\frac{\delta V_a}{\delta P_T}\frac{\delta V_b}{\delta G_T} - \frac{\delta V_a}{\delta G_T}\frac{\delta V_b}{\delta P_T}}. \tag{4.1.24}$$

This way, two $B \times B$ correction matrices can be computed consisting of correction values for each bus combination (a, b), where $\overset{a,a}{\Delta G_T} = \overset{b,b}{\Delta P_T} = \infty$.

$$\boldsymbol{\Delta P_T} = \begin{bmatrix} \infty & \overset{1,2}{\Delta P_T} & ... & \overset{1,B}{\Delta P_T} \\ \overset{2,1}{\Delta P_T} & \infty & ... & \overset{2,B}{\Delta P_T} \\ \vdots & \vdots & & \vdots \\ \overset{B,1}{\Delta P_T} & \overset{B,2}{\Delta P_T} & ... & \infty \end{bmatrix}, \quad \boldsymbol{\Delta G_T} = \begin{bmatrix} \infty & \overset{1,2}{\Delta G_T} & ... & \overset{1,B}{\Delta G_T} \\ \overset{2,1}{\Delta G_T} & \infty & ... & \overset{2,B}{\Delta G_T} \\ \vdots & \vdots & & \vdots \\ \overset{B,1}{\Delta G_T} & \overset{B,2}{\Delta G_T} & ... & \infty \end{bmatrix} \tag{4.1.25}$$

Choosing the corrections

$$\Delta P_T[m] = \min_{a,b}\Big[|\boldsymbol{\Delta P_T}|\Big], \quad \Delta G_T = \min_{a,b}\Big[|\boldsymbol{\Delta G_T}|\Big] \tag{4.1.26}$$

where $|\boldsymbol{x}|$ denotes the absolute value of all elements in matrix $\boldsymbol{x}$, ensures the correction is made such that the new maximum and minimum bus voltages are always $V_{\max}, V_{\min}$. For fairness vectors $[k_1, ..., k_B]^T$ and $[l_1, ..., l_B]^T$ defined at the respective curtailment triggers, this constitutes the maximum load and DG that can be delivered in the network without voltage deviation out of bounds.

4.2 Performance under Zero Latency

Under zero latency the corrections $\Delta P_T[m]$ and $\Delta G_T[m]$ can be calculated and applied instantly in response to voltage events. By adjusting EV load and DG according to voltage requirements, the COR scheme can harness natural synergies

between EV charging and renewable generation. By example, Fig. 4.1 shows COR under 95% EVs and 59MW DG input at bus 18. Several observations can be made:

Voltage Control

During P-COR, any change in DG is reflected in ΔP_T such that V_b^{low} stays rigid at $V_{\min}$. Similarly, during G-COR, any change in power demand is reflected in ΔG_T such that V_b^{high} stays rigid at $V_{\max}$. Thus all unacceptable voltage deviation is removed.

Peak Shaving

Peak load and peak DG tend to coincide. Under COR, peak load may rise above that of random uncoordinated charging, which was impossible under CUR. This degraded peak shaving performance is a key tradeoff of the COR scheme.

User Inconvenience

The maximum available charging load and DG is used at any time, while keeping voltage within bounds. This minimises EV charging delay and maximises DG power input, alleviating user inconvenience. Power transfer is at optimum for EV owners and investors in DG.

CO_2 Emissions

DG energy input is maximised given voltage constraints. Meanwhile, the EV charging load is shifted from peak in the early evening to low-emission hours in the night and early morning. Therefore CO_2 emissions are significantly reduced.

EV & DG Capacity

G-COR prevents overvoltage from excessive DG by adjusting generation limit according to load. Similarly, P-COR prevents undervoltage from excessive EV penetration

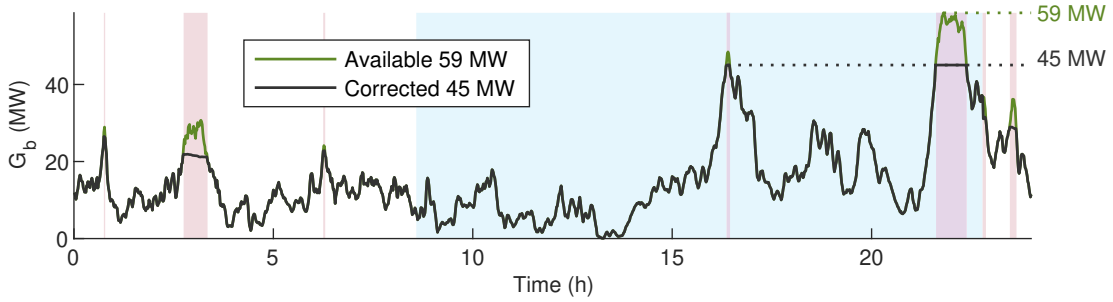

(a) DG Power Input at Bus 18

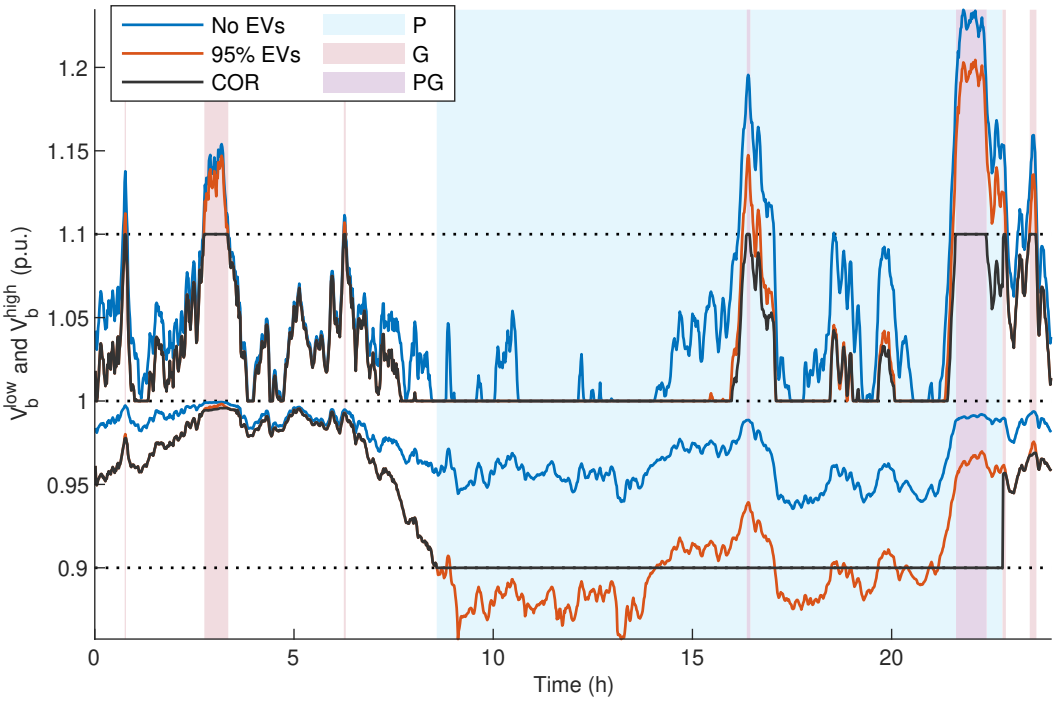

(b) Maximum (top) and minimum (bottom) worst bus voltages. Under zero latency COR keeps all bus voltages within upper and lower bounds.

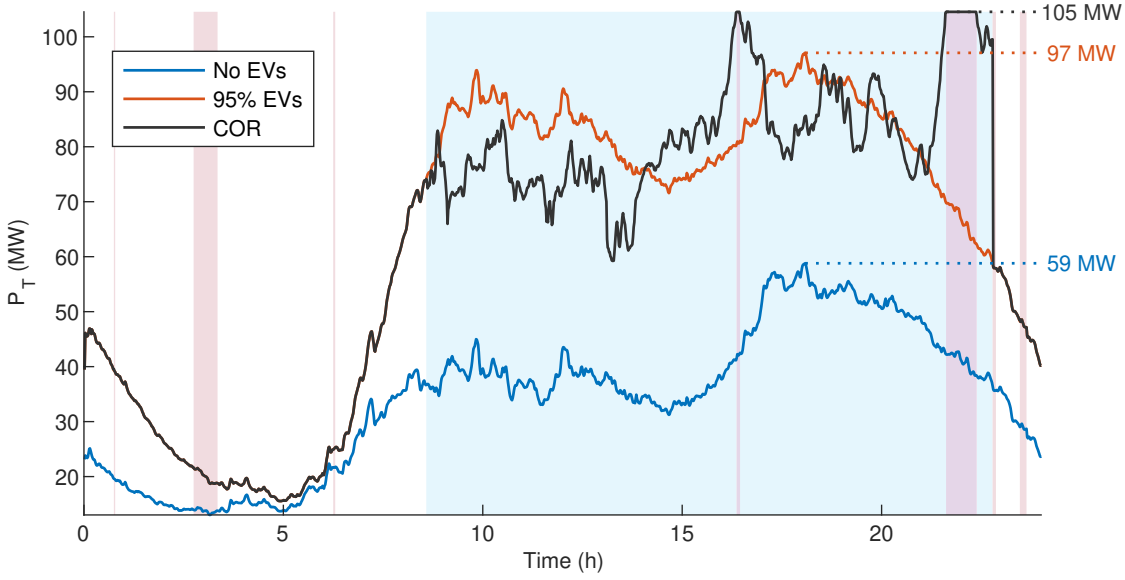

(c) Total Power Demand

Figure 4.1: COR can make strong improvements to both DG and EV capacity.

by adjusting charging limit according to available DG. As a result, EV and DG penetrations can be increased to very high levels with no voltage deviation out of bounds. The capacity of both is significantly improved over the CUR scheme.

4.3 Practical Latency Constraints

The COR scheme shows marked improvement in performance over CUR under zero latency conditions, when the system can detect and respond immediately to voltage events anywhere in the network. However, zero latency is not practical and, as discussed in Chap. 3, operational latency presents a key design decision relating to a multitude of performance tradeoffs. Fig. 4.2 shows the COR scheme for update interval $t_u = 10$min. Several effects are observed.

Voltage deviations are again divided into two categories: Trigger Deviation (TD) and Continuous Deviation (CD). TD occurs due to variation in both $\overrightarrow{P}$ and $\overrightarrow{G}$ in between the over- or under-voltage event and effective curtailment actuation. CD occurs continuously following the curtailment trigger, due to variation in the unconstrained variable. In P-COR, CD is due to changes in unconstrained $\overrightarrow{G}$, and in G-COR, CD is due to unconstrained $\overrightarrow{P}$.

The same trigger latency effects encountered for CUR in Chap. 3 also occur in COR, since curtailment in both is triggered following a voltage event. Therefore, TD is again prominent at the G-COR trigger. CD is also visible, however takes a different shape. The COR scheme involves a repetitive control action every update interval that corrects V_b^{low} to V_{min} and V_b^{high} to V_{max} by adjustments in P_T and G_T, respectively. As a result, CDs only appear in 10 minute windows in between correction intervals. Both TD and CD are stochastic in nature and can be modelled via statistical distribution.

As described in Sec. 3.1.5, household and EV charging load are governed by the law of large numbers, meaning their profile will approximate closer to the expected mean

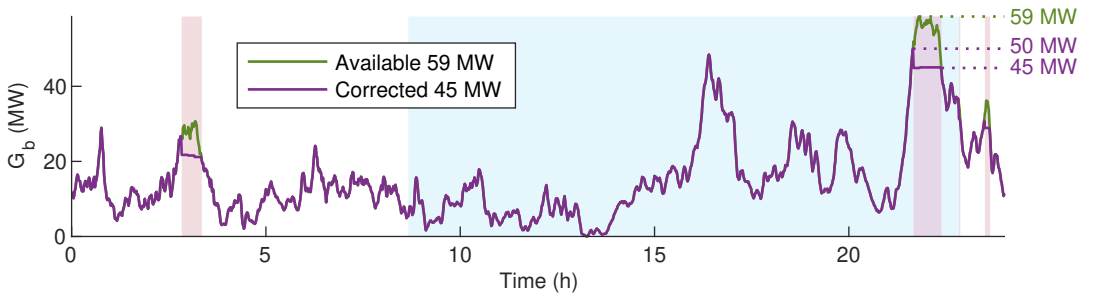

(a) DG Power Input at Bus 18

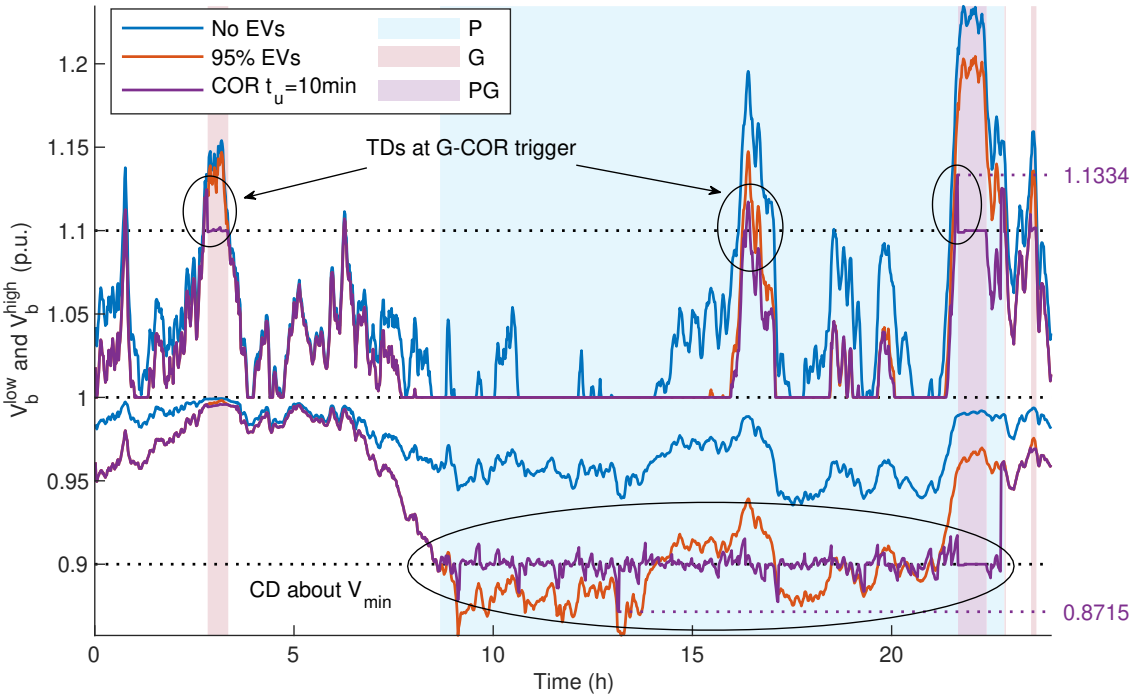

(b) Maximum (top) and minimum (bottom) worst bus voltages

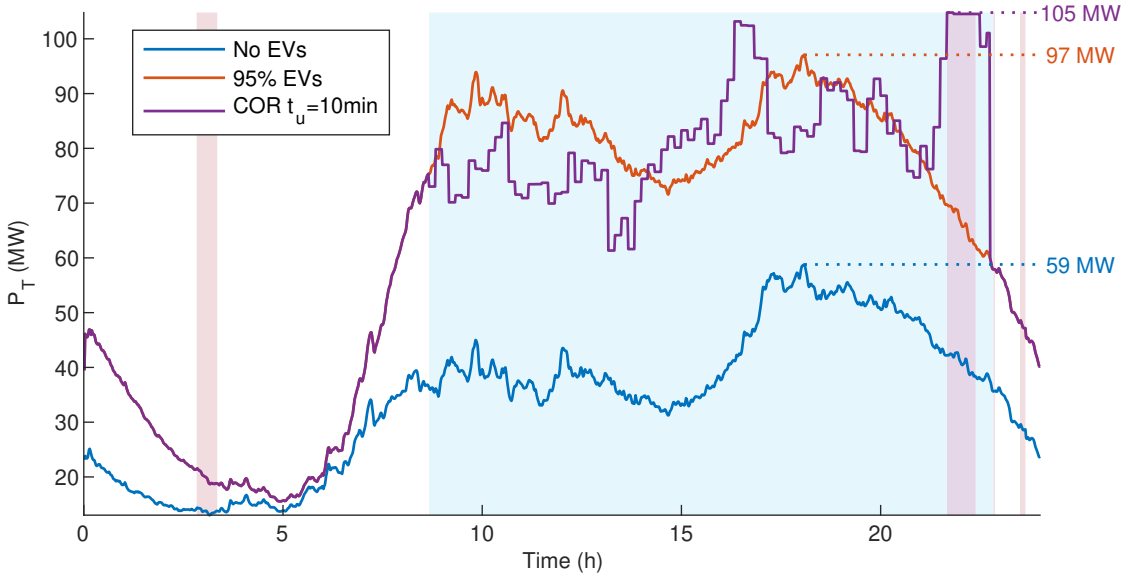

(c) Total Power Demand

Figure 4.2: Practical latency effects of update interval $t_u = 10$min. TDs and CDs appear bringing voltage out of bounds.

curve as the number of users increases. On the other hand, renewable generation depends strongly on weather conditions, and cannot be approximated by an expected mean on any single day. As a result, DG is in general much more volatile than aggregated load. Further, this is compounded here by concentration of renewable generation at the end of the feeder. This is visible in Fig. 4.2. TD is most prominent in G-COR, since DG can vary a great deal more in between update intervals than the load at any individual bus. Once G-COR is triggered, and DG curtailed to a maximum value, CDs about $V_{\max}$ are relatively small since the change in load per bus is less significant. In contrast, TD and CD under P-COR are comparable, since they are both mainly sourced from variation in unconstrained $\overrightarrow{G}$. During PG-COR, only TD is visible since, following the trigger, neither $\overrightarrow{P}$ nor $\overrightarrow{G}$ undergo significant change.

A key advantage of COR is that it provides a third mitigation strategy - Trigger Margin Reduction (TMR) - to combat TD spikes at the G-curtailment trigger that avoids the costly associations of heavy G-CMR. The three latency-mitigation strategies to deal with latency effects will be described in turn.

4.3.1 Continuous Margin Reduction (CMR)

As seen for CUR in Chap. 3, the margin formed by $V_{\min}$ and $V_{\max}$ can be reduced to mitigate the severity of voltage deviations. This is shown Fig. 4.3, using 0.91 and 1.09pu, respectively. Both CD and TD during P-COR are improved, since fewer deviations are now of sufficient magnitude to breach the lower technical limit.

Statistically, the same is true for G-COR, since reducing $V_{\max}$ means that G-COR is triggered earlier in anticipation of overvoltage, reducing the probability of a deviation out of bounds. However, since the trigger can only happen at 10 minute intervals, the volatility of the DG input means that reducing $V_{\max}$ to 1.09pu does not lead to G-COR being triggered any sooner here. Even, since increasing $V_{\min}$ also reduces P_T during P-COR, peak voltage increases to 1.14p.u.

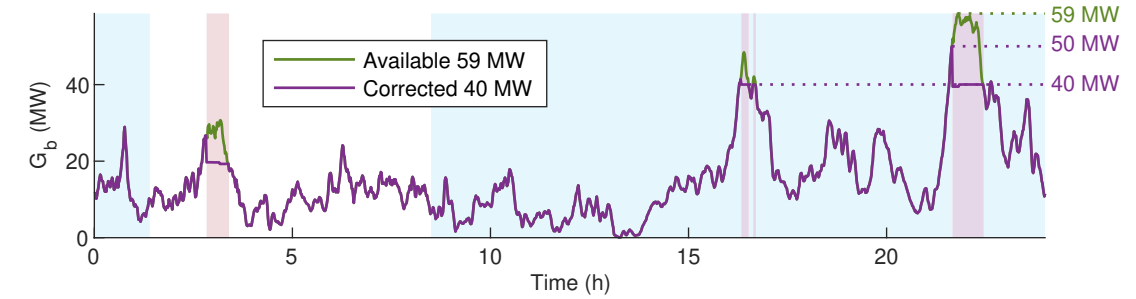

(a) DG Power Input at Bus 18

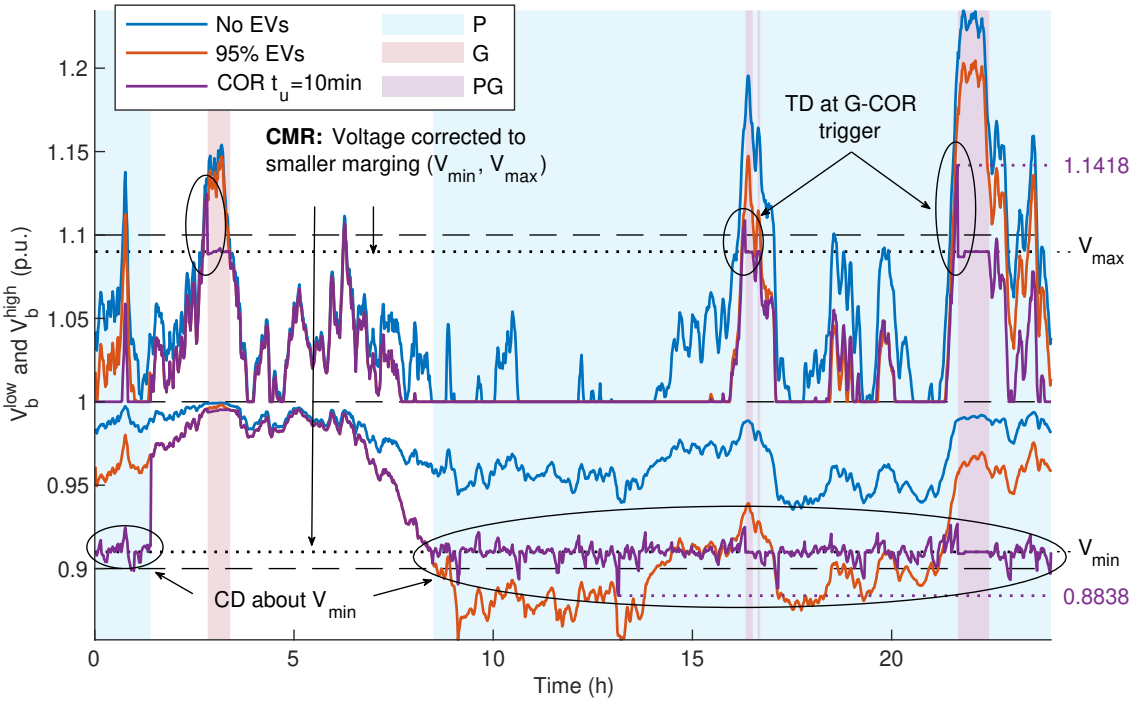

(b) Maximum (top) and minimum (bottom) worst bus voltages. Voltage limits $V_{\min} = 0.91$pu, $V_{\max} = 1.09$pu.

Figure 4.3: Continuous Margin Reduction (CMR) for $P-$ and G-COR with $t_u = 10$min. CDs about $V_{\min}$ are effectively mitigated, however TDs remain for G-COR.

Adjusting the margins $V_{\max}$ and $V_{\min}$ also affects P_T and G_T during correction. Peak charging load is now reduced to 96MW (from 105MW before CMR in Fig. 4.2c), and while peak DG input remains unchanged, the peak curtailed limit has reduced from 45MW to 40MW. These changes are visible in the amount of time spent in P-G- and PG-COR, which is larger in all categories. The drawbacks of CMR are shared with CUR. Lower average curtailment power increases EV charging delay, and lower average DG input reduces carbon savings as well as the return from investment in renewable systems.

As with CUR, increasing the severity of CMR by reducing $V_{\max}$ eventually eliminates voltage deviation above bounds, since correction is then triggered at an earlier

interval. But this incurs an impractical penalties regarding the key performance-cost tradeoffs. A significant advantage of COR over CUR is it presents a solution to this key tradeoff. TDs above bounds can be effectively limited with Trigger Margin Reduction (TMR) without the negative effects incurred by CMR.

4.3.2 Trigger Margin Reduction (TMR)

In all analysis so far, G-COR has been triggered by a voltage deviation above $V_{\max}$, and the voltage is then corrected to the same $V_{\max}$. The same is true for P-COR and $V_{\min}$. However, in COR this does not need to be the case. Under TMR, the voltage at which correction is triggered (V_{trig}) is not the same as the voltage to which it is then corrected. Triggering G-COR at a voltage $V_{\text{trig}} < V_{\max}$ allows for G-corrective limits to be applied in anticipation of an over- or under-voltage event, therefore avoiding TD without impeding on P_T and G_T.

This is shown Fig. 4.4 where, like before, G-COR is calculated to bring maximum bus voltage to $V_{\max} = 1.1$pu, but, unlike before, the limit is applied when any bus voltage is detected above $V_{\text{trig}} = 1.05$pu.

Any bus voltage above V_{trig} will trigger G-corrective iterations, applying an upper generation limit on all DG sources. This curtailment limit pre-empts a sudden spike in generation, meaning the limit is applied even if DG does not rise to this limit. If the limit is not reached and generation stays low, no change in DG will occur. This effectively reduces TD, since to breach the upper technical limit a spike in generation must be sufficiently sharp to bring bus voltage from below V_{trig} to above $V_{\max}$ in the space of one update interval. It also leads to none of the drawbacks associated with CMR since the curtailment limit G_T is unchanged.

TMR can be used to effectively mitigate TD spikes. However, CD is not affected, since this occurs due to variation in the unconstrained variable while the corrective limit is already applied. Since CDs during G-COR are comparatively small, CMR is applied only for P-COR here.

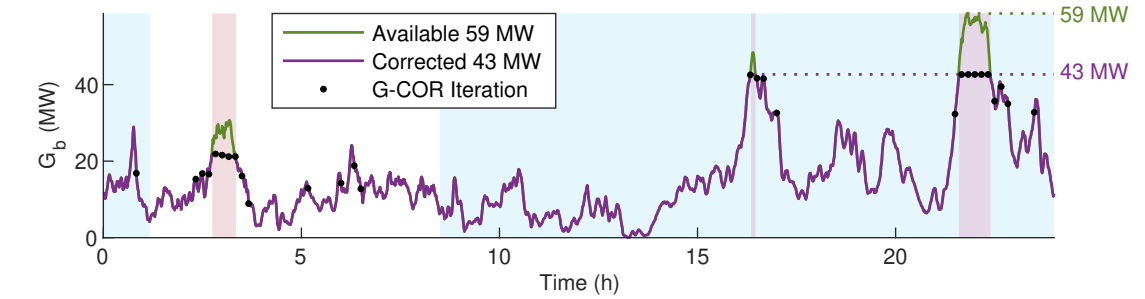

(a) DG Power Input at Bus 18

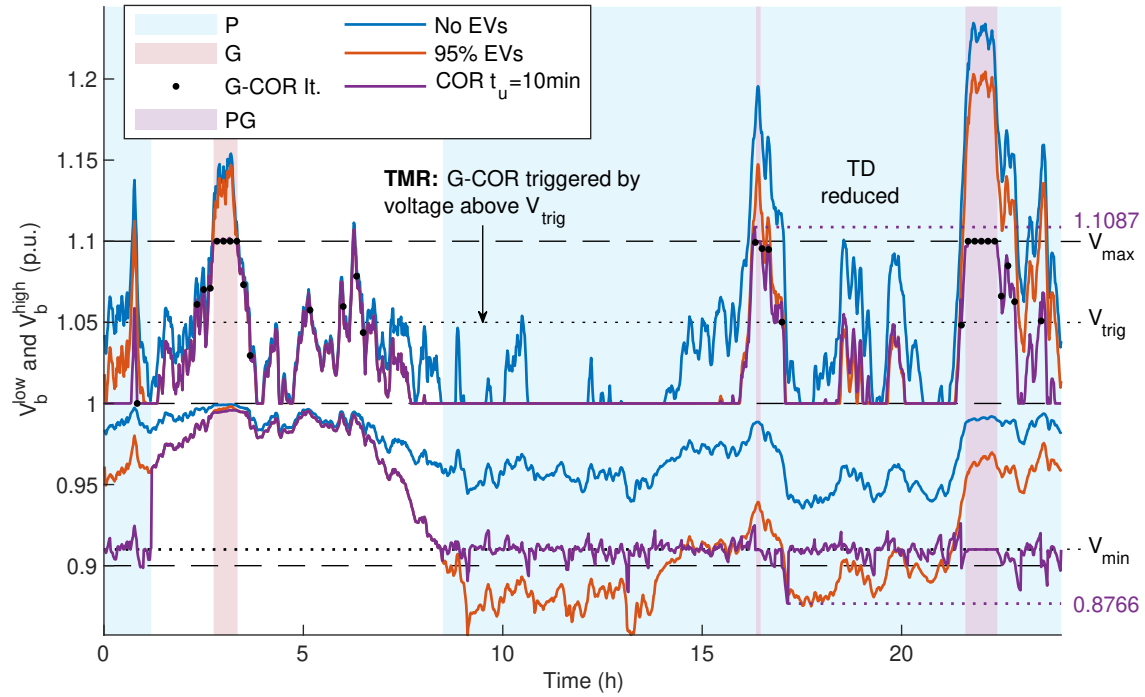

(b) Maximum (top) and minimum (bottom) worst bus voltages. G-COR is now triggered by any voltage above $V_{\text{trig}} = 1.05$pu.

Figure 4.4: Trigger Margin Reduction for G-COR with $t_u = 10$min. $V_{\text{trig}} = 1.05$pu, $V_{\max} = 1.1$p.u., $V_{\min} = 0.91$p.u.

The drawback of TMR is that it leads to numerous false corrections in anticipation of an overvoltage event that never occurs. For each corrective iteration, numerous messages must be gathered, sent through multiple network tiers, limits computed at the CCU and then distributed to all ICUs and smart devices in order for the corrected curtailment limit to be effectively applied. This occurs every corrective iteration even if the limit is never reached. G-corrective iterations are shown by black dots in Fig. 4.4b, 4.4a, of which there are roughly twice as many as for CMR in Fig. 4.3 with a similar G- curtailment time. Effectively, this means twice the correction iterations for the same amount of curtailment.

False corrections raise data traffic in the network, which may be significant for a large number of nodes and short update intervals, however the overall traffic increase

is likely negligible compared to the equivalent traffic increase of severe interval reduction (IR). More importantly, in the case of multiple DG input sources, false corrections may also unnecessarily limit renewable energy in the system: Curtailment is applied to all nodes in the system at once with l_b proportional to available power input at the G-curtailment trigger. If the balance of availability changes then the l_b values and vector $\overrightarrow{G}^{\max}$ are out of date. In this case, G_b at one bus may be curtailed to an upper limit even if generation at remaining buses remains low, in which case the curtailment is unnecessary. Ultimately, this may impair renewable energy input. Quantifying this effect is beyond the scope of this thesis, however, it is acknowledged that excessive TMR is to be avoided if possible.

Since system update interval means that detection and control actions only occur here at 10 minute update intervals, a particularly sharp spike in generation may still lead to overvoltage if it rises rapidly enough, as occurs for the peak in Fig. 4.4b. Lowering V_{trig} further can eliminate these spikes, however this also leads to numerous false corrections which may impede overall performance.

4.3.3 Interval Reduction (IR)

Unlike CUR, where reducing the update interval t_u served only to mitigate the TD spike, IR in COR can significantly reduce both CD and TD. Since t_u defines the frequency of corrective iterations, reducing t_u leads to a smaller window within which both TD and CD can occur, and therefore strongly reduces the severity of both. This is shown Fig. 4.5 for $t_u = 5$ and 3min.

IR reduces all voltage deviations about both upper and lower technical limits. This allows the severity of CMR and TMR to be significantly relaxed while simultaneously improving voltage control. The result is more tightly constrained voltage deviations about both upper and lower limits, improved EV charging delay and renewable input, as well as lower percentage of false corrections. Further, by allowing CMR to be reduced, IR can raise both EV and DG capacity, while at the same time improving

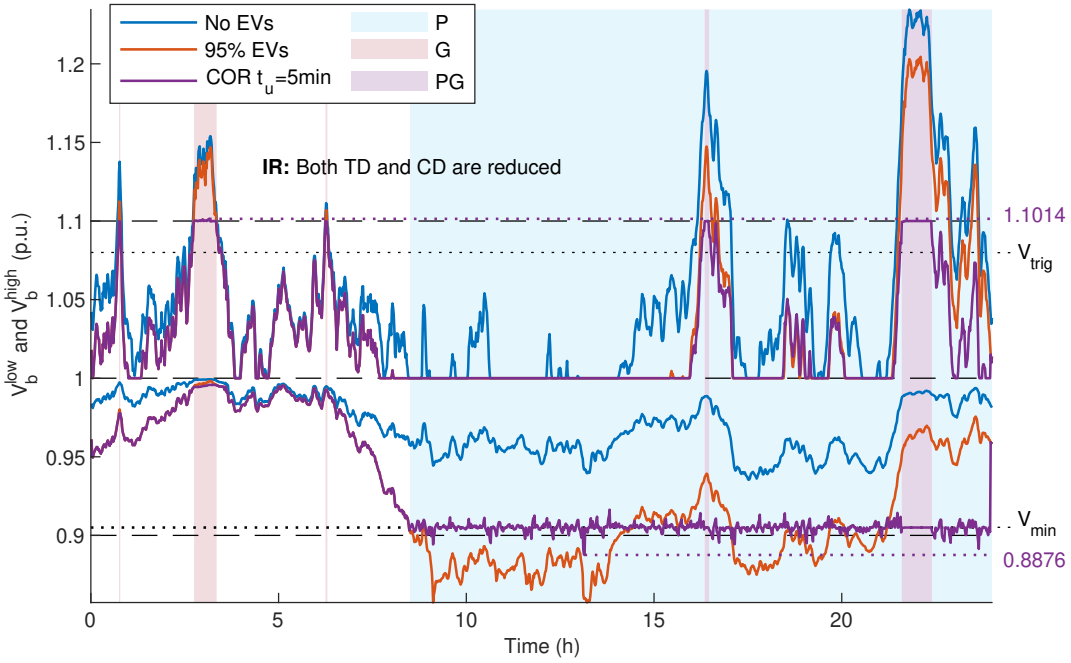

(a) IR: $t_u = 5$min

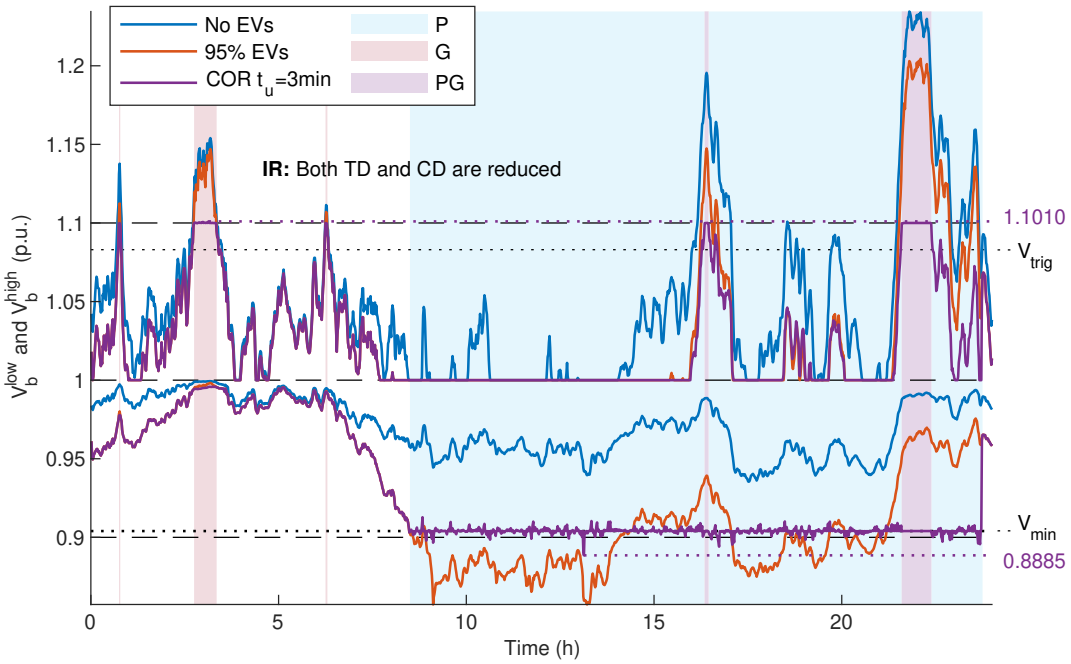

(b) IR: $t_u = 3$min

Figure 4.5: Interval Reduction: Decreasing update interval t_u can bring significant system improvement. $V_{\text{trig}} = 1.08$p.u., $V_{\text{min}} = 0.905$p.u.

peak upper and lower voltage. As the update interval reduces, the system approaches asymptotically to that of the zero latency system, as shown in Tab. 4.1.

Table 4.1: IR can simultaneously improve both EV and DG capacity as well as voltage deviations in the network. (All with $V_{\max} = 1.1$pu)

t_u (min)	10	5	3	0
$V_{\min}$ (p.u.)	0.91	0.905	0.903	0.9
$\eta_{EV}^{\max}$ (%)	208	222	226	234
$\eta_{DG}^{\max}$ (%)	40.9	42.3	42.8	43
V_b^{low} (p.u.)	0.8838	0.8876	0.8885	0.9000

4.4 Simulation

To evaluate performance-cost tradeoffs for KPIs under COR, and for direct comparison with CUR, statistical evaluation from Sec. 3.5 was repeated using the same 172 days of wind power profiles with 80% EV penetration and 40MW wind farm input at bus 18. The analysis is divided between latency mitigation strategies, first CMR/TMR and then IR.

4.4.1 Continuous/Trigger Margin Reduction (TMR/CMR)

Statistical analysis of CMR and TMR is conducted separately.

First, CMR is evaluated by varying $V_{\min}$ and $V_{\max}$ in turn from 0.9-0.96pu and 1.1-1.04pu, respectively, while the other is kept constant. Voltage, load and generation profiles were simulated at each bus for each of the 172 days of wind power input, and KPIs relating to Voltage Control, Peak Shaving, User Inconvenience, Carbon Emissions and Deployment Cost were evaluated. Repetition is avoided where possible by focusing on the differences between CUR and COR.

Second, TMR is a strong advantage of COR. To demonstrate this, the same inputs were simulated for V_{trig} from 1.1pu to 1.04pu, while $V_{\min}$ and $V_{\max}$ are held constant at 0.9pu and 1.1pu. The same KPIs are evaluated for comparison between three categories: CUR with G-CMR, COR with G-CMR and COR with TMR.

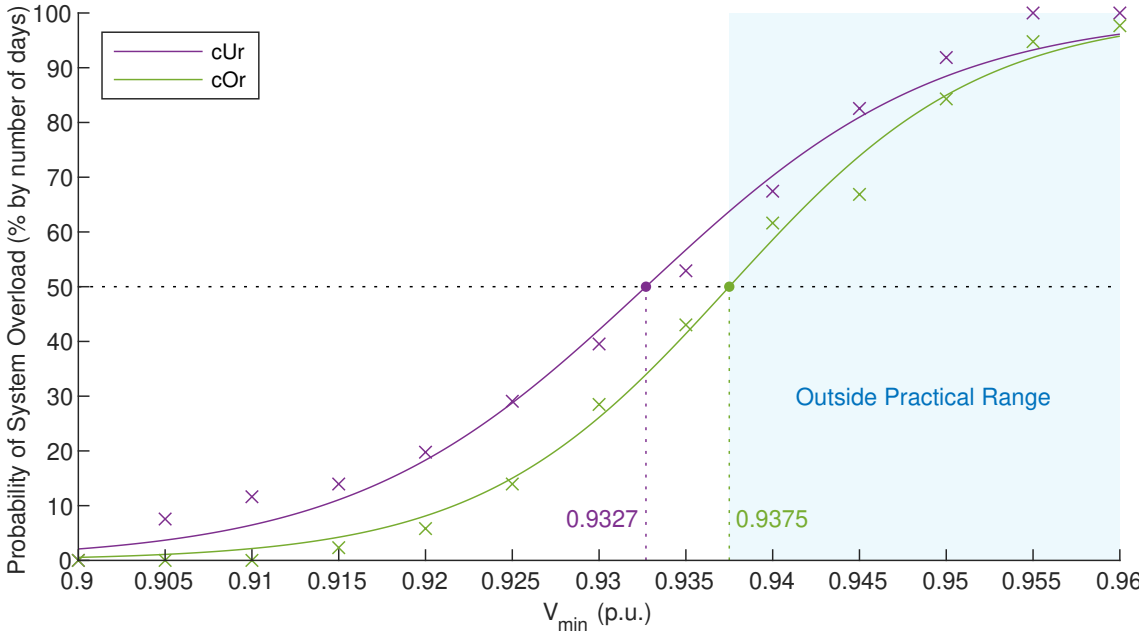

Figure 4.6: COR - Probability of system overload with increasing $V_{\min}$.

Percentage Overload

Whether the daily EV charging load can be satisfied in a single 24 hour period depends on both the severity of P-CMR and the available incoming DG. System overload was defined in Sec. 3.5.1 to be a 24 hour period during which the daily EV charging load could not be satisfied. The probability of system overload must be less than 50% if the active penetration of EVs can be sustained long term. Therefore, this 50% requirement defines the highest extent of practical P-CMR in the system and the useable range of $V_{\min}$.

Percentage overload for the 172 days in each $V_{\min}$ category is compared for CUR and COR in Fig. 4.6, where the best fit logistic curve is drawn according to eq. (3.5.1). Only the values for $t_u = 10$ min. are shown since update interval has negligible effect on this characteristic. By extrapolating for both at the 50% mark, it can be seen that COR can tolerate a wider practical range of $V_{\min}$. This reflects the increased EV charging capacity now that charging load is adaptive to DG input and can take full advantage of the available power in the network.

This lower overload probability also reflects that time spent in curtailment is lower overall, meaning that more flexible load can be delivered on demand and peak

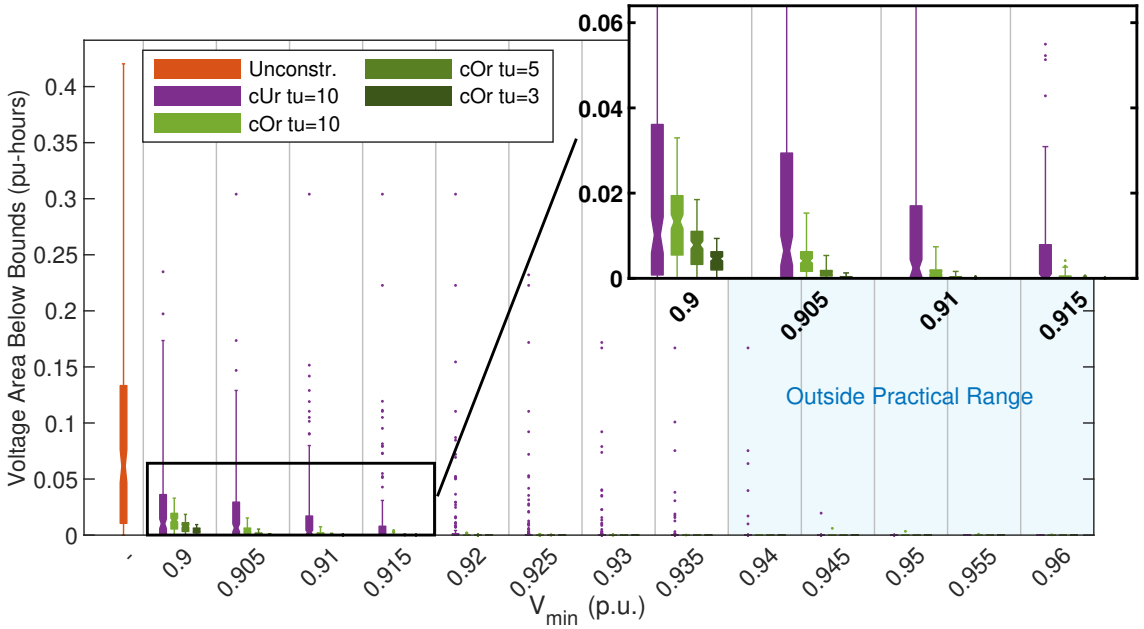

(a) Voltage Area Below Bounds for varying $V_{\min}$ (units volt-minutes).

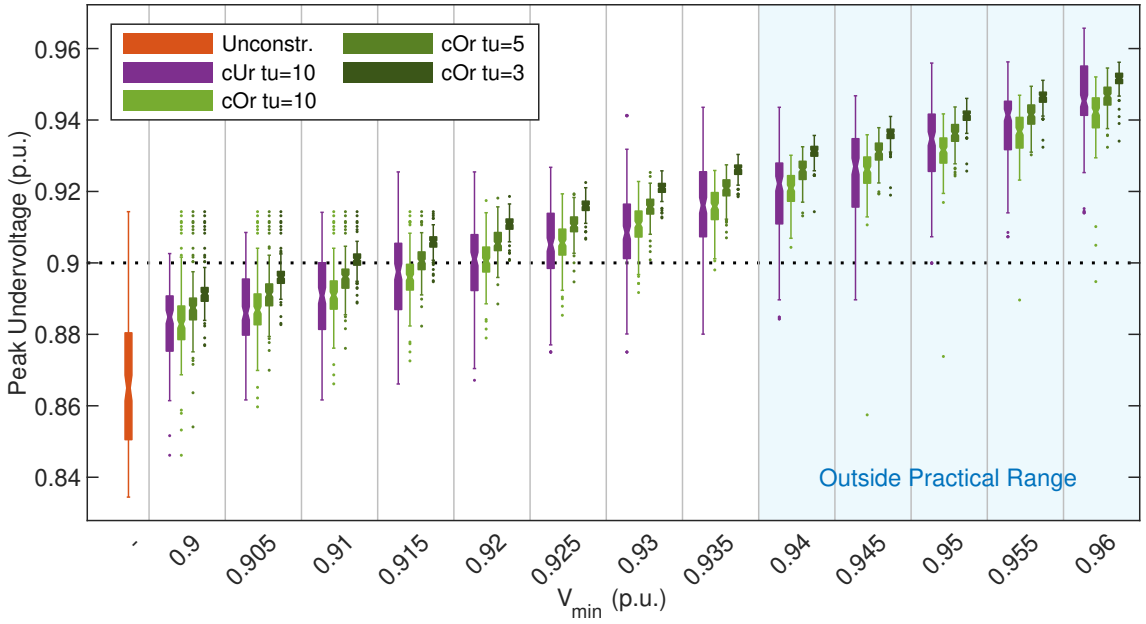

(b) Peak Daily Minimum Voltage for varying $V_{\min}$

Figure 4.7: COR - Undervoltage performance and P-CMR.

hours - time during which charging delay is incurred - is reduced. Further, this implies EV penetration can be increased in the network under the same practical performance requirements.

Voltage Control

Voltage control is assessed via voltage area above and below statutory limits as well as peak upper and lower voltage. Analysis is split between P-CMR and G-CMR/TMR.

***P*-CMR** Voltage area below bounds (units pu-hours) and peak daily undervoltage are shown for varying degrees of P-CMR in Fig. 4.7 for the following categories: Unconstrained system; CUR under $t_u = 10$min and COR under $t_u = 10$, 5 and 3min.

First, referring to Fig. 4.7a, clearly the COR scheme dramatically limits overall voltage deviation out of bounds compared to CUR. This is due to the repetitive control action during curtailment which bring V_b^{low} back to the limit V_{min} every update interval. The only deviation out of bounds then occurs due to CD in between update intervals, which is reduced to effectively zero for $V_{\text{min}} > 0.92$, which is also now well within the practical long term range.

Next, referring to peak undervoltage in Fig. 4.7b, it is clear from the length of each box in the box-whisker plot that the COR scheme also leads to more tightly grouped voltages about the lower limit. Again, since the repetitive control action continuously brings V_b^{low} back within bounds every update interval, it is no longer free to deviate with DG input for the length of the curtailment period. Not only does this mean the system is more predictable in terms of behaviour, but also that CMR can be deployed closer to technical limits under the same voltage constraints, which allows for marked advantage over the key performance tradeoffs.

Finally, by comparing Fig. 4.7 to the equivalent for CUR in Fig. 3.15a and 3.15b, an opposing response to system update interval can be observed. Under CUR, using a smaller t_u reduced overcurtailment in the system which led to curtailment limits marginally closer to the statutory voltage boundaries. Since curtailment limit under CUR is then static, this slightly increased the statistical voltage deviation below bounds. In contrast, Fig. 4.7 shows a clear positive relation between voltage deviation and t_u. Since update interval now defines the window in which CDs can take place, not only does using a smaller t_u effectively reduce the severity of these deviations, it also reduces the standard deviation - this can be seen by comparing the vertical length of the COR box plots in each category.

Under CUR, a certain amount of voltage deviation must be tolerated if V_{min} is to remain static within practical range. However, under COR, all unacceptable

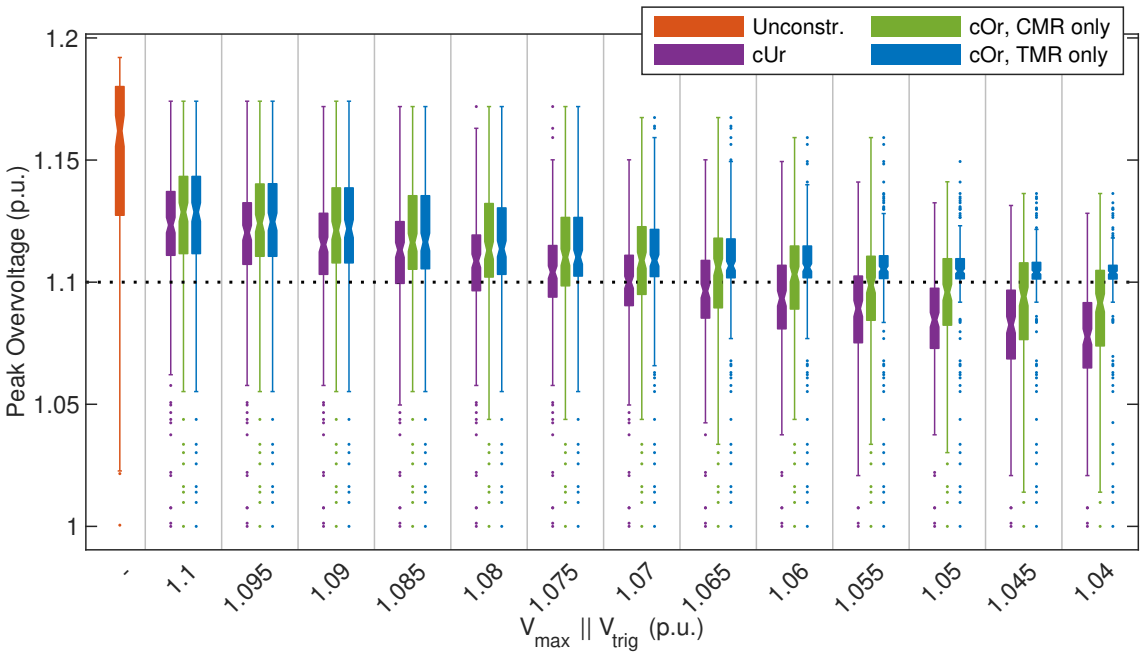

Figure 4.8: COR - Peak Daily Maximum Voltage for varying $V_{\max}$ (for red, purple and green) or V_{trig} (for blue).

voltage deviation can be entirely eliminated from the system, even for 10min update interval, while keeping the system within practical range of P-CMR. These figures demonstrate comprehensively improved voltage control about the lower boundary.

G-CMR and TMR Peak overvoltage and voltage area above bounds are shown in Fig. 4.8 and 4.9, which compare performance of G-CMR in CUR and COR, and TMR under COR. Here, to avoid clutter, only $t_u = 10$min is shown in each case, with in depth analysis of update interval saved for IR in Sec. 4.4.2. There are several factors at play here.

First, referring to CUR (purple) and COR-CMR (green) for peak overvoltage in Fig. 4.8, it can be seen that both behave comparably under increasing levels of CMR - peak overvoltage decreases steadily while spread (vertical length of the box plots) stays roughly the same. This is to be expected, since TD in both occurs due to the same process and is limited by the same factor. However, more interestingly, it can be seen that CMR actually performs better in CUR along all categories of $V_{\max}$. Peak overvoltage is strongly dominated by TD at the G-curtailment trigger. Since the COR scheme curtails both power and DG at the optimum level with regard

to $V_{\min}$ and $V_{\max}$, the curtailed power limit of both $\overrightarrow{P}^{\max}$ and $\overrightarrow{G}^{\max}$ is significantly higher than under CUR. This leads to two contributing factors towards this higher TD spike:

- First, for G-COR, the higher curtailment limit means that DG is more likely to drop below this limit. If, at the next update interval, DG is still below this limit and all bus voltages are below $V_{\max}$ then G-COR is ended and unconstrained DG resumes. If DG rises again, another TD is incurred. The result is G-COR endures in shorter bursts, therefore statistically the COR scheme undergoes more TD spikes per day than CUR, and the probability of a sharp spike is higher.

- Second, the higher curtailment limit in P-COR means that delayed EV charging load is satisfied faster, and less time is spent in P-curtailment each day. The effect is to expose the system to more hours of low power demand, since less charging load endures into off-peak hours in the night and early morning. It was seen in Fig. 4.3 that TD coinciding with a lower power demand led to a higher voltage spike (in that case the lower demand was due to more severe P-COR, but the effect is the same). Spikes in DG are more consequential when there is lower power demand in the system. Since EV charging queues are served faster in COR, the off-peak hours expose the system to sharper overvoltage spikes.

As a result, peak overvoltage is higher in COR when only G-CMR is compared. However, TMR under COR (blue) brings the COR scheme significant advantage. In this category, the x-axis shows values only for V_{trig}, since $V_{\max}$ is held constant at 1.1pu. When V_{trig} is comparable in magnitude to $V_{\max}$, there is little noticeable effect. However, as V_{trig} drops further, peak overvoltage is significantly reduced since the G-corrective limit is applied in advance, in anticipation of overvoltage, and a spike in DG fast enough to breach the upper statutory limit becomes less likely. Further, since the corrective limit is always applied for $V_{\max} = 1.1$pu, all overcurtailment

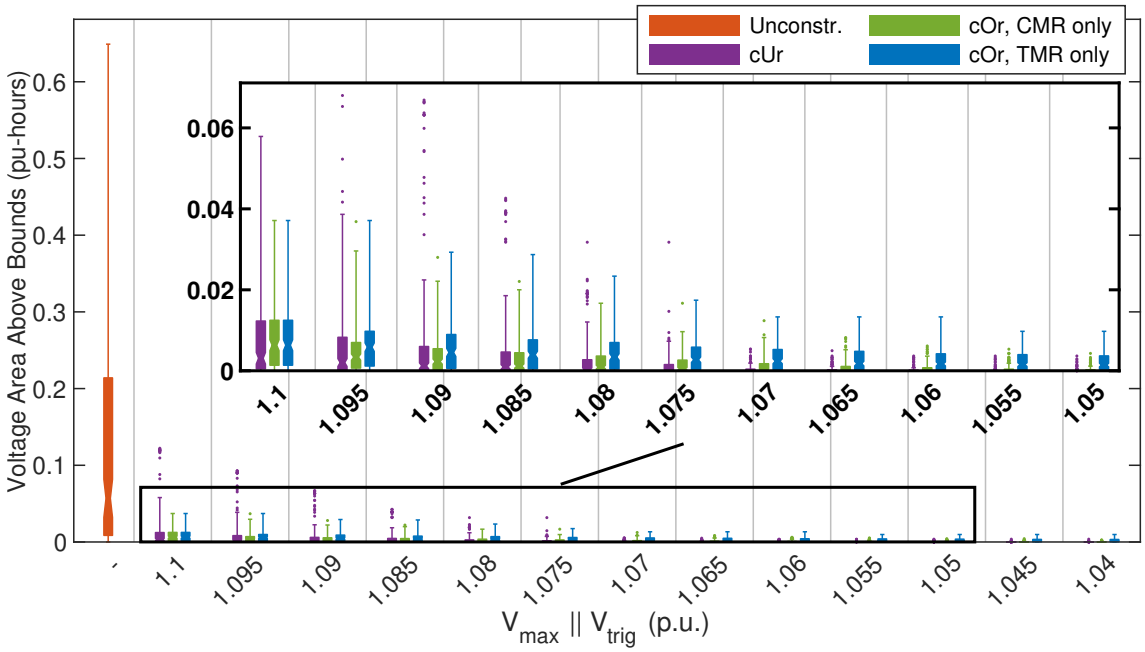

Figure 4.9: COR - Voltage area above bounds for varying $V_{\max}$ (for red, purple and green) or V_{trig} (for blue). Units in pu-hours.

effects of G-CMR are eliminated. Any peak maximum voltage significantly below the statutory limit under COR-TMR is due to a particularly low wind power day rather than a whole day in overcurtailment. The grouping of peak overvoltages under heavy TMR is so dense that it achieves better peak overvoltage performance than either CMR category.

Finally, it can be seen that the 'box' of the TMR box plots changes size very little from $V_{\text{trig}} = 1.045$ and 1.04pu, and rests at roughly the same height a little above the statutory limit. This dense collection of peak voltages is due to CDs about $V_{\max} = 1.1$pu, which is not affected by V_{trig}, and can be eliminated by combining G-CMR and TMR (as will be shown in Sec. 4.4.2)

Next, referring to Fig. 4.9, it can be seen that voltage area above bounds reduces with $V_{\max}$ in CUR (purple) and COR CMR (green), however, not at the same rate. The area for CUR begins larger at $V_{\max} = 1.1$pu, then falls faster. By $V_{\max} = 1.09$, the area above bounds for COR categories is larger than CUR. Area above bounds is a combination of TD and CD. In CUR, CD is significant only when $V_{\max}$ is near the statutory limit 1.1p.u. This is mitigated quickly by CMR, until the area above

bounds is dominated by TD, beyond which both categories of COR remain larger, since here TD is more significant.

CMR successfully mitigates this area above bounds in COR (green) since it limits both TD and CD. However, under TMR (blue), which only reduces TD, area only reduces up to around $V_{\text{trig}} = 1.055\text{pu}$, beyond which it stays roughly the same. This area is due to CD about the limit $V_{\max} = 1.1\text{pu}$, and can be reduced by combining CMR and TMR (this will be shown in Sec. 4.4.2).

These two figures demonstrate several points. First, that overvoltage control is significantly improved under COR provided ample TMR is employed. In this case, not only does overvoltage improve, but also overcurtailment (as a result of heavy CMR) is eliminated. Second, that CDs about $V_{\max}$ are not negligible, and a small amount of G-CMR is still required.

Peak Shaving

An inevitable consequence of P-COR compared to P-curtailment only is an increase in curtailed power limit, since power demand now directly scales with available DG. This has two effects.

First, since curtailed power demand is by definition the highest allowed total power demand in the system, peak load increases significantly. Fig. 4.10 shows that peak power demand is on average 30% higher across all categories of $V_{\min}$. This is key tradeoff of the enhanced voltage control, since higher rated power equipment may have to be replaced to support this increase. However, it is worth noting that peak load is only significantly higher than unconstrained loading patterns for $V_{\min} < 0.92$, beyond which a universal peak load decrease is incurred.

Second, a marked effect on standard deviation for peak load values is visible from the difference in vertical length of the box plots. Under CUR, peak load is primarily a result of the TD spike that occurs before load has been effectively curtailed. The magnitude of this is dependent on many factors such as the length of the TD window,

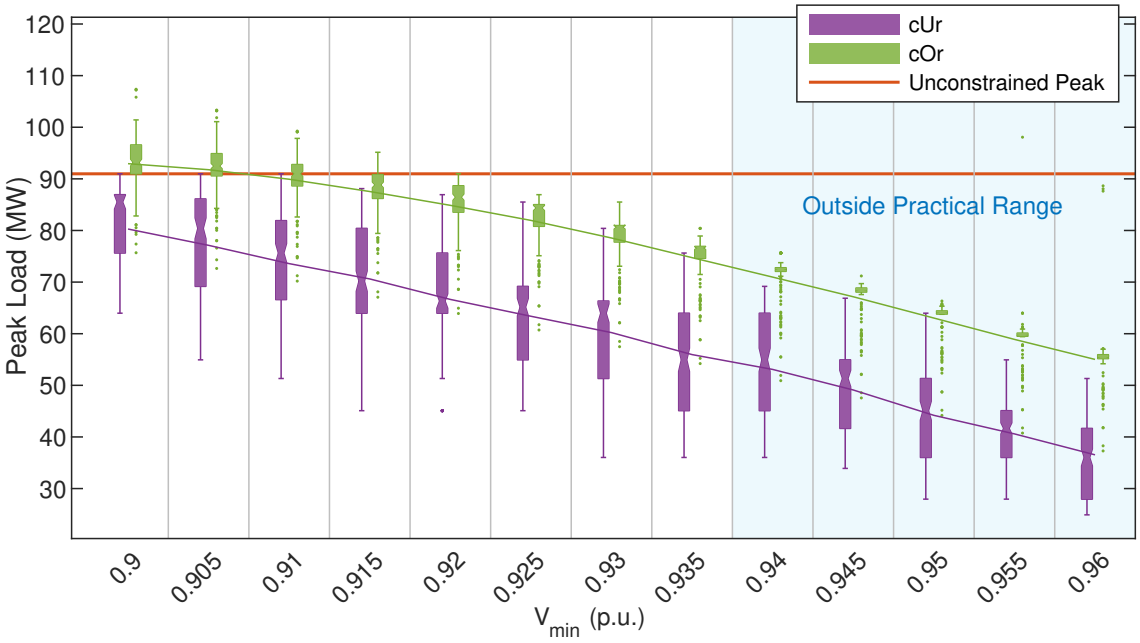

Figure 4.10: COR - Daily peak total power demand with $V_{\min}$

when in the day the trigger takes place and available DG at this instant. In contrast, peak load under COR is rarely due to the TD spike. Instead it coincides with peak DG input during P-COR. If DG is low then COR means that EV charging power is low, meaning that more charging delay is accumulated and curtailment tends to persist. However, as soon as DG then rises, so does EV charging power. Since COR allows the system to 'wait' for a spike in DG, the coincidence of peak load and peak DG input is more likely. The result is that peak load is more densely populated near the mean than with CUR.

User Inconvenience

Peak load under both schemes can be reduced by increasing the severity of P-COR (increasing $V_{\min}$). However, both schemes undergo the same performance tradeoff with respect to EV charging delay, shown Fig. 4.11. Reducing peak load in the system by heavier P-CMR leads to increased inconvenience to subscribing users. On the other hand, the higher average power associated with the COR scheme leads to a reduced charging delay compared to CUR.

This presents a key tradeoff of the COR scheme - enhanced voltage control

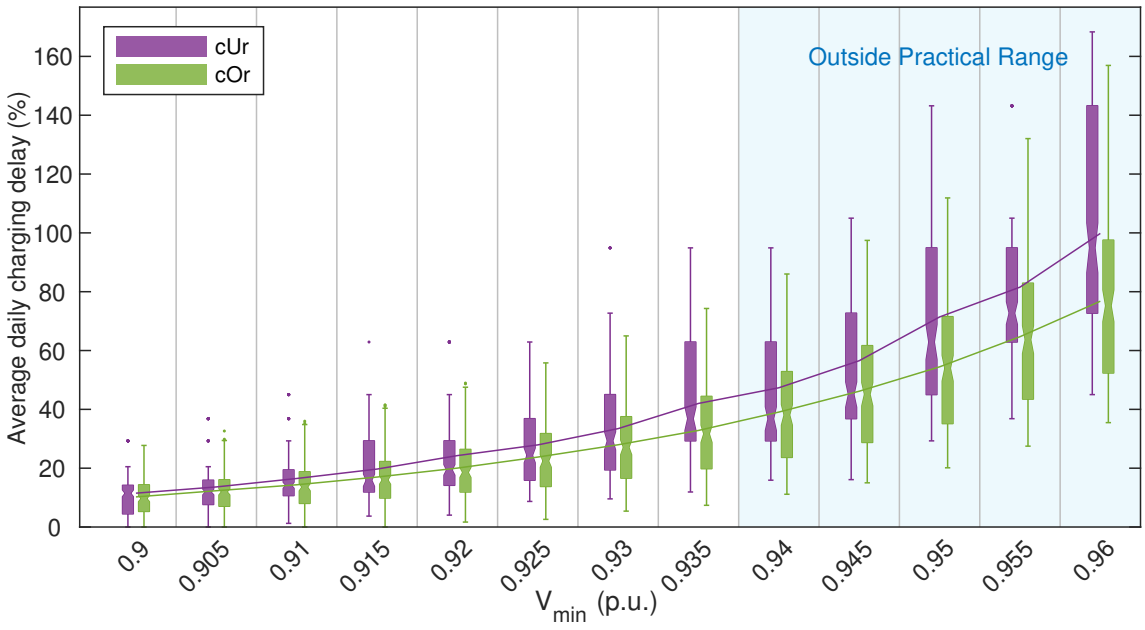

Figure 4.11: COR - Average EV charging delay per user during peak hours under progressive severity of P-CMR.

combined with lower EV charging delay comes at the price of a rise in peak load in the system. This is important from the perspective of the system operator, since peak load is a key budgeting concern, and user satisfaction is imperative to maintain the high rates of subscription required for scheme operation.

While the nominal 40MW DG input is constant across all test variables in both schemes, COR demonstrates strong improvement in practical DG penetration. Under CUR, heavy G-CMR is required to restrict sharp overvoltage spikes, which is accompanied by penalties in renewable energy input. However, under COR-TMR (blue), shown in blue in Fig. 4.12, mean values daily energy supplied by DG remain flat across all V_{trig} categories, since correction is always made for $V_{\text{max}} = 1.1$pu. A comparable graph exists for peak DG, however, is not included since instalment of a 40MW wind farm will naturally be accompanied by equipment capable of supporting a 40MW peak power input, and it is less of a budgeting concern.

It is desirable to increase DG input where possible, to maximise return on investment in renewable systems. Under COR, the percent of total daily energy supplied by renewable generation is significantly higher than CUR. At $V_{\text{max}} = 1.04$pu, CUR delivers on average 16% of daily generation to the network. At $V_{\text{trig}} = 1.04$ and

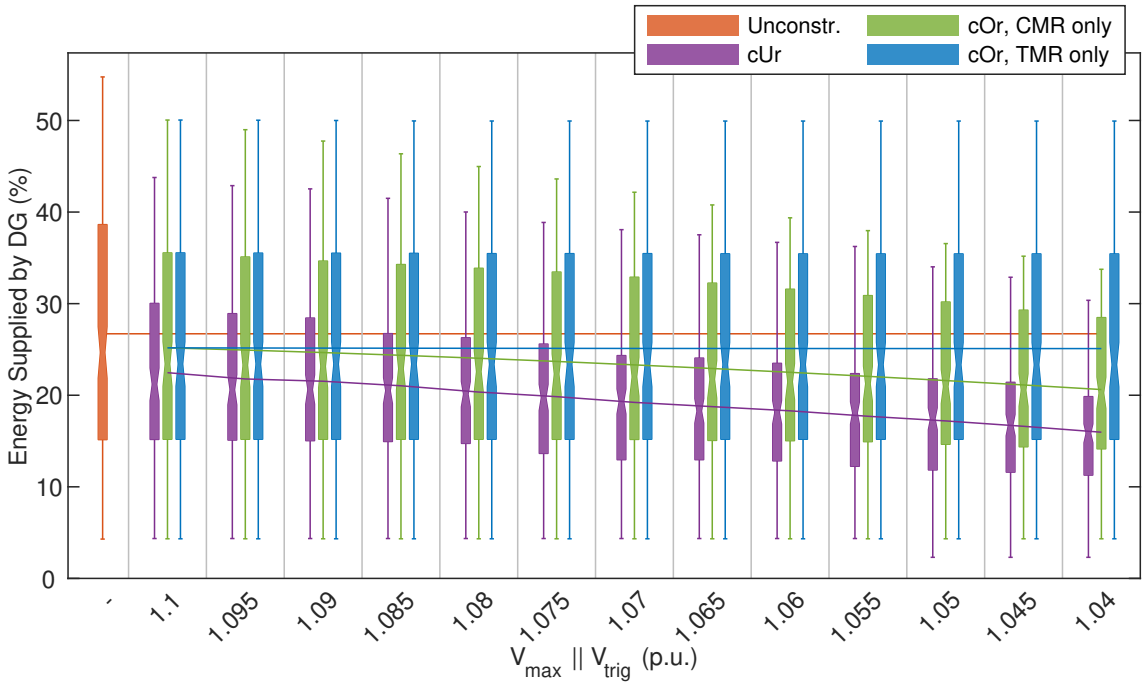

Figure 4.12: COR - Daily Energy supply from DG under progressive severity of G-CMR and TMR.

$V_{\text{max}} = 1.1$pu, COR delivers 25%, while also improving overvoltage performance. Clearly, the COR scheme stands to significantly improve energy input from renewable sources as well as supporting significant improvement in voltage control.

Carbon Emissions

CO_2 emissions between the CUR and COR schemes behave similarly under increasing V_{min}, shown Fig. 4.13a. In raising the severity of P-curtailment, more charging load is delayed into off-peak hours in the night and early morning where the emissions per kWh are significantly lower, therefore overall carbon emissions reduce. However, certain differences are noticeable.

For $0.9 \leq V_{\text{min}} \leq 0.91$ in CUR, the delay in EV charging load is not sufficient to counteract the offset rise in emissions from curtailing DG. The result is that CO_2 emissions are slightly higher than unconstrained loading. In contrast, since curtailed DG and load complement one another under COR, the result is lower emissions, roughly equal to that of unconstrained loading. As severity of P-CMR increases

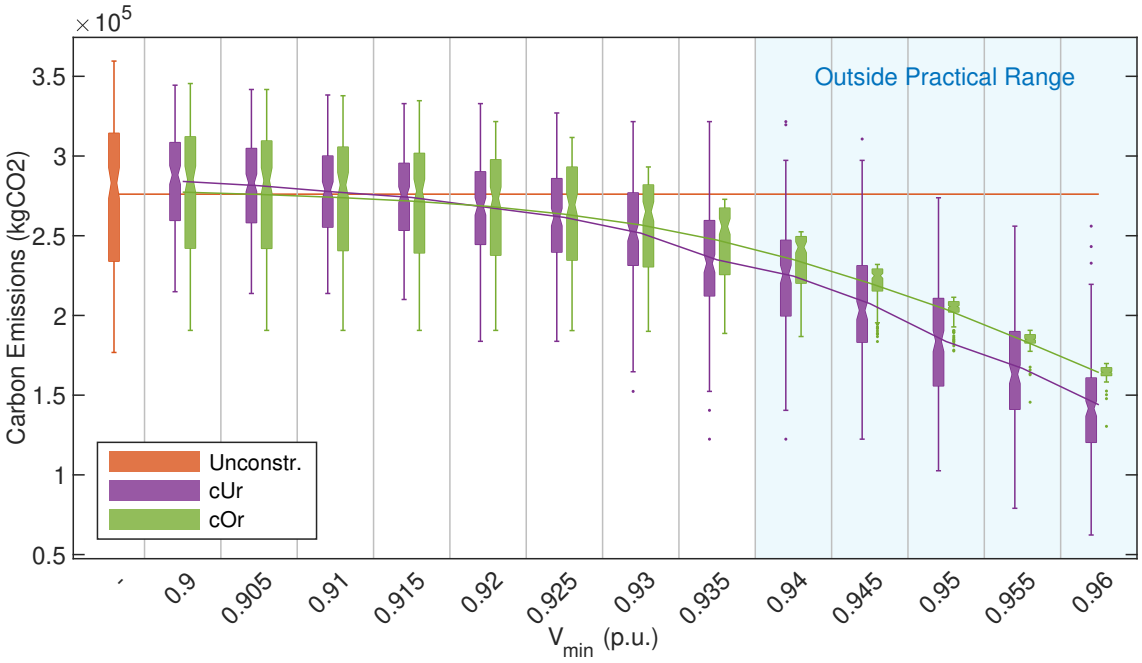

(a) Total Daily CO_2 Emissions for $V_{\min}$.

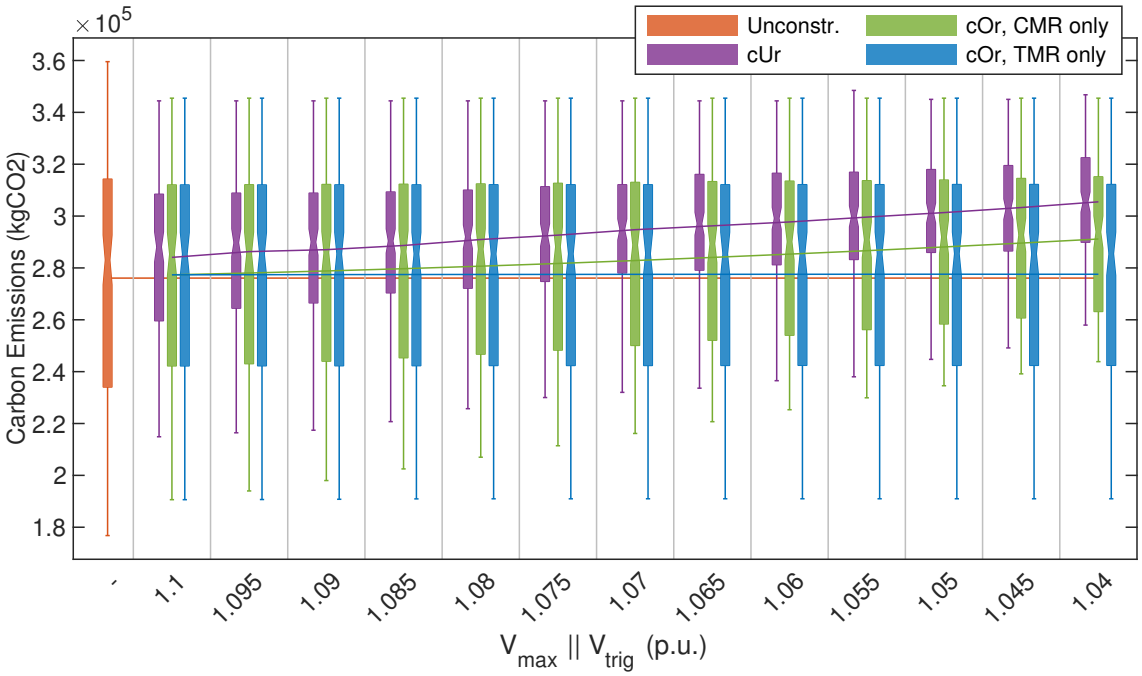

(b) Total Daily CO_2 Emissions for $V_{\max}$.

Figure 4.13: COR - Carbon Emissions of CMR.

for $V_{\min} > 0.91$, the delayed EV charging load begins to reduce carbon emissions. However, since under COR curtailment power is significantly higher, the EV charging is less delayed, so carbon emissions reduces more slowly.

A similar relation can be seen for G-CMR in Fig. 4.13b. Since a lower $V_{\max}$ reduces the G-curtailment power limit, increasing the severity of G-CMR leads to an

Table 4.2: COR systems tested under varying degrees of IR

	$V_{\min}$	$V_{\max}$	V_{trig}
CUR	0.9	1.1	-
COR1	0.9	1.1	1.04
COR2	0.92	1.095	1.03
COR3	0.93	1.09	1.02

increase in carbon emissions in both CUR and COR. The COR scheme incurs lower emissions since it has significantly higher average G-curtailment limit. COR-TMR does not affect the G-curtailment limit, therefore incurs no increase in emissions as V_{trig} changes in value.

This has several implications. First, since mean carbon emissions of COR-TMR are roughly equal to the unconstrained system, COR will lead to no increase in emissions compared to unconstrained charging. Second, since the COR scheme is tested here well below its charging capacity, increasing η_{EV} will lead to increased EV charging load delayed to off peak and low-emissions hours, therefore CO_2 emissions per EV user will decrease as penetration of EVs in the network rises.

4.4.2 Interval Reduction (IR)

Finally, performance under varying degrees of IR was tested by repeating the experiment for update interval t_u, which is a key determinant in Deployment Cost. The same performance metrics were evaluated for t_u incremented between 10 and 2 minutes for each of the COR systems outlined in Tab. 4.2.

Deployment Cost

In all performance categories except voltage control, effect of t_u in COR is negligible. This is because effects of TD, which had strong influence on peak load and DG in CUR, as well as overcurtailment, which had significant effect on EV charging delay, renewable energy input and CO_2 emissions, have now been outsized by the repetitive

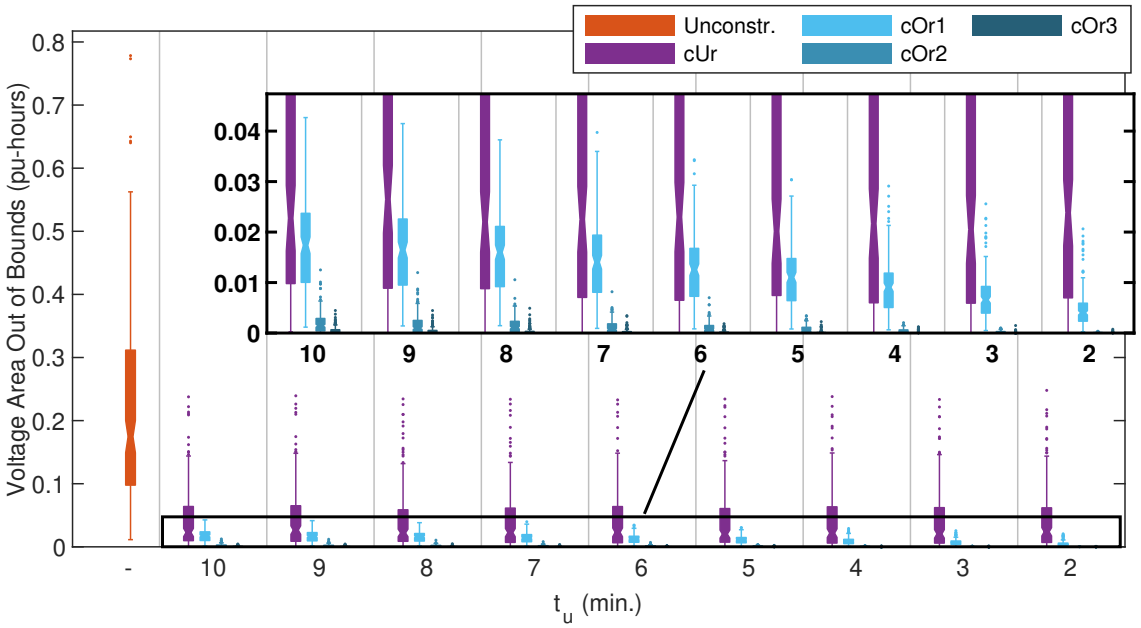

(a) Voltage area out of bounds (units pu-hours).

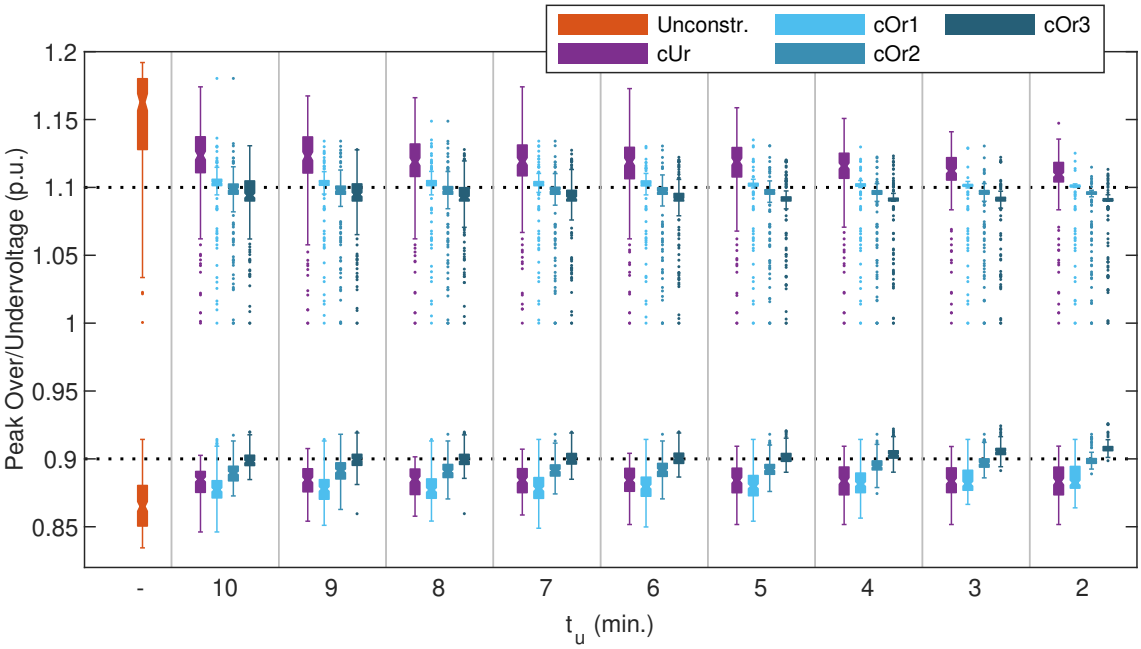

(b) Peak maximum and minimum voltage.

Figure 4.14: Voltage effects of three COR systems under IR, CMR and TMR.

load and DG corrections inherent in the COR running process. Instead, system update interval defines the window in which voltage deviations can occur.

Total voltage area out of bounds and peak over- and undervoltage are shown in Fig. 4.14 under successive degrees of IR for each of the COR test schemes. First, referring to Fig. 4.14a, it can be seen that total voltage area out of bounds reduces significantly with t_u for all COR schemes. For COR3, this reduces to effectively

zero, showing it is possible to completely eliminate voltage deviations out of bounds with properly calibrated CMR, TMR and IR. Similarly, referring to Fig. 4.14b, IR significantly reduces both peak over- and under-voltage for each of the three COR schemes. This figure demonstrate that the four critical variables $V_{\min}$, $V_{\max}$, V_{trig} and t_u can be tweaked to achieve any desired range of peak voltage deviations, depending on what is considered tolerable in the network.

Importantly, Fig. 4.14 demonstrates better performance of COR at long update intervals (t_u = 7-10 min). This means better voltage control can be achieved at lower deployment cost than CUR, providing strong advantage over the key performance-cost tradeoffs.

4.5 Conclusion

In response to growing penetration of EVs and DG, this chapter designs a correction-based Smart Charging scheme that can adjust EV charging load and DG according to mutual availability. This allows jointly optimised cost-efficiency for subscribing users and improved voltage control in the distribution network. KPIs and key performance-cost tradeoffs of this scheme are directly compared with those identified for CUR in Chap. 3.

The first key tradeoff is between voltage control and peak shaving. COR brings improved voltage control performance over CUR, particularly in overvoltage. In contrast, CUR displays significantly lower peak load. However, critically, COR achieves better voltage control under low-severity CMR and IR, which brings strong advantage when weighed against the other key tradeoffs. Peak load in COR is also less variable, so equipment can be run closer to its limits.

The second key tradeoff is between peak shaving and user inconvenience. COR has marked advantage in EV charging delay so more severe P-CMR can be tolerated for the same user inconvenience. COR also has higher DG energy delivery, and further

gains can be achieved since heavy G-CMR is unnecessary to avoid overvoltage. Finally, both schemes show reduced CO_2 emissions compared to unconstrained output. This is important, since high user subscription is required for scheme operation, and higher DG input promotes investment in renewable energy and helps deliver on emissions targets.

The third key tradeoff is between deployment cost and user inconvenience. Excessive IR is undesirable since it may require extensive replacement and reconfiguration of ICT infrastructure and hardware. Excessive CMR is undesirable since it increases EV charging delay and reduces DG energy input. In CUR, these are the only latency-mitigation options. COR gains strong advantage over this tradeoff with TMR, capable of achieving voltage control with low-severity IR and CMR.

COR can deliver better performance to the operator, users and investors without the need for a low-latency system. Further, reduced user inconvenience encourages subscription, which is a key functional requirement. These offset costs to the operator from added peak load. Ultimately, some compromise, where correction is applied up to a certain maximum load, may adequately marry the interdependent performance objectives of the operator and subscribing user.

The contributions of this chapter are as follows:

- An adaptive Smart Charging scheme is proposed to optimally adapt EV charging load and DG input according to mutual availability. This maximises cost-efficiency for subscribing users, significantly improves both EV and DG capacity and delivers strong advantage over key performance-cost tradeoffs compared to CUR.

- COR maintains the same distributed multi-tier hierarchical communications framework from Chap. 3. Therefore maintains all of its advantages - jointly minimised computation and traffic load as well as scalability and adaptability to a wide range of network sizes. Further, the COR power allocation algorithm takes into account computation at the central controller and user fairness

throughout the network in a way that is robust to non-uniform loading patterns during the correction process within one iteration phase.

- Latency constraints on KPIs are evaluated, and COR is shown to be significantly more robust to practical operational latency compared to CUR.
- Key performance-cost tradeoffs relating to Voltage Control, Peak Shaving, User Inconvenience, Carbon Emissions and Deployment Cost are evaluated statistically over 172 days of wind power profiles.

4.6 Evaluation

The work in this chapter can be aptly compared with several studies in the literature.

The Smart Charging scheme proposed in [44], that allocates EV charging power for cost minimisation based on three user-selected charging time zone priorities with Maximum Sensitivities Selection by Jacobian approximation, was improved on in [46]. Wind DG input is added, and the algorithm seeks to minimise energy costs through proper coordination of EVs during off peak hours while taking advantage of wind DG during their peak generation periods. Detailed simulations of Voltage Control and Peak Shaving were performed for a modified IEEE 23kV distribution system with three DG inputs and 22 residential networks populated with EVs. However, conclusions from introducing DG are limited and unquantified. Overvoltage is not considered. Further, only one DG profile is used, which is shifted by a certain number of hours to achieve diversity. Synergy between EVs and DG is not properly exploited, nor is scheme proven to be statistically robust to a large number of input profiles. Constant $t_u = 5$min update interval is used and again it is unclear how to handle users who cannot charge their vehicles during their preferred time zone due to network constraints.

In [49], the impact of various Smart Charging strategies on distribution grids with varying amounts of wind generation is assessed. Insights are provided into

power and finance-related impacts of different strategies and wind scenarios. Two cases are modelled, first minimising charging costs, second minimising peak load. The scheme allocates power for EV charging via quadratic programming formulation including feedback on electricity prices and uses constraints relating to driving requirements and battery parameters. However, it is unclear how this optimisation method would cope with large networks as the importance of computation complexity grows. Further, there is no consideration for user fairness in the network. Only peak shaving is considered.

Finally, [45] proposes a distributed Smart Charging solution for grid support services with dynamic pricing. For local (internal) active power management, the leading control signal is the voltage magnitude at the point of common coupling. DG is modelled in this system in the form of varying energy prices only, and just limited qualitative analysis is provided relating to power losses, voltage variation and line overload.

Again, all these studies present Smart Charging solutions for only a limited set of KPIs. None of them consider the comprehensive list modelled in this thesis. None consider User Inconvenience parameters such as EV Charging Delay, DG energy input and CO_2 emissions. Further, all these studies assume perfect knowledge of energy prices, driving patterns and network load is available everywhere in the network instantly and that control actions can be actuated without delay. None consider how practical operational latency affects each respective KPI, and it remains unclear how sensors and actuators within the schemes should be efficiently implemented via supporting ICT architecture. This chapter delivers on all of these issues.

4.7 Summary

First, the power allocation algorithm for COR is analytically derived. Unlike CUR where curtailment limits remain static for the full duration of curtailment, in COR the limit is 'corrected' every update interval to bring the worst bus voltage back to

the upper or lower statutory limit. This is achieved via Taylor Series approximation assuming small changes in the interval t_u, where an additional fairness condition is enforced to prevent power concentration at specific low-sensitivity buses. This fairness condition also reduces computation load meaning it can be extended to larger networks. Power delivery is then optimised such that the maximum available renewable generation is used at any time, and voltage deviation out of bounds is eliminated.

Performance under zero latency conditions is then examined, assuming corrections can be calculated and applied instantly in response to over- or undervoltage conditions. Since power delivery is optimised for the user, EV charging delay is significantly reduced. The tradeoff is that peak load in the system inevitably increases.

Practical latency constraints are then introduced. Resulting voltage deviations are categorised into CDs and TDs. Under COR, CDs occur only between update intervals, since the repetitive control action continuously brings worst bus voltage back within bounds. Meanwhile, TDs persist at the G-curtailment trigger. Three latency-mitigation strategies are proposed. CMR is effective to limit CDs; however, demonstrates noticeable detriment to curtailed power limits and does not effectively eliminate TD spikes. TMR involves separating the curtailment trigger voltage and the upper voltage limit such that the curtailed power limit is applied in anticipation of overvoltage. This effectively eliminates TD spikes without the drawbacks of heavy G-CMR. IR can decidedly reduce both TD and CD about upper and lower voltage limits, therefore bypassing the associated drawbacks of CMR.

Finally, statistical performance was demonstrated by exposing the system to 172 days of wind power profiles. Analysis showed COR has strong advantage over the CUR scheme in all key performance-cost outcomes except peak load.

Overload probability showed COR to have a wider practical range of $V_{\min}$ than CUR, reflecting its increase in EV capacity. Further, voltage deviation below bounds can be comfortably eliminated for $V_{\min}$ well within this practical range, even at high

latency. Overvoltage control also showed strong improvement provided ample TMR is employed.

The primary tradeoff of COR is increased peak load. However, this can be mitigated for the same user requirements by deploying higher P-CMR, since marked advantage in EV charging delay also occurs. COR by definition maximises DG in the network and avoids heavy G-CMR, it leads to notably higher daily energy delivery from renewable sources. This renewable energy advantage also translates to reduced carbon emissions.

Finally, IR is evaluated on three COR test systems, illustrating how correctly calibrated CMR, TMR and IR can be used to tailor the statistical range of voltage deviations and associated key performance-cost tradeoffs as desired. IR incurs costs relating to ICT deployment cost, therefore understanding of these key design tradeoffs is vital to the success of any Smart Charging system.

Chapter 5

Traffic Load and Deployment Cost in Large-Scale Hierarchical ICT Topologies

The global interconnectedness of machines and devices over the internet, often called the 'internet-of-things' (IoT) [78], stands to be a defining characteristic of 21st century technology. Smart Grids and Smart Charging are a direct application of IoT to the power network.

Previous chapters have proposed two schemes to optimise power flow in the distribution network using two-way information exchange between connected sensors and actuators. Additionally, a distributed multi-tier hierarchical communications framework is proposed to support both schemes such that they are scalable and adaptable to a wide range of network sizes. This chapter models traffic load in the proposed communications architecture as the number of SDs and addressable end-points in the network grows.

Three key infrastructural challenges relate to Smart Grid and IoT technology:

1. The fast growing quantity of power system data needs to be supported by the network [79]. Deployment of numerous and diverse interconnected devices

is accompanied by rise in data traffic and diverging Quality-of-Service (QoS) requirements (e.g. reliability, throughput, latency and security). As Smart Grid systems grow more prevalent, the number of SDs will increase dramatically, which will inevitably add load to ICT infrastructure. This chapter considers how to optimise the underpinning ICT network topology to meet growing traffic and QoS requirements.

2. The numerous competing communications standards for broad-network Smart Grid demand-response services (e.g. OCPP, OpenADR, Open Smart Charging Protocol (OSCP), ISO 15118) render practical evolution of the ICT system unclear. Two-way information flow between SDs is enabled by integration of many advanced communication technologies, and a cooperation of multiple protocols are required to meet Smart Grid requirements. This chapter draws conclusions general to numerous emerging industry standards.

3. Deployment of necessary supporting hardware, SDs and communications infrastructure also involves significant financial investment. Once the infrastructure has been deployed, any modifications can also be costly. This chapter explicitly models key performance-cost tradeoffs relating to ICT deployment cost to balance traffic and QoS provision as the network size grows.

This chapter simulates traffic load in multi-tier hierarchical ICT network topologies as the number of connected devices grows. The conclusions support assertions made on the proposed Smart Charging communications architecture in Chap. 3, however are also general to a broad range of applications in Smart Grids and IoT. The contributions are as follows.

- A testbed simulator is developed to model data traffic in large-scale mutli-tier hierarchical ICT topologies. Simulations for a large number of SDs using point to point, unicast and multicast communication under various heterogenous layouts are used to gauge demand-response latency for growing network sizes.

- This simulator is used to gain key design insights relating to mid-tier node deployment: Given a known network size and demand-response latency requirement, the number of ICUs required is quantified.

- A model is provided for demand-response latency including all congestion delays, protocol overheads and retransmissions, and the processing time of the testbed computers is eliminated. Using this model, key performance-cost tradeoffs relating to network size, QoS provision and ICT deployment cost are discerned.

The rest of the paper is laid out as follows. Section 5.1 describes the testbed simulation model concerning topology, communication protocols, module structure and graphic user interface. The demand-response latency model relevant to traffic accumulation in the hierarchical topology is presented in Section 5.2. Statistical simulation results are presented and analysed in Section 5.3, where key performance-cost tradeoffs are identified relating to demand-response latency, network size, topology, and ICT Deployment Cost. Finally, Section 5.4 concludes the topic.

5.1 Testbed Simulator

The aims of the testbed simulator are to analyse the effect of the telecommunications infrastructure on the overall network performance and to provide crucial insight into network optimisation. Specifically, it is designed to model how traffic load and QoS provision changes for large network sizes and varying topologies.

The scope is for networks where: Hundreds to thousands of nodes are organised in a specific topology to serve a large number of users via smart meters and actuation devices; point-to-point, unicast and multicast communication between nodes is considered, to simulate a complex directional arrangement of network traffic; Traditional network and transport layer internet protocols with IPv4 and IPv6 address space

are used. This allows general application to the majority of Smart Grid and Smart EV Charging communications standards and requirements.

The testbed is designed to be flexible, scalable and reconfigurable, oriented by and accessible to communication providers to optimise for large scale metrics. Scalability and customisability is key, since the testbed requires network arrangements of 1000+ nodes spread over multiple connected computers. For this reason Microsoft Visual Studio VB.NET platform [80], [81], which is free and widely accessible, was chosen over standard network simulators such as OPNET (which is proprietary software and has limited customisability) or NS-3 (which has limited scalability over multiple computers) [90].

5.1.1 Contributions of the Testbed

The simulation must be able to test varieties of communication standards combined in assorted arranged network topologies, so as to find the optimum solutions prior to capital investment in hardware and deployment. In this respect, Smart Grid simulations have gained significant attention in the recent years:

A testbed for demand-focused energy management in the end-user environment is designed and implemented in [82]. The testbed consists of three levels - the base station, gateways and smart devices. The gateways are implemented via RaspberryPi with multiple radio front ends, including Z-wave, Zigbee, Bluetooth, Wifi and Ethernet. The on-site test was performed only on a small scale.

A testbed based on wireless communication technology involving both centralised and distributed architectures is studied in [83]. Hardware interfaces between energy and communication components is designed and implemented, and a small scale laboratory test is performed investigating real-time demand response and disruption resilience. There are also works that focus on ICT architecture.

In [84], a three-tier framework is proposed based on the IoT, while in [85], an interoperability framework based on data distribution services is proposed. Mean-

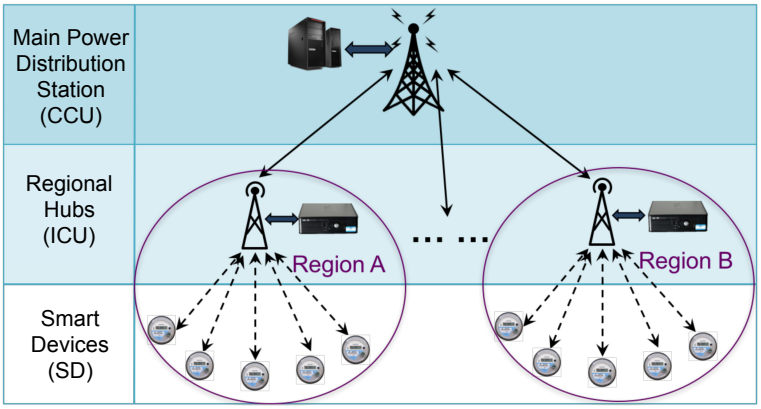

Figure 5.1: Three-Tier Hierarchical Topology

while, in [86], a comprehensive survey on Smart Grid cyber-physical system testbeds is performed. Existing testbeds are compared and discussed from several design aspects, including heterogeneous communication support, security and privacy, multiple protocol support and remote connection access.

These trials and tests pave the way for the successful deployment of Smart Grid ICT architectures, however these are restricted to small and medium-scale studies, and large-scale simulation has not been fully addressed. Analysis of a large networks is of great importance to physical implementation of Smart Grid ICT architectures from the perspective of communication service providers. This chapter presents a Smart Grid testbed designed for large-scale network simulations and derives key performance-cost tradeoffs and insights that are not visible on smaller systems.

5.1.2 Topology

The simulation consists of three component types forming a three-tier heterogenous network: SDs, ICUs and a CCU module. A three-tier hierarchical topology is used (as proposed for the two Smart Charging schemes in Sec. 3.2).

A hierarchical topology is an arrangement of two or more star networks connected together by one central administrator at the highest tier. In each star network there is an ICU to which all the lower tier SDs are directly linked. The ICUs are then directly connected to the CCU, as in Fig. 5.1. This topology is ideal when the nodes are located in groups, such as at a particular power distribution bus, with each group

occupying a relatively small physical region, and is favoured by many open Smart Charging standards such as OCPP and OpenADR.

5.1.3 Communication Protocols

TCP/IP is commonly used in Smart Grid and IoT standards for several reasons. First, it is widely used and well understood, so is supported by the majority of available routers and servers, reducing cost of system development. Second, since it is transparent to real networks, more routes are available for transmission. A wide choice of encryption algorithms can also guarantee information security, the complexity of which can be assigned according to the specific application. Further, IPv6 is already rolled out for commercial use and is able to support the rapidly growing number of devices expected in the network. Finally, it allows for easy accessibility and scalability to new devices due to its general prevalence across all manner of practical applications.

TCP/IP is used in this simulation for communication between all nodes and tiers. The simulation supports both wireless or wired communication, requiring only input of data rate and bit error rate (BER) on each communication link.

5.1.4 Module Structure

The simulation is developed in a Windows application environment. In this application, the user selects all the simulation parameters through the application graphic user interface (GUI). The application then calls the three described functions (`SmartDeviceModule.exe`, `ICUModule.exe`, `CCUModule.exe`) in order to build the 3-level hierarchical topology. For example, if a user has selected 1 node for the CCU in the upper tier, 10 nodes for the ICU in the middle tier and 10 nodes (SDs) per ICU in lower tier, the application will call `CCUModule.exe` once, `ICUModule.exe` ten times, `SmartDeviceModule.exe` 100 times. The CCU knows the IP addresses of its ICU nodes. Each ICU node knows the IP address of the CCU, as well as the

IP addresses of its regional SDs. Each SD knows the IP address of its ICU. The function of each module will be described in turn, before the operation of the GUI inputs and outputs is explained.

Each node in the network (and each module) has a unique IP address, and each module consists of a listener and sender submodule which communicate on separate ports. In theory, the maximum supported port number is 65,536, however this simulation requires only two ports per module for the listener and sender. This feature makes the testbed highly flexible, since more functions can easily be added and assigned with different ports to cooperate with existing modules. Each submodule has functions to generate and receive TCP/IP packets and log device events.

Smart Device (SD) Module

SDs are lower tier nodes that conduct measurements and/or actuations in a Smart Grid system. They receive and respond to control commands from the CCU, via their regional ICU. The proposed SD module consists of two submodules, the Listener and Sender, as illustrated in Fig. 5.2.

The SD module algorithm has several capabilities. The Listener submodule listens to a specific IP:port address and receives data (command packets) from the upper layers. The Sender sub-module can send data (measurement or status packets) to the upper layer in two ways, either periodically every predefined fixed period of time, or on demand, upon receipt of a measurement command from the upper layer by the Listener sub-module. There are several measurement commands, chosen for the needs of the simulation, for example “send now values”, “send last values”, “send a fixed value”, “send a random value”, etc. The Listener and Sender sub-module write into the `SmartDevice_Listener.log` file and `SmartDevice_Sender.log` file, respectively, for every received data packet.

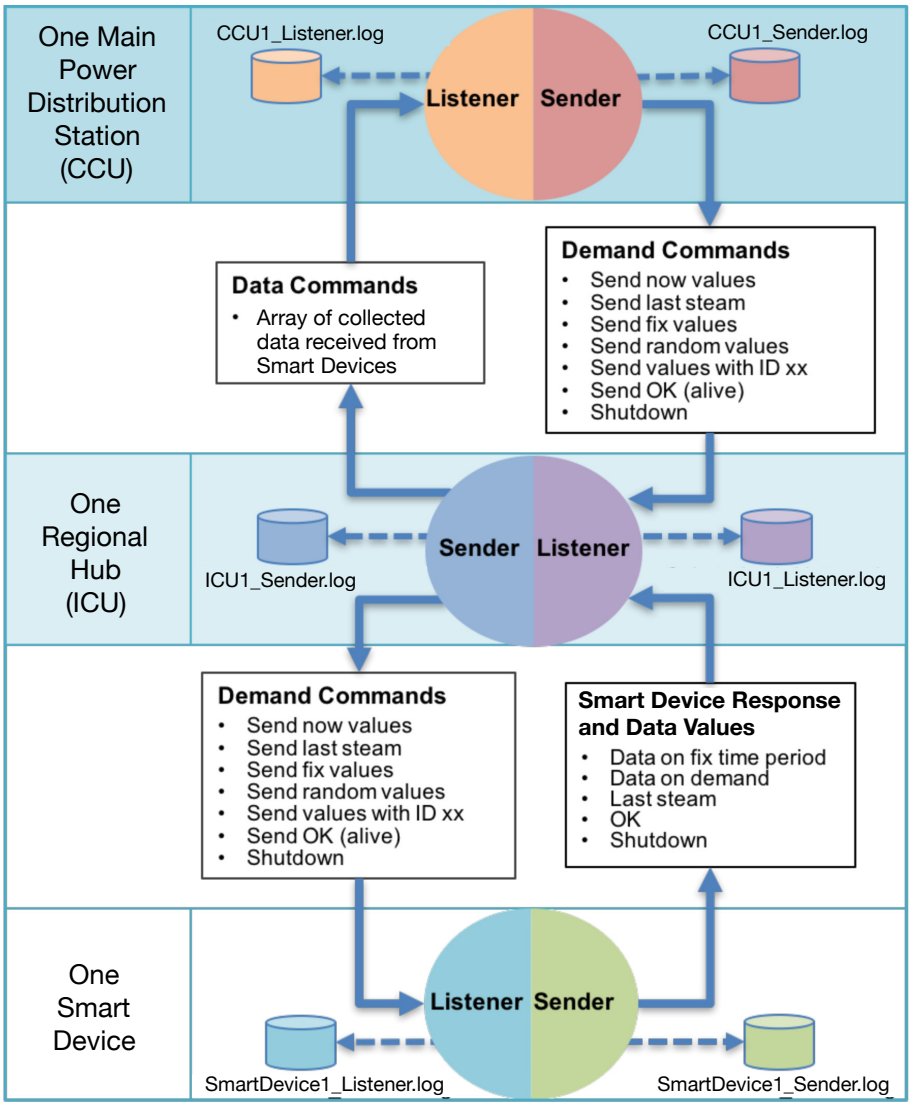

Figure 5.2: Overview of the Simulation Module Structure

Regional Hub / ICU Module

ICU modules are the mid-tier nodes, which aggregate measurements from their associated SDs and forward the data to the CCU. Like the SD module, the ICU module consists of a Listener and Sender submodule, as illustrated in Fig. 5.2.

Capabilities of the ICU module involve TCP/IP traffic coordination, SD control and device event logging, so the algorithm has a number of functions. On starting the ICU module, both Listener and Sender sub-modules begin. The Listener listens to a specific IP:port address, receiving command packets from the CCU and measurement/status packets from its SDs. For every received packet it writes a record into the `ICU_Listener.log` file. The Sender sub-module may send status

request packets to SDs or aggregated readings to the CCU, and writes each packet transmission into log data in the `ICU_Sender.log` file.

When the ICU Listener receives a measurement command from the CCU, the Sender submodule forwards the command to its regional SDs in a broadcast manner. Once the Listener has received each of the status reply packets from all of its affiliated SDs, the Sender submodule aggregates and sends the data to the CCU.

Central Control Unit (CCU) Module

The CCU module is the main network coordinator, where data from the entire network is gathered. Again, it consists of Listener and Sender submodules, shown Fig. 5.2. Its functions are to send commands to the lower tier ICU nodes and receive replies. It also logs device events into a Sender and Listener log file and may be instructed to request SD data in three ways:

- Periodically: The CCU sends measurement commands to its ICUs every update interval or fixed period of time.
- On demand: The CCU may send measurement commands in between update intervals, in which case an additional demand-response cycle is generated.
- Randomly: The CCU may be programmed to send measurement commands randomly during the overall simulation time period with a frequency following the Poisson distribution.

In the CCU module algorithm, the Listener submodule listens to a specific IP:port address and receives data (aggregated status packets) from the ICUs. It writes a record of each received packet into the `CCU_Listener.log` file. The Sender submodule sends measurement commands to all ICUs with a broadcast function, and writes log data to the `CCU_Sender.log` file.

This communications structure is general to a large number of centralised demand-response architectures. However, it also specifically emulates that of the two Smart

Charging schemes designed in previous chapters. SDs could be Charging Stations, DG controllers or home energy managements systems in a residential LV feeder. ICUs may be located anywhere in the network where a certain power curtailment may be required, for example at a MV distribution bus. The CCU could be the DSO or other operator body. The demand-response latency process described here emulates a power curtailment or measurement command coming from the CCU and the reply from SDs via their regional ICU.

5.1.5 Graphic User Interface (GUI)

Simulation data is input by the user in four GUI input forms:

1. *Initialisation* - shown Fig. 5.3a, the user selects if the simulation environment should be distributed over multiple computers or stand-alone on a single computer. In the stand-alone environment the Upper, Middle and Lower tiers are all on the same computer with the same IP address. Each node then uses different ports. In the distributed environment, any of the three tiers Upper, Middle or Lower may be built on different computers, and hence with different IP addresses as required.

2. *Topology* - shown Fig. 5.3c, the network topology is chosen by selecting the number of nodes for each tier.

3. *Data Send* - shown Fig. 5.3b, the user decides the type of SD measurement data (either fixed values or random values for purposes of simulation) and activity of the CCU measurement commands (either periodically, randomly or on demand).

4. *Simulation Time* - shown Fig. 5.3d, the simulation time preferences are specified, which includes when, if at all, the nodes in each tier should send their periodic messages, whether there should be a random time delay before each

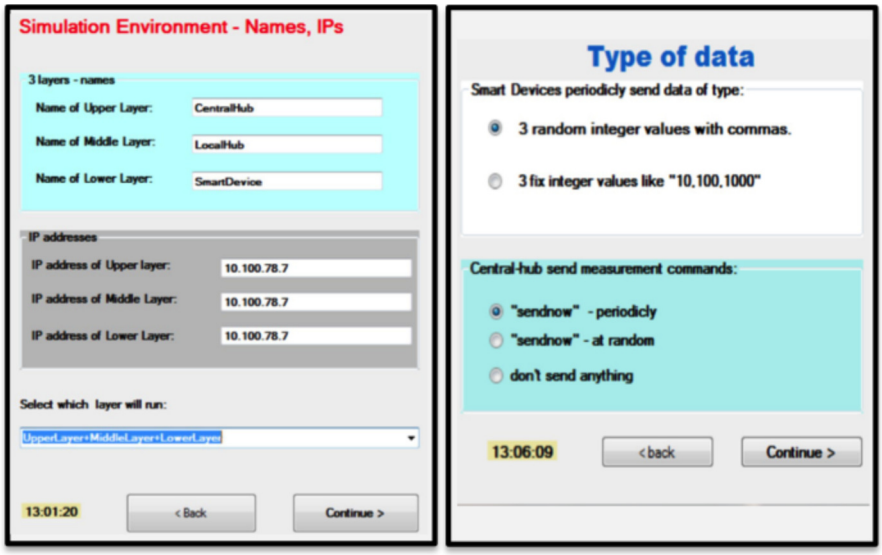

(a) Initialization Form of GUI Input (b) Data Send Form of GUI Input

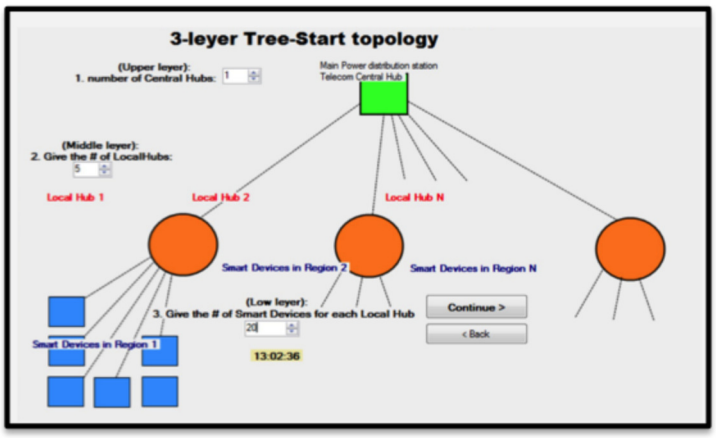

(c) Topology Form of GUI Input

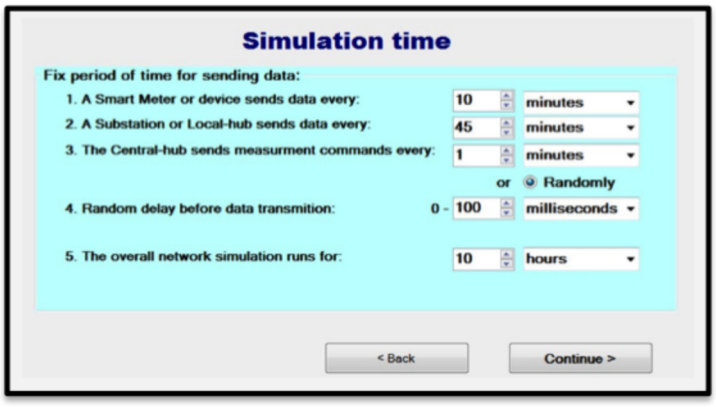

(d) Simulation Time Form of GUI Input

Figure 5.3: GUI Input Forms

transmission so that the computer's processor is not overloaded by a large number of nodes sending messages all at once, and how long the total simulation should run for.

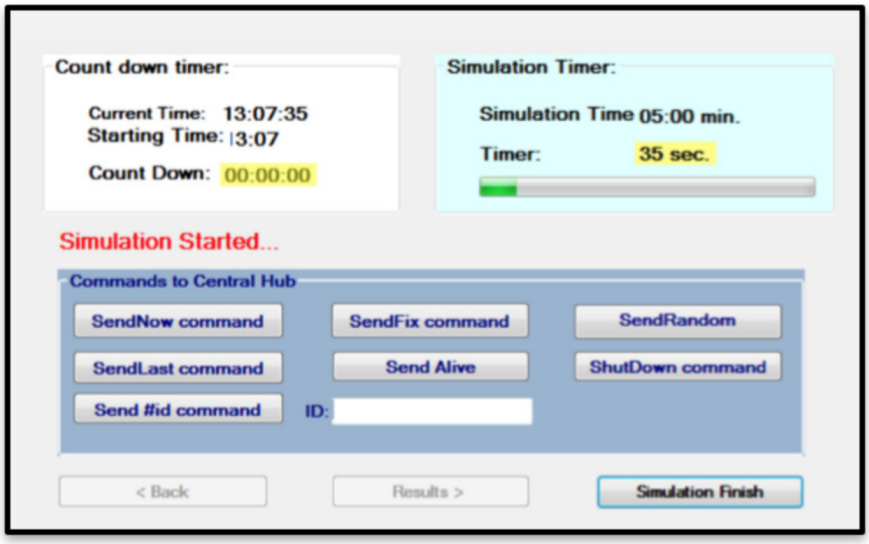

(a) Simulation Running GUI Output

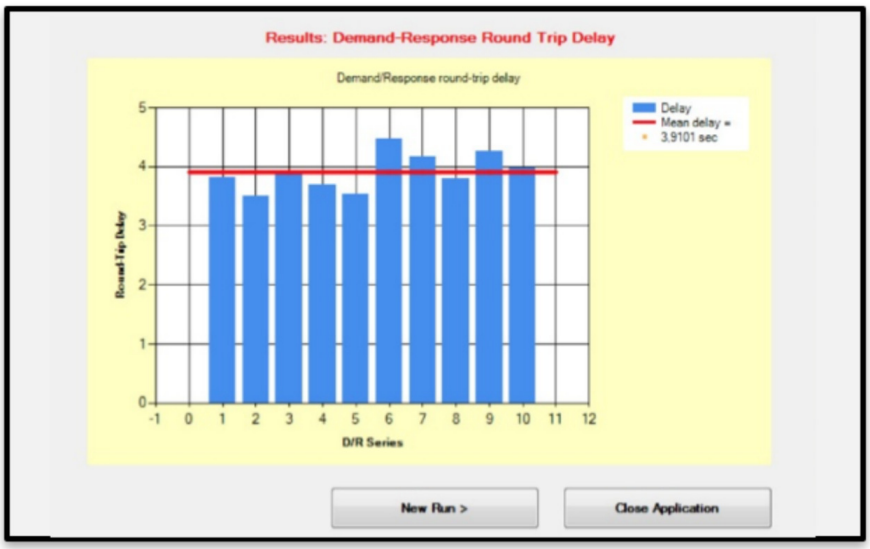

(b) Latency Graph of GUI Output

Figure 5.4: GUI Outputs

While the simulation is running, the GUI displays the output window shown in Fig. 5.4a. During this time, the user can choose to send additional commands from the CCU, such as 'send now', 'send alive', etc. Once the simulation is complete, the GUI displays a bar graph of the demand-response latencies for all the commands sent from the CCU during the simulation, and displays the mean with a red line, as shown in Fig. 5.4b.

With this testbed simulation platform the statistical effect of Smart Grid network topology on demand-response latency is analysed. With a specific latency constraint,

this can be used to gauge the maximum number of devices that can be supported for a given network structure. Analysis can then serve to optimise the system configuration, and gain crucial insights into design characteristics for QoS provision in Smart Grid/IoT networks as the number of served users increases.

5.2 Demand-Response Latency Modelling

For any ICT system supporting a Smart Grid or IoT function, the maximum number of devices that the network can support for a given set of QoS requirements is a key feature. The total number of SDs and number of ICUs per CCU will be independent variables in this experiment, which aims to gauge the relation between network topology and demand-response latency. Ultimately, an optimal topology is sought to maximise the number of supported SDs in a large network. This section evaluates how the three-tier hierarchical centralised topology for SD aggregation may affect the resulting latency in the system.

While the Smart EV Charging schemes in Chap. 3 and 4 assumed there is one ICU at each distribution bus, this definition is now generalised such that there may be more or less than one ICU per distribution bus, e.g. a particularly large bus might be split between two ICUs, or two small buses might be served by the same ICU. Further, to properly model this effect it is assumed that each ICU has the same number of SDs. Since number of SDs per ICU is a key performance variable with respect to QoS provision and ICT network design, this assumption is valid.

The demand-response latency in this case consists of the time required for the CCU to request measurements from all subsidiary SDs and receive a complete reply, emulating the control action carried out each update interval in the COR scheme. This demand-response latency includes all protocol overheads, retransmissions and traffic congestion at the respective nodes. For total number of SDs N_T, the number

of SDs per ICU N_{SD}, and number of ICUs N_{ICU} are related by the formula

$$N_T = N_{SD} N_{ICU}. \tag{5.2.1}$$

Given that measurement data from each SD must pass through two hops in order to reach the CCU (SD to ICU and ICU to CCU), the bottleneck in the system occurs in the middle tier, at the ICU level. Thus N_{SD} is a critical network parameter.

The traffic load at any node in the network can be quantified by the utilisation factor ρ. This is defined as the ratio between the packet arrival rate λ and the packet service rate μ

$$\rho = \frac{\lambda}{\mu}. \tag{5.2.2}$$

Assuming an M/M/1 queueing process, since there is one queue per ICU, the average queuing latency due to congestion at ICU is given by

$$L_q = \frac{1}{\mu(1-\rho)} = \frac{1}{\mu - \lambda} \tag{5.2.3}$$

Assuming constant average packet service rate from ICU to CCU, the packet arrival rate at each ICU should increase linearly with N_{SD}, and the queueing delay at each ICU will increase proportional to the inverse of this. However, the demand-response latency incurs four queueing delays from CCU to ICU, from ICU to SD, from SD to ICU and ICU to CCU. Each node has only one listener and one sender submodule, so there may be congestion at any of these steps, and each queueing delay is also affected by the delay incurred in the previous queue. Latency is further incurred by processing time, transmission time and the number of retransmissions. This simulation testbed aims to gauge the overall effect of number of SDs and number of ICUs on network demand-response latency.

5.3 Results & Analysis

Using the testbed described in Section 5.1, ten different network sizes were simulated using N_T from 100 to 1000. These nodes were spread over three computers connected

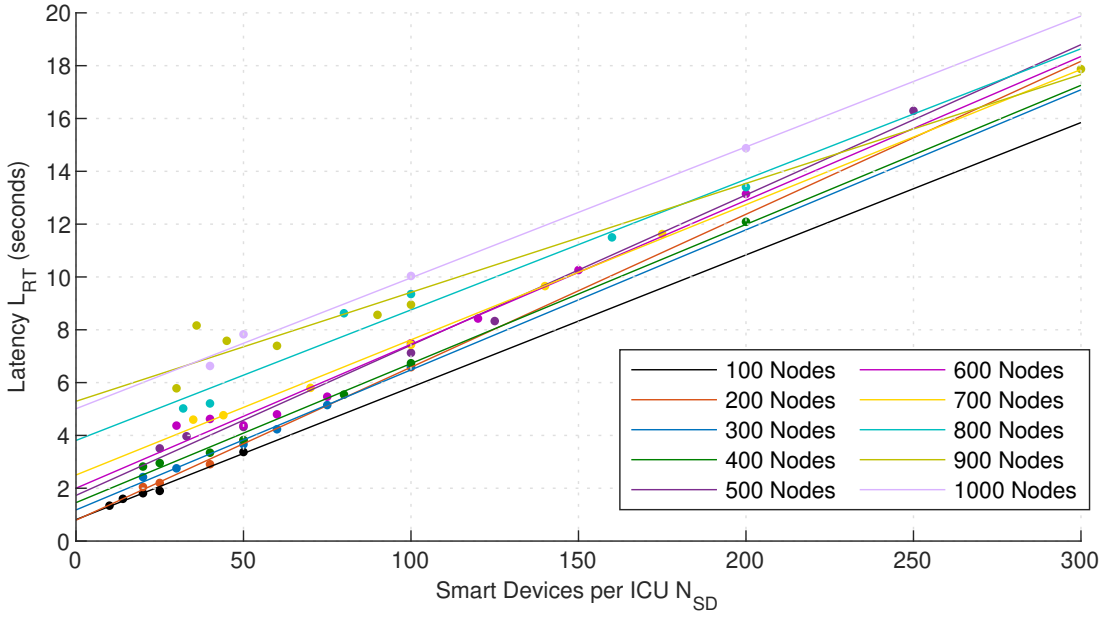

Figure 5.5: Demand-Response delay variation for SDs per ICU

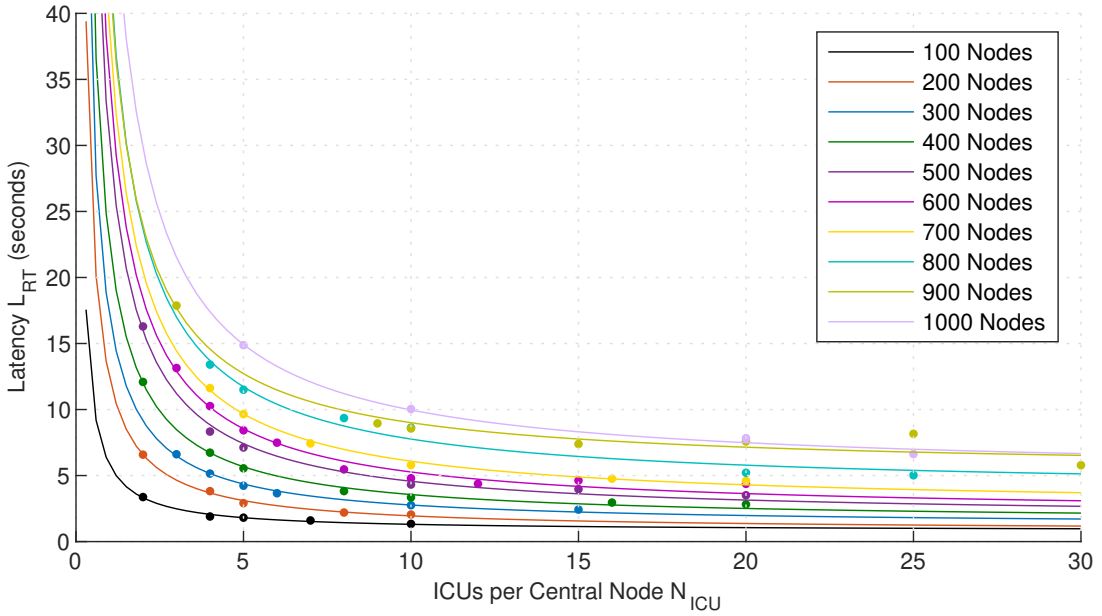

Figure 5.6: Demand-Response delay variation for ICUs per CCU

via RS232 cable. One computer held the CCU, the second held the ICUs and the third held all SDs. Within each network size, N_{SD} and N_{ICU} were varied, to gain an idea of the effect of network topology on demand-response delay. The data links were modelled with a data rate of 50 Mbps to simulate the VDSL backbone, and BER of 10^{-7}.

Fig. 5.5 shows how the demand-response latency L_{RT} varies with N_{SD} for the different network sizes. It can be seen that the delay increases linearly with the

number of SDs per ICU, in the form

$$L_{RT}(N_{SD}) = \alpha N_{SD} + \beta \tag{5.3.1}$$

where α, β are fitting coefficients. This relation is seen even more clearly when L_{RT} is plotted against the number of ICUs N_{ICU},shown in Fig. 5.6, following an inverse relationship of the form

$$L_{RT}(N_{ICU}) = \alpha \frac{N_T}{N_{ICU}} + \beta \tag{5.3.2}$$

In this case α, β are found by nonlinear least squares regression.

The fewer SDs per ICU, or the more ICUs for a given number of devices, the less congestion during the aggregation process, and less overall delay. This makes intuitive sense, since the sensor data is then sent along more parallel data streams to and from the CCU and incurs less queueing delay. However, Fig. 5.6 also shows a crucial design insight: for a constant total number of devices, the delay benefits of using more ICUs diminishes with the inverse of the number of ICUs. This is important, since the number of mid-tier devices in the communications architecture will have a significant effect on deployment cost.

Also notice that the demand-response delay appears to rise with the total number of nodes. This is unexpected, since the data traffic bottlenecks occurs at the ICU, which are unaffected by the number of parallel data streams in adjacent ICUs. This proportional increase is accountable to the processing time of the computer itself - generating measurement packets for 1000 nodes will take ten times the time to generate packets for 100 nodes. It is desirable to remove the processing time from the overall delay calculation, since packet generation for the entire system would not normally be undertaken by only one processor.

To remove this processing delay, the average delay for each fit in Fig. 5.5 was used to compute the average difference between each successive network size, which is taken to be the processing time for 100 nodes T_{p100}, in this case 457 milliseconds. This time delay was then subtracted from the data for every 100 node increase,

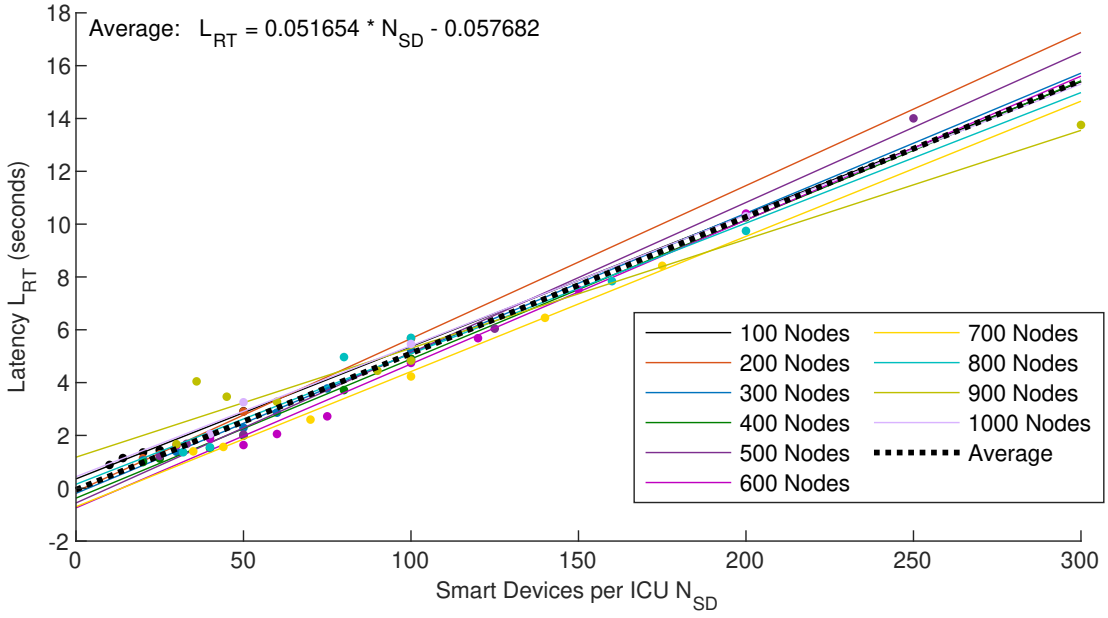

Figure 5.7: Demand-Response delay minus processing time for Devices per ICU

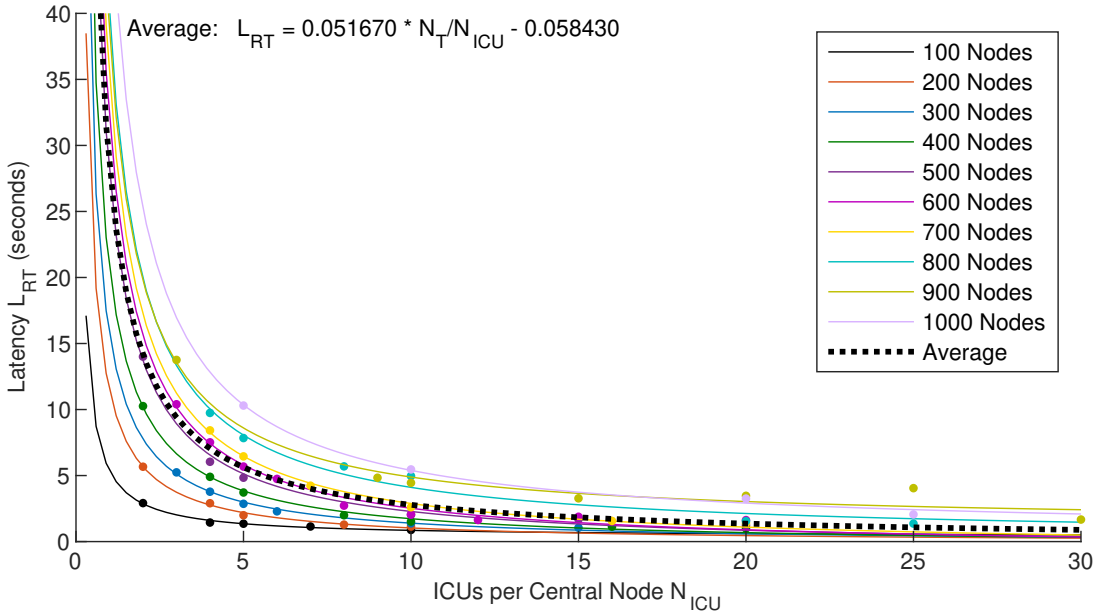

Figure 5.8: Demand-Response delay minus processing time for ICU number

giving the plots shown in Fig. 5.7 and 5.8. This allows the coefficients α and β to be estimated as the average gradient and y-intercept. The average curve in each case is shown by the black dotted line, which runs approximately through the origin in Fig. 5.7, and tends to zero and infinity in Fig. 5.8.

Fig. 5.9 shows the same in a 3D surface plot for the number of ICUs and total number of devices. For comparison, plots both with and without the processing time T_{p100} are included. From this it is clearly visible that for a constant total number

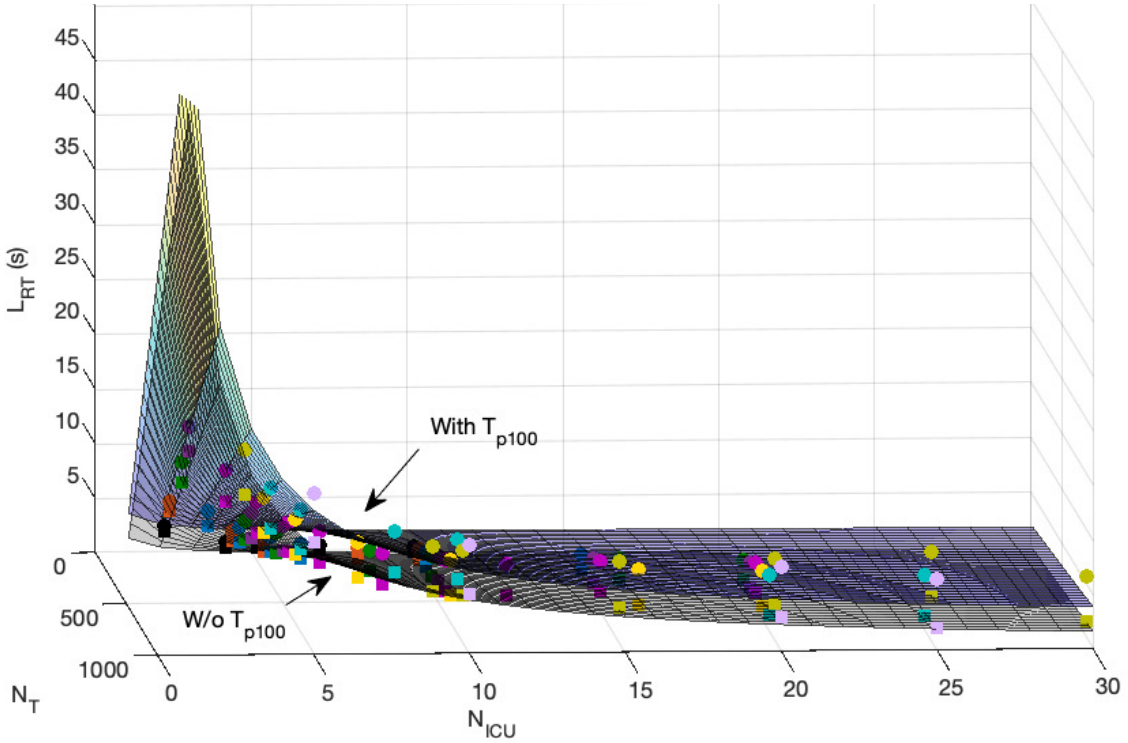

Figure 5.9: 3D plot of L_{rt} with N_{ICU} and N_T with and without processing time. (Uses the same data point colour scheme as previous graphs)

of devices N_T, the minimum delay will occur with the maximum number of ICUs N_{ICU}. For $N_{\text{ICU}} > 15$ there is very little variation in latency for each additional ICU. The exact number must then be chosen accounting for QoS requirements specific to the application, and budget constraints of the overall system.

Several outcomes can be drawn from the results of this chapter. First, they demonstrate example of a key assumption that has persisted throughout this thesis: that latency in the underlying communications system is subject to capital investment in backhaul communications infrastructure. Deployment of ICT devices such as ICUs in a hierarchical network involves significant financial investment for the operator. Further, once installed, any modifications can be costly. If traffic in the system increases for the same number of ICUs, either by increasing the number SDs (by serving more users) or by sending more data from each SD (e.g. by reducing the update interval), traffic load, queueing delay and/or demand-response latency will rise in the system.

This exposes the second, more important, outcome of this chapter. That by

deploying more ICU units for the same number of served users, demand-response latency will reduce; however, latency falls by an increasingly small amount with each additional mid-tier node, while the cost of deploying each new node stays the same. This leads to an inevitable key performance-cost tradeoff between latency reduction and deployment cost in the system.

5.4 Conclusion

Infrastructural challenges relating to Smart Grid and IoT communications networks can be summarised in three aspects. First, the growing number of served users implies a rapidly growing quantity of SDs which share a diverse set of QoS requirements. How to guarantee these QoS requirements under increasing traffic load is a significant concern. Second, this problem is complicated by numerous competing communications standards that each entail a cooperation of advanced communication techniques, and a single unifying industry standard has yet to emerge. Third, deployment of ICT hardware to support the power network is a significant investment, and once committed, modifications are costly.

How best to deliver the diverse QoS requirements of emerging power applications under a restricted communications budget remains a significant challenge for future Smart Grid systems. To this end, this chapter assesses how ICT infrastructure must be deployed to deliver QoS requirements with regard to rapidly growing networks and confined backhaul communications budgets. This evaluation of large scale smart grid architectures is of great interest to service providers for optimisation of deployment cost-efficiency.

The contributions of this chapter are as follows:

- A large-scale simulation testbed is designed to study the demand-response latency of heterogeneous multi-tier hierarchical network topologies. The simulation is general to a broad range of Smart Grid and IoT applications and

communications standards using traditional network and transport layer internet protocols.

- Using this simulation testbed, three-tier hierarchical topologies are evaluated with three distinct node types. Networks with up to 1000 client nodes are simulated, where various lower and mid-tier node configurations are studied. The number of SDs that can be supported per mid-tier aggregator and the total number of SDs are key assessed variables since this decides the queueing latency at critical bottlenecks along the demand-response path.

- A model for demand-response latency across large-scale multi-tier hierarchical network topologies is provided, where the evaluated latency includes all congestion delays, protocol overheads and retransmissions, and the processing time of the testbed computers is successfully eliminated from analysis with data post-processing. Using this model, key performance-cost tradeoffs relating to QoS provision and ICT investment are evaluated.

Demand-response latency requirements can be provided for a certain number of client users by deploying an appropriate number of aggregator nodes in the middle tier. However, each new ICU incurs an additional cost to the operator. Further, each addition of a mid-tier node reduces the latency by a smaller amount. Thus a balance must be found dependent on the number of SDs, latency requirements of the application messages, and overall communications budget. The curves provided can be used for cost-optimisation of the underpinning data infrastructure in any centralised or distributed Smart Grid / IoT application environment, however are apt to support the latency-driven cost-performance tradeoffs exposed for the two Smart Charging schemes in previous chapters.

Chapter 6

Conclusion

The growing penetration of EVs into the market is driving sharper spikes in consumer power demand. Meanwhile, growing renewable DG is driving sharper spikes in power supply. This is leading to growing temporally unsynchronised spikes in generation and consumption, which manifest as localised over- or undervoltage and disrupt grid service quality. By harnessing a vast network of cyber-enabled sensors and actuators, Smart Charging solutions can respond to over or under-voltage by curtailing EV charging or DG in strategic locations. In this way, Smart Charging stands to deliver precise and colocated actuation at fine granularity in the distribution network, and can synergise with renewable supply such that the capacity of both EVs and DG can be improved.

This thesis proposes two Smart Charging schemes for secondary voltage control in the distribution network, and models key performance-cost tradeoffs between various interrelated KPIs in the power grid and supporting ICT infrastructure.

6.1 Summary

Chap. 1 begins with an introduction to Smart Grids and the open research topics targeted by Smart Charging. Specific research objectives of this thesis are then defined and explicit research contributions are listed.

A background and literature survey then begins in Chap. 2. First, background material is reviewed, where two mathematical models are derived to describe prevalent power flow issues in the transmission and distribution network. These models are used to identify key shortcomings of traditional grid control methods that are targeted by Smart Grid solutions for provision of future energy services. Second, recent literature is surveyed on key research topics in this thesis. ICT constraints relevant to data exchange between sensors and actuators are introduced, and networked control paradigms in Smart Grid communications architectures are reviewed. Smart Charging is then presented, along with relevant extension to Vehicle-to-Grid configurations, as a means to deliver various KPIs in the power network. Recent open Smart Charging and Demand-Response communications standards are then summarised.

The research contributions of this thesis begin in Chap. 3, where the first Smart Charging scheme (Smart Curtailment, CUR) is presented relevant to Peak Shaving and Voltage Control to minimise costs of network operation. First, the system model is described. Household, EV charging and DG inputs to the system are defined, along with the test IEEE bus distribution network. The supporting ICT architecture for both schemes is then established, before operation of CUR is explained in detail, beginning with operation under zero latency. Key practical latency effects on KPIs are then identified, and two latency mitigation strategies are defined. Scheme performance is then consolidated statistically against 172 days of 1s windpower profiles, and key performance-cost tradeoffs are established relating to KPIs: Voltage Control, Peak Shaving, User Inconvenience, DG Energy Input, CO_2 Emissions and ICT Deployment Cost.

Having demonstrated a benchmark performance improvement with CUR over random unconstrained charging, Chap. 4 gains advantage over the key performance-cost tradeoffs with the second scheme (Smart Correction, COR) by reformulating scheme optimisation for power consumers and/or investors in DG systems. By maximising power delivery when it is cheap - e.g. during non-peak times or when

renewable generation is strong, natural synergies between EV charging and DG can be exploited. First, mathematical formulation of the COR scheme is defined. Operation under zero latency is then explained. Practical latency effects are identified and three latency-mitigation solutions are presented. Statistical performance consolidation is repeated for COR under 172 days of 1s windpower profiles. Significant advantage over CUR is demonstrated for many key performance-cost tradeoffs in the same KPIs.

Finally, Chap. 5 models data traffic accumulation in the proposed multi-tier hierarchical ICT architecture as the number of client devices in the network grows, and resulting cost-performance tradeoffs between QoS provision and ICT Deployment Cost. A testbed simulator is developed to model data traffic in networks of hundreds to thousands of nodes. The simulation is first described concerning topology, communication protocols, module structure and graphic user interface. A model for demand-response latency relevant to traffic accumulation in the hierarchical topology is then presented. Finally, statistical simulation results are analysed where key performance-cost tradeoffs are identified relating to demand-response latency, network size, topology and ICT Deployment Cost.

6.2 Conclusion

This thesis targets four critical research areas in Smart Charging development. Conclusions can be categorised correspondingly:

6.2.1 Divergent Optimisation Standpoints

Smart Charging can be approached from two optimisation objectives. For the network operator, EV charging can be rescheduled to flatten peak loads, reducing operating costs by allowing for power equipment to be minimally replaced. For consumers and generators, power transfer can be maximised when it is ‘cheap’, for

example during non-peak times or when renewable generation is strong. These two objectives can be misaligned, and this dichotomy is largely unanswered in Smart Charging research. This thesis explicitly models the performance implications of both optimisation standpoints via targeted case study.

The two Smart Charging schemes proposed in this thesis correspond to the two optimisation standpoints. Both can simultaneously achieve secondary voltage control in the distribution network and dramatic rise in EV and DG capacity. CUR, optimised for peak shaving, is capable of significantly reducing peak load, and therefore reducing costs for the system operator. This is important, since costs for the operator eventually translate to costs for the user in the form of energy prices. However, the COR scheme, optimised for consumer/generator, demonstrated that considerable advantage over many performance-cost tradeoffs and KPIs can be achieved by removing peak load constraints. Further, much greater EV and DG capacity is achievable.

Importantly, the advantages of COR also eventually translate to cost reductions for the operator. COR can deliver better performance to the operator, users and investors without the need for a low-latency system. Further, reduced user inconvenience encourages user subscription, which is a key functional requirement. These offset costs to the operator from added peak load. Ultimately, some compromise between CUR and COR, where correction is applied up to a certain maximum load, may adequately marry the interdependent performance objectives of the operator and subscribing user.

6.2.2 Practical Latency Constraints

Smart Grid solutions require a pervasive ICT infrastructure to connect numerous sensors and actuators. Fine-granularity control also requires optimisation over increasingly numerous links and buses. For this reason, cost of data collection as well as computation complexity in the optimisation algorithm are significant investment

concerns relating to operational latency. Further, operating bodies in the power network are traditionally unaccustomed to latency-critical applications and this is reflected in deployed hardware. The result is that practical operational latency up to several minutes often exists before actuations can be effectively implemented.

This thesis explicitly models effects of varying practical operational latency on KPIs. Both Smart Charging schemes are modelled under practical latency constraints via the system update interval. Multiple latency-mitigation strategies are identified for each Smart Charging scheme, and success of each relating to key performance-cost tradeoffs is statistically evaluated. Further, performance under practical operational latency is used to gauge the cost of ICT Deployment relevant to each proposed scheme.

COR permits strong advantage over CUR in various key performance-cost tradeoffs by providing improved latency-mitigation capability. With the ability to apply curtailment limit in anticipation of overvoltage (with TMR), voltage control is significantly improved without the heavy IR and CMR required for the same in CUR. Effectively this means improved Voltage Control, User Inconvenience, DG Energy Input and CO_2 emissions without the need to reduce system update interval. This offsets the additional costs associated with peak load increase by limiting deployment costs associated with interval reduction.

6.2.3 Balancing KPIs over multiple concerned parties

Successful Smart Charging requires coordination from various concerned participants in the power network, each with their own prioritised KPIs. How to guarantee satisfaction for each participant remains unanswered in the literature. This thesis explicitly models key performance-cost tradeoffs relating to six KPIs: Voltage Control, Peak Shaving, User Inconvenience, DG Input, CO2 Emissions and Deployment Cost. Additionally, Chap. 5 models key performance-cost tradeoffs between Traffic Load and Deployment Cost in the supporting ICT network.

Voltage Control vs Peak Shaving

The first key tradeoff is between Voltage Control and Peak Shaving. COR brings improved voltage control over CUR, particularly in overvoltage. In contrast, CUR displays significantly lower peak load. However, critically, COR achieves better voltage control under low-severity CMR and IR, which brings strong advantage when weighed against the other KPIs. Peak load in COR is also less variable, so power equipment can be run closer to its limits.

Peak Shaving vs User Inconvenience, DG Input and CO_2 Emissions

The second key tradeoff is between Peak Shaving and User Inconvenience, DG Input and CO_2 Emissions. COR shows significantly lower EV charging delay compared to CUR, meaning that more severe P-CMR can be tolerated for the same delay requirement. COR also has higher DG energy delivery, meaning further gains can be achieved since heavy G-CMR is unnecessary to avoid overvoltage. Finally, both schemes show reduced CO_2 emissions compared to unconstrained output. This is important, since high user subscription is required for scheme operation, and high DG input promotes investment in renewable energy and helps deliver on emissions targets.

User Inconvenience vs ICT Deployment Cost

The third key tradeoff is between User Inconvenience and ICT Deployment Cost. Excessive IR is undesirable since it may require extensive replacement and reconfiguration of ICT infrastructure and hardware. Excessive CMR is undesirable since it increases EV charging delay and reduces DG energy input. In CUR, these are the only latency-mitigation options. COR gains strong advantage over this tradeoff with TMR, capable of achieving voltage control with low-severity IR and CMR.

QoS Provision vs ICT Deployment Cost

Finally, Chap. 5 identifies a final tradeoff between QoS Provision and ICT Deployment Cost in growing multi-tier hierarchical network topologies, such as that proposed to support the two Smart Charging schemes. Each new mid-tier aggregator reduces latency in the system. However, the marginal latency reduction of each diminishes as the number of aggregators grows. Since each aggregator node represents additional cost to the system operator, an inverse relation between QoS provision and deployment cost occurs that scales with the overall number of client devices. This is important for Smart Charging scheme implementation; however, this conclusion is also general to numerous Smart Grid and IoT solutions with the same underlying topology.

6.2.4 Steps towards Decentralisation

There is a notable progression of 'decentralisation' evident in the literature on Smart Grid control, as the need for finer granularity and number of connected devices grows larger. However, existing practical solutions adopt a centralised communications paradigm only. Moreover, decentralisation is a formidable step, involving at the very least significant installation and reprogramming of new and existing infrastructure. To avoid this, a distributed communications architecture is proposed that serves to decentralise computation and traffic load in the network without radical infrastructural overhaul.

A multi-tier hierarchical distributed communications architecture is designed that alleviates computation load on the central controller as well as traffic load on the underpinning communications system by offloading coordination of regionally colocated demand-response assets onto mid-tier aggregators. Importantly, the architecture is compatible with recent Smart Charging and Demand-Response communications standards such as OCPP and OpenADR, and therefore requires minimal infrastructural overhaul beyond what is already envisaged for Smart Grid systems. As a

result, the scheme is scalable and adaptable to a variety of network sizes and asset arrangements that comprise modern power systems, and is readily applicable in the industrial environment.

Traffic load within this architectural topology as network size grows is studied in Chap. 5. Addition of mid-tier aggregators is shown to alleviate traffic load in the system by reducing queueing latency at the mid-tier node. The analysis permits provision for demand-response latency requirements of a known number of client users by the deployment of an appropriate number of mid-tier aggregators. In addition, since each new mid-tier aggregator constitutes an additional cost to the operator, this same relation can be used to relate QoS provision and ICT deployment cost as the network size grows. This directly applies to the proposed Smart Charging scheme; however, the conclusion is general to numerous Smart Grid and IoT solutions with a similar topology.

6.3 Future Work

Several extensions may branch from the work in this thesis.

First, by repeating the simulation test system under varying EV and DG penetrations, the described Smart Charging performance-cost tradeoffs may be explicitly compared in the two schemes to understand how the key performance outcomes contend with rising distributed load and generation challenges. In this way, three-dimensional relationships for each performance outcome can be attained for system update interval and penetration of EVs and DG. This would enable illustration of how each scheme will cope as envisaged future energy services are realised.

Second, the conclusions of this thesis suggest that a combination of the CUR and COR schemes to adjust EV charging load according to available DG up to a certain maximum peak load may beneficially combine the interrelated performance objectives of operator, consumer and generator. Thus, development and testing of a

combined CUR-COR scheme to combine the peak shaving advantages of CUR with the voltage control, user satisfaction and DG energy advantages of COR in a way that benefits both operator and consumer/generator is a strong research direction.

Finally, the significance of the key performance-cost tradeoffs identified in this thesis may be consolidated by attaching a cost function to each performance outcome. Deriving accurate cost functions in this way would require significant further practical investigation, however, this would enable a thorough economic analysis to evaluate a cost-optimal Smart Charging compromise for the system operator.

These research topics will be explored in future study.

Bibliography

[1] Department for Business, Energy & Industrial Strategy, 'Digest of United Kingdom Energy Statistics (DUKES),' Jul. 2020, https://www.gov.uk/government/statistics/digest-of-uk-energy-statistics-dukes-2020.

[2] ExtraLink, 'New figures reveal 6% rise year on year in largely 'invisible' embedded energy generation,' May 2017, http://www.electralink.co.uk/2017/05/new-figures-reveal-6-rise-year-year-largely-invisible-embedded-energy-generation/.

[3] National Grid, 'Future Energy Scenarios,' Jul. 2019, http://fes.nationalgrid.com/media/1409/fes-2019.pdf.

[4] S. M. Ismael, S. H. A. Aleem, A. Y. Abdelaziz and A. F. Zobaa, 'State-of-the-art of hosting capacity in modern power systems with distributed generation,' *Renewable Energy*, vol. 130, pp. 1002–1020, 2019, doi:https://doi.org/10.1016/j.renene.2018.07.008.

[5] Ofgem, 'Typical domestic consumption values,' 2018, http://www.ofgem.gov.uk/gas/retail-market/monitoring-data-and-statistics/typical-domestic-consumption-values.

[6] Chevrolet, 'Chevrolet Bolt EV,' 2018, http://www.chevrolet.com/electric/bolt-ev-electric-car.

[7] Honda, 'Honda Clarity Electric,' 2018, http://automobiles.honda.com/clarity-electric#technology.

[8] Nissan, 'Nissan LEAF,' 2018, https://www.nissan.co.uk/vehicles/new-vehicles/leaf.html.

[9] Tesla, 'Tesla Model S,' 2018, http://www.tesla.com/models.

[10] IEEE Innovation at Work, 'The smart grid could hold the keys to electric vehicles,' Apr. 2020, https://innovationatwork.ieee.org/the-smart-grid-could-hold-the-keys-to-electric-vehicles.

[11] H. Sun, N. Hatziargyriou, H. V. Poor, L. Carpanini and M. A. A. Sanchez-Fornie, *Smarter energy: from smart metering to the smart grid*. The Institution of Engineering and Technology, 2016.

[12] S. Boyd and L. Vandenberghe, *Convex Optimization*. Cambridge University Press, Mar. 2004.

[13] K. G. Murty and S. Kabadi, 'Some np-complete problems in quadratic and nonlinear programming,' *Mathematical Programming*, vol. 39, pp. 117–129, 1987.

[14] P. Srikantha and D. Kundur, 'Intelligent signal processing and coordination for the adaptive smart grid: An overview of data-driven grid management,' *IEEE Signal Processing Magazine*, vol. 36, no. 3, pp. 82–102, May 2019, doi:10.1109/MSP.2018.2877001.

[15] S. H. Low, 'Convex relaxation of optimal power flow? Part I: Formulations and equivalence,' *IEEE Transactions on Control of Network Systems*, vol. 1, no. 1, pp. 15–27, Mar. 2014, doi:10.1109/TCNS.2014.2309732.

[16] C. Mitra, T. Kittel, A. Choudhary, J. Kurths and R. V. Donner, 'Recovery time after localized perturbations in complex dynamical networks,' *New Journal of Physics*, vol. 19, no. 10, p. 103 004, 2017.

[17] C. Coffrin and P. V. Hentenryck, 'A linear-programming approximation of AC power flows,' *INFORMS Journal on Computing*, vol. 26, pp. 718–734, 2014.

[18] J. R. Pillai, P. Thøgersen, J. Møller and B. Bak-Jensen, 'Integration of electric vehicles in low voltage danish distribution grids,' in *2012 IEEE Power and Energy Society General Meeting*, Jul. 2012, pp. 1–8, doi:10.1109/PESGM.2012.6343948.

[19] M. E. Baran and F. F. Wu, 'Optimal capacitor placement on radial distribution systems,' *IEEE Transactions on Power Delivery*, vol. 4, no. 1, pp. 725–734, Jan. 1989, doi:10.1109/61.19265.

[20] M. Baran and F. F. Wu, 'Optimal sizing of capacitors placed on a radial distribution system,' *IEEE Transactions on Power Delivery*, vol. 4, no. 1, pp. 735–743, Jan. 1989, doi:10.1109/61.19266.

[21] F. Kennel, D. Görges and S. Liu, 'Energy management for smart grids with electric vehicles based on hierarchical MPC,' *IEEE Transactions on Industrial Informatics*, vol. 9, no. 3, pp. 1528–1537, Aug. 2013, doi:10.1109/TII.2012.2228876.

[22] A. A. Eajal, M. F. Shaaban, E. F. El-Saadany and K. Ponnambalam, 'Fuzzy logic-based charging strategy for electric vehicles plugged into a smart grid,' in *Proc. 2015 IEEE International Conference on Smart Energy Grid Engineering (SEGE)*, Sep. 2015, pp. 1–6, doi:10.1109/SEGE.2015.7324606.

[23] T. Adefarati and R. C. Bansal, 'Integration of renewable distributed generators into the distribution system: A review,' *IET Renewable Power Generation*, vol. 10, no. 7, pp. 873–884, 2016.

[24] M. Bollen and F. Hassan, *Integration of Distributed Generation in the Power System*. Hoboken, USA: IEEE Press, 2011, doi:10.1002/9781118029039.

[25] M. Ebad and W. M. Grady, 'An approach for assessing high-penetration pv impact on distribution feeders,' *Electric Power Systems Research*, vol. 133, pp. 347–354, 2016,

http://www.sciencedirect.com/science/article/pii/S0378779615004034 doi:https://doi.org/10.1016/j.epsr.2015.12.026.

[26] M. Karimi, H. Mokhlis, K. Naidu, S. Uddin and A. Bakar, 'Photovoltaic penetration issues and impacts in distribution network – a review,' *Renewable and Sustainable Energy Reviews*, vol. 53, pp. 594–605, 2016, http://www.sciencedirect.com/science/article/pii/S136403211500903X doi:https://doi.org/10.1016/j.rser.2015.08.042.

[27] Y. Yang and M. Bollen, 'Power quality and reliability in distribution networks with increased levels of distributed generation,' *Elforsk*, 2008.

[28] J. Moura, *Accommodating high levels of variable generation*, Jul. 2009.

[29] F. Katiraei and J. R. Agüero, 'Solar pv integration challenges,' *IEEE Power and Energy Magazine*, vol. 9, no. 3, pp. 62–71, 2011.

[30] S. Repo, H. Laaksonen, P. Jarventausta, O. Huhtala and M. Mickelsson, 'A case study of a voltage rise problem due to a large amount of distributed generation on a weak distribution network,' in *2003 IEEE Bologna Power Tech Conference Proceedings,*, vol. 4, Jun. 2003, p. 6, doi:10.1109/PTC.2003.1304703.

[31] P. Srikantha and D. Kundur, 'Distributed demand curtailment via water-filling,' in *Proc. 2015 IEEE International Conference on Smart Grid Communications (SmartGridComm)*, Nov. 2015, pp. 350–355, doi:10.1109/SmartGridComm.2015.7436325.

[32] ——, 'Resilient distributed real-time demand response via population games,' *IEEE Transactions on Smart Grid*, vol. 8, no. 6, pp. 2532–2543, Nov. 2017, doi:10.1109/TSG.2016.2526651.

[33] ——, 'A game theoretic approach to real-time robust distributed generation dispatch,' *IEEE Transactions on Industrial Informatics*, vol. 13, no. 3, pp. 1006–1016, Jun. 2017, doi:10.1109/TII.2016.2610951.

[34] C. Chen, J. Wang and S. Kishore, 'A distributed direct load control approach for large-scale residential demand response,' *IEEE Transactions on Power Systems*, vol. 29, no. 5, pp. 2219–2228, Sep. 2014, doi:10.1109/TPWRS.2014.2307474.

[35] C. Chu and H. H. Iu, 'Complex networks theory for modern smart grid applications: A survey,' *IEEE Journal on Emerging and Selected Topics in Circuits and Systems*, vol. 7, no. 2, pp. 177–191, Jun. 2017, doi:10.1109/JETCAS.2017.2692243.

[36] C. Zhao, U. Topcu, N. Li and S. Low, 'Design and stability of load-side primary frequency control in power systems,' *IEEE Transactions on Automatic Control*, vol. 59, no. 5, pp. 1177–1189, May 2014, doi:10.1109/TAC.2014.2298140.

[37] H. Kakigano, Y. Miura and T. Ise, 'Distribution voltage control for DC microgrids using fuzzy control and gain-scheduling technique,' *IEEE Transactions on Power Electronics*, vol. 28, no. 5, pp. 2246–2258, May 2013, doi:10.1109/TPEL.2012.2217353.

[38] R. R. Negenborn, A. G. Beccuti, T. Demiray, S. Leirens, G. Damm, B. D. Schutter and M. Morari, 'Supervisory hybrid model predictive control for voltage stability of power networks,' in *2007 American Control Conference*, Jul. 2007, pp. 5444–5449, doi:10.1109/ACC.2007.4282264.

[39] J. W. Heron, J. Jiang, H. Sun, V. Gezerlis and T. Doukoglou, 'Demand-response round-trip latency of IoT smartgrid network topologies,' *IEEE Access*, vol. 6, pp. 22 930–22 937, May 2018, doi:10.1109/ACCESS.2018.2831254.

[40] S. Islam, M. Zaber and A. A. Ali, 'A smart grid prerequisite: Survey on electricity demand forecasting models and scope analysis of demand fsorecasting in bangladesh,' in *2017 IEEE Region 10 Humanitarian Technology Conference (R10-HTC)*, Dec. 2017, pp. 691–696, doi:10.1109/R10-HTC.2017.8289052.

[41] A. S. Nair, P. Ranganathan, H. Salehfar and N. Kaabouch, 'Uncertainty quantification of wind penetration and integration into smart grid: A survey,' in *2017 North American Power Symposium (NAPS)*, Sep. 2017, pp. 1–6, doi:10.1109/NAPS.2017.8107196.

[42] P. Palensky and D. Dietrich, 'Demand side management: Demand response, intelligent energy systems, and smart loads,' *IEEE Transactions on Industrial Informatics*, vol. 7, no. 3, pp. 381–388, Aug. 2011, doi:10.1109/TII.2011.2158841.

[43] J. Dai, M. Dong, R. Ye, A. Ma and W. Yang, 'A review on electric vehicles and renewable energy synergies in smart grid,' in *2016 China International Conference on Electricity Distribution (CICED)*, Aug. 2016, pp. 1–4, doi:10.1109/CICED.2016.7575995.

[44] S. Deilami, A. S. Masoum, P. S. Moses and M. A. S. Masoum, 'Real-time coordination of plug-in electric vehicle charging in smart grids to minimize power losses and improve voltage profile,' *IEEE Transactions on Smart Grid*, vol. 2, no. 3, pp. 456–467, Sep. 2011, doi:10.1109/TSG.2011.2159816.

[45] R. Stanev, 'A control strategy and operation paradigm for electrical power systems with electric vehicles and distributed energy resources,' in *2016 19th International Symposium on Electrical Apparatus and Technologies (SIELA)*, May 2016, pp. 1–4, doi:10.1109/SIELA.2016.7543047.

[46] A. S. Masoum, S. Deilami, M. A. S. Masoum, A. Abu-Siada and S. Islam, 'Online coordination of plug-in electric vehicle charging in smart grid with distributed wind power generation systems,' in *2014 IEEE PES General Meeting | Conference Exposition*, Jul. 2014, pp. 1–5, doi:10.1109/PESGM.2014.6939133.

[47] A. Tahir and A. Massoud, 'Load shedding and forecasting in distribution systems with PV-based distributed generation and electric vehicles,' in *2017 4th International Conference on Information Technology, Computer, and Electrical*

Engineering (ICITACEE), Nov. 2017, pp. 71–76, doi:10.1109/ICITACEE.2017.8257678.

[48] F. Rassaei, W. Soh and K. Chua, 'Demand response for residential electric vehicles with random usage patterns in smart grids,' *IEEE Transactions on Sustainable Energy*, vol. 6, no. 4, pp. 1367–1376, Oct. 2015, doi:10.1109/TSTE.2015.2438037.

[49] E. Veldman and R. A. Verzijlbergh, 'Distribution grid impacts of smart electric vehicle charging from different perspectives,' *IEEE Transactions on Smart Grid*, vol. 6, no. 1, pp. 333–342, Jan. 2015, doi:10.1109/TSG.2014.2355494.

[50] C. Liu, K. T. Chau, D. Wu and S. Gao, 'Opportunities and challenges of vehicle-to-home, vehicle-to-vehicle, and vehicle-to-grid technologies,' *Proceedings of the IEEE*, vol. 101, no. 11, pp. 2409–2427, Nov. 2013, doi:10.1109/JPROC.2013.2271951.

[51] V. Monteiro, J. G. Pinto and J. L. Afonso, 'Operation modes for the electric vehicle in smart grids and smart homes: Present and proposed modes,' *IEEE Transactions on Vehicular Technology*, vol. 65, no. 3, pp. 1007–1020, Mar. 2016, doi:10.1109/TVT.2015.2481005.

[52] C. Pang, P. Dutta and M. Kezunovic, 'BEVs/PHEVs as dispersed energy storage for V2B uses in the smart grid,' *IEEE Transactions on Smart Grid*, vol. 3, no. 1, pp. 473–482, Mar. 2012, doi:10.1109/TSG.2011.2172228.

[53] Z. Wang and S. Wang, 'Grid power peak shaving and valley filling using vehicle-to-grid systems,' *IEEE Transactions on Power Delivery*, vol. 28, no. 3, pp. 1822–1829, Jul. 2013, doi:10.1109/TPWRD.2013.2264497.

[54] Y. Ota, H. Taniguchi, T. Nakajima, K. M. Liyanage, J. Baba and A. Yokoyama, 'Autonomous distributed V2G (vehicle-to-grid) satisfying scheduled charging,' *IEEE Transactions on Smart Grid*, vol. 3, no. 1, pp. 559–564, Mar. 2012, doi:10.1109/TSG.2011.2167993.

[55] O. Erdinc, N. G. Paterakis, T. D. P. Mendes, A. G. Bakirtzis and J. P. S. Catalão, 'Smart household operation considering bi-directional EV and ESS utilization by real-time pricing-based DR,' *IEEE Transactions on Smart Grid*, vol. 6, no. 3, pp. 1281–1291, May 2015, doi:10.1109/TSG.2014.2352650.

[56] 'Electric Cars to charge Johan Cruyff Arena,' Dec. 2019, https://www.thestadiumbusiness.com/2019/12/10/electric-cars-charge-johan-cruyff-arena/.

[57] International Electrotechnical Commission, 'IEC 61851-1:2017 Electric vehicle conductive charging system - Part 1: General Requirements,' 2017.

[58] International Organisation for Standardisation, 'ISO 15118 Road Vehicles – Vehicle to grid communication interface,' 2017.

[59] EnelX, 'The Different EV Charging Connector Types,' 2019, https://evcharging.enelx.com/eu/about/news/blog/552-ev-charging-connector-types.

[60] 'EV Connectors and EV Charging Cables,' Feb. 2020, https://evse.com.au/ev-charging-cables-leads/.

[61] OpenADR Alliance, 'Open automated demand response,' 2019, https://www.openadr.org.

[62] U. Herberg, D. Mashima, J. G. Jetcheva and S. Mirzazad-Barijough, 'OpenADR 2.0 deployment architectures: Options and implications,' in *Proc. 2014 IEEE International Conference on Smart Grid Communications (SmartGridComm)*, Nov. 2014, pp. 782–787, doi:10.1109/SmartGridComm.2014.7007743.

[63] A. Robinson, P. Blythe, M. Bell, Y. Hübner and G. Hill, 'Analysis of electric vehicle driver recharging demand profiles and subsequent impacts on the carbon content of electric vehicle trips,' *Energy Policy*, vol. 61, pp. 337–348, 2013, doi:10.1016/j.enpol.2013.05.074.

[64] J. Zimmerman, M. Evans, J. Griggs, N. King, L. Harding, P. Roberts and C. Evans, 'Household Electricity Survey A study of domestic electrical product usage,' *Intertek Testing & Certification Ltd*, pp. 213–214, May 2012, R66141 Final Report Issue 4.

[65] J. Palmer and I. Cooper, 'United Kingdom housing energy fact file,' *Department of Energy & Climate Change*, pp. 46, 49, 2013.

[66] A. Evans, J. Cummings, M. Slocombe and F. Corvaglia, 'National Travel Survey: England 2017,' *Department for Transport*, 2017, Statistical Release: Table NTS9902.

[67] 'MyGridGB,' Feb. 2020, `https://www.mygridgb.co.uk`.

[68] M. E. Baran and F. F. Wu, 'Network reconfiguration in distribution systems for loss reduction and load balancing,' *IEEE Transactions on Power Delivery*, vol. 4, no. 2, pp. 1401–1407, Apr. 1989, `doi:10.1109/61.25627`.

[69] R. D. Zimmerman, C. E. Murillo-sánchez and R. J. Thomas, 'MATPOWER steady-state operations, planning and analysis tools for power systems research and education,' *IEEE Transactions on Power Systems*, pp. 12–19, 2011.

[70] R. A. Shayani and M. A. G. de Oliveira, 'Photovoltaic generation penetration limits in radial distribution systems,' *IEEE Transactions on Power Systems*, vol. 26, no. 3, pp. 1625–1631, Aug. 2011, `doi:10.1109/TPWRS.2010.2077656`.

[71] 'LDT TURBINE SCADA-1SEC,' Feb. 2020, `https://pod.ore.catapult.org.uk/product/2`.

[72] *Vestas V164-8.0*, `https://en.wind-turbine-models.com/turbines/318-vestas-v164-8.0`, Online, Jul. 2020.

[73] R. Seguin, J. Woyak, D. Costyk, J. Hambrick and B. Mather, 'High-penetration PV integration handbook for distribution engineers,' Jan. 2016, `doi:10.2172/1235905`.

[74] A. Alyousef and H. de Meer, 'Design of a TCP-like smart charging controller for power quality in electrical distribution systems,' in *Proceedings of the Tenth ACM International Conference on Future Energy Systems*, ser. e-Energy '19, Phoenix, AZ, USA: ACM, 2019, pp. 128–138, doi:10.1145/3307772.3328293.

[75] O. Ardakanian, S. Keshav and C. Rosenberg, 'Real-time distributed control for smart electric vehicle chargers: From a static to a dynamic study,' *IEEE Transactions on Smart Grid*, vol. 5, no. 5, pp. 2295–2305, Sep. 2014, doi:10.1109/TSG.2014.2327203.

[76] Open Charge Alliance, 'Open Charge Point Protocol 2.0,' 2018, https://www.openchargealliance.org/protocols/ocpp-20/.

[77] T. Ma and O. Mohammed, 'Real-time plug-in electric vehicles charging control for V2G frequency regulation,' in *IECON 2013 - 39th Annual Conference of the IEEE Industrial Electronics Society*, Nov. 2013, pp. 1197–1202, doi:10.1109/IECON.2013.6699303.

[78] S. E. Collier, 'The emerging enernet: Convergence of the smart grid with the internet of things,' *IEEE Industry Applications Magazine*, vol. 23, no. 2, pp. 12–16, Mar. 2017, https://doi.org/10.1109%5C%2Fmias.2016.2600737 doi:10.1109/mias.2016.2600737.

[79] J. Jiang and Y. Qian, 'Distributed communication architecture for smart grid applications.,' *IEEE communications magazine.*, vol. 54, no. 12, pp. 60–67, Dec. 2016, http://dro.dur.ac.uk/24179/.

[80] T. Doukoglou and V. Gezerlis, 'Smart homes in smart grids,' in *InfoCom World Conference, under the title Fiber to the people: The Gigabit Era, Athens, Greece*, Oct. 2017.

[81] V. Gezerlis and T. Doukoglou, 'Software network topology and traffic simulation for overlay telecommunication network in smart grids,' in *InfoCom World Conference, under the title Fiber to the people: The Gigabit Era, Athens, Greece*, Oct. 2017.

[82] W. Tushar, C. Yuen, B. Chai, S. Huang, K. L. Wood, S. G. Kerk and Z. Yang, 'Smart grid testbed for demand focused energy management in end user environments,' *IEEE Wireless Communications*, vol. 23, no. 6, pp. 70–80, Dec. 2016, doi:10.1109/MWC.2016.1400377RP.

[83] W. Song, D. De, S. Tan, S. K. Das and L. Tong, 'A wireless smart grid testbed in lab,' *IEEE Wireless Communications*, vol. 19, no. 3, pp. 58–64, Jun. 2012, doi:10.1109/MWC.2012.6231160.

[84] J. Jin, J. Gubbi, S. Marusic and M. Palaniswami, 'An information framework for creating a smart city through internet of things,' *IEEE Internet of Things Journal*, vol. 1, no. 2, pp. 112–121, Apr. 2014, doi:10.1109/JIOT.2013.2296516.

[85] T. A. Youssef, A. T. Elsayed and O. A. Mohammed, 'DDS based interoperability framework for smart grid testbed infrastructure,' in *2015 IEEE 15th International Conference on Environment and Electrical Engineering (EEEIC)*, Jun. 2015, pp. 219–224, doi:10.1109/EEEIC.2015.7165544.

[86] M. H. Cintuglu, O. A. Mohammed, K. Akkaya and A. S. Uluagac, 'A survey on smart grid cyber-physical system testbeds,' *IEEE Communications Surveys Tutorials*, vol. 19, no. 1, pp. 446–464, First Quarter 2017, doi:10.1109/COMST.2016.2627399.

[87] S. Boyd, N. Parikh, E. Chu, B. Peleato and J. Eckstein, *Distributed Optimization and Statistical Learning via the Alternating Direction Method of Multipliers*. 2011, https://ieeexplore.ieee.org/xpl/articleDetails.jsp?arnumber=8186925.

[88] S. E. Collier, 'The emerging enernet: Convergence of the smart grid with the internet of things,' in *2015 IEEE Rural Electric Power Conference*, Apr. 2015, pp. 65–68, doi:10.1109/REPC.2015.24.

[89] H. Guo, Y. Wu, F. Bao, H. Chen and M. Ma, 'UBAPV2G: A unique batch authentication protocol for vehicle-to-grid communications,' *IEEE Transactions on*

Smart Grid, vol. 2, no. 4, pp. 707–714, Dec. 2011,
doi:10.1109/TSG.2011.2168243.

[90] S. Rampfl, 'Network simulation and its limitations,' *Network Architectures and Services*, Aug. 2013,
doi:10.2313/NET-2013-08-1_08.

[91] W. R. Stevens, *TCP/IP Illustrated (Vol. 1): The Protocols*. USA: Addison-Wesley Longman Publishing Co., Inc., 1993.

[92] D. P. Tuttle and R. Baldick, 'The evolution of plug-in electric vehicle-grid interactions,' *IEEE Transactions on Smart Grid*, vol. 3, no. 1, pp. 500–505, Mar. 2012,
doi:10.1109/TSG.2011.2168430.

[93] X. Yu, C. Cecati, T. Dillon and M. G. Simões, 'The new frontier of smart grids,' *IEEE Industrial Electronics Magazine*, vol. 5, no. 3, pp. 49–63, Sep. 2011,
doi:10.1109/MIE.2011.942176.

Publications

Publication A

J. W. Heron and H. Sun, "Smart Electric Vehicle Charging with Ideal and Practical Communications in Smart Grids," in *Proc. 2019 IEEE Global Communications Conference (GLOBECOM)*, Waikoloa, HI, USA, 2019, pp. 1-6.

Smart Electric Vehicle Charging with Ideal and Practical Communications in Smart Grids

John W. Heron and Hongjian Sun
Department of Engineering, Durham University, Durham, DH1 3LE, United Kingdom
john.w.heron@durham.ac.uk, hongjian.sun@durham.ac.uk

***Abstract*—The growing number of electric vehicles (EV) in the automotive market is leading to ever sharper spikes in consumer power demand. Smart EV charging techniques seek to adjust EV charging load to compensate for supply-demand mismatch. However, all schemes are vulnerable to communications inefficiencies. This paper models implications of communications-driven latency in smart EV charging relevant to secondary voltage control in the distribution network. EV charging load and driving pattern data are gathered from verified statistical studies. A smart charging scheme is proposed enabling high EV penetration with no peak load increase and minimal infrastructure additions. Further, it is applicable to all flexible loads and permits power allocation via a number of possible algorithms. A communications structure for this scheme is then developed, and system performance under ideal and practical communications constraints are studied.**

I. Introduction

The United Kingdom's (UK) National Grid estimates by 2040 all cars sold will be purely electric [1]. Typical UK daily household energy consumption ranges 5-20kWh/day [2], while typical electric vehicle (EV) battery capacity ranges 20-100kWh [3]–[6]. Ownership of an EV will represent significant increase in household energy consumption. Further, numerous EV owners arriving home from work between already peak loading hours of 6-10pm and immediately charging their vehicles is plausible. The growing number of EVs, as well as other grid-connected devices, is leading to ever sharper spikes in consumer power demand. Predictions of effects of random uncoordinated charging in the power network range from significant to disastrous [7]–[9], compounded by rising embedded renewable generation [10], [11].

Locally, supply-demand imbalance manifests as over- or under-voltage conditions that may trigger passive protection elements or lead to mandatory load shedding and blackouts. Growing temporally unsynchronised spikes in generation and consumption lead to question whether the traditional power grid can continue to be operated within stable limits. Smart Load Management techniques exploit the discretionary power requirement of flexible loads: it does not matter exactly when EV charging takes place, so long as it is charged when the consumer requires. Thus it is possible, within certain timing constraints, to compensate for supply-demand mismatch by adjusting net demand according to grid stability requirements. This can achieve flatter power profile and more predictable disturbances, meaning power equipment (sized according to peak load) need not be supplemented to accommodate rising peak demand. Equipment can be operated closer to its limits and power efficiency more effectively optimised, reducing technical losses and operating costs.

There has been some work in this field. In [8], an EV charging scheme with distributed wind power cost-efficiently meets consumer charging requirements based on real-time pricing. Peak shaving under EV load curves incorporating embedded generation is analysed in [12]. A fuzzy logic strategy in [13] keeps distribution system minimum voltage within operating limits. A fast-converging scheme in [14] incorporates randomness of arrival time, departure time and charging time to minimise peak demand in the system. An algorithm based on charging time zone priorities in [7] improves voltage profile, where over 63% EV penetration could be tolerated with no peak load increase.

All these schemes assume perfect knowledge of grid status, energy prices, driving patterns and loading is available everywhere in the network, reliably and with zero latency. Where delay is mentioned, as in [15], [16], it refers to convergence time and/or control action period of the power optimisation scheme. Latency from backhaul communications constraints such as message congestion, packet loss and overhead, as well as actuation latency at the charging point, is unquantified, and resulting system performance effects are not analysed.

This paper models practical communications and actuation latency in Smart EV Charging schemes relevant to secondary voltage control in a distribution network, demonstrating profound effect on maximum EV penetration. To the authors' knowledge, this is the first paper to consider such constraints. Contributions are threefold:

- Base power load, EV charging load and driving patterns are modelled using verified statistical data.
- A new EV charging scheme is proposed enabling 81% EV penetration with no rise in peak load and minimal infrastructure additions.
- Effects of latency on system performance are then studied to model practical system constraints.

The rest of this paper is laid out as follows. Section II describes accurate estimation of random uncoordinated charging load and the network model used for simulation. Section III introduces the proposed Smart EV Charging scheme assuming ideal communication in the network. Section IV then elaborates on protracted implications of communications latency for system performance. Section V concludes the topic.

This work was supported by the European Commissions Horizon 2020 framework programme (H2020/2014-2020) under grant agreement no. 734325 TESTBED project (http://testbed-rise.com/), and by the UK EPSRC (grant no. EP/P005950/1). Manuscript written August 6, 2019.

978-1-7281-0962-6/19/$31.00 ©2019 IEEE

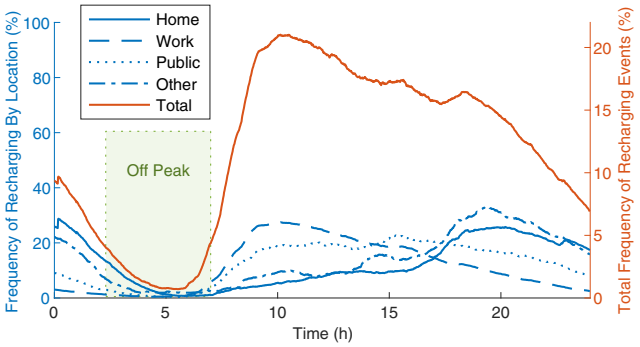

Fig. 1. Statistical probability distribution for active charging events.

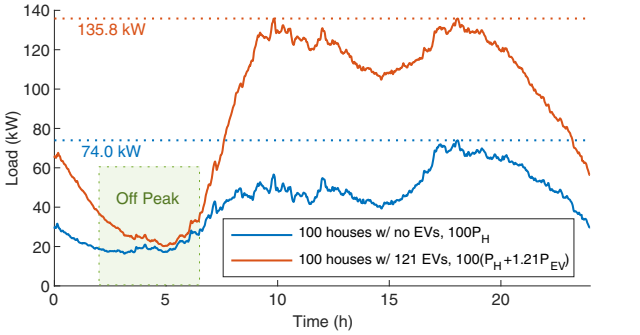

Fig. 2. The average household in the UK has 1.21 vehicles. This plot shows the increase in expected load profile of 100 households on a cold winter day if all vehicles were electric ($H_b = 100,\ \eta_{EV} = 1.21$).

II. Electric Vehicles in the Power Network

Effective modelling of EV charging in the power network requires accurate expected load estimation. Recharging behaviour of EVs is statistically quantified in [17], which gathers data from 31,765 EV trips and 16,229 EV charging events. Charging frequency with time of day is given for 'home', 'work', 'public' and 'other' locations. With this data, a statistical probability distribution for expected number of active charging events with time is constructed, shown Fig. 1.

Load curves for 'home' and 'other' charging locations have peak roughly synchronised with household peak hours 6-10pm, when many users return home from work. However, the majority of charging events occurred at 'work' locations, leading to peak total charging load around 10am. All locations saw roughly synchronised off-peak hours 2.30-7am, during which users are unlikely to be driving and most EV charging is complete. Mean charging power encountered per vehicle was 3.18kW. An expected load curve per vehicle $P_{EV}(t)$ was then constructed for random uncoordinated charging.

Electrical power demand of 251 selected households with and without electric heating in the UK is presented in [18]. Approximately 10% of households use electric heating [19]. With this data, expected load curve per household $P_H(t)$ on a cold winter day is constructed. Average vehicle number per household in the UK was 1.21 in 2017 [20]. When the corresponding EV and household load profiles are combined, shown Fig. 2 for 100 households, peak load rises 83%. However, off-peak times are roughly matched 2-6am, presenting favourable conditions for Smart Charging.

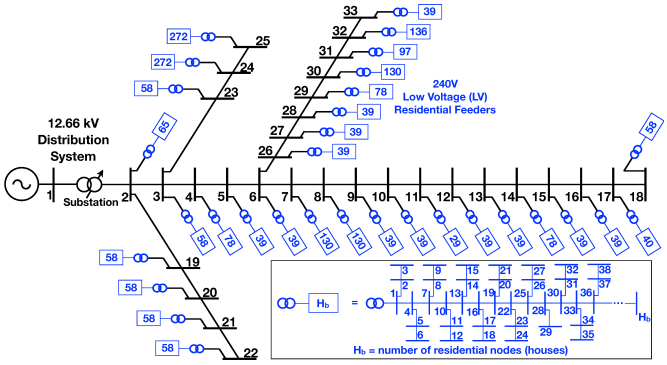

Fig. 3. IEEE 33 bus 12.66kV distribution network.

The impact of this additional EV load on a distribution network of B buses is then modelled. Power demand $S_b^{\text{norm}}[n] = P_b^{\text{norm}}[n] + jQ_b^{\text{norm}}[n],\ (j = \sqrt{-1})$ at each distribution bus $b \in \mathbf{B} = \{1, 2, ..., B\}$ at time $t = n\Delta t,\ n \in \mathbb{Z}^+$ is defined

$$\left.\begin{aligned} P_b^{\text{norm}}[n] &= H_b\Big(P_H[n] + \eta_{EV} P_{EV}[n]\Big) \\ Q_b^{\text{norm}}[n] &= 0 \end{aligned}\right\} \forall\, 0 \le n < \tfrac{24}{\Delta t} \quad (1)$$

H_b is number of houses supplied at each bus b, η_{EV} is network-wide EV penetration, P_H and P_{EV} are average expected household and EV charging load profiles, respectively, per household and per EV. Time interval $\Delta t = \frac{1}{60}$ (1 minute). Power flow between sequential nodes $a, b, c \subset \mathbf{B},\ a \neq b \neq c$ in the network is then defined by the Branch Flow Model [21]

$$\sum_{c=1}^{C} S_{b,c}[n] = S_{a,b}[n] - Z_{a,b}|I_{a,b}[n]|^2 - S_b^{\text{norm}}[n] \quad (2)$$

$$V_b[n] - V_c[n] = Z_{b,c} I_{b,c}[n] \quad (3)$$

$$S_{b,c}[n] = V_b[n] I_{b,c}^*[n] \quad (4)$$

where $c \in [1, 2, ...C]$ are all child nodes of node b, which is in turn child of a. Along the branch $b \to c$: $S_{b,c} = P_{b,c} + jQ_{b,c}$ is sending end complex power transfer, $I_{b,c}$ is current phasor and $Z_{b,c} = R_{b,c} + jX_{b,c}$ is line impedance. S_b^{norm} is net power drawn from bus b and V_b is voltage phasor. This model allows complex power flow and voltage deviation at each link and bus to be calculated iteratively for each time step n.

This was simulated for the IEEE 33-bus 12.66kV distribution network shown Fig. 3, adapted from [22]. Each bus b has a low voltage (LV) 240V residential feeder with a varying number of households H_b. Real power demand at each LV node follows the expected average load curve for households P_H and EVs P_{EV}. Power factor correction is perfectly implemented at each bus and line impedance in the LV feeders is negligible (i.e. the only reactive load is from capacitive and inductive effects of the 12.66kV lines). Bus 1 is the reference bus with constant voltage $V_1 = 1$p.u., zero net power demand $P_1^{\text{norm}} = 0$ and phase angle $\theta_1 = 0$.

Expected load without ($\eta_{EV} = 0$) and with 41% EVs ($\eta_{EV} = 0.41$) is then applied, and voltage deviation at each

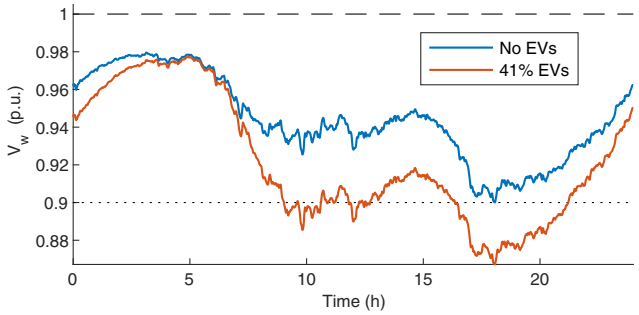

Fig. 4. Voltage deviaton at worst bus V_w for random uncoordinated charging.

bus derived using Matpower [23]. In normal grid operations, voltage at the worst bus should not exceed the statutory limit of 0.9 per unit (p.u.). At worst bus w, voltage V_w is shown Fig. 4. Without EVs, V_w touches this limit. The added EV load is then sufficient to bring V_w well outside of its acceptable range. In practice this may lead to mandatory load shedding and system outage to bring V_w back within acceptable limits. As proportion of EVs rises, an effective load management solution is required to reduce peak load and optimise power transfer for the expected network-wide load increase.

III. Ideal Smart EV Charging

Peak load may be alleviated via numerous dispersed cyber-enabled sensors and actuators that characterise Smart Grid solutions. Peak voltage deviation coincides with peak network load. If EV charging can be rescheduled during peak times so V_w stays within technical limits, a higher penetration of EVs can be served with minimal infrastructure additions. To do this, a curtailment-based load management scheme is designed. Ideal operation is first considered, before practical constraints are introduced in Sec. IV.

The proposed scheme uses a three-tier tree-star communications topology described in [24]. This involves a Central Control Unit (CCU), Intermediary Control Units (ICU$_b$) and Smart Devices (SDs), shown Fig. 5 for the 33-bus distribution system. The CCU is the main network coordinator, where information from the entire network is gathered. It is connected via data link to an ICU$_b$ at each distribution bus b. ICUs are mid-tier nodes which aggregate measurements from their associated SDs and forward data to the CCU. Each ICU$_b$ is connected to various SDs at all EV charging points and aggregators in its LV feeder. SDs are the lower tier nodes that conduct measurements and/or actuations. These update their ICU$_b$ with power, voltage and EV charging status information on demand. Based on CCU commands, each ICU$_b$ may control/curtail EV charging by communicating with its SDs.

EV charging priority is decided by user input. 'High priority' users are treated as non-flexible load, and 'low priority' users compensated for potential charging delay with cheaper energy prices. Conceivably, many users with daytime jobs do not care if their EV is charged early evening or overnight, and will accept this scheme to save money. Henceforth, EV charging refers to scheme subscribers, unless otherwise stated.

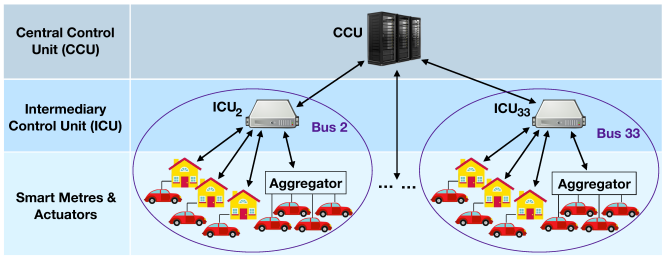

Fig. 5. Three-tier tree-star communications topology for the IEEE 33-bus distribution system from Fig. 3.

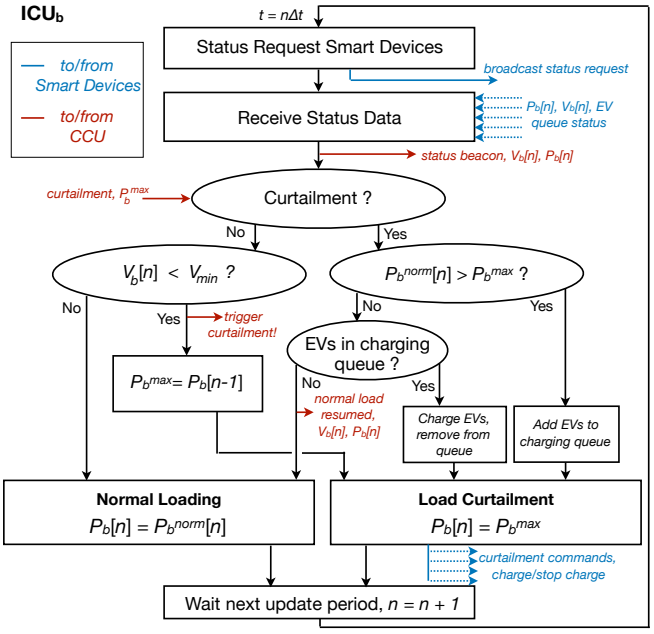

Fig. 6. Smart EV Charging algorithm at ICU$_b$.

The role of each ICU$_b$ is summarised in Fig. 6. Every update period n, ICU$_b$ requests status information of bus voltage $V_b[n]$, active power demand $P_b[n]$ (composed of non-flexible power requirements and active EV charging load), and incoming EV charging requests from its SDs. It then updates the CCU with $V_b[n], P_b[n]$. Thus, the CCU receives two complete status vectors every update interval n

$$\mathbf{V}[n] = [V_1[n], ..., V_B[n]]^{\mathrm{T}} \tag{5}$$

$$\mathbf{P}[n] = [P_1[n], ..., P_B[n]]^{\mathrm{T}} \tag{6}$$

If $V_b[n] < V_{\min}$, ICU$_b$ begins curtailment at bus b and notifies the CCU, which then identifies bus b as the worst bus w.

Due to the radial topology of the distribution network, V_w will be affected by load changes in any other bus. Therefore, the CCU calculates maximum power vector based on the last received values before the curtailment trigger

$$\mathbf{P}^{\max} = [P_1^{\max}, ..., P_B^{\max}]^{\mathrm{T}} = \mathbf{P}[n-1] \tag{7}$$

The CCU then notifies each ICU$_b$ of its maximum power $P_b^{\max}$, which launches curtailment at every other bus $b \neq w$.

During curtailment, every update period n, each ICU$_b$ coordinates with its SDs to ensure $P_b[n] = P_b^{\max}$. It does this

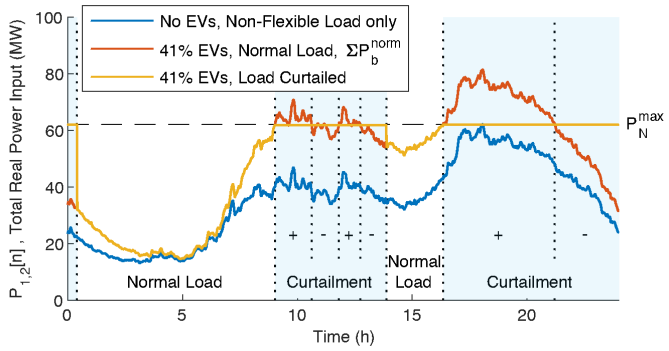

(a) Total real power demand.

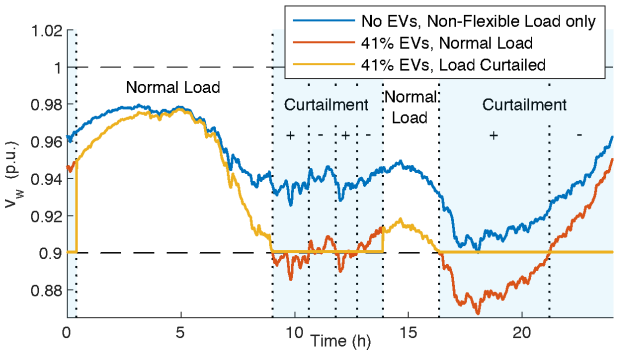

(b) Voltage at worst bus

Fig. 7. Power and voltage deviaton in the smart EV charging scheme. Regions of EV charging queue growth and decline are marked with '+' and '-', respectively.

by prioritising requirements of non-flexible load and filling the remaining available power with EV charging. This limits total overall network load to $P_N^{\max} = \sum_{b=1}^{B} P_b^{\max}$, and limits V_w to $V_{\min}$, shown Fig. 7.

Behaviour during curtailment is explained by interaction between curtailment load $P_b^{\max}$ and uncurtailed normal load $P_b^{\text{norm}}[n]$ from (1). EV charging requests are accepted on a first come first serve basis, however curtailment requires some requests be denied. All denied requests are logged in a queue at ICU_b. With each new n, if $P_b^{\text{norm}}[n] > P_b^{\max}$ there are more arriving charging requests than can be serviced, and the queue will grow. If $P_b^{\text{norm}}[n] < P_b^{\max}$, more requests are accepted than are arriving, so the queue will shrink. On a network-wide scale the same interaction is represented by $\sum_{b=1}^{B} P_b^{\text{norm}}[n]$ and $P_N^{\max}$, shown Fig. 7a. Regions of net queue growth and decline are marked by '+' and '-', respectively.

If EV penetration η_{EV} is within system capacity, eventually all EV charging requests at bus b will be active or complete (i.e. the charging queue is empty). At this point ICU_b resumes normal load $P_b^{\text{norm}}[n]$ and notifies the CCU of its reduced power. CCU then recalculates power vector $\mathbf{P}^{\max}$, seeking to maximise the charging queue service rate for $V_w \geq V_{\min}$. Assuming linear $\frac{\delta P_b}{\delta V_w}$ at each bus for small changes in P_b, $\mathbf{P}^{\max}$ is rearranged such that $P_N^{\max}$ remains constant. The CCU then updates each ICU_b with its new $P_b^{\max}$. This process continues until all EV charging queues at all ICUs are empty, and normal load is resumed.

Energy is available for charging in this scheme by virtue of the difference between $P_N^{\max}$ and $\sum_{b=1}^{B} P_b^{\text{norm}}[n]$. Daily surplus energy available for EV charging is formulated

$$E_{\text{charge}} = \int_0^{24} P_N^{\max} - \sum_{b=1}^{B} H_b \Big[P_H(t) + \eta_{EV} P_{EV}(t) \Big] \, dt. \quad (8)$$

$P_N^{\max}$ is inherently the maximum total power demand such that $V_b \geq V_{\min}$, $\forall\ b \in \mathbf{B}$. If perfect communication exists in the network, the CCU may be instantly aware of $V_w < V_{\min}$, and may instantly respond with curtailment. Therefore the statutory limit may be used $V_{\min} = 0.9$p.u. For illustration, $P_N^{\max}$ in this simulation is also equal to maximum load in the 33-bus distribution system under zero EVs.

As η_{EV} is increased, E_{charge} is reduced. When $E_{\text{charge}} = 0$ the network may be considered fully utilised, and any further charging load cannot be satisfied in a single 24h period. This defines maximum EV charging capacity

$$\eta_{EV}^{\max} = \frac{24 P_N^{\max} - \sum_{b=1}^{B} H_b \int_0^{24} P_H(t) dt}{\sum_{b=1}^{B} H_b \int_0^{24} P_{EV}(t) dt}. \quad (9)$$

With known H_b, statistically-derived $P_H(t), P_{EV}(t)$ and simulation-derived $P_N^{\max}$ this is calculated numerically to be 81.2%. This is matched in simulation, which cannot compute solution for $\eta_{EV} > 0.81$.

Hence this scheme achieves EV capacity of 81% with no peak load increase from conditions without EVs. It is applicable beyond EVs to all flexible loads in general. It requires minimal additions to existing power infrastructure, since it harnesses real-time sensor technology and ICT connection that is increasingly permeated in Smart Grid systems. Finally, calculation of $\mathbf{P}^{\max}$ at the CCU adds flexibility, permitting power allocation via a multitude of algorithms, e.g. maximum sensitivities selection [7], [8], fuzzy logic [13], distributed dual decomposition [16], genetic algorithms [25], etc. bringing scope for optimisation.

IV. Practical Smart EV Charging

Without the assumption of perfect communication, multiple messages must be exchanged in sequence upon detection of $V_w < V_{\min}$ before load curtailment is effectively actuated. This latency, shown Fig. 8, inherently affects the minimum update interval Δt and has strong impact on EV capacity.

To model this latency, a communications structure for the Smart EV Charging scheme is designed. Hardware and backhaul infrastructure additions will represent large investment for a system as ubiquitous as the power network, and cost will be a significant performance constraint. Thus a minimum of communications resources are assumed.

The system is based on that in [24], which analyses demand-response latency in TCP/IP tree-star network topologies. Each node in the three-tier hierarchical structure (CCU, ICU and SD) has a unique IP address shared by one listener and one sender port. This allows for reduced hardware complexity as well as added flexibility, permitting easy implementation of more port functions and scope for scheduled multicast packet

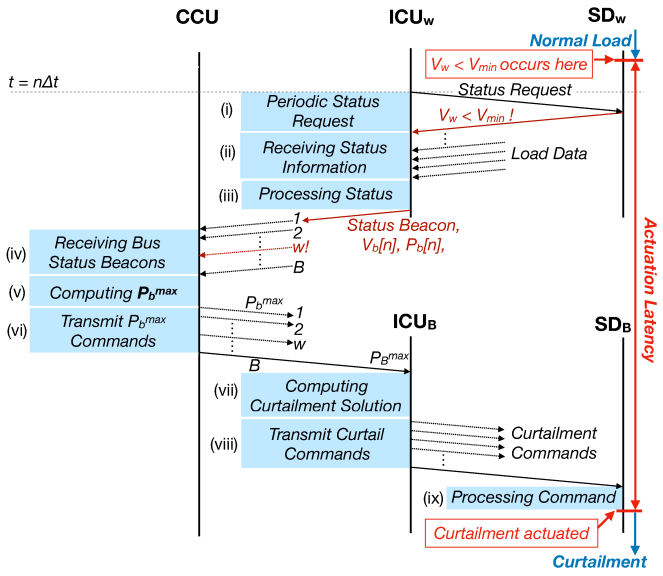

Fig. 8. Latency accumulation in the Smart EV Charging scheme. Curtailment is triggered in bus w and actuated in last bus B.

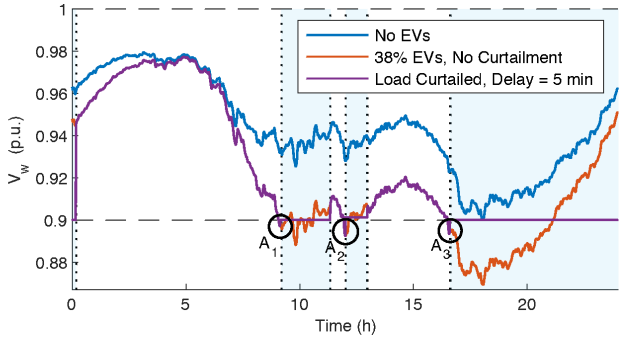

(a) $V_{\min} = 0.9$p.u.

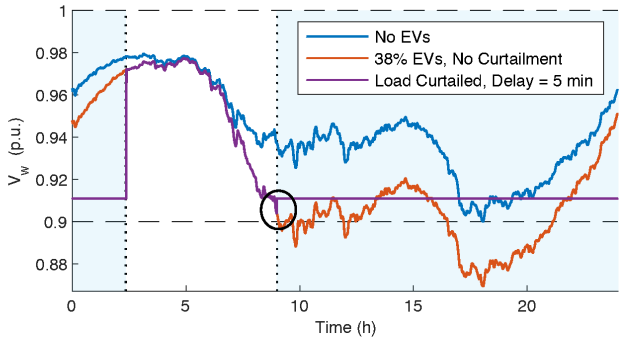

(b) $V_{\min} = 0.91$p.u.

Fig. 9. Voltage at worst bus V_w with 5 minute actuation latency. Shaded: curtailment, Unshaded: normal load.

transmissions. This reduces backhaul data load and implementation cost, however, simultaneous outgoing/incoming messages must be buffered at the transmitter/receiver, incurring queueing delay. Listener/sender operation in each tier is as follows:

1) SDs: These will be numerous and pervasive, so operation is kept simple. The listener port receives control commands from ICU$_b$, and sender responds with status messages.

2) ICUs: Every update period n, the sender port broadcasts 'Status Request' to all its SDs, (i) in Fig. 8, and the listener port receives each of their replies (ii). Once all replies are received, the sender forwards a status beacon to the CCU. The listener port also receives command messages from the CCU (e.g. $P_b^{\max}$ commands (vi) or status requests). During curtailment, the sender transmits instructions to SDs to control EV charging load (viii).

3) CCU: The listener receives periodic status beacons from each ICU$_b$ (iv). Once all beacons are received, if curtailment is triggered, CCU computes $\mathbf{P}^{\max}$ (v) and the sender transmits $P_b^{\max}$ individually to each ICU$_b$ (vi). The CCU sender may at any time broadcast additional status request messages or commands, maintaining complete centralised network control.

Queueing latency will occur at (ii,iv,vi,viii) at the ICU and CCU, where there are many transmitters/receivers and packets can only be serviced serially at each port. This scheme includes four queues where all packets in one queue must be serviced before the next queue can begin. Total queueing delay D_q is then quantified by average packet service rate μ and the number of arriving packets in each queue. At ICU$_b$, packet arrival will scale with the number of SDs. At CCU, it will scale with the number of distribution buses B. Assuming one SD at each LV node, one status packet per SD and equal μ in each tier, queueing delay per curtailment trigger is given

$$D_q = 2\left(\frac{\max[H_b]}{\mu_{ICU}} + \frac{B}{\mu_{CCU}}\right) \tag{10}$$

Computation of $\mathbf{P}^{\max}$ may also be intensive for a large number of nodes, incurring significant processing latency at the CCU (v). This also occurs for ICU$_b$ curtailment operation (iii,vii), where EV charging must be managed request-by-request every update period. Finally, transmission latency will depend on type and quality of data links used. Link bandwidth may also affect average packet service rate at CCU and ICU.

Communications latency decides minimum update interval Δt. However, halving Δt will also lead to twice the system traffic, which will be significant for the large number of SDs inherent in the Smart Grid. Increased system traffic will raise cost of communications infrastructure, thus its reduction is desirable. A tradeoff ensues between granularity of control and weight on system backhaul.

To illustrate effects of these latency accumulations on Smart EV Charging performance, a 5 minute update interval is chosen, Fig. 9a. Latency effects are noticeable at the curtailment trigger shown by A_{1-3}. Here, after $V_w < V_{\min}$, there is a delay period during which load at each bus remains uncurtailed, meaning voltage deviation is allowed to exceed the statutory limit. The amount exceeded depends on rate of load increase during this actuation delay, so is stochastic in real terms.

Under practical communications constraints, actuation latency requires that $V_w < V_{\min}$ cannot be instantly detected at CCU nor curtailment instantly actuated at SDs. This delay

must be accounted for by raising $V_{\min}$, allowing the system time for effective actuation. Fig. 9b shows V_w where $V_{\min} = 0.91$p.u. V_w is now comfortably within acceptable limits. However, since $P_N^{\max}$ is by definition the maximum total power demand such that $V_w \geq V_{\min}$, raising $V_{\min}$ inherently reduces $P_N^{\max}$. This slows charging queue service rate at all buses in the network since less power is available for charging, meaning more time spent in curtailment and longer charging delays for subscribing users. Using the new reduced $P_N^{\max}$ in (9), maximum EV capacity is 64%.

V. Conclusion

Growing penetration of EVs will drive ever sharper spikes in consumer power demand, and how to keep the power grid within stable operating limits is uncertain. Smart EV Charging schemes have demonstrable applicability for reducing peak load and maintaining stable network conditions; however, inefficiency in underlying communications infrastructure is a routinely neglected system constraint.

This paper studies effects of communications-driven latency for Smart EV Charging in a distribution network. Predicted EV charging power profile is first quantified based on verified statistical studies alongside residential load. A model is hence constructed based on statistical results for driving patterns, charging locations and power ratings. If all vehicles in the UK were purely electric, random uncoordinated EV charging demonstrates a peak load increase of 83%.

A smart EV charging scheme is then designed based on load rescheduling via user subscription, with compensation for delayed charging in the form of reduced energy prices. This scheme maintains maximum voltage deviation within acceptable limits, satisfies all EV charging requirements and causes no increase in peak load. Further, it is applicable beyond EVs to all flexible loads in general, and permits power allocation via a number of possible algorithms. Under ideal conditions, this scheme can sustain 81% EV penetration with minimum infrastructure additions.

Finally, a communications structure for the scheme is designed, involving a three-tier centralised architecture. The effect of latency on scheme performance is analysed and simulated, where a 5 minute update interval was shown to induce unacceptable voltage drops at the curtailment trigger. This was compensated by raising the minimum voltage threshold to accommodate actuation delay. However, effects are significant, leading to increased charging delays. When practical communications constraints are considered, maximum EV penetration fell to 64%.

References

[1] National Grid, "Future Energy Scenarios," http://fes.nationalgrid.com/media/1409/fes-2019.pdf, July 2019.

[2] Ofgem, "Typical domestic consumption values," http://www.ofgem.gov.uk/gas/retail-market/monitoring-data-and-statistics/typical-domestic-consumption-values, 2018.

[3] Honda, "Honda Clarity Electric," http://automobiles.honda.com/clarity-electric#technology, 2018.

[4] Nissan, "Nissan LEAF," https://www.nissan.co.uk/vehicles/new-vehicles/leaf.html, 2018.

[5] Chevrolet, "Chevrolet Bolt EV," http://www.chevrolet.com/electric/bolt-ev-electric-car, 2018.

[6] Tesla, "Tesla Model S," http://www.tesla.com/models, 2018.

[7] S. Deilami, A. S. Masoum, P. S. Moses, and M. A. S. Masoum, "Real-time coordination of plug-in electric vehicle charging in smart grids to minimize power losses and improve voltage profile," *IEEE Transactions on Smart Grid*, vol. 2, no. 3, pp. 456–467, Sept 2011.

[8] A. S. Masoum, S. Deilami, M. A. S. Masoum, A. Abu-Siada, and S. Islam, "Online coordination of plug-in electric vehicle charging in smart grid with distributed wind power generation systems," in *2014 IEEE PES General Meeting | Conference Exposition*, July 2014, pp. 1–5.

[9] E. Veldman and R. A. Verzijlbergh, "Distribution grid impacts of smart electric vehicle charging from different perspectives," *IEEE Transactions on Smart Grid*, vol. 6, no. 1, pp. 333–342, Jan 2015.

[10] "Digest of United Kingdom Energy Statistics (DUKES)," *Department for Business, Energy & Industrial Strategy*, July 2018.

[11] ExtraLink, "New figures reveal 6% rise year on year in largely 'invisible' embedded energy generation," http://www.electralink.co.uk/2017/05/new-figures-reveal-6-rise-year-year-largely-invisible-embedded-energy-generation/, May 2017.

[12] A. Tahir and A. Massoud, "Load shedding and forecasting in distribution systems with PV-based distributed generation and electric vehicles," in *2017 4th International Conference on Information Technology, Computer, and Electrical Engineering (ICITACEE)*, Oct 2017, pp. 71–76.

[13] A. A. Eajal, M. F. Shaaban, E. F. El-Saadany, and K. Ponnambalam, "Fuzzy logic-based charging strategy for electric vehicles plugged into a smart grid," in *2015 IEEE International Conference on Smart Energy Grid Engineering (SEGE)*, Aug 2015, pp. 1–6.

[14] F. Rassaei, W. Soh, and K. Chua, "Demand response for residential electric vehicles with random usage patterns in smart grids," *IEEE Transactions on Sustainable Energy*, vol. 6, no. 4, pp. 1367–1376, Oct 2015.

[15] A. Alyousef and H. de Meer, "Design of a TCP-like smart charging controller for power quality in electrical distribution systems," in *Proceedings of the Tenth ACM International Conference on Future Energy Systems*, ser. e-Energy '19. New York, NY, USA: ACM, 2019, pp. 128–138. [Online]. Available: http://doi.acm.org/10.1145/3307772.3328293

[16] O. Ardakanian, S. Keshav, and C. Rosenberg, "Real-time distributed control for smart electric vehicle chargers: From a static to a dynamic study," *IEEE Transactions on Smart Grid*, vol. 5, no. 5, pp. 2295–2305, Sep. 2014.

[17] A. Robinson, P. Blythe, M. Bell, Y. Hübner, and G. Hill, "Analysis of electric vehicle driver recharging demand profiles and subsequent impacts on the carbon content of electric vehicle trips," *Energy Policy*, vol. 61, pp. 337–348, 2013.

[18] J. Zimmerman, M. Evans, J. Griggs, N. King, L. Harding, P. Roberts, and C. Evans, "Household Electricity Survey A study of domestic electrical product usage," *Intertek Testing & Certification Ltd*, pp. 213–214, May 2012, R66141 Final Report Issue 4.

[19] J. Palmer and I. Cooper, "United Kingdom housing energy fact file," *Department of Energy & Climate Change*, pp. 46,49, 2013.

[20] A. Evans, J. Cummings, M. Slocombe, and F. Corvaglia, "National Travel Survey: England 2017," *Department for Transport*, 2017, Statistical Release: Table NTS9902.

[21] S. H. Low, "Convex relaxation of optimal power flow? Part I: Formulations and equivalence," *IEEE Transactions on Control of Network Systems*, vol. 1, no. 1, pp. 15–27, March 2014.

[22] M. E. Baran and F. F. Wu, "Network reconfiguration in distribution systems for loss reduction and load balancing," *IEEE Transactions on Power Delivery*, vol. 4, no. 2, pp. 1401–1407, April 1989.

[23] R. D. Zimmerman, C. E. Murillo-sánchez, and R. J. Thomas, "MATPOWER steady-state operations, planning and analysis tools for power systems research and education," *IEEE Transactions on Power Systems*, pp. 12–19, 2011.

[24] J. W. Heron, J. Jiang, H. Sun, V. Gezerlis, and T. Doukoglou, "Demand-response round-trip latency of IoT smartgrid network topologies," *IEEE Access*, vol. 6, pp. 22 930–22 937, 2018.

[25] T. Ma and O. Mohammed, "Real-time plug-in electric vehicles charging control for V2G frequency regulation," in *IECON 2013 - 39th Annual Conference of the IEEE Industrial Electronics Society*, Nov 2013, pp. 1197–1202.

Publication B

J. W. Heron, J. Jiang, H. Sun, V. Gezerlis and T. Doukoglou, "Demand-Response Round-Trip Latency of IoT Smart Grid Network Topologies," in *IEEE Access*, vol. 6, pp. 22930-22937, 2018.

IEEE Access
Multidisciplinary | Rapid Review | Open Access Journal

Received March 9, 2018, accepted April 11, 2018, date of publication April 30, 2018, date of current version May 16, 2018.

Digital Object Identifier 10.1109/ACCESS.2018.2831254

Demand-Response Round-Trip Latency of IoT SmartGrid Network Topologies

JOHN W. HERON[1], (Student Member, IEEE), JING JIANG[1], (Member, IEEE), HONGJIAN SUN[1], (Senior Member, IEEE), VELISSARIOS GEZERLIS[2], AND TILEMACHOS DOUKOGLOU[2]

[1]Department of Engineering, Durham University, Durham DH1 3LE, U.K.
[2]COSMOTE (OTE group), 151 22 Athens, Greece

Corresponding author: Hongjian Sun (hongjian.sun@durham.ac.uk)

This work was supported in part by the European Commissions' Horizon 2020 Framework Program (H2020/2014-2020) through TESTBED Project under Grant 734325, and in part by the U.K. EPSRC under Grant EP/P005950/1.

ABSTRACT Smart grids are the next generation of power distribution network, using information and communications technologies to increase overall energy efficiency and service quality of the power grid. A significant challenge in smart grid development is the rapidly rising number of smart devices and how to meet the associated load on the backbone communication infrastructure. This paper designs an Internet-of-Things smart grid testbed simulator to provide crucial insight into communication network optimization. Simulation for a large number of smart devices under various heterogeneous network topologies is used to analyze the maximum number of clients supportable for a given demand-response latency requirement. This latency includes all protocol overheads, retransmissions and traffic congestion, and simulator processing time is successfully eliminated from the final delay calculation via data post-processing. For a specific three-tier topology, given a round-trip latency requirement, the effect of number of smart devices per local hub and overall number of local hubs on network performance is analyzed, and crucial design insights are drawn relevant to cost-efficiency optimization of network deployment.

INDEX TERMS Internet-of-Things, network topology, round-trip latency, smart grids, testbed simulator.

I. INTRODUCTION

The global interconnectedness of machines and devices over the internet, often called the 'internet-of-things' (IoT), proves to be a defining characteristic of 21^{st} century technology [1]. Smart Grids, the extension of this idea to the power distribution network, use two-way information exchange between connected components to optimise energy flow. Application of Smart Grid systems are capable of dramatically reducing energy consumption and improving overall service quality [2]. However, as the prevalence of Smart Devices grows exponentially, the problem of increasing traffic load and addressable end-points is of rising concern.

Internet and communications technology (ICT) infrastructure is the backbone of future Smart Grid enhancement, providing scalable and reliable services to all kinds of IoT applications. In light of the rapid growth of IoT and Smart Grid technology, the infrastructural challenges to be addressed come down to three aspects: Firstly, the fast growing amount of power system data needs to be supported by the network [3]. A persisting challenge in IoT systems, both in Smart Grids and otherwise, is that the deployment of numerous and diverse interconnected devices is accompanied by equally numerous traffic increase with equally diverse set of Quality of Service (QoS) requirements, such as reliability, throughput, latency and security. The number of these Smart Devices is predicted to increase dramatically in the near future, and this will inevitably add load to ICT infrastructure. How best to optimise the Smart Devices' network topology to meet these QoS requirements remains an open issue. Secondly, there are many competing communication standards for IoT, but with which to communicate these data is still an open issue. Two-way information flow between Smart Devices is enabled by integration of many advanced communication technologies. A cooperation of multiple technologies are required to meet the Smart Grid requirements, and a single industry standard unifying all these technologies has yet to emerge. Finally, the cost of deploying the necessary supporting hardware is high. Deployment of devices and infrastructure also involves significant financial investment. Once the infrastructure has been deployed, any modifications can also be costly.

Thus, simulation is required to tackle these three infrastructural challenges. The simulation must be able to test varieties of communication standards combined in assorted arranged network topologies, so as to find the optimum solutions prior to capital investment in hardware and deployment. In this context, Smart Grid simulations have gained significant attention in the recent years: A testbed for demand-focused energy management in the end-user environment is designed and implemented in [4]. The testbed consists of three levels - the base station, gateways and Smart Devices. A testbed based on wireless communication technology involving both centralised and distributed architectures is studied in [5]. Hardware interfaces between energy and communication components is designed and implemented, and a small scale laboratory test is performed investigating real-time demand response and disruption resilience. There are also works that focus on ICT architecture. In [6], a three-tier framework is proposed based on the Internet of Things, while in [7], an interoperability framework based on data distribution services is proposed. Meanwhile, in [8], a comprehensive survey on Smart Grid Cyber-Physical System testbeds is performed. Existing testbeds are compared and discussed from several design aspects, including heterogeneous communication support, security and privacy, multiple protocol support and remote connection access. These trials and tests pave the way for the successful deployment of Smart Grid ICT architectures, however these are restricted mainly to small or medium scale studies, and large scale simulation has not been fully addressed. Analysis of a large scale network is of great importance to physical implementation of Smart Grid ICT architectures from the perspective of communication service providers.

In this respect, this paper presents the smart grid testbed design toward large scale network simulations. The testbed is designed to be flexible, scalable and reconfigurable, oriented by communication providers to optimise for large scale metrics. The major contributions are listed as follows.

- An IoT smart grid testbed simulator is designed and developed to provide crucial insight into the effect of ICT backbone topology on overall network performance. Simulations for a large number of smart devices under various heterogenous network topologies are used to analyse critical performance limits given minimum QoS requirements.
- For a specific three-tier heterogeneous topology using point to point, unicast and multicast communication, given a demand-response latency requirement, investigations are carried out on the number of smart devices that a local hub can support, and with a fixed number of smart devices, the number of local hubs that a central server can support.
- A model is provided for demand-response round-trip latency, where the latency includes all congestion delays, protocol overhead and retransmissions, and the processing time of the testbed computers is successfully eliminated from analysis with data post-processing. Using the model, critical design constraints concerning network topology are optimised.

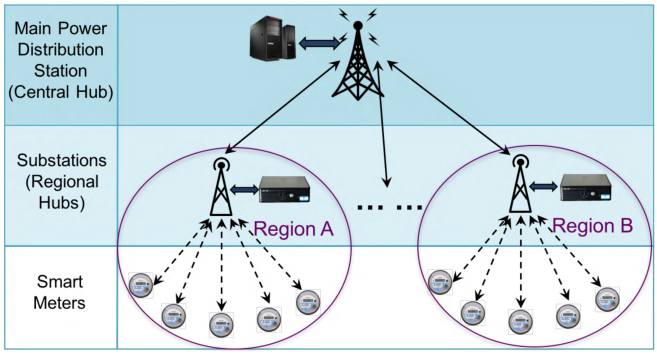

FIGURE 1. Three-tier tree-star topology.

The rest of the paper is laid out as follows. Section II describes the testbed simulation model of this paper. Demand-response round-trip latency modelling is presented in Section III, and analysis of simulation results are presented in Section IV, where critical findings are demonstrated. Finally, Section VI summarises the key points of this study.

II. SIMULATOR OVERVIEW

The aims of the smart grid testbed simulator are to analyse the effect of the telecommunications infrastructure on the overall network performance and be used to provide crucial insight into network optimisation. Scope of the simulator is to simulate networks where: up to hundreds of nodes are organized in a specific topology; point to point, unicast and also multicast (or even broadcast) communication, between nodes is being considered; and traditional layer 3 Internet protocols (TCP/IP) with IPv4 (upgradeable to also use IPv6) address space are used.

A. SIMULATION TOPOLOGY

The smart grid testbed needs to be flexible, scalable and reconfigurable. To meet these needs, the simulator consists of three component types forming a three-tier heterogenous network: a Smart Device module, a Substation or Local Hub module and a Central Hub module. To enable large scale testing, these modules have been implemented using Microsoft Visual Studio VB.NET platform [9], [10]. The chosen system topology is a three tier tree-star network. A tree-star network topology can be considered as a combination of two or more star networks connected together. In each star network comprising the tree, there is a Local Hub to which all the lower tier Smart Devices are directly linked. The Local Hubs of each star network are then directly connected to a central administrator node call the Central Hub, as in Fig. 1. This topology is ideal when the nodes are located in groups, with each group occupying a relatively small physical region, such as households or groups of households.

B. COMMUNICATION PROTOCOLS

The simulation supports communication via wireless or wired communication, requiring only input of data rate and bit error rate (BER) (or packet error rate (PER)) on each communication link. Transmission Control Protocol (TCP) / Internet Protocol (IP) [11] communication is used to simulate communication on the ICT backbone. The TCP/IP protocol has several advantages for a Smart Grid testbed. It is widely used and well understood, so it is supported by the majority of available routers and servers, which will serve to reduce the cost of system development. Furthermore, since it is transparent to real networks, more routes will be available for the transmission. A wide choice of encryption algorithms can guarantee information security, the complexity of which can be assigned according to the specific application. Finally, IPv6 is already rolled out for commercial use and is able to support vast amount of devices within the network. A main criticism of TCP/IP in IoT applications is it's energy performance on power-limited devices, however the simulation can also utilize the User Datagram Protocol (UDP).

C. SIMULATION MODULE STRUCTURE

The simulation is developed in a windows application environment. In this application a user selects all the simulation parameters through the application graphic user interface (GUI). The application then calls the three described functions (SmartMeterModule.exe, SubstationModule.exe, CentralHubModule.exe) in order to build the 3-level Tree-Star topology. For example, if a user has selected 1 node for the Central-hub in the upper layer, 10 nodes for the Substations in the middle layer and 10 nodes (Smart Meters) per Substation in lower layer, then the application will call CentralHubModule.exe once, SubstationModule.exe ten times, SmartMeterModule.exe 100 times. The central-hub knows the IP addresses of its Substation nodes. Each Substation node knows the IP address of the Central-hub, as well as the IP addresses of its regional Smart Meters. Each Smart Meter knows the IP address of its Substation. The function of each module will be described in turn, before the operation of the GUI inputs and outputs is explained.

1) SMART METER/DEVICE MODULE

Smart Meters (or Smart Devices) are the lower tier nodes, conducting measurements and/or actuations within a Smart Grid system. They receive and respond to control commands from the Central Hub, via their Local Hub. The proposed Smart Meter module consists of two submodules, the Listener and Sender, as illustrated in Fig. 2.

Each Smart Meter is assigned a unique IP address which is shared by the two submodules. In theory, the maximum supported port number is 65,536, although this simulation requires only one per node for the listener submodule. This feature also makes the proposed testbed highly flexible, since more functions can easily be added and assigned with different ports to cooperate with existing modules. Each submodule

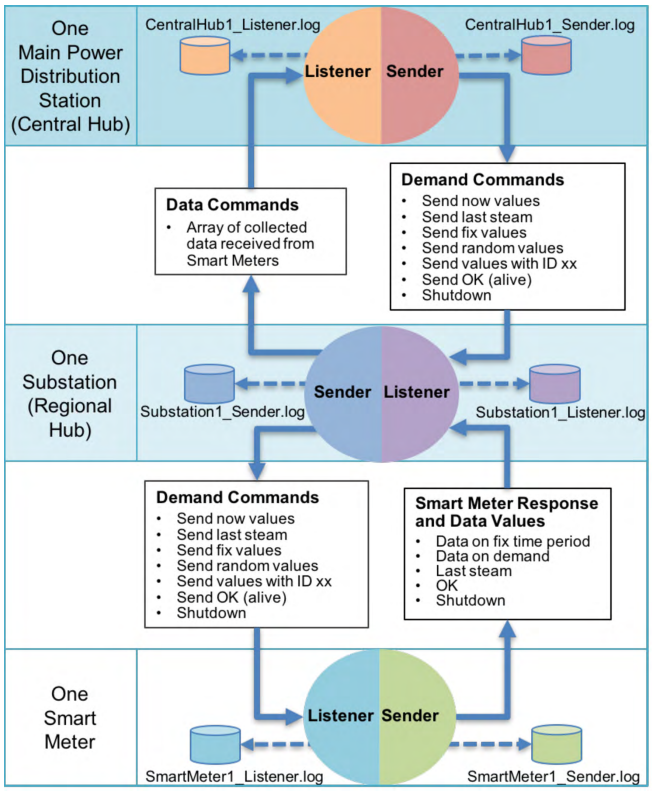

FIGURE 2. Overview of the simulation module structure.

has functions to generate and receive TCP/IP packets and log device events.

The Smart Meter module algorithm has several capabilities. The Listener sub module listens to a specific IP:port address and receives data (command packets) from the upper layers. The Sender sub-module can send data (measurement packets) to the upper layer in two ways, either periodically every predefined fixed period of time, or on demand, upon receipt of a measurement command from the upper layer by the Listener sub-module. There are several measurement commands, chosen for the needs of the simulation, for example "send now values", "send last values", "send a fix value", "send a random value", etc. The Listener and Sender sub-module write a record into the SmartMeter_Listener.log file and SmartMeter_Sender.log file, respectively, for every received data packet.

2) SUBSTATION/LOCAL HUB MODULE

Substation modules are the mid-tier nodes, which aggregate measurements from their associated Smart Meters and forward the data to the Central Hub. Like the Smart Meter module, the Substation module consists of a Listener submodule and a Sender submodule, as illustrated in Fig. 2.

Capabilities of the Local Hub involve TCP/IP traffic coordination, Smart Meter control and device events logging, and the algorithm has a number of functions. On starting the Substation module, both Listener and Sender sub-modules start. The Listener sub-module listens to a specific IP:port

address and receives data (command packets) from the Central Hub and data (measurement packets) from its Smart Meters. For every received packet it writes a record of data into Substation_Listener.log file.

When the Substation Listener receives a measurement command from the Central Hub, the Sender submodule forwards the command to its regional Smart Meters in a broadcast manner. Upon receipt of the measurement packets from all of its affiliated Smart Devices, the Sender submodule aggregates and sends the data to the Central Hub in two ways:

- Periodically (every predefined fixed period of time): The substation collects all the data received from its regional Smart Devices and sends them to the Central Hub.
- On demand: Once the substation has sent a measurement command to its regional Smart Devices, it waits to collect all the replies before sending an array of data to the Central Hub.

The Sender sub-module writes log data to the Substation_Sender.log file.

3) CENTRAL HUB MODULE

The Central Hub module is the main network coordinator, where data from the entire network is gathered. Again it consists of Listener and Sender submodules, shown in Fig. 2. It's functions are to send commands to the lower tier nodes and receive replies. It also logs device events into a Sender and Listener log file and may be instructed to request Smart Meter data either periodically, on demand, or randomly during the overall simulation time period.

In the Central Hub module algorithm, the Listener submodule listens to a specific IP:port address and receives data (aggregated measurement packets) from the the Local Hubs, then writes a record of the data into the Central-Hub_Listener.log file. The Sender submodule, sends measurement commands to all Substations with a broadcast function, and writes log data to the Central-Hub_Sender.log file.

D. GRAPHIC USER INTERFACE (GUI)

Simulation data is input by the user in four GUI forms:

- Initialisation Input Form
- Data Send Input Form
- Topology Input Form
- Simulation Time Input Form

In the first form, shown in Fig. 3 (a), the user selects if the simulation environment should be distributed over multiple computers or stand-alone on a single computer. In the stand-alone environment the Upper layer, Middle layer and Lower layer will all be built in the same computer, with the same IP address. Each node will then use different ports. In the distributed environment, any of the three layers Upper, Middle or Lower may be built in different computers (and hence with different IP addresses) as required. In the second form, shown in Fig. 3 (c), the network topology is chosen by selecting the number of nodes for each layer. In the third form,

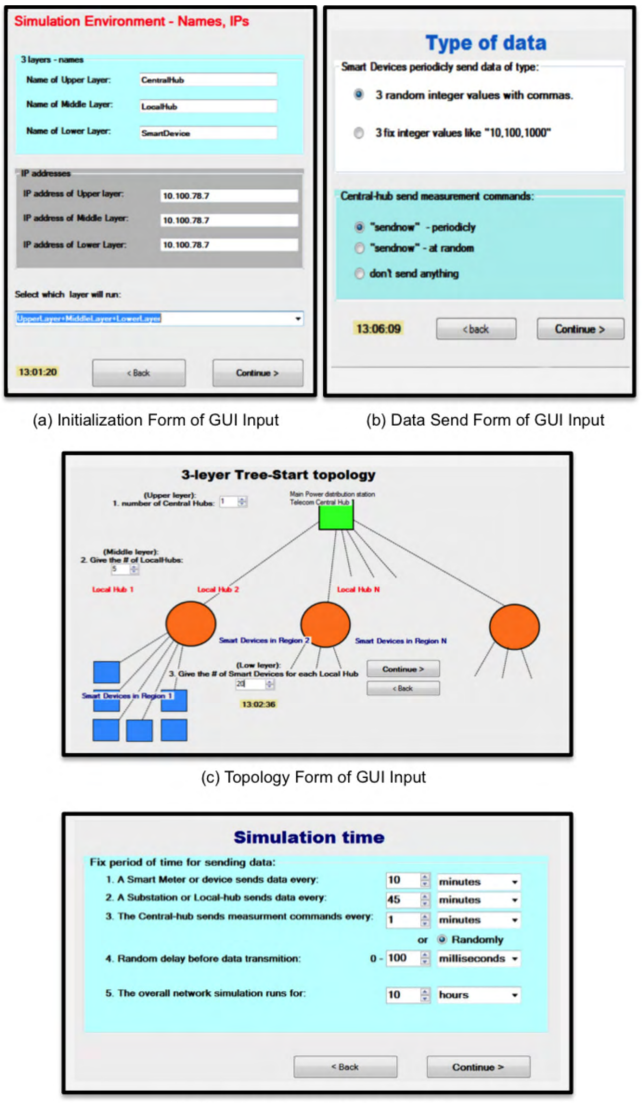

(a) Initialization Form of GUI Input (b) Data Send Form of GUI Input

(c) Topology Form of GUI Input

FIGURE 3. GUI input forms.

shown in Fig. 3 (b), the user decides the type of Smart Device measurement data (either fixed values or random values for purposes of simulation) and activity of the Central Hub measurement commands (either periodically, randomly or on demand). In the last form, shown in Fig. 3 (d), the simulation time preferences are specified, which includes when, if at all, the nodes in each tier should send their periodic messages, whether there should be a random time delay before each transmission (so that the computer's processor is not overloaded by a large number of nodes sending messages all at once) and how long the total simulation should run for.

While the simulation is running, the GUI displays the output window shown in Fig. 4 (a). During this time, the user can chose to send additional commands from the Central Hub, such as 'send now', 'send alive', etc. Once the simulation is complete, the GUI displays a bar graph of the round-trip latencies from all the commands sent from the Central Hub during the simulation, and displays the mean with a red line, as shown in Fig. 4 (b).

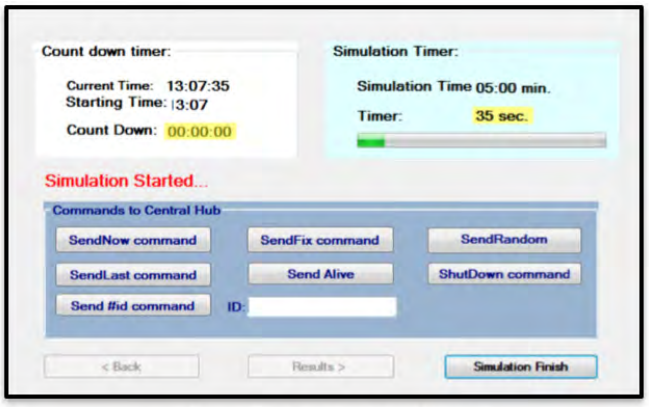

(a) Simulation Running GUI Output

(b) Latency Graph of GUI Output

FIGURE 4. GUI outputs.

With this testbed simulation platform it is possible to analyse the effect of Smart Grid network topology on round-trip latency, and use this to gauge the maximum number of devices that can be supported for a given network structure. Analysis can then serve to optimise the system and gain crucial insights into relevant design characteristics.

III. ROUND-TRIP LATENCY MODELLING

It is of great importance to know the maximum number of devices that a Smart Grid network can support for a given set of QoS requirements. The maximum number of Smart Devices per Substation and Substations per Central Hub will be a target metric in this experiment, and finding the optimal topology to maximise the number of supportable Smart Devices is key. In this section, we seek to find how the three-tier centralised topology and Smart Device aggregation affects the resulting demand-response or round-trip latency.

The round-trip latency in this case consists of the time required for the Central Hub to request measurements from all subsidiary Smart Metres and receive a complete reply. This includes all protocol overheads, retransmissions and traffic congestion at the respective nodes. For total number of Smart Devices N_D, the number of Smart Devices per Substation (Local Hub) S_L and number of Local Hubs per Central Hub L are related by the formula

$$N_D = LS_L \tag{1}$$

Given that measurement data from each Smart Device must pass through two hops in order to reach the Central Hub (Smart Device to Substation and Substation to Central Hub), the bottleneck in the system occurs in the middle tier, at the Substation level. Thus S_L is a critical network parameter.

The traffic load ρ in a network is defined as the ratio between the packet arrival rate λ and the packet service rate μ.

$$\rho = \frac{\lambda}{\mu} \tag{2}$$

Assuming an M/M/1 queueing process in this case, since there is one queue per substation server, the average delay due to congestion at the local hub is given by

$$D_A = \frac{1}{\mu(1-\rho)} = \frac{1}{\mu - \lambda} \tag{3}$$

Assuming constant average packet service rate from Substation to Central Hub, the arrival rate at each local hub should increase linearly with S_L, and the delay should increase proportional to the inverse. However, this is only one link. The round-trip delay incurs a transmission delay from central hub to substation, from substation to smart device, from smart device to substation and substation to central hub. Each node has only one listener and one sender submodule, so there may be congestion at any of these steps. And that is without considering the delay incurred by processing time, transmission time and the number of retransmissions. Hence the need for a simulation testbed.

IV. NETWORK SIMULATION RESULTS & ANALYSIS

Using the testbed described in Section II, ten different network sizes were simulated using N_D from 100 to 1000. Within each network size, S_L and L were varied, to gain an idea of the effect of network topology on round-trip delay. The data links were modelled with a data rate of 50 Mbps to simulate the VDSL backbone, and BER of 10^{-7} to allow for zero PER with convolutional coding.

Fig. 5 shows how the round-trip delay D_{rt} varies with S_L for the different network sizes. It can be seen that the delay increases linearly with S_L of the form

$$D_{rt}(S_L) = C_1 S_L + C_2 \tag{4}$$

where C_n are fitting coefficients. This relation is seen even more clearly when D_{rt} is plotted against L, following an inverse relationship of the form

$$D_{rt}(L) = \frac{C_1 N_D}{L} + C_2 \tag{5}$$

shown in Fig. 6. In this case C_n are found by nonlinear least squares regression.

The fewer devices per local hub, or the more local hubs for a given number of devices, the less congestion during the aggregation process, and less overall delay. This makes intuitive sense. However, Fig. 6 also shows a crucial design

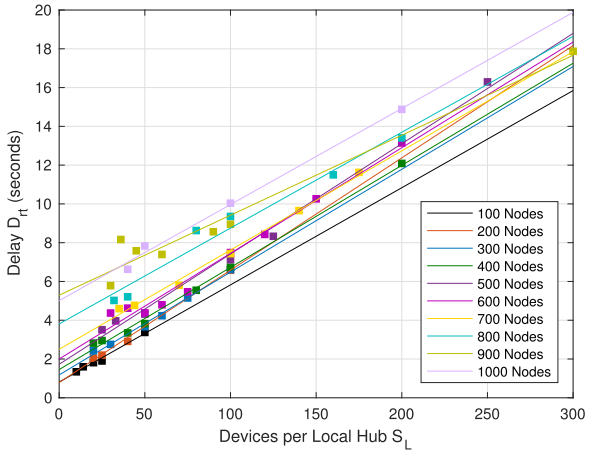

FIGURE 5. Round-trip delay variation for smart devices per local hub.

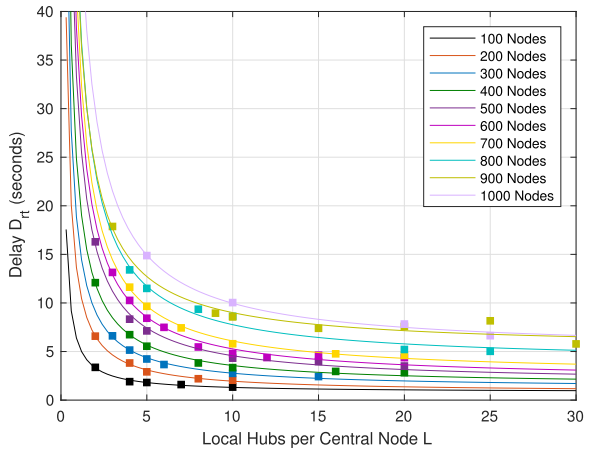

FIGURE 6. Round-trip delay variation for local hubs per central hub.

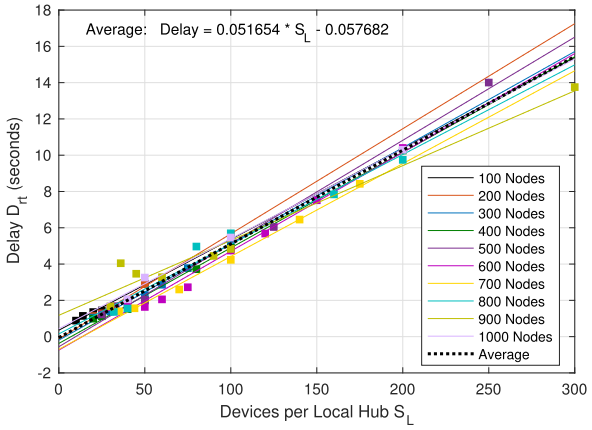

FIGURE 7. Round-trip delay minus processing time for devices per local hub.

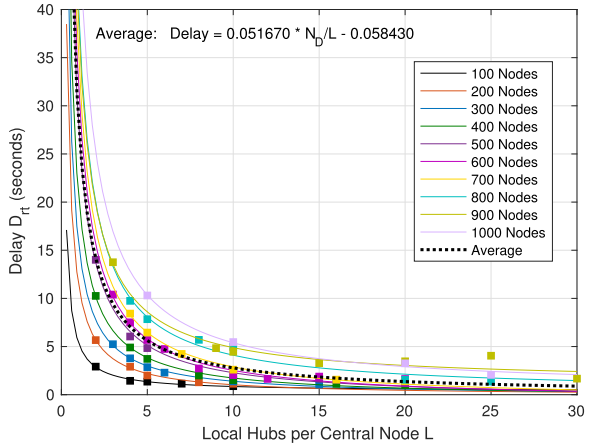

FIGURE 8. Round-trip delay minus processing time for substation number.

insight: for any constant number of devices, the delay benefits of using more local hubs diminishes with the inverse of the number of substations. This is important, since the number of substations within a smart grid network will have a significant effect on deployment cost.

Also notice that the round-trip delay appears to rise with the number of nodes. This is unexpected, since the bottleneck occurs at the local hub, which is unaffected by the number of parallel data streams in different substations. This proportional increase is accountable to the processing time of the computer itself: Generating measurement packets for 1000 nodes will take ten times the time to generate packets for 100 nodes. It is desirable to remove the processing time from the overall delay calculation, since packet generation for the entire system would not normally be undertaken by only one processor.

To remove the processing delay, the average delay for each fit in Fig. 5 was used to compute the average difference between each successive network size, which is taken to be the processing time for 100 nodes T_{p100}, in this case 457 milliseconds. This time delay was then subtracted from the data for every 100 node increase, giving the plots shown in Fig. 7 and 8. This allows the coefficients C_1 and C_2 to be estimated as the average gradient and y-intercept. The average curve in each case is shown by the black dotted line, which runs approximately through the origin in Fig. 7, and tends to zero and infinity in Fig. 8.

Fig. 9 shows the same in a 3D surface plot for the number of substations and total number of devices. For comparison, plots both with and without the processing time T_{p100} are included. From this it is clearly visible that for any number of devices N_D, the minimum delay will occur with the maximum number of local hubs. For $L > 15$ there is a constant convergence with very low variation. The exact number must then be chosen accounting for cost efficiency of the overall system.

V. DISCUSSION

How best to structure the IoT power and communications network remains a significant challenge for future smart grid systems. This paper improves analysis over existing models by successfully simulating demand-response latency for various large scale network topologies, where all protocol overheads, retransmissions and traffic congestion are taken into account, and simulator processing time is removed from the final latency assessment.

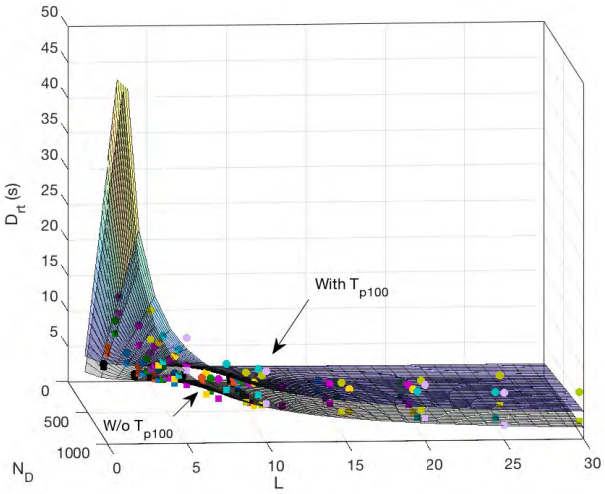

FIGURE 9. 3D plot of D_{rt} with L and N_D with and without processing time. (Uses the same data point colour scheme as previous graphs).

Analysis of large scale smart grid architectures is of great interest to communication service providers for optimisation of deployment cost-efficiency. Deployment of ICT devices and infrastructure, such as local hubs in a network, involves significant financial investment. The analysis in this paper exposes an opportunity to compromise between latency gain and deployment cost, on the grounds that the demand-response latency falls by an increasingly smaller amount with each addition of a mid-layer node.

VI. CONCLUSION

This paper presents a large scale simulation testbed to study the demand-response latency of various heterogeneous smart grid network topologies. A three-tier tree-star topology is simulated with three distinct node types. Networks with up to 1000 client nodes are simulated, and various lower and mid-tier node configurations are studied. Round trip delay includes all congestion delays, protocol headers and retransmissions, and the processing time of the testbed computers was successfully eliminated from analysis with data post-processing. It was found that the round-trip delay varies with the inverse of number of substation nodes, meaning that the system is optimised with the maximum of local hubs. Moreover, regardless of the number of Smart Devices in a Smart Grid, beyond a certain number of middle layer local-hubs (in this simulation 15 and above), the Demand-Response round trip delay changes very little, slowly converging to zero. This can be used for easy analysis of network implementation cost-efficiency and network performance limitations given certain QoS requirements, quantity of client devices and implementation budget.

REFERENCES

[1] S. E. Collier, "The emerging Enernet: Convergence of the smart grid with the Internet of Things," *IEEE Ind. Appl. Mag.*, vol. 23, no. 2, pp. 12–16, Mar./Apr. 2017.

[2] H. Sun, N. D. Hatziargyriou, H. V. Poor, L. Carpanini, and M. A. Fornié, *Smarter Energy: From Smart Metering to the Smart Grid* (Energy Engineering), Edison, NJ, USA: IET, 2016, accessed: 2016. [Online]. Available: https://books.google.co.uk/books?id=sYoxDQAAQBAJ

[3] J. Jiang and Y. Qian, "Distributed communication architecture for smart grid applications," *IEEE Commun. Mag.*, vol. 54, no. 12, pp. 60–67, Dec. 2016.

[4] W. Tushar *et al.*, "Smart grid testbed for demand focused energy management in end user environments," *IEEE Wireless Commun.*, vol. 23, no. 6, pp. 70–80, Dec. 2016.

[5] W.-Z. Song, D. De, S. Tan, S. K. Das, and L. Tong, "A wireless smart grid testbed in lab," *IEEE Wireless Commun.*, vol. 19, no. 3, pp. 58–64, Jun. 2012.

[6] J. Jin, J. Gubbi, S. Marusic, and M. Palaniswami, "An information framework for creating a smart city through Internet of Things," *IEEE Internet Things J.*, vol. 1, no. 2, pp. 112–121, Apr. 2014.

[7] T. A. Youssef, A. T. Elsayed, and O. A. Mohammed, "DDS based interoperability framework for smart grid testbed infrastructure," in *Proc. IEEE 15th Int. Conf. Environ. Elect. Eng. (EEEIC)*, Jun. 2015, pp. 219–224.

[8] M. H. Cintuglu, O. A. Mohammed, K. Akkaya, and A. S. Uluagac, "A survey on smart grid cyber-physical system testbeds," *IEEE Commun. Surveys Tuts.*, vol. 19, no. 1, pp. 446–464, 1st Quart., 2017.

[9] V. Gezerlis and T. Doukoglou, "Software network topology and traffic simulation for overlay telecommunication network in smart grids," in *Proc. InfoCom World Conf.*, Athens, Greece, Oct. 2017, pp. 1–34, accessed: 2017. [Online]. Available: http://www.infocomworld.gr/19o-infocom-world-2017/erevnitika-programmata-o-t-e/programma-erevnitikon-programmaton-o-t-e/

[10] T. Doukoglou and V. Gezerlis, "Smart homes in smart grids," in *Proc. InfoCom World Conf.*, Athens, Greece, Oct. 2017, pp. 1–14, accessed: 2017. [Online]. Available: http://www.infocomworld.gr/19o-infocom-world-2017/erevnitika-programmata-o-t-e/programma-erevnitikon-programmaton-o-t-e/

[11] W. R. Stevens, *TCP/IP Illustrated: The Protocols*, vol. 1. Boston, MA, USA: Addison-Wesley, 1993.

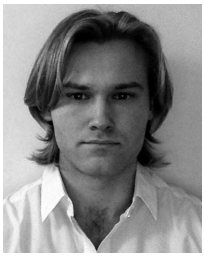

JOHN W. HERON (S'17) received the master's degree (M.Eng.) in electronics engineering from Durham University, U.K., in 2016, where he is currently pursuing the Ph.D. degree in communications engineering. He spent two months co-located in collaboration with COSMOTE (OTE group) in 2017, presented at INFOCOM World 2017 Conference in Athens and has co-authored one paper in the 2017 IEEE 86th Vehicular Technology Conference in Toronto. His current research interests include visible light communications, vehicular networks, smart grids, Internet-of-Things, and cooperative relay.

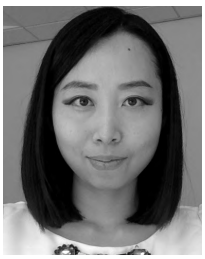

JING JIANG (S'10–M'12) received the Ph.D. degree in electronic and electrical engineering from the University of Edinburgh, U.K. From 2011 to 2014, she was a Research Fellow with the Centre for Communication Systems Research, University of Surrey, U.K. She is currently a Research Associate with the Department of Engineering, Durham University, U.K. Her current research interests include smart grid, next generation wireless communications, massive MIMO, cyber security, cognitive radio networks, wireless sensor networks, and Internet of Things in smart energy applications. She is on the Editorial Board of the Journal IET *Smart Grid* and the EURASIP *Journal on Wireless Communications and Networking*.

HONGJIAN SUN (S'07–M'11–SM'15) received the Ph.D. degree in electronic and electrical engineering from The University of Edinburgh, U.K., in 2011. He held post-doctoral positions with King's College London, U.K., and Princeton University, USA. Since 2013, he has been with Durham University, U.K., as a Reader in smart grid (Lecturer from 2013 to 2017). He has authored or co-authored over 90 papers in refereed journals and international conferences. He has made contributions to and co-authored the IEEE 1900.6a-2014 Standard. He has authored or co-authored five book chapters, and edited two books: IET book *Smarter Energy: From Smart Metering to the Smart Grid*, and CRC Book *From Internet of Things to Smart Cities: Enabling Technologies*. His research mainly focuses on smart grid: communications and networking; smart grid: demand side management and demand response; and smart grid: renewable energy sources integration.

He is an Editor-in-Chief for IET *Smart Grid* and an Editor for the *Journal of Communications and Network*. He also served as a Guest Editor of the IEEE *Communications Magazine* for three feature topics, including: Integrated Communications, Control, and Computing Technologies for Enabling Autonomous Smart Grid, 2016.

VELISSARIOS GEZERLIS received the B.Sc. degree (Hons.) in computer science from the Department of Informatics and Telecommunications, University of Athens, in 1993, the M.Sc. degree (Hons.) in advanced information systems in 1996, and the Ph.D. thesis from the Department of Informatics in the area of pattern recognition, optical character recognition and Byzantine music technology in 2001. He also holds the Diploma of Byzantine Music. He is currently a Telecom Engineer with the New Technologies Labs of OTE/COSMOTE Group of companies. He worked for 15 year from 2000 to 2015 with the IT Department of OTE as a System Administrator, an Office Automation Programmer and Analyst and the Head of user support section. In addition, he was responsible for OTE IT Equipment procurements.

He is currently responsible for Smart Home platform validation and Lab Test Automation procedures. He also participates in EU funded research projects, such as SmarterEMC2, TESTBET, SliceNet, and 5GMedia. His research interests include smart grids, smart home, automations & robotics, and network simulation.

TILEMACHOS DOUKOGLOU received the Diploma degree in electrical engineering from the Aristotle University of Thessaloniki, Greece, in 1986, and the M.Eng. and Ph.D. degrees in electrical and biomedical engineering from McGill University, Montreal,Canada, in 1989 and 1994, respectively. He was a Visiting Research Engineer and a Post-Doctoral Researcher with the Bioinstrumentation Laboratory, Massachusetts Institute of Technology, Cambridge, MA, USA, from 1994 to 1995.

He is currently the Head of OTE's Group Laboratories responsible for new technologies test and evaluation. His research interests are in the area of broadband network technologies and services (G.fast, Super-Vectoring, NG/XG-PON, and Hybrid Access), development of platforms for new service and service-support, like IMS, SDN/NFVs, Telemetry (SmartGRID & Smart Metering), and networking and cloud (i.e. Vitrual CPEs and Virtual SBCs).

Since 1995, he has been involved in various EU Funded Research and Development Programs as Technical Responsible and Project Manager in the areas of biomedical engineering, telemedicine, IT, networking and telecommunications.